Effect of Equalisation Time and Temperatures on Microstructures of Simulated Directly and Conventionally Charged V-Microalloyed Steels

by

Jiansu Zhang

A thesis submitted to the University of Strathclyde
in fulfilment of the requirements for the award
of the degree of Doctor of Philosophy

Metallurgy and Engineering Materials Group
Department of Mechanical Engineering
University of Strathclyde
Glasgow, UK

March, 2003

Preface

The work presented in this thesis was carried out in the Metallurgy and Engineering Materials Group, Department of Mechanical Engineering, University of Strathclyde during the period November 1998 to March 2003 under the supervision of Professor T. N. Baker.

The work is original except where otherwise stated, and no part of this thesis has been submitted for any degree in this University or any other Universities.

The project was off shoot of an EPSRC grant, No GRIM 22818/01, awarded to Professor T. N. Baker with Corus group and Vanitec as industrial collaborations.

Acknowledgements

I wish to express my sincere gratitude to my supervisor, Professor T. N. Baker, for his invaluable guidance, advise and encouragement throughout the course of this work.

Many thanks also due to all academic and technical staff in Metallurgy and Engineering Group for their kind assistance, to all classmates for their useful help, and to Dr. D. N. Crowther, Swinden Technology Centre, Rotherham, Corus Group, for providing the steels used in this study, for his early work and for helpful discussions, and to Oversea Research Scheme committee, Corus Group, and Vanitec for their generous financial support.

Here, I also like to extend my cordialest thanks to all members of my family, especially my wife - Wei Wang and my parents for their continuous encouragement, support and understanding during my stay in Glasgow. Without their help, this work would have been impossible.

Finally, I want to show my special thanks to my newborn son, Michael. His coming brings me a lot of joys during the last period of my study.

Jiansu Zhang

March 2002

Contents

ABSTRACT

Two equalisation or reheating temperatures (1050°C and 1150°C) and three equalisation or reheating times (53 min, 318 min, and 1333 min) were applied to three V- and V-Ti- microalloyed steels, which contain a low carbon content (0.067 ~ 0.073 wt%) and high nitrogen content (0.017 ~ 0.021 wt%), by the simulated direct charging or conventional cold charging processes.

The experimental results show that in directly charged V-microalloyed steels, MnS provides the main pinning effect but does not have a sufficient ability to prevent the austenite grains from growing during the equalisation. Because of the slow precipitation, AlN only precipitates at the longest equalisation time and is the main compound which has an obvious pinning effect on the austenite grain growth in V-microalloyed steels. Austenite grain growth appears more likely to be abnormal as a result of the direct charging than of the cold charging due to the precipitation of fine AlN particles during the phase transformations. The experimental results also show that the longer equalisation or reheating time in the furnace does not result in a significant change in the microstructures and in the austenite grain size, because of the precipitation of AlN during equalisation or reheating.

However, in V-Ti-microalloyed steels, the existence of titanium can promote the precipitation of complex $(Ti_xV_{1-x})N$ particles during equalisation or reheating. In the cold charged V-Ti-N microalloyed steel, the fine austenite grains produced (<10μm) can be observed after the reheating and water-

quenching due to the significant pinning effect of $(Ti_xV_{1-x})N$. When the reheating time of V-Ti-N microalloyed steels at 1150°C is longer than 318 min, the coarsening of $(Ti_xV_{1-x})N$ precipitates occurs and leads to abnormal austenite grain growth. The TEM results also show that cruciform $(Ti_xV_{1-x})N$ particles can only be found in directly charged steels but not in cold charged steels.

Symbols

A_i, B_i ($i=1,2,3$)	Constants
c_i ($i=1,2,3,4,5,6,7,8$)	Constants
c_M, c_X	Constants related to concentrations and activities of M and X, respectively
C_b	Solute concentration within grain boundary
C_e^{∞}	Equilibrium solute concentration at planar interface
C_I	Solute concentration in the matrix at the interface
C_p, C_M	Solute concentration in precipitate and in matrix, respectively
C_{HV/σ_y}	A conversion factor
CCR	Conventional controlled rolling
d	Ferrite grain diameter
D_{Al}	Bulk diffusivity of Al in Fe
D_b	Grain boundaries diffusivity
D_{diff}	diffusion coefficient
D_{lim}	Limiting grain diameter
D_M	Mean diameter of grains
D_0	diffusion constant

D_s	Volume diffusion diffusivity
f	Volume fraction of precipitate
f_{AlN}	Volume fraction of AlN particles
f_{MnS}	Volume fraction of MnS particles
H_v	Vickers hardness
k	Experimental constant
k_1	Rate constant
k_0	Constant
K^{∞}, K_I	Solubility product for planar and nonplanar precipitate/matrix interface, respectively
m	Mobility of grain boundaries
M	Metals
$[M]$	Concentration of M
n	Constant
P	Driving pressure for general grain growth
P_m	Driving pressure for abnormal grain growth
P_Z	Particle pinning pressure
Q	Heat of dissolution
Q_b	Activation energy for grain growth
Q_{diff}	Activation energy for diffusion
r	Radius of second phase particle

r_{AlN}	Radius of AlN particles
r_{MnS}	Radius of MnS particles
R	Gas constant or radius of grains
R_0	Initial mean grain radius
R_i $(i=1,2,)$	Radius of curvature
R_a	Radius of abnormal grain
R_C	Critical maximum grain radius
R_g	Radius of a grain
$\overline{R}_g$	Mean radius of grains
R_G'	Radius of austenite grains
R_{lim}	Limiting grain Radius
R_m	Mean radius of an individual grain
t	Time
T	Temperature
T_C	Ductile-brittle transition temperature
$TSDR$	Thin slab direct rolling
T_{nr}	Non-recrystallisation temperature
V_p	Molar volume of precipitate
X	C, N, S, etc.
$[X]$	Concentration of X

X_V	Fraction of recrystallised material
Z	Ratio of the radii of growing grains to matrix grains
α, β_i $(i=1,2,3,4)$	Constants
α_M, α_X	Activities of M, X
α_{MnS}	The percentage of MnS volume in each diameter group
α_γ	The percentage of austenite volume in each diameter group
δ	Grain boundary thickness
γ	Precipitate/matrix interfacial energy
γ_b	Grain boundary energy
$\varphi_{\gamma GF}$	Grain-refining strain
$\varphi_{\gamma S}$	Strengthening strain
φ_Σ	Total rolling reduction
σ_0	Experimental constant
σ_{LYP}	Lower yield point
σ_y	Yield stress

CHAPTER 1 INTRODUCTION

In 1985, Woodhead (**1985**) wrote that microalloyed steels developed since 1960's offer an excellent combination of strength, ductility, toughness, formability and weldability at relatively low cost and are a very important member in the current world steel market, and this is still true today.

The development of microalloyed steels has been one of the most significant achievements of the past four decades in the field of steel metallurgy. It has been succeeded by the development of low carbon steels (≤ 0.1%C) with yield strength of higher than 400 N/mm^2 and microalloying additions of Nb, V or Ti (**Eissa, et al, 1998**). On laboratory-scale experiments, ferritic-pearlitic HSLA steels with higher yield strength levels of about 470 N/mm^2 and low carbon equivalent have been successfully produced by increasing Si and decreasing C and Mn contents of Nb-Ti microalloyed steels(**Richter, 1993**). However, there is still a need for producing low carbon steels with high strength levels to replace high strength alloy steels containing significant amounts of expensive elements such as nickel, chromium and molybdenum (**Eissa, et al, 1998**). It seems very attractive to attain these high strength levels by a combination of vanadium and a most abundant and cheap alloying element, such as nitrogen.

There are two main types of production routes used for microalloyed steels, i.e. conventional controlled rolling (CCR), and, more recently, thin slab direct

rolling (TSDR). The microstructures and mechanical properties of the steels will be determined by the different processing routes.

CCR is the process where the continuously cast steels, normally of 160-250mm thickness, are cooled to room temperature after casting and reheated to a soaking temperature prior to rolling to homogenise the chemical composition and microstructure. This route requires energy to reheat the steels from room temperature to the designed soaking temperature and requires more than 7 passes to reduce the slabs to a thickness of 2- 7 mm.

Direct hot charge rolling, developed in late 1970s, is a process where after casting, the thin slabs (about 50~100mm) are directly fed into an equalisation furnace set close to rolling temperature and then rolled into sheets by several passes. This process can be economic in production (**Lubensky, et al, 1995**) (**Flemming, 1993**) (**Leroy, 1995**) and also can lead to changes in the microstructures and mechanical properties of microalloyed steels compared to steels produced by the THE COLD CHARGING PROCEDURE process, because of the changes of cooling rates and phase transformation conditions.

However, the austenite microstructure prior to the rolling procedure of the TSDR process, known as direct charging, differs in several ways from that prior to the rolling procedure of the CCR process, the conventional cold charging. The prior austenite in the direct charging procedure is

characterised by a very large austenite grain size, up to several millimetres. This size is influenced by the chemical composition of the steels, the equalisation temperature and the equalisation time prior to rolling. The former two factors can be controlled satisfactorily during the process. Normally, the equalisation time can be satisfactorily controlled, too. However, in some special circumstances such as the breaking down of the rolling mill, the steel may have to be held in the equalisation furnace for longer times. This situation would be expected to lead to further growth of the prior austenite grains and hence lead to a possible change of microstructures and mechanical properties of the steels. So it is of importance to understand what will happen to the microstructures and how this affects the mechanical properties.

The aim of the present work is to study the change of microstructural parameters, the development of precipitates and their effects on particle strengthening and prior austenite grain growth during equalisation and reheating for three different times at three different equalisation or reheating temperatures in both the direct charging and the cold charging for several steel compositions.

CHAPTER 2 LITERATURE REVIEW

2.1 What is "Microalloyed Steel"?

It is very interesting to find that there are several different descriptions of "Microalloyed Steel". It is also very difficult to separate the terms "microalloyed steels" and "HSLA steels". There is no general agreement on which alloying elements qualify a steel for the term nor the levels below which a low-alloy steel turns into a microalloyed steel (**Stuart, 1983**).

Woodhead (1985) mentioned that "Microalloyed steel" was probably first introduced by Noren in 1962 as "Microalloy steel". These type of steels were defined as a steel, whose basic composition is simply an un-alloyed structural steel or, in many cases a carbon-manganese steel or even a low alloy steel, to which a small amount of usually a transition alloying element has been added which has a very strong and sometimes remarkable effect on one or several of the steel properties. It was thought that this type of steel could contain aluminium, vanadium, titanium, niobium and boron.

Gladman (1997) considered "microalloyed steels" as a name that was reserved for the steels containing small additions of an alloying element that will produce grain refinement and/or dispersion strengthening by the formation of relatively stable carbides or nitrides. Thus, microalloyed steels will typically contain niobium, titanium or vanadium, either singly or in combination, and their specific effects may be influenced by other alloying

elements such as aluminium, boron, or indeed any of the other more conventional alloying elements used in steel manufacture.

Summing up the development of steels in recent decades, **Woodhead (1985)** pointed out that nowadays grain refined, pearlite reduced or pearlite free, bainitic, acicular, controlled rolled, accelerated cooled, low sulphur, shape controlled etc. were all terminologies that fall within the category of microalloy or HSLA steels. Thus microalloyed steels and HSLA steels in the present period are widely considered as the same category of materials since the objectives and applications of microalloyed and HSLA steels largely coincide, and they contain small amounts of carbide and/or nitride-forming elements such as aluminium, niobium, titanium and vanadium, etc.

2.2 The development of microalloyed steels

The use of vanadium to increase the strength of mild steels can be dated back to as early as 1916. Then the use of aluminium deoxidation led to the important discovery that precipitation of AlN in normalising high nitrogen steels gave rise to a fine ferrite grain size and to an increase in yield strength **(Houdremont & Schrader, 1936)**. Niobium was employed in mild steels in the late 1950's **(Starratt,1959)**, much later than vanadium because niobium became much cheaper and readily available. Titanium did not seem to have been used to any marked extend as an addition to mild steel at an early date. Some data for properties of as-rolled and normalised Ti steels were given by **Wiester (1957)**. However, the early work had no reference to grain size

effects or to the influence of nitrogen until the late 1960's, when the effect of titanium on grain growth inhibition in low carbon steels had been reported by George and Irani (**Gladman, 1997**).

Even though the microalloying additions were used in mild steels before 1940, no major studies were initiated at the laboratory level into the strengthening mechanisms, especially the relationships of the grain size with the yield stress built up by **Hall (1951)** and **Petch (1953)**, before the early 1960's. Woodhead at the University of Sheffield was probably the first who made many important contributions to the fundamental understanding of the mechanisms whereby niobium influences the properties of steel (**Morrison & Woodhead, 1963**) (**Morrison, 1963**) (**Stuart, 1983**). Perhaps the contribution which stands out more than others was that the application of Hall-Petch analysis to structure property relationships could demonstrate unequivocally that, in addition to refining the ferrite grain size of steel, niobium also caused precipitation hardening (dispersion strengthening).

Because of more and more industrial interests on microalloyed steels, a new process, which can save the energy and manpower and reduce the steel cost, was employed in the late 1970s (**Ohkuma, et al, 1981**). The details about this type of direct charging process will be mentioned later.

2.3 Strengthening theories of microalloyed steels

Due to wide application of microalloyed steels, a physical metallurgical understanding was required to explain the effects of the elements on the microstructure and mechanical properties of these new steels.

Like many other metallic materials, the most important strengthening mechanisms of the microalloyed steels are considered as:

a. solid solution strengthening;
b. particle dispersion strengthening;
c. dislocation strengthening;
d. grain size refinement.

These strengthening mechanisms may affect the properties of microalloyed steels singly or in combination. The weighting will be dependent on the composition and processing details.

Hall (1951) and **Petch (1953)** independently developed the relationship between the lower yield point σ_{LYP} and the ferrite grain size, *d*

$$\sigma_{LYP} = \sigma_0 + kd^{-\frac{1}{2}} \qquad 2.1$$

where σ_0 and *k* are experimental constants. σ_0 was described by **Cracknell & Petch (1955)** as a stress which opposes the motion of the dislocations, and this can be increased by increasing solute concentration, dislocation density or volume fraction of particles.

Heslop and **Petch (1958)** went on to establish a relationship between the ductile-brittle transition temperature, T_C, and grain size, d, for mild steels

$$T_C = A_1 - B_1 \ln d^{-\frac{1}{2}} \qquad 2.2$$

Over the range of grain sizes which are readily obtainable, an approximate expression is

$$T_C = A_2 - B_2 d^{-\frac{1}{2}} \qquad 2.3$$

where A_1, B_1, A_2, and B_2 are constants.

The above equations show that the grain refinement can improve not only the yield stress but also toughness.

Subsequent wide-ranging work into the factors controlling the grain size and properties of steels containing niobium, vanadium, titanium and aluminium was undertaken. The research showed the influence of the complex interactions of carbon, nitrogen, sulphur and oxygen on stability of the various possible compounds which may precipitate out in either austenite or ferrite (**Irvine, *et al.* 1967**).

2.4 Grain growth

There are many factors which may influence grain growth. The main factors are:

- **Temperature:** Grain growth involves the migration of high angle grain boundaries and the kinetics will therefore be strongly influenced

by the temperature dependence of boundary mobility. As the driving force for grain growth is usually very small, significant grain growth is often found only at high temperatures.

- **Solutes and particles:** Although grain growth is inhibited by a number of factors, grain boundary pinning by solutes and by second-phase particles is particularly important.

The technological importance of grain growth stems from the dependence of properties, and in particular the mechanical behaviour, on grain size. In materials for structural applications at ambient temperatures, a small grain size is normally required to optimise the strength and toughness. However, in order to improve the high temperature creep resistance of a material, a large grain size is required. A good understanding of grain growth is therefore a prerequisite for the control of the microstructures and properties of metallic materials during solid state processing.

Grain growth may be divided into two types, normal grain growth and abnormal grain growth or secondary recrystallisation. During normal grain growth, the microstructure changes in a rather uniform way, there is a relatively narrow range of grain sizes and shapes, and the form of the grain size distribution in usually independent of time and hence of scale. During abnormal grain growth, a few grains in the microstructure grow and consume the matrix of smaller grains and a bimodal grain size distribution develops.

However, eventually these large grains impinge and normal grain growth may then resume (see **Fig. 2.1**) (**Humphreys, 1995**).

2.4.1 Grain growth kinetics

Burke (1949) and **Burke** & **Turnbull** (1952) deduced the kinetics of grain growth on the assumption that the driving pressure (P) on a boundary arises only from the curvature of the boundary. If the principal radii of curvature of a boundary of energy γ_b are R_1 and R_2 then

$$P = \gamma_b \left(\frac{1}{R_1} + \frac{1}{R_2} \right) \qquad 2.4$$

with the following assumptions:

1) the boundary is the part of a sphere, then $R_1 = R_2$.

2) γ_b is the same for all boundaries.

3) the radius of curvature (R_i) is proportional to the mean radius (R_m) of an individual grain, and thus

$$P = \frac{\alpha \gamma_b}{R_m} \qquad 2.5$$

where α is a small geometric constant.

4) the boundary velocity is proportional to the driving pressure P and to dR/dt. i.e. $dR/dt = c \cdot P$, where c is a constant.

Hence,

$$\overline{R}_m^{\,2} - \overline{R}_0^{\,2} = k_1 t \qquad 2.6$$

Or equation 2.6 can be written in general form

$$\overline{R}_m^{\,n} - \overline{R}_0^{\,n} = k_1 t \qquad 2.7$$

where R_m is the mean grain radius at time t, R_0 is the initial mean grain radius, n is the grain growth exponent which could be over 2, and k_1 is a rate constant, which is temperature dependent and follows the usual Arrhenius relationship

$$k_1 = k_0 \exp(-Q_G / RT) \qquad 2.8$$

where k_0 is a constant, Q_G is the activation energy for grain growth, T is the absolute temperature (K), and R is the gas constant.

2.4.2 The effect of second phase particles

A dispersion of particles will exert a retarding force on a low or high angle grain boundary and this may have a profound effect on the processes of recovery, recrystallisation and grain growth. The effect is known as **Zener drag**. The Zener equation

$$R_c = 4r / 3f \qquad 2.9$$

was first published by **Smith** in **1948**. According to this equation, it was proposed that the driving pressure for grain growth due to the curvature of the grain boundary would be counteracted by a pinning (drag) pressure exerted by the particles on the boundary. As a consequence, normal grain growth would be completely inhibited when the grain size reached a critical maximum grain radius (R_C) given by Equation 2.9, where r is the radius of the pinning particles and f is the volume fraction of particles. The Zener equation (2.9) embodies the major features of grain growth inhibition by

second phase particles. A finer grain size can be stabilised by an increased volume fraction of particles for a given particle size and finer particles are capable of stabilising a finer grain size for a given volume fraction of particles.

Gladman (1966) adopted a more realistic approach by considering the pinning force exerted by a single particle on a planar boundary and then derived the driving force for grain growth. In his equation,

$$R = \frac{\pi r}{6 f}\left(\frac{3}{2} - \frac{2}{Z}\right) \qquad 2.10$$

an important feature is Z, which is related to the ratio of the radii of maximum grains to average grains and lies between $\sqrt{2}$ and 2.

Hellman and **Hillert (1975)** considered the curvature in the grain boundary and introduced into Zener's equation a correction factor β_1 which equalled to 0.1251(R/r), and for abnormal grain growth the equation was derived as

$$R_C = 4r / 3f\beta_1 \qquad 2.11$$

where β_1 was normally between 1.3 to 1.6.

In recent years, computer modelling has been developed to predict particle-size / grain-size relationships. **Hillert (1988)** compared these models with both two and three dimensional approaches discussed in the literature. He concludes that in three dimensional systems

$$R_C = 4r / 9f^{0.93} \qquad 2.12$$

is recommended, except for large values of f, where the exponent decreases to lower values.

Rios (1987) derived an equation to predict grain growth in systems in which particles are coarsening and dissolving, where

$$R_c = r / 6f \qquad 2.13$$

Another model, developed by **Elst *et al.* (1988)**, can be modified to accommodate elongated particles, a bimodal particle distribution and a distribution of grain boundary precipitates. Here

$$R_C = \frac{4r}{3f\beta_2}\left(\frac{3}{2} - \frac{2}{Z}\right) \qquad 2.14$$

where β_2 is an increasing function of R/r and R_C approximated to $0.056\sim0.067(r/f)$ **(Gao & Baker, 2000)**.

2.4.3 Coarsening of dispersed second phase particles during grain growth

Grain growth can stagnate due to the particle dispersion according to the analysis above. The particle coarsening (**Ostwald ripening**) will reduce this effect and promote grain growth. In this situation, the grain size (R_g) is equal to a limiting grain size R_{lim}, and the rate of growth is controlled by the rate of change of particle size. Thus

$$\frac{dR_g}{dt} = c\frac{dr}{dt} \qquad 2.15$$

where the constant c is equal to $2\alpha_1 / 3f$ for low volume fractions and to $\beta_3 / 2f^{1/3}$ for large volume fractions, α_1, β_3 are constants.

The rate of particle coarsening will depend on the rate controlling mechanisms (**Hillert 1965) (Gladman 1966) (Ardell, 1972**). If the particle growth is controlled by volume diffusion (diffusivity =D_s) then

$$\overline{R}_g^{\,3} - \overline{R}_0^3 = c_1 D_s t \qquad 2.16$$

whereas for particle growth controlled by diffusion along the grain boundaries (diffusivity =D_b), which is commonly found for large volume fractions then

$$\overline{R}_g^{\,4} - \overline{R}_0^4 = c_2 D_b t \qquad 2.17$$

where c_1, c_2 are constants.

Coarsening of the particles by grain boundary diffusion will of course only affect those particles which are on grain boundaries, and other particles will coarsen more slowly. However, as grain growth occurs, the boundaries will lose some particles and acquire others, and therefore the overall particle coarsening rate may be uniform, although the rate constant c_1 in equation 2.16 should include a correction factor to account for the fraction of the time a particle is not attached to a boundary.

To predict the dissolution and coarsening of aluminium nitride precipitates in low carbon steels, **Cheng (2000)** developed a theoretical model. He assumed that

1) all precipitates are spherical;

2) the kinetics of particle dissolution and/or coarsening process is controlled by the diffusion of the substitutional alloy element Al;

3) the local equilibrium is considered exist at the precipitate/matrix interface.

The rate of dissolution (or growth) of a precipitate in a finite matrix can be approximated as

$$\frac{dr}{dt} = -k_2 \cdot \left[\frac{D_{Al}}{r} + \left(\frac{D_{Al}}{\pi t} \right)^{\frac{1}{2}} \right] \qquad 2.18$$

with $$k_2 = \frac{C_I - C_M}{C_P - C_I} \qquad 2.19$$

where r is the radius of a particle, D_{Al} is the bulk diffusivity of Al in Fe, C_P is the solute concentration in the precipitate, C_I is the solute concentration in the matrix at the precipitate/matrix interface and C_M is the average solute concentration in the matrix. Under local equilibrium conditions at the precipitate/matrix interface, the Gibbs-Thomson equation shows that the equilibrium composition in the matrix at the curved precipitate/matrix interface C_I varies with precipitate radius r as

$$C_I = C_e^{\infty} \cdot \exp\left(\frac{2\gamma V_P}{RTr} \right) \qquad 2.20$$

where γ is the precipitate/matrix interfacial energy, which is assumed to be constant, V_P is the molar volume of the precipitate, R is the gas constant, T is the absolute temperature and C_e^∞ is the equilibrium solute concentration at a planar interface. In the case of dissolution, the presence of the curvature tends to speed up the rate of dissolution. This is particularly important for small particles. For AlN precipitates, the solubility product for a non-planar precipitate/matrix interface K_I can be written as

$$K_I = [Al]_I[N]_I = K^\infty \cdot \exp\left(\frac{4\gamma V_P}{RTr}\right) \qquad 2.21$$

where $[Al]_I[N]_I$ is the equilibrium content (wt%) of Al and N respectively in the matrix at the curved precipitate/matrix interface and K^∞ is the solubility product for a planar interface.

It can be seen from Equation 2.18 that a precipitate is dissolving when $k>0$ and growing when $k<0$. In a multi-particle system an individual particle may dissolve while at the same time other particles are growing. Moreover, each individual particle may have a different growth or dissolution rate. For precipitates along grain boundaries, the dissolution (or growth) rate of a precipitate is approximated as

$$\frac{dr}{dt} = -k_3\left[\frac{D_{Al}}{r} + \frac{\delta D_b}{4r^2} + \frac{\delta D_b \beta_4}{2r} + \left(\frac{D_b}{\pi t}\right)^{\frac{1}{2}}\right] \qquad 2.22$$

with $$\beta_4 = \sqrt{\frac{4 D_{Al}}{D_b \delta d_0}} \qquad 2.23$$

where D_b is the grain boundary diffusivity, δ is the thickness of the grain boundary, d_0 is the mean grain diameter, and β_4 is a constant.

2.4.4 Abnormal grain growth

In addition to the normal grain growth discussed above, there are, however, some circumstances when the microstructure becomes unstable and a few grains may grow excessively, consuming the smaller recrystallised grains (**Fig 2.1b**). Usually, this process occurs in the steels where normal grain growth is strongly inhibited by nitrides, carbides or sulphides. If the grain growth inhibition fails, the grain growth may become abnormal (**Flores & Martinez, 1997**). This process may lead to grain diameters of several millimetres or greater. Because this discontinuous growth of selected grains has similar kinetics to primary recrystallisation and has some microstructural similarities, it is sometimes known as secondary recrystallisation. The avoidance of abnormal grain growth at high temperatures is an important aspect of grain size control in steels and other alloys.

The driving force for abnormal grain growth is usually the reduction in grain boundary energy, as for normal grain growth. Abnormal grain growth originates by the preferential growth of a few grains which have some special growth advantage over their neighbours, and the progress of abnormal grain

growth may be described in some cases by the JMAK equation (**Dunn & Walter, 1966**).

$$X_V = 1 - \exp(-c_3 t^n) \qquad 2.24$$

where X_V is the fraction of recrystallised material, t the recrystallisation time, n and B_1 are constants.

An important question to consider is whether or not abnormal grain growth can occur in an "ideal grain array", i.e. one in which there are no impurities and the boundary energy is constant. The answer to this question can be deduced from **Hillert's (1965)** theory of grain growth. From his equation

$$\frac{dR_g}{dt} = c_4 m \gamma_b \left(\frac{1}{R_{crit}} - \frac{1}{R_g} \right) \qquad 2.25$$

we see that the rate of growth of a grain of radius R_g is proportional to ($1/R_{crit}$ - $1/R_g$), where R_{crit} is the radius of a grain that will neither grow nor shrink, which was shown by Hillert to equal the mean grain radius of the assembly ($\overline{R}_g$). R_{crit} can be shown as

$$\frac{dR_{crit}}{dt} = \frac{c_4 m \gamma_b}{4 R_{crit}} \qquad 2.26$$

Here c_4=0.5 for a 2-D array and 1 for a 3-D array, m the mobility of grain boundaries, and γ_b the grain boundary energy.

Thompson *et al.* (1987) developed Equation 2.25 and pointed out that if we consider a large grain of radius R in the structure, then its growth rate relative to that of the normally growing grains is

$$\frac{d}{dt}\left(\frac{R_g}{\overline{R}_g}\right)=\frac{1}{\overline{R}_g^{\,2}}\left(\overline{R}_g\frac{dR_g}{dt}-R_g\frac{d\overline{R}_g}{dt}\right) \qquad 2.27$$

Thus the large grain will grow faster than the normally growing grains and lead to abnormal grain growth if

$$\overline{R}_g\frac{dR_g}{dt}-R_g\frac{d\overline{R}_g}{dt}>0 \qquad 2.28$$

substituting for dR_g/dt and $d\overline{R}_g/dt$ from Equations 2.25 and 2.26 (putting $\overline{R}_g=R_{crit}$), then it is seen that although $\overline{R}_g\,dR_g/dt = R_g\,d\overline{R}_g/dt$ when $R_g=2\overline{R}_g$, the condition of Equation 2.28 is never achieved. Thus a very large grain will always grow more slowly than the average grain and will eventually rejoin the normal size distribution. Therefore abnormal grain growth cannot occur in an "ideal grain assembly". It can, therefore, only occur when normal grain growth is inhibited, unless the abnormally growing grain enjoys some advantage other than size over its neighbours. The second-phase particles are considered the main factor which lead to abnormal grain growth although the rolling texture can also cause abnormal grain growth when materials are rolled (**Humphreys and Hatherly, 1995**). The latter factor is not the case in the present research and is not discussed here.

Conditions for abnormal grain growth

If we consider an assembly of grains of mean diameter D_M, whose growth is prevented by the particles, then this grain structure provides the driving force for abnormal grain growth. If the boundaries are of energy γ_b then the driving pressure for abnormal grain growth is (**Humphreys, 1998**)

$$P_m = \frac{3\gamma_b}{D_M} \qquad 2.29$$

This is opposed by the particle pinning pressure, P_Z (**Smith, 1948**)

$$P_Z = \frac{3f\gamma_b}{2r} \qquad 2.30$$

where f is a volume fraction of randomly distributed spherical particles of radius r , and therefore the condition under which a very large grain will grow, is $P_m > P_Z$, or

$$D_M \leq \frac{2r}{f} \qquad 2.31$$

If the grain size following primary recrystallisation is less than the particle-limited grain size, then D_M can be taken to be limiting grain diameter D_{lim}.

Equation 2.31 is based on the propagation of a planar boundary (infinitely large grain), whereas in practice the "nucleation" of abnormal grain growth (i.e. growth of a favoured large grain) may be the limiting factor. The above analysis may be modified to take into account the finite size of the abnormally growing grain, by adding a retarding force due to the radius of curvature of the grain ($c_5\gamma_b/R_a$) where R_a, is the radius of curvature of the abnormal

grain, and c is a constant, often taken as 2, so that the condition for its growth becomes

$$P_m > P_z + \frac{c_6 \gamma_b}{R_a} \qquad 2.32$$

or

$$D_M < \frac{2r}{f}\left(1 - \frac{2c_7}{3x}\right) \qquad 2.33$$

where $x = D_a / D_M$ and $D_a = 2R_a$.

Although this analysis is not rigorous, it does indicate that whereas abnormal grain growth may be viable in most particle-containing alloys, its nucleation may be the critical factor in alloys containing larger particle volume fractions, and this will be sensitive to the grain size distribution.

In research work on bulk copper, **Kronberg** and **Wilson (1949)** found that the size of the abnormally growing grains decreased with increasing heating rate up to the annealing temperature, and the incubation time for the initiation of abnormal grain growth decreased with increasing annealing temperature. **Koo** and **Yoon (2001)** pointed that the grain boundary migration rate will increase nonlinearly with the driving force, causing rapid growth of only large grains and, hence, abnormal grain growth. If the faceted grain boundaries migrate by growth on the steps produced by dislocations, the migration rate at low driving forces would be substantially higher than that by two dimensional nucleation, as shown by a dashed curve in **Fig. 2.4**. But at high

driving forces, the growth can be still occur by two dimensional nucleation, and, with either type of non-linear migration behaviour with driving force shown in **Fig. 2.4**, abnormal grain growth can occur in a system of many grains.

Feppon *et al.* (2002) compared the local parameters of a grain with the average parameters for the assembly and established the condition of instability (or abnormal grain growth) for a special grain. It was clarified that low misoriented assemblies have the strongest effect on the occurrence of abnormal grain growth because the rate of growth of the average is small enough to allow the abnormal development of some special grains.

2.5 The effect of processing details on microstructures of microalloyed steels

As mentioned above, there are two main types of processes used for microalloyed steels, i.e. conventional controlled rolling (CCR), and the newly developed thin slab direct rolling (TSDR). The difference between CCR and TSDR is shown in **Fig. 2.2** (**Priestner, 1998**). Now the newer process has recently become a potentially more important process for microalloyed steels due to its advantages both in the economics and microstructures. The microstructures and mechanical properties of steels will be significantly changed due to the differences of the processing routes.

2.5.1 Conventional controlled rolling (CCR)

Conventional charge rolling is the process where the steels leaving the mould of the caster are cooled to room temperature and reheated to a soaking temperature and then rolled into plates, sections or sheets by several passes. In this process, the fine austenite grains are due mainly to recrystallisation following deformation and the fine ferrite grains from γ-α phase transformation. More energy is required to reheat the steels from room temperature to the designed soaking temperature and requires a rolling process of normally about 15 passes to reduce the slabs from about $\geq$ 250 mm thick to 2~25 mm thick. This process route creates new austenite grains, homogenisation, precipitates and some solid solutions. The mechanical properties of the microalloyed steels depend on the accumulation of dislocations, and the recovery and recrystallisation of microstructure during the process of deformation.

In a conventional integrated plant, the production of hot rolled plate or strip steel begins with continuously cast slabs approximately 250mm thick. The slabs are allowed to cool to ambient temperature, and are then inspected and their surfaces conditioned for hot rolling to strip or plate. They are reheated, typically over a period of 6-8 hours to 1200-1250°C, during which as much as 10% is lost as scale, which must be removed before rolling. The reheating conditions affect the austenite by recrystallising the as-cast microstructure and creating a reproducible austenite grain size of about 200 μm, achieving a degree of homogenisation, and, in the case of microalloyed high strength

steels, by bringing precipitated species into equilibrium with their solution in the austenite. This usually means aiming to take the transition metal nitrides and carbonitrides into solution (**Crowther *et al.*, 1997**)(**DeArdo, 1998**).

The main objective of the thermomechanical processing of steels is to develop a small ferrite grain size, which is well known to be the only parameter which can simultaneously improve the strength and toughness in steels. One method that can lead to a significant refinement of the ferrite grain size is to accumulate as much strain as possible in the austenite before transformation occurs. The strain retained during the finishing rolling operations causes the austenite grains to be flattened and elongated and introduces intragranular defects, such as deformation bands and twin boundaries. The strained austenite is thus effectively refined, in the sense that its grain boundary area, including intragranular defects, is significantly increased and it transforms to a much finer ferrite grain structure (**Ouchi, *et al.*, 1982**).

Accumulation of deformation takes place when the austenite is deformed at temperatures low enough to produce strain induced precipitation of carbonitrides during deformation, which in turn inhibit recrystallisation. The temperature below which this occurs is known as the no-recrystallisation temperature (T_{nr}). Increasing this temperature allows the finishing rolling operations to be performed at higher temperatures which translates into lower loads to be applied by the mills. Some data found in the literature point

out the beneficial effect of the addition of titanium to the niobium microalloyed steels in increasing the value of the T_{nr} (**Abad *et al*, 1998**).

2.5.2 Thin slab direct rolling (TSDR)

Thin slab direct rolling, developed in late 1970s, is the process where continuously cast steels are kept above the rolling temperature and directly rolled into sheets by several passes without cooling and reheating. This process often uses the thin slabs (about 50~100 mm) instead of the thick slabs (over 150 mm) in CCR. It can be economic in production (**Flemming, 1993**) (**Leroy, 1995**) (**Lubensky, *et al.*, 1995**) and also, lead to changes of microstructures and mechanical properties of microalloyed steels.

2.5.3 Laboratory simulation of TSDR

The methodology of laboratory-based metallurgical research into conventional reheating and rolling processes is relatively straightforward and well established. A single plate of homogeneous composition and initial microstructure can be divided into many samples, and reproducible results obtained for many variations of experimental parameters (**Priestner, 1998**). For example, identical samples may be reheated to different temperatures and rolled to different strains, either by real rolling or by simulation in a plane strain or torsion testing machine, and realistic temperature histories can be simulated. For research into hot direct rolling of as-cast austenite, a newly melted and cast slab, however, is needed for every experiment and each parametrical variation. Early work in this area (**Wada *et al.*, 1988**) used large

cast ingots, and demonstrated that low carbon steels could be successfully hot direct rolled, but that microalloying resulted in a degree of grain size heterogeneity in the final product. In the case of Ti-microalloyed steel containing small additions of Ti (**Kunishige & Nagao, 1985**), it was shown that the strength was increased by direct rolling, probably as a result of a higher supersaturation of Ti in solution at the rolling temperature, in austenite cooled from the solidification temperature, than in reheated austenite. However, experiments with large castings are expensive in the use of material, and it is difficult to quench large samples efficiently enough for investigation of sequential microstructural changes throughout processing.

2.5.4 Comparison of CCR and TSDR

2.5.4.1 The thickness of slabs

Part of the impetus for HDR was the economic and ecological benefits gained by retaining the heat of the casting within the slabs, but improvements in strength were also reported, as described above for Ti-microalloyed steels (**Kunishige & Nagao, 1985**).

Since 1990, a number of plants have been commissioned around the world, but particularly in the USA, for casting thin or "thinner" slabs for hot direct rolling. The trend has been towards slabs thicker than 50 mm (but still considerably thinner than conventional, thick slab casting – about 250mm), using electric arc furnace steel derived mainly from scrap. Capital costs per tone are less than half those of a conventional BF-BOF hot strip mill

(**Edington, 1997**) and productivity (with respect to manpower) can be nearly three times as great. It seems certain, therefore, that the hot direct rolling of thin slab cast steel will continue to expand. In order to do so, however, it must match or exceed the quality produced by conventional plants in higher grades, particularly in microalloyed, HSLA steels.

As is seen in **Fig. 2.3** (**Priestner, 1998**), the characteristic difference is the much more rapid solidification and the faster cooling rates in the thin slab. The thin slab, in this case of 80 mm thickness, solidified completely within 2 $^1/_2$ minutes and the bulk mean temperature of the slab reached about 1000°C within a further 3 minutes. In the thick slab, the austenite grain size of low carbon steel soon after solidification is about 3 mm, whereas in the thin slab it is about 1 mm, and may be less if the sulphur content is appreciable. The rapid solidification can also lead to an additional result. The secondary dendrite arm spacing is considerably finer in the thinner slab, and, consequently, so is the scale of segregation of solutes such as manganese, with obvious consequences with respect to homogeneity in the final product.

2.5.4.2 Austenite grain size

In contrast to TSDR process, the austenite after the CCR process is significantly refined by the γ/α and α/γ transformations on cooling and reheating respectively, which also results in an homogenisation of the composition. It is not directly known if the interactions between deformation, precipitation and recrystallisation in austenite during TSDR are different from

those in reheated austenite during CCR. However, it has been found that the final microstructure and the mechanical properties of the microalloyed steels processed by TSDR can differ significantly from those obtained by CCR. The different thermal conditions can influence such microstructural changes as dynamic and static recrystallisation, and also precipitation characteristics during hot working.

The microstructures and mechanical properties of steels made by the TSDR process can be influenced by the composition of steels, the austenite grain sizes (including the austenite grain sizes after equalisation), the equalisation temperatures and time, the rolling temperatures, the rolling schedules, the amount of reduction, cooling rates after rolling, and the end coiling temperature.

Priestner (1995) mentioned that the phase transformation for γ-α/α-γ would lead to the fine austenite grain size. However, the final grain size of steels is the one of the most important factors which decides the mechanical properties of steels. The grain refinement may become a real problem in TSDR because the total possible reduction for the grain refinement is limited. But, on the other hand, **Gibbs (1992)** simulated the hot direct rolling of Ti microalloyed steel in his laboratory and found the finer ferrite grain size of rolled plate compared to conventional reheating and rolling. This was thought to be due to retained strain in the austenite prior to the transformation to ferrite in the TSDR steel. Many very small titanium precipitates, which were not observed in the conventionally processed steels, were found and it was

believed that these fine, possibly strain induced, precipitates are responsible for preventing recrystallisation at low temperatures during rolling, thus producing a controlled rolling effect in the TSDR titanium steel.

2.5.4.3 Cooling rate

Changes in the cooling rate will lead to changes in the microstructure of steels. Bainite instead pearlite can be produced using a faster cooling rate from austenite; 20°C/s rather than 1 to 10°C/s. For 20 mm thickness Nb-microalloyed steel, increasing the cooling rate from 0.9 K s^{-1} to 8.5 K s^{-1} will result in the decrease of ferrite grain size from 16.6 μm to 6.8 μm (**Singh *et al.*, 1999**) because accelerated cooling remarkably enhances the ferrite nucleation rate by controlling the stored energy.

It was known that when steels experience a low cooling rate through the $\gamma \rightarrow \alpha$, a pearlite transformation would take place. When the cooling rate is higher than about 1°C/s, a bainite transformation may occur. The higher cooling rates depress the bainite transformation to a lower temperature region. Also, the amount of pearlite decreases drastically with the increased cooling rates. With cooling rates higher than 4°C/s, the pearlite structure will be completely eliminated (**Wang *et al.*, 1992**). For an ultra low carbon microalloyed steel (about 0.03~0.04 wt.%), the critical cooling rate to avoid ferrite formation can reach about 2°C/s (**Wang *et al.*, 1993**).

The as-cast austenite grain size is increased when the cooling rate is decreased (**Crowther *et al.*, 1997**). For thick slab of 250 mm thickness, the cooling rate in the centre is slower than on the surface. An experiment on the thick as-cast slabs revealed the usual slab structure, with a narrow layer of fine equiaxed austenite grains near the slab surface, a region of columnar grains and a region of coarse equiaxed grains near the slab mid-thickness position. During rolling, the average austenite grain size decreased from over 800 to about 300μm as the cooling rate increased due to a reduced slab thickness from 80 to 30 mm. **Essadiqi (Woodhead, 1985)** described three zones of solidification structure in a thick steel slab: an undercooled zone of about 30μm along both sides; a zone of columnar structure; and an equiaxed zone at the middle of the strip. **Kaspar (1994)** found that the structures produced with a cooling rate of 0.1K/s had uniform equiaxed grains compared to the columnar dendritic structure observed at a cooling rate of 1.2 K/s.

2.5.4.4 Deformation schedules

In hot deformation processes, the total strain, in addition to reducing the cross sectional area, can be employed either for austenite grain refinement through complete recrystallisation (grain-refining strain, $\varphi_{\gamma\text{-}GF}$) and/or for the strengthening of austenite in the non-recrystallisation region (strengthening strain, $\varphi_{\gamma\text{-}S}$).

Experiments have been performed by **Zentara and Kaspar (1994)**, on an industrial Nb-V steel with the following chemical composition in weight percent: 0.11%C, 1.45%Mn, 0.34%Si, 0.068%Nb, 0.087%V, and 140ppmN. When rolling, the total amount of reduction, φ_{Σ}, was divided into two components: firstly, the high temperature reduction (1150-1100°C) which ensured an effective grain refinement through a static recrystallisation mechanism, and secondly, the low temperature reduction (850°C), which occurred in strained austenite, and produced grain refinement at the phase transformation stage. The experiments showed that when $\varphi_{\Sigma}<1$, the increase of $\varphi_{\gamma\text{-}S}$ had little effect on the mechanical properties, but when $\varphi_{\Sigma}>1.4$, the increase of $\varphi_{\gamma\text{-}S}$ led to a clear decrease in the transition temperature. This improvement is based on a finer ferrite-bainitic microstructure observed in the direct-rolled material as a result of a higher microalloying potential in austenite. Additional results were obtained by **Leroy (1995)** which showed that the yield strength is influenced by strain in the non-recrystallisation region and not by φ_{Σ}. Transition temperature would be improved much more when $\varphi_{\Sigma}>1.4$, which is similar to the result from the Zentara and Kaspar experiment.

Essadiqi (1995) studied a steel, of composition 0.05%C, 1.3%Mn, 0.2%Si, 0.015%Ti, 0.05%Nb, 90 ppm N, and found that the poorer properties of the direct rolled thin slab resulted from insufficient austenite grain refinement during the low reduction rolling schedule because there are no refining effects of phase transformation and less rolling reduction. Therefore, new

rolling strategies, new control of the solidification process, and new alloying additions will be required.

2.5.4.5 Equalisation/reheating temperature and time

Priestner (1995), studying TSDR Nb-Ti steel, pointed out that the carbonitride precipitated only below 1000 °C, or at 1100 °C after a long time (8 hr). The precipitates were Nb-rich and generally arranged in a linear group, suggesting that they had formed in interdendritic volumes or at austenite grain boundaries. But when a sample which had cooled in the mould to room temperature was reheated at 1250°C in the austenite phase field and quenched, titanium rich cubes were then observed.

Crowther (1997) showed that by using the direct charging, there was a continual increase in both yield strength and UTS as the equalisation temperature was increased from 1130 to 1200°C. The yield strength increased from 498 to 558 MPa, and UTS from 601 to 639 MPa. In parallel, there was a decrease in the Charpy toughness as the equalisation temperature increased. The structures for all the equalisation temperatures used were generally a fine grained ferrite-pearlite structure, with grain sizes in the range 4.7~5.9 μm. A torsion simulation experiment on a Ti steel by **Gibbs (1992)** showed that after hot deformation, the ferrite grain size of specimens previously heated to 1400°C was 11.3μm, compared to those previously heated to 1150°C with a grain size of 8.3μm. The bigger ferrite grain size when the steel was heated at 1400°C is due to the complete

dissolution of second phase particles which led to a bigger austenite grain size.

2.6 The effect of composition on microstructures of microalloyed steels

2.6.1 Carbon

It is known that at carbon levels within the range found in mild steels, changes in pearlite content have little, if any, effect on yield strength, whereas increasing the amount of pearlite raises the impact transition temperature (**Woodhead, 1985**). The reduction of carbon content in steels can result in a significant increase of the bainitic transformation temperature (**Honeycombe *et al.*, 1995**) and promote the bainitic transformation at higher cooling rates. So there will be advantages in using steels of carbon content as low as 0.03-0.10% and therefore with reduced amounts of pearlite. Further reduction of the carbon content down to about 0.01% gives a pearlite-free steel. It is, however, doubtful whether there is any real gain in the properties. In his research on high manganese low carbon steels, **Mårtensson (1972)** found that when the carbon content is below 0.015% and the steel is austenitised at 900°C, no martensite can be formed at realistic cooling rates (not higher than 90°C/s) and the hardenability of steels will markedly decrease.

Zajac (1996) stated that the strengthening effect depends also on the carbon content of microalloyed steels. An increase in carbon increases the intensity of precipitation of V(C,N) in ferrite at a given V and N. This effect of carbon is

due to the high carbon content of ferrite in equilibrium with metastable austenite.

It was found that low carbon levels below the peritectic range (0.05 wt.%) were an attractive option because they discouraged the formation of columnar grains, refined the as-cast grain size, and produced a greater improved ductility than the peritectic steel (**Banks, 2001**).

2.6.2 Nitrogen

For a long time, nitrogen has been considered as an enemy for steelmakers due to its detrimental effect being associated with various embrittlement phenomena. However, in recent years, nitrogen has attracted much attention due to certain beneficial effects resulting from its interaction with the alloying elements present, which has led to the development of many different steels containing an enhanced nitrogen content.

Kunishige *et al.* (**1989**) studied the microstructures and mechanical properties of Ti steels by HDR, HCR and CCR. The results showed that the amount of nitrogen in the steels is important. When the nitrogen content in steels is at 45 ppm level, the highest tensile strength was attained in the whole titanium range investigated (from 0.005% to 0.02%). In the conventional process, approximately 80% of the total titanium was in precipitation after soaking at 1150°C. The insoluble titanium is considered to have existed in the form of titanium nitride. In the HDR process, however,

only about 20% of the total titanium was present in the form of titanium nitride after keeping the slabs at 1150°C, but after rolling was completed the amount of the insoluble titanium increased up to about 73% of the total titanium in the form of titanium nitride, which was also fine and numerous. For higher nitrogen steels, the main strengthening factor was due to TiN precipitation which was incoherent with the ferrite matrix while a superior low temperature toughness results from the dispersion hardening by fine TiN particles which precipitate on a high density of dislocations introduced by rolling and produce the smaller grain size. In lower nitrogen steels, the main strengthening particle is TiC which initially is coherent with the ferrite matrix and may caused an embrittlement.

In his studies on low C-V and low C-V-Nb steels, **Banks (2001)** pointed out that although higher nitrogen contents increased the precipitate mole fraction, the vanadium and nitrogen levels did not influence particle size in vanadium steels.

2.6.3 Manganese and Sulphur

The addition of manganese to a low carbon steel is an efficient way to form MnS to reduce sulphur effects in the steels and affect final properties of the steels adversely. MnS precipitates are unavoidable because a manganese addition is the best and the most economic way to reduce free sulphur. Indeed sulphur is a well-known deleterious element in steel.

Previous work (**Frawley, 1998**) shows that Increasing the sulphur content of thin slab cast and direct rolled mild steel, refined the ferrite grain size of the product and increased strength. The sulphur had two principal effects. The high supersaturation with respect to MnS present in the just-cast austenite caused precipitation of MnS, preferentially on the austenite grain boundary. These precipitates have a pinning effect on the grain boundary, resulting in a finer austenite grain size prior to rolling. The other effect is that the strain induced precipitate dispersion, or the sulphur in solid solution, or both, retarded austenite recrystallisation, augmenting a similar tendency arising from the coarseness of the just-cast austenite grain size. The retained strain in the banded, unrecrystallised fraction of the austenite caused that fraction to transform to fine grained ferrite. The yield strength was greater in the TSDR material and increased to a maximum at a sulphur content which was inversely related to the level of Mn. This concentration of sulphur, where peak strength occurs, corresponds to its maximum solubility in austenite at the peritectic temperature. Edge cracking originated in the first pass at 1100°C, and was related to sulphur in solid solution rather than to precipitated MnS. The addition of Ti significantly reduced the severity of edge cracking because Ti apparently increased the kinetics of sulphide precipitation, thereby reducing the free sulphur at the time of rolling.

A study on the forged low carbon steels (0.1%C) with manganese contents from 0.75 wt.% to 3.5 wt.% was carried out by **Eissa *et al.* (1998)**. It was found that with up to 1.5 wt.% Mn, the general nature of the microstructure

comprises ferrite-pearlite. The higher manganese contents from 2.7 to 3.5 wt.% result in the formation of bainitic structure. Manganese has a pronounced effect on the mechanical properties of steels with lower manganese contents (< 1.5 wt.%), due to solid solution and grain refining effects, and higher manganese contents (2.7~3.5 wt.%) will produce the increase of the yield and ultimate tensile strengths due to the solid solution and transformation strengthening. Manganese contents in the range of 1.5~2.3% have a less pronounced effect due to solely solid solution hardening.

2.6.4 Microalloying elements

It had been well-known that microalloying elements are added to structural steels for three principal reasons (**DeArdo, 1998**):

(1) to refine the austenite grain size during rolling and therefore, to aid in refining the ferrite grain size after transformation.

(2) to lower the transformation temperature, thereby also refining the ferrite grain size and increasing its dislocation density.

(3) to possibly impart precipitation hardening or solute hardening.

Four microalloying elements -- aluminium, vanadium, titanium, and niobium -- are widely used in various combinations to improve the mechanical

properties of structural steels. Addition of these four elements brings about the extreme refinement of grain size of steel and the rise of coarsening temperature austenitic grain. It is considered that this grain refinement is due to the precipitation of very fine carbides or carbonitrides of vanadium, titanium, niobium or nitrides of vanadium, titanium, niobium and aluminium, which act as nuclei for the newly precipitating phases at the transformation of steel, and that the rise of grain coarsening temperature is a result of a restraint of grain growth by the precipitates (**Narita, 1975**).

Vanadium, niobium, titanium have a high quenching-hardening effect on steels. The hardenability of steel, however, is reduced by the refining of the grains by increasing the amount of additions. This may be caused by the fact that the solubility of carbides or carbonitrides of these elements in austenite is considerably low, their solution rate is also very low, and moreover vanadium, niobium, titanium markedly reduce the diffusion of carbon.

As is well known, vanadium, titanium, niobium and aluminium do not have a significant influence on the tensile strength, the elongation and the reduction of area, but have a marked effect on the yield strength and the impact value. In particular, the effect of vanadium and niobium is remarkable. It is considered that the improvement of the tensile strength depends upon the grain refinement in the case of a comparatively low temperature heat treatment or normalizing, and mainly upon the precipitate hardening in the case of the heat treatment at comparatively high temperatures of solution

treatment. Such a characteristic of vanadium or niobium is based on the fact that carbides, nitrides or carbonitrides of these elements have an appropriate solubility in solid steel at the heating temperatures, besides their solubility changes, in very suitable range for the metallurgical processing. Because of restraint of dislocation movement by these fine precipitates, and grain refinement, the yield strength of steel is raised and the impact transition temperature may be lowered, and then toughness of steel at low temperature is improved.

2.6.4.1 Niobium

The use of niobium in mild steels was initiated in 1950s. However it was probably first studied theoretically by Morrison & Woodhead (1963). The clearest evidence of the effect of a Nb addition to steels was the grain refinement, which brought about the increase of strength without the increase of brittleness, and provided good formability and weldability. So Nb steels were employed throughout the world and a number of facts about niobium steels had become well established by the end of 1959 (**Woodhead, 1985**).

These are:

(a) the addition of 0.01%-0.05%Nb to mild steel base compositions gives improved yield strength in hot rolled steels;

(b) the toughness (transition temperature) of hot rolled Nb steels is little affected; sometimes it is improved but, in general, it is slightly impaired, compared Nb free steels;

(c) normalising after rolling caused a marked improvement in toughness and a slight increase in strength of Nb steels as compared with plain carbon steels;

(d) niobium additions are more effective in steels with higher manganese levels;

(e) grain refinement is observed in Nb steels, both in the as-rolled condition and when normalised.

The addition of Nb to the steels will lead to the precipitation of fine Nb(CN) particles which could have a greater effect in retarding softening processes in the ferrite, and which may lead to the cracks at the grain boundaries **(Crowther, 1998)**.

Niobium additions can also decrease the stability of TiN and result in a lower grain coarsening temperature (GCT) (**Feng et al., 1989**). Typical particle morphologies in Ti/Nb bearing steel slab are dispersed dendritic (TiNb)N particles and fine spherical TiNb(CN) particles. The dendritic TiNbN particles have cuboidal Ti-rich cores and Nb-rich arms. The arms dissolve readily on reheating leaving the Ti-rich core.

2.6.4.2 Vanadium

Vanadium microalloying is effective in increasing the strength of steels either solely through dispersion strengthening, or through both dispersion strengthening and grain refining effects. The strengthening effect of vanadium seems to have no negative effect on elongation; the effectiveness of vanadium is greatly enhanced by increasing the nitrogen content. **Eissa *et al.* (1998)** studied a forged microalloyed steel bar and found that increments of 194 and 110 N/mm^2 in the yield and ultimate tensile strengths, respectively, were attained by increasing the nitrogen content from 0.015 to 0.025% for steel with a base composition of 1.8% Mn and 0.15% V; the grain refinement of vanadium/nitrogen microalloying seems to be due to the inhibition of austenite grain growth as a result of the precipitation of vanadium nitride in austenite during forging. Dispersion strengthening of these steels is achieved by the precipitation of vanadium carbide and nitride in ferrite or bainite; electrolytic analysis clarified the simultaneous formation of vanadium carbide and nitride, irrespective of the content of either vanadium or nitrogen in steels; nitrogen enhances the dispersion strengthening of vanadium microalloyed steels which could be attributed to the finer vanadium nitride precipitates compared to vanadium carbide; up to 70% of the total nitrogen content of steel precipitates as vanadium nitride which could be achieved with V/N ratio of about 6-7 (**Eissa, 1998**).

Vanadium is the most soluble of the four microalloying elements and does not readily precipitate in austenite (**Zajac, 1998**). VN is considerably more

stable than the carbide and it hardly affects the hot deformation process but rather precipitates during cooling in ferrite, thereby increasing the strength level of steels. This precipitation hardening is markedly enhanced with increasing nitrogen in the steel, and so nitrogen is considered as a beneficial alloying element in vanadium microalloyed steels. Since the nitrogen contents of commercial structural steels, up to 200 ppm, are generally below the solubility limit in both ferrite and austenite, all the nitrogen is available for precipitate formation, where this occurs homogeneously or by an interphase mechanism.

2.6.4.3 Titanium

In commercial V-microalloyed steels, small amounts of Ti (~0.01 wt.%) are commonly added to prevent excessive grain coarsening at high temperatures (**Lagneborg, 1999**). After studying the effect of increasing titanium content on V-microalloyed steels using a CCT diagram, **Peñalba (1996)** concluded that increasing of the Ti percentage produced a translation of the CCT diagram towards the right side of the time axis, and when Ti content in steels is over 0.020 wt%, this translation is great (**Fig. 2.5~2.7**). It was reported that the addition of a small amount of titanium to steel could not only inhibit the grain growth of austenite, but also raise the austenite grain coarsening temperature during reheating. The austenite and the subsequent transformed ferrite grain size can be refined as long as the reheating temperature is not higher than the austenite grain coarsening temperature of the steel. In niobium-microalloyed steels, the grain refinement effect from titanium is

surpassed by niobium itself (**Wang, 1990**). The technical background to this is that Ti reacts with the nitrogen in the steel to form a fine dispersion of very stable TiN.

The TiN precipitation may be affected by a second microalloy addition, such as V, in various ways. This alone, but especially together with the formation of a second precipitate, may affect the grain coarsening behaviour significantly (**Kaspar 1994**). Titanium additions to steels can make the precipitation of carbides and/or nitrides easier, or form TiN to hinder boundary movement and influence the grain growth (**Priestner, 1998**) This will be beneficial through the formation of a fine grain size which improves the mechanical properties, particularly the Charpy toughness (**Crowther, 1997**).

Abad *et al.* (**1998**) compared the effect of Nb alone with Nb-Ti on the no-recrystalisation temperature (T_{nr}) in the microalloyed steels and pointed out that the T_{nr} of the Nb-Ti steel is significantly lower than that observed for the Nb-steel. The explanation of this phenomenon is that a reheating temperature of 1200°C would be enough to dissolve all the niobium in Nb-steel, but not high enough to dissolve the (Ti,Nb)N particles, and a significant fraction of added niobium may remain undissolved in the austenite. Consequently, the supersaturation becomes lower and results in the necessity of going to lower temperatures for the precipitation of Nb

carbonitrides, which are able to pin the dislocations and halt the recrystallisation process (decrease of T_{nr}).

Other research (**Feng, 1989**) (**Matsuda *et al.*, 1979**) had shown that Ti has a great effect on the austenite grain coarsening temperatures (GCT). It was found that titanium and nitrogen, whose levels were in a ratio near to the stoichiometric value, can substantially increase the austenite GCT for Ti- and for Ti/Nb-bearing steels. The stable precipitates responsible for grain boundary pinning in high temperature austenite are fine TiN or TiNbN cuboids. Titanium steels with Ti : N ratio well in excess of the stoichiometric ratio have a relatively low GCT due to the formation of coarse TiN particles and coarse titanium carbosulphides. Rapid austenite grain growth results from the solution of fine (~15 nm) TiN (or TiNbN) particles and the consequent increase in the mean size and decrease in volume fraction of these particles. The reduction in the GCT after solution treatment and hot rolling is attributed to a substantial loss of fine TiN or TiNbN particles at the reheating or soaking temperature. Reprecipitation of fine particles during air-cooling and hot rolling only partially compensates for this loss. The starting austenite grain size on reheating after solution treatment or hot rolling is also a factor which can influence the GCT. GCT is a function of time and temperature and typically is 50-75°C lower for a 4 hour treatment time than for 0.5 hour. The apparent activation energies for the coarsening process in the 0.016Ti and 0.019Ti/ 0.024Nb steels were 340 $kJ \cdot mol^{-1}$ and 270 $kJ \cdot mol^{-1}$, respectively.

Some research has found that the large cuboidal TiN precipitates (>0.5μm) might form in the liquid due to the significant segregation of titanium and nitrogen during casting (**Chen *et al.*, 1987**). These precipitates would not be useful in inhibiting austenite grain growth at high temperatures despite their stability. Furthermore, they remove titanium from solution, so reducing dispersion strengthening. The authors also mentioned that these kinds of particles could be avoided by decreasing the concentrations of titanium and nitrogen, which reduces the segregation of titanium and nitrogen in the liquid. However, a decrease of nitrogen below the content used in the Nb-V-Ti steel would significantly reduce the volume fraction of precipitates in austenite and thus is not desirable. It would be better to reduce the titanium content. The size of the TiN precipitates may also be reduced by using a fast cooling rate during the solidification.

2.6.4.4 Aluminium

Aluminium is almost universally present in C-Mn steels for purposes of deoxidisation but may also react together with nitrogen to form aluminium nitride. The aluminium is normally dissolved in austenite at high temperatures prior to rolling but the nitride phase is thermodynamically stable at lower temperatures (**Li *et al.*, 2000**).

It is well-established that steels containing a small amount of aluminium resist grain coarsening up to ~ 1273 K because of the pinning effect of

aluminium nitride precipitates in the austenite (**Gladman *et al.*, 1967**) (**Hall *et al.*, 1967**). The small values of solubility product [Al][N] in austenite (**Wilson *et al.*, 1988**) suggest that aluminium nitride can be an effective grain boundary pinning phase in austenite. However, insufficient amounts of nitrogen in steels, typically less than 0.01 wt.% N, will limit the potential of AlN precipitation (**Matsuo *et al.*, 2000**).

In the research on vanadium microalloyed steels which contains 0.025% aluminium, **Li (2000)** found that AlN particles usually did not precipitate when steel specimens were equalised at 1100°C or 1200°C, but precipitated at 1050°C, both on the austenite grain boundaries and in the matrix, and were often associated not only with MnS particles, but also with VN particles (**Li, *et al.*, 2001**).

It was also clarified that both the volume fraction and particle size of aluminium nitride will determine the matrix grain size. However, the aluminium nitride precipitates can locally promote the appearance of abnormal grain growth, because their relatively rapid dissolution can eventually favour a local reduction in the pinning force (**Cabrera, *et al.*, 1996**). Cabrera also considered that the appearance of abnormal grain growth was attributed to the heating-rate effect. The steel which was directly introduced into the furnace at the austenitizing temperature might show abnormal grain growth, while normal grain growth would be observed with

slower heating rates, because dissolution curves would tend to those of equilibrium.

CHAPTER 3 EXPERIMENTAL PROCEDURES

3.1 Composition and Processes of Steels

Three Al-V-N steels, whose composition (wt%) is given in **Table 3.1**, were used in the research.

Steel 1 was treated using the simulated thin slab directly charged process at Swinden Technology Centre, Corus Group. **Figs. 3.1 ~ 3.2** show diagrams of the simulated TSDR process program and a time - temperature diagram of this program. The ingots of the experimental steel were stripped from the mould at T_1 = 1450°C ~ 1500°C. During stripping, the temperature of the ingots may drop to temperatures between 1000°C and 1100°C (T_2). These ingots were than equalised at 1150°C (T_3) for 53min, 318min, or 1333min respectively and then water-quenched. All the ingots were cut into 10x10x10mm specimens from both the equiaxed and columnar as-cast austenite zones. Half were tempered at 650°C (T_4) for 30min. The temperature in the furnace was calibrated by placing a thermocouple at the position of specimens and relating the controller display temperatures to the correct temperatures.

Steel 2 was treated by the simulated conventional charging process. All the ingots were cast, stripped, and then quenched to room temperature at Swinden Technology Centre, Corus Group. They were then cut into specimens 10x10x10mm and 3x10x10mm. The latter specimens were

encapsulated in quartz tubes. All the specimens were equalised at 1050°C or 1150°C for 53min, 318min, or 1333min in the furnace and quenched in the icy water. The cooling rate of encapsulated specimens in the water was about 300~500°C/s and that of non-encapsulated specimens was about 100°C/s~200°C/s.

Steel 3 was treated using both the simulated direct charging process, in which the entry temperature T_2, the equalisation temperature T_3 and equalisation time were 1018-1095°C, 1100°C and 47 min respectively, and a simulated conventional charging process with the same conditions as Steel 2 in an encapsulated condition. The cast microstructure of Steel 3 was also analysed. The addition of titanium in Steel 3 was used to study the influence of Ti on austenite grain growth.

3.2 Hardness Testing

A Vickers hardness testing machine was used to obtain the hardness of steels on the equiaxed and columnar grain zones for Steel 1 and the surface and centre of specimens for Steels 2 and 3. The surfaces of specimens are divided into 12 divisions. The average hardness values are obtained from 12 indents located in the centres of these 12 divisions with 30 kg load. Before testing, the test machine was calibrated using standard test block following the procedure described in BS427 [1990]. As hardness tests always reveal close parallels to the tensile test, the yield strength could be estimated from the hardness data, using the following relationship

$$\sigma_y = C_{H_V/\sigma_y} H_V \qquad 3.1$$

where H_V is the Vickers hardness value, σ_y is yield stress in MPa, and C_{HV/σ_y} a conversion factor given as 2.15 in similar microalloyed steels containing vanadium (**Lapointe and Baker, 1982**).

3.3 Austenite Grain Size

A cast structure of Steel 1 was retained during the direct charging and quenching treatment (**Fig. 3.3**). This structure can be clearly divided into two zones - the equiaxed zone and columnar zone. The grain sizes in the columnar zone need to be measured in two vertical directions (**X** and **Y** direction) because of the significant size difference of up to 15 times in the two directions. The microstructures were examined by optical microscopy after etching in 2% nital. 100 austenite grains in each condition were measured by the optical microscope at 7 times magnification. This small number of measurement was due to the large austenite grain size in the steel which was over 1mm in the diameter.

For conventionally charged Steels 2 and 3, the austenite grains were equiaxed and 200 grains were measured by the optical microscope at 400 times magnification. A linear intercept method recommended by ASTM [1976] was used to obtain the austenite grain size.

3.4 Transmission Electron Microscopy

Extraction replicas were obtained by a standard method of evaporating carbon on to the etched surface of specimens in a Mikro BA3 Balzers Vacuum Coating Unit at a vacuum of better than $5x10^{-3}$ Pa. The specimens which were covered by carbon coating were cut into 3mm×3mm square and etched by 5% nital. The floated carbon replicas were cleaned in pure alcohol, collected by copper grits.

The examination for precipitate morphology, size, distribution, and composition was performed in a Philips EM 400T transmission electron microscope, operated at 80 or 100 KV, which was interfaced to a Phoenix EDX energy dispersive system.

Precipitate sizes and their distributions were obtained by measuring 100 ~ >300 particles while lath widths and their distributions were obtained by measuring more than 200 laths. The lath width was measured on the TEM screen. The reading error was estimated beyond 10%. The particle diameter and grain diameter analysis was dealt with by using the commercial software called as Image-pro Plus. Every particle diameter was obtained by measuring 50 diameters in every 18 degrees and calculating the average.

3.5 About identifying nitrogen peak with titanium peak in EDX spectrum

It is well understood that it is impossible to distinguish the nitrogen N_k peak from the titanium Ti_L peak in EDX spectrum. This is because that the energy of nitrogen K peak is 0.392 KeV and very close to the energy of titanium L peak which is 0.452 KeV. These peaks overlap in an EDX spectrum as the detector resolution is about 0.13 eV and the difference between N_k and Ti_L peaks is only 0.06 KeV. When the samples contain both nitrogen and titanium, identifying the existence of these two elements becomes a real challenge. Usually either a TEM with an energy loss spectrometer, or if the particles are big enough (>1μm), a wavelength spectrometer on an SEM can be used.

Another easier way to solve this problem may depend on the energy peak heights in the EDX spectrum. It is easy to identify titanium from titanium K peak at 4.6 KeV. When titanium is identified, the energy peak height of the titanium L peak can be estimated (see **Fig. 3.4**). When the real peak is higher than the estimated titanium L peak height, this difference may be due to nitrogen. It can be seen that when nitrogen is considered for analysis of EDX spectrum an almost perfect overlap occurs in **Fig. 3.5**. Therefore, this method should be suitable for the identification of nitrogen in EDX spectrum analysis.

CHAPTER 4 EXPERIMENTAL RESULTS

4.1 Hardness

4.1.1 Steel 1

The hardness of Steel 1 before and after tempering is shown in **Fig. 4.1** and **Fig. 4.2.** It can be seen that there is no significant difference in the hardness values between specimens from either columnar zones or equiaxed zones. When the specimens were equalised at 1150°C and water-quenched, the hardness values decrease very quickly from about 360 to 260 when the equalisation time increases from 53 min to 318 min and then there is a slight increase of hardness value from 260 to 290 when the equalisation time increases from 318 min to 1333 min. Tempering leads to the changes in the hardness values for the three equalisation times, but these changes are different. For 53min, 318min, and 1333min equalisation time, the hardness values decrease about 20, increase about 25, and remain almost same, respectively, after tempering.

4.1.2 Steel 2

Fig. 4.3 presents the hardness values of Steel 2 reheated at 1050°C or 1150°C in the encapsulated or non-encapsulated conditions. Compared with the simulated directly charged Steel 1, the hardness values of non-encapsulated Steel 2, from about 230~340, are lower for the three reheating times while the hardness values of encapsulated Steel 2, from about 380~420, are much higher for the three reheating times.

The hardness values of the encapsulated specimens are much higher than those of non-encapsulated specimens, especially for 318min and 1333min reheating times.

It is found that when the reheating time increases from 53 min to 318 min, the hardness values of non-encapsulated specimens do not decrease as quickly as encapsulated specimens. However, when the reheating time increases from 318 min to 1333 min, the decrease rates of hardness of both types of specimens are almost the same. The hardness change of non-encapsulated specimens is similar to that of the simulated direct charged Steel 1.

The change of reheating temperatures from 1050°C to 1150°C, however, does not have a significant influence on the hardness of both the encapsulated and non-encapsulated specimens.

4.1.3 Steel 3

At a reheating temperature of 1150°C, the hardness values of the encapsulated specimen increase slightly from 378 to 384 when the reheating time increases from 53 min to 318 min. However, as the reheating time increases from 318 min to 1333 min, the hardness decreases quickly from 384 to 334. The decrease tendency of non-encapsulated specimens is similar to that of Steel 2 non-encapsulated specimens. The hardness values decrease in non-encapsulated specimens from 279 to 213.

The hardness values of non-encapsulated Steel 3 specimens reheated at 1050°C almost remain unchanged when the reheating time increases from 53 min to 318 min. As the reheating time increases from 318 min to 1333 min, the hardness values slightly decrease from 340 to 330.

All the changes of hardness values of Steel 3 are shown in **Fig. 4.4**.

4.2 Austenite grain growth

4.2.1 Steel 1

4.2.1.1 Before tempering

The austenite grain coarsening behaviour as the functions of equalisation times, in both equiaxed zone and columnar zones, are shown in **Fig. 4.5 and Fig. 4.6**. In **Fig. 4.5**, the square diameters of austenite grains were obtained from the average diameters measured from the equiaxed zone. The non-linear curve indicates that the growth of austenite grains does not follow the parabolic law. In the columnar zone, austenite grain growth are roughly linear in either X or Y direction. Their grain size distributions (times frequency) are given in **Figs. 4.7~4.9**. The austenite grains can be as large as several millimetres (**Figs. 4.7~4.11**).

The austenite grain size in both the equiaxed and columnar zones increased with an increase of the equalisation time. Initially, the grain growth rates are high, then they slow down as the equalisation time increases. The methods reported by **Kaspar *et al* (1994)** and **Ralph (1990)** were used here to

distinguish abnormal grain growth from normal grain growth. No obvious bimodal shape of austenite grain size in 53min and 318min equalisation times shows that no significant abnormal grain growth occurs in equiaxed zones and Y directions of columnar zones during these two equalisation stages. However, as the equalisation time increases to 1333min, a bimodal shape, indicating abnormal grain growth, can be seen clearly. In X directions of columnar zones, the abnormal grain growth can be seen for all three equalisation times. This fact indicates that since the growth rate in the length direction of columnar austenite grains is much quicker than that in the width direction, it is more likely for the columnar austenite grains to grow abnormally in the length direction.

After the equalisation and quenching, the microstructures for 53min and 318min equalisation times are mainly lower bainite (**Figs. 4.12~4.13**) where many carbides precipitate in ferrite laths.

4.2.1.2 After tempering

Figs. 4.14~4.15 show the austenite grain size and the diameter distribution in the equiaxed zone of Steel 1. It can be observed that tempering the specimens which were quenched after equalisation does not lead to obvious change of the austenite grain sizes and size distribution,.

4.2.2 Steel 2

Quenching at a cooling rate of about 100~200°C/s for non-encapsulated specimens and at about 300~500°C/s for encapsulated specimens leads mainly to the formation of martensite (**Fig. 4.16**). Only a few laths (about 2~5 %) were bainitic ferrite laths where cementite could be found (**Fig. 4.17**).

When Steel 2 is reheated, the austenite grains are much smaller, less than 100μm in diameter, than in directly charged Steel 1. **Figs. 4.18~4.23** show the austenite grain sizes and their distribution histograms for three reheating times at 1050°C and 1150°C in both encapsulated and non-encapsulated specimens. There are almost no differences between these two types of specimens in both the average grain sizes and in the distribution. Unlike the distribution in directly charged Steel 1, all distribution curves of austenite grain sizes in Steel 2 have only a single peak. This means that only normal austenite grain growth occurs in conventionally charged Steel 2. The diameters of most austenite grains reheated at 1050°C are between 20 and 60 μm while the diameters of most austenite grains reheated at 1150°C are between 100 and 500 μm. The optical microstructure reheated at 1050°C is shown in **Fig. 4.24.**

The austenite grain growth in Steel 2 is strongly influenced by the reheating temperatures. The effect of reheating temperatures is illustrated in **Figs. 4.18 and 4.21.** When the reheating temperature increased from 1050°C to

1150°C, the average austenite grain sizes increased from about 40~50μm to about 100-150μm.

4.2.3 Steel 3

The average austenite grain sizes in the conventionally charged Steel 3 at 1050°C reheating temperature are much smaller than those in either Steel 1 or Steel 2, being only about 20μm in diameter. **Figs. 4.25~4.27** show the microstructure and relationships between the austenite grain sizes and the reheating times for encapsulated specimens. Like Steel 2, the normal grain growth is indicated by the single peak distribution of its austenite grain sizes.

When the specimens are reheated at 1150°C, significant changes of the austenite grain sizes occur in the different reheating times. The austenite grain growth remains normal in 53 minutes reheating time (**Figs. 4.28~4.30**). The increase of reheating time from 53 min to 318 min leads to the abnormal austenite grain growth (**Figs. 4.28 and 4.29**). A small amount of huge austenite grains (>500 μm) appears. The further increase of reheating time from 318 min to 1333 min results in the recovery of the normal austenite grain growth in the larger grain size (>500 μm). The changes of microstructure for three different reheating times are shown in **Fig. 4.30~4.32.**

4.3 Lath width

4.3.1 Steel 1

4.3.1.1 Before tempering

The ferrite lath width and distribution histogram in Steel 1 are shown in **Figs. 4.33, 4.35, and 4.36**. Differences in the columnar zones and equiaxed zones were observed. In the columnar zones, the lath width values increased following the increases of equalisation time. The average lath widths are about 0.65μm, 0.69μm, 0.88μm, respectively for 53min, 318min, 1333min equalisation times. However, as the standard deviation of these lath width values are 0.4~0.6μm, the lath width for these three equalisation times can be considered to be constant. In the equiaxed zones, the lath widths are almost same for 53min and 1333min equalisation times. However, in 318min equalisation time, the value is much higher, about 1.6μm.

4.3.1.2 After tempering

Figs. 4.34, 4.37, and 4.38 show the effect of tempering on the changes of the ferrite lath width. Tempering can at least double the lath width, compared to the lath width without tempering. The effect in columnar zones is stronger than in equiaxed zones. The lath width in 318min equalisation time has the highest values while the values in 1333min equalisation time are only a slightly higher than that in 53min equalisation time.

4.3.2 Steel 2

Reheated at 1050°C, the increasing rates of the lath width in non-encapsulated and encapsulated Steel 2 specimens are very different (**Fig. 4.39**). As the reheating times increase, the lath widths in the non-encapsulated specimens increased much faster than those in the encapsulated specimens did. The lath widths in encapsulated specimens, about 1μm, are much smaller than those in non-encapsulated specimens, which are about 2.8~4.4μm. The distribution histograms of lath width in both non-encapsulated and encapsulated specimens are shown in **Figs. 4.40 and 4.41.** Most lath widths of encapsulated specimens were located in a single range of 0.6~1.2 μm while most lath widths of non-encapsulated specimens were located in the two ranges of 0~2 μm and 2~4 μm for 53 min reheating time, 2~4 μm and 4~6 μm for 318 min and 1333 min reheating times.

4.3.3 Steel 3

For encapsulated Steel 3 specimens which contain 0.09 wt% titanium, after reheating at 1050°C, the lath widths (between 0.6~0.8 μm) are a little smaller than those of titanium-free Steel 2, under the same conditions (**Fig. 4.42**). Considering the standard deviation of lath width in Steel 3 (**Fig. 4.43**), it can be agreed that the lath widths in these encapsulated specimens are almost constant. The lath widths are mainly located in two ranges: 0.3~0.6 μm and 0.6~0.9 μm.

4.4 Particles

4.4.1 Steel 1

4.4.1.1 Before tempering

After equalisation at 1150°C and water-quenching, several different kinds of particles existed in the microstructure. The particles with the size over 250 nm were almost MnS. They were often found along the austenite grain boundaries. The average particle size, the distribution, and the microstructure were shown in **Figs. 4.44~4.46**.

Many particles (about 40~75nm) were observed by TEM in the microstructure of the steels. An analysis on these particles showed that most were cementite which is considered to form during quenching. Some cuboid particles (>20nm) could be seen in the bainitic lathes and along the lath boundaries when Steel 1 was equalised for 53 min and 318 min. Occasionally larger particles with a size of about 40 nm can be found. EDX analysis indicated that these particles are $(Ti_xV_{1-x})N$ (**Figs. 4.46~4.47**). In 1333 minute equalisation, no vanadium was detected and only a few AlN particles (average size 104nm) (**Fig. 4.48**) and some AlN-MnS can be found (**Fig. 4.49**).

4.4.1.2 After tempering

After tempering, vanadium nitride particles were observed as non-complex particles for 53 minute equalisation. However, when the equalisation times were longer, vanadium nitride can not be found. The complex particles were

found which were the combinations of manganese sulphide/ aluminium nitride and vanadium nitride/aluminium nitride (**Figs. 4.49 and 4.50a**). The diffraction pattern is shown in **Fig. 4.50b**. The plate spacing relation of AlN and VN is $(11\bar{1})_{VN}//(011)_{AlN}$ and the direction relation of AlN and VN is $[101]_{VN}//[31\bar{1}]_{AlN}$ (**Fig. 4.50c**).

4.4.2 Steel 2

It was found that the particles, which exist in the martensite laths after quenching, are mainly aluminium nitrides. **Fig. 4.51** gives the size of the AlN precipitates in the non-encapsulated and encapsulated specimens during the reheating at 1050°C and 1150°C for different times. It is shown that the reheating temperature plays an important role in the particle growth. The increase of the reheating temperature from 1050°C to 1150°C leads to a dramatic increase of particle diameters from about 0.2~0.5 μm to about 0.7~1.0 μm. The size and distribution are shown in **Fig. 4.52~4.53**.

4.4.3 Steel 3

4.4.3.1 Hot direct charging

When Steel 3 was directly charged and equalised at 1100°C for 47 min, in addition to cuboid $(Ti_xV_{1-x})N$ particles (**Fig. 4.54**), many cruciform particles were also found in the microstructure with a average size of 140 nm (**Figs. 4.55~4.56**). EDX analysis showed that ratio of concentration of titanium to vanadium in the core of a cruciform particle is higher, about 7:3 (**Fig. 4.57**),

than that in the arm of the cruciform particle, about 6:4 (**Fig. 4.58**), same as the ratio of these two elements in cuboids.

4.4.3.2 Cast

Many fine $(Ti_xV_{1-x})N$ (2~30 nm) particles were found in the quenched cast slab and most of them were spheroidal (**Fig. 4.59**). Some large cuboids (80 ~ 110 nm) were found as MnS (**Fig. 4.60**). No cruciform particles were found in the cast microstructures.

4.4.3.3 Conventional cold charging

Many $(Ti_xV_{1-x})N$ particles were found in the microstructure of Steel 3 reheated at 1150°C (**Fig. 4.61**). Most of them existed along the ferrite lath boundaries and some were in the ferrite lath. **Figs. 4.62 and 4.63** showed that there was only a slight increase of the average $(Ti_xV_{1-x})N$ particle size from 30nm to 33nm. However, the standard deviation of particle sizes increases as the reheating time increases. When the reheating time increases to 318 min, the larger particles (>60nm) appear.

CHAPTER 5 DISCUSSION

5.1 Solubility temperatures of precipitates in Steel 1~3

5.1.1 Evaluation of solubility temperatures of precipitates

Vanadium, aluminium, titanium, and niobium are the most important alloying elements in microalloyed steels for conferring grain refinement and dispersive strengthening through the formation of carbides, nitrides or carbonitrides. The solution and precipitation of these compounds in commercial steels produce many important effects. However, niobium was not added to Steels 1~3 used in this present research and will not be discussed in the thesis.

AlN particles inhibit austenite grain growth in Al-killed steels (**Cheng *et al.*, 2000**). Solution and precipitation of the carbides and nitrides (or carbonitrides) of V, or Ti in austenite during hot-working can inhibit recrystallisation of the austenite, minimise grain growth of austenite, and add a component of dispersion hardening in ferrite to the strength of the as-rolled steel at room temperature (**Abad et al., 1998**) (**DeArdo, 1998**). Manganese is another important element in microalloyed steels. Solution of MnS during the reheating of austenite at temperatures in excess of 1300°C and subsequent precipitation during cooling produces the phenomenon called overheating (**Hale *et al.*, 1986**). Precipitation or pre-precipitation stages of MnS during annealing of cold-rolled, low-Mn steels for porcelain enamelling

can prevent recrystallisation at all temperatures below that required for transformation to austenite (**Gladman, 1997**).

The general precipitation or dissolution formula can be written in the form of

$$MX \Leftrightarrow M + X \qquad 5.1$$

where *M* represents metals such as Mn, V, Al, Ti, *X* represents C, N, S.

The reaction equilibrium constant, K_P, can be written as

$$K_P = \frac{\alpha_M \alpha_X}{\alpha_{MX}} \qquad 5.2$$

where α_M, α_X are the activity of M, X respectively, $\alpha_M = c_M[M]$, $\alpha_X = c_X[X]$ and the activity of compound MX, α_{MX}, is considered as 1.

$$\left(\ln c_M c_X + \ln[M][X]\right) = -Q/RT + c_8 \qquad 5.3$$

where $[M]$, $[X]$ are the concentration of M and X dissolved in austenite respectively, Q is the heat of dissolution, R is the gas constant, T is the temperature, in Kelvin, at which the dissolution or precipitation in austenite occurs. Since c_M, c_X, and Q are constants, equation 5.3 can be rewritten as following general equation:

$$\lg[M][X] = -\frac{A_3}{T} + B_3 \qquad 5.4$$

where A_3, B_3 are constants.

The determination of the temperature dependence of the solubility of sparingly soluble compounds in austenite is a difficult task. The precipitates

in microalloyed steels are usually less soluble in ferrite than in austenite. Here a term, **solubility temperature**, is used to describe the temperature in the equilibrium condition at which precipitates completely dissolve and are then part of the solid solutions, such as austenite or ferrite.

Many researchers have worked on the determination of solubility temperatures of the precipitates which may appear during the processes. Numerous equations, which are dependent on the specific compositions and working processes of steels employed by the authors, have been developed to calculate the equilibrium solubility of the precipitates. Some equations relevant to the present work are listed in **Table 5.1.** According to the conditions and the equations used, the calculated results of the solubility temperature of precipitates are very different. In the present research, the steels explored are vanadium-microalloyed steels. VN is the most important precipitate in the steels which may affect the final microstructures and mechanical properties, together with vanadium carbide or carbonitride, which have also been cited in the literatures (**Zajac, 1998**) (**Lagneborg, 1999**). It is also well accepted that, at low temperatures (about 900°C), the precipitates must be mainly considered as a carbide while at high temperatures (about 1100°C) as a nitride (**Cabrera *et al.*, 1998**). However, recent research has cast doubt on this view for some process routes and steel compositions (**Wilson, *et al.*, 1988**)

Many equations can be used to calculate the solubility temperature of VN with different steel compositions and processes, and some results have be

obtained from Fe-V-N or Fe-C-V-N alloys (**Frohberg, 1960**)(**Irvine, 1967**)(**Narita, 1975**); others were developed from a much higher carbon content steel than those of the present study (**Erasmus, 1964b**)(**Roberts, 1993**). **Erasmus** also mentioned that his equation was obtained from experiments where the specimens were kept in the furnace for 2 hours at 800°C~1200°C. Undoubtedly, vanadium and nitrogen in the steels are the most important elements to decide the VN solubility temperatures. However, some other elements, such as manganese, aluminium etc., may still have an influence on the solubility of VN.

Irvine (1967) pointed out that the solubility of VN in the austenite depended not only on the temperature, but also on the content of manganese. Adding manganese into HSLA steels would reduce the solubility temperature of VN in austenite. **Gladman (1976)** mentioned that Irvine's equation had to be used for the steels which contained a high manganese content. He also pointed out (**Gladman, 1997**) that reducing the manganese content close to zero would reduce the solubility product at any given temperature by 0.06 and would give even better agreement with the results of Roberts et al. and Narita. The effect of aluminium depends greatly on the compositions of the steels (**Gao *et al.*, 1997**). For 0.1%C and 0.008%N containing steels, virtually all the aluminium is in solution in the austenite. But for higher N contents, aluminium generally causes the concentration of vanadium to increase at the lower austenitising temperature (**Adrian, 1992**), so that the solubility temperature is reduced. Aluminium can remove the nitrogen from

carbonitrides due to its higher affinity to nitrogen. It will result in the easier solution of carbonitrides in austenite (**Eckstein, 1993**). Similarly, for the same quantity of nitrogen in the steels, an increase in the carbon content leads to an increase in the AlN content owing to the larger quantity of vanadium combined with carbon in the C-rich carbonitrides. Aluminium carbides do not form in microalloyed steels.

None of the steels employed to develop the solubility equations have similar compositions to the steels used in the present experiments. However, considering the greater effect of manganese on the solubility of VN, the Eckstein and Irvine equations (Equations VN-7 and VN-8), where high manganese steels were used, are considered to be more suitable than the others. The calculated results for Steel 1 and Steel 2 or 3 show that the solubility temperatures are 1152°C and 1093°C (**Fig. 5.1**) respectively using equations VN-7 and VN-8. Considering that the manganese content in the steel substituted into equation VN-7, is less than that in Steel 1, the solubility temperature of VN in austenite in Steel 1 can certainly be a little lower than 1152°C. This means that when Steel 1 is equalised at 1150°C, as in the present work, VN will be expected to dissolve in austenite and even if some particles are still out of solution, they will be too small to play a role in pinning austenite grain boundaries. Since there are lower vanadium and nitrogen contents in Steel 2 and Steel 3 than in Steel 1, the solubility temperatures of VN are less than those in Steel 1. All the calculated results are below 1150°C

(1038°C~1130°C) (**Fig. 5.2**). The precipitation of VN is expected to be more difficult in Steel 2 in the absence of titanium.

In addition to VN, AlN, TiN, and MnS are three other possible precipitates predicted from the composition of the steels. Their calculated solubility temperatures are much higher than VN, for example, it can be found that the calculated solubility temperatures of AlN, using a similar manganese content to that in Steels 1 to 3, are about 100°C higher than VN (**Figs. 5.3~5.4**). Equation AlN-4 is considered as a suitable equation because the similar composition to the present research was used. That of MnS is about 150°C higher than that of AlN (**Figs. 5.5~5.6**). However, the solubility temperature of TiN is 200 ~ 300°C higher than that of MnS (**Fig. 5.7**), and TiN may precipitate in the liquid steel or during the early stages of solidification (**Narita, 1975**). All these three precipitates will remain undissolved during the processing and may, depending on size and volume fraction, play an important role in pinning austenite grain boundaries. They may also, in certain instances, be the heterogeneous nuclei for the precipitation of VN.

Although vanadium carbide is one of the possible precipitates, it is very difficult for this compound to form in the steels used in the present research and under the present experimental conditions. The calculated solubility temperature of Steel 1, using VC-1 equation, is 824 °C, which is much lower than the equalisation temperature of 1150°C. All the calculated solubility

results of vanadium carbide in Steel 1, Steel 2, and Steel 3 are shown in **Figs. 5.8 ~5.9.**

When vanadium exists in the form of vanadium carbonitride, the solubility temperatures will be higher than for vanadium carbide alone. But, the equalisation temperature is still too high for vanadium carbonitride to exist in austenite. This will be discussed in **5.1.3.**

5.1.2 Equilibrium solubility of VN and AlN in austenite

According to the above discussion, when the steels are kept at a temperature which is equal to or higher than the solubility temperatures of precipitates, there will be no precipitation occurring during the equalisation or reheating stage. However, if the equalisation or reheating temperature of steels is lower than the solubility temperatures, precipitation will occur. **Figs. 5.10~5.11** show calculated solubility limits of VN and AlN at different temperatures using Equations **VN-7** and **AlN-4.** Clearly, if the contents of vanadium, aluminium, and nitrogen in the steels are beyond and on the left of the lines, no precipitation will be expected to occur in the equilibrium status.

It is also understandable that when the precipitation of VN and AlN occurs under equilibrium conditions, the loss of vanadium, aluminium, and nitrogen contents in austenite should be in the stoichiometric relation. So, Equations **VN-7** and **AlN-4** can be rewritten, by considering the partition of vanadium,

aluminium, and nitrogen between VN, AlN, and austenite, following (**Matsuo, 2000**)

$$\log\{([V]_{tot} - [V]_{VN})([N]_{tot} - [N]_{VN})\} = -\frac{7840}{T} + 3.03 \qquad 5.6$$

$$\log\{([Al]_{tot} - [Al]_{AlN})([N]_{tot} - [N]_{AlN})\} = -\frac{7750}{T} + 1.8 \qquad 5.7$$

where:$[V]_{VN}$, $[N]_{VN}$, $[Al]_{AlN}$, and $[N]_{AlN}$ are the contents of vanadium, aluminium, and nitrogen combined as VN and AlN, respectively. $[V]_{tot}$, $[Al]_{tot}$, and $[N]_{tot}$ are the total contents of vanadium, aluminium, and nitrogen in the steel chemical composition, respectively. **Figs. 5.12~5.13** plot the calculated maximum volume fraction of VN or AlN, which precipitate from austenite, in austenite against temperatures for steels that contain different contents of vanadium, aluminium, and nitrogen. There are no significant differences in the precipitation of AlN between the three steels at the different equalisation or reheating temperatures, while the differences in the precipitation of VN are quite obvious. This means that the change of the temperatures can significantly change the precipitation of VN in austenite so that the mechanical properties of the steels will be changed.

5.1.3 About solubility of vanadium carbonitride and the effect of aluminium

Depending on steel composition and temperature, vanadium may precipitate as nitride, carbonitride or carbide. Since the solubility controls the coarsening tendency of precipitated particles, preference should be given to nitrides rather than to carbides, as VN is more capable of maintaining a fine particle

dispersion than VC or a low nitrogen V(C, N). The greater the supersaturation ratio of VN, which determines the driving force, means that vanadium will tend to react first with nitrogen and subsequently with carbon, but only when all the former has been consumed (**Aronsson, 1969**).

The microalloying addition, such as vanadium, in microalloyed steels is very important. Continuing development of microalloyed steels requires the ability to predict the fraction and composition of particles, such as VN, VC, or V(C, N), and of the matrix, for a given microalloying content. To estimate the equilibrium compositions of the austenite and carbonitride phases at different austenitising temperatures, a useful model, which is called the two parameter thermodynamic model, was developed by **Rios (1992)**.

$$f_P = \frac{C_0 + N_0 - C_S - N_S}{1 - 2(C_S + N_S)} \qquad 5.8$$

$$V_S = \frac{V_0}{1 - 2f_P + f_P(C_S / K_{VC} + N_S / K_{VN})} \qquad 5.9$$

$$C_S = \frac{f_C}{(V_0 / K_{VC}) / [1 - 2f_P + f_P(C_S / K_{VC} + N_S / K_{VN})]} \qquad 5.10$$

$$N_S = \frac{f_N}{(V_0 / K_{VN}) / [1 - 2f_P + f_P(C_S / K_{VC} + N_S / K_{VN})]} \qquad 5.11$$

where f_P is the mole fraction of carbonitride, V_0, C_0, N_0 are the atomic fraction of vanadium, carbon, and nitrogen content in steels, V_S, C_S, N_S are the atomic fraction of vanadium, carbon, and nitrogen in solution in austenite, while $K_{VC} = 10^{6.72 - 9500/T}$ and $K_{VN} = 10^{3.03 - 7840/T}$ are the solubility products of vanadium carbide and VN.

Aluminium is also an important microalloying element in microalloyed steels. Because it has the stronger binding force with nitrogen than vanadium, its existence will affect the formation of vanadium carbonitride. To estimate this effect, the modified equations can be used as follows

$$f_{AlN} = Al_0 - Al_S\left[1 - \frac{2(C_0 + N_0 - C_S - N_S)}{1 - 2(C_S + N_S)}\right] \qquad 5.12$$

$$f_P = \frac{C_0 + N_0 - C_S - N_S}{1 - 2(C_S + N_S)} - f_{AlN} \qquad 5.13$$

$$V_S = \frac{V_0}{1 - 2f_P - 2f_{AlN} + f_P(C_S / K_{VC} + N_S / K_{VN})} \qquad 5.14$$

$$C_S = \frac{f_C}{(V_0 / K_{VC}) / [1 - 2f_P - 2f_{AlN} + f_P(C_S / K_{VC} + N_S / K_{VN})]} \qquad 5.15$$

$$N_S = \frac{f_N}{(V_0 / K_{VN}) / [1 - 2f_P - 2f_{AlN} + f_P(C_S / K_{VC} + N_S / K_{VN})]} \qquad 5.16$$

where f_{AlN} is the atomic fraction of aluminium, $Al_S = K_{AlN} / N_S$ is the atomic fraction of aluminium in solution in austenite, and $K_{AlN} = 10^{1.8 - 7750/T}$ is the solubility products of AlN.

A C-language computing program was been designed to do the calculation of above equations (**Appendix A**). The calculated results from both sets of equations for Steel 1 and Steel 2 are shown in **Table 5.2** and **Figs. 5.14~5.17**. It can be found that when the equalisation temperatures of steels are higher than 1000°C, carbon will completely dissolve into the austenite matrix and the precipitates will be VN only, rather than complex vanadium carbonitride. These calculated results match the results from electron

microscopy EDX analysis, where only VN particles were found in equalised, water-quenched, and then tempered Steel 1.

From the calculated results, it is also found that aluminium does not produce significant differences in the solubility of carbon, nitrogen, and vanadium in austenite. This is because of the relatively high vanadium and nitrogen contents in the steels used in present research.

5.1.4 The calculated solubility of VC, VN, AlN, and MnS in Steels 1~3 with or without the effect of Ti using ChemSage

Although many equations describing the dissolution or precipitation of precipitates, such as VC, VN, AlN, or MnS, are available, these equations were developed according to the specific compositions of steels. The change of the steel composition and additional elements will probably lead to a change in the dissolution or precipitation of precipitates. In these circumstances, it is more important to ensure that the calculation is based on the compositions of steels which are used in the present research. ChemSage is commercial software which allows the development of a personal database and undertake the calculation. Using ChemSage and the database built by Corus Group (**Rose, 2002**), some results are shown in **Table 5.3 ~ 5.6** and **Figs. 5.18 ~ 5.21**. The results show some similarity to the calculated data for Steels 1~3 by using Rios Equations (**Table 5.2** and **Figs 5.14~5.17**), in which only nitrides are predicted to appear in the austenitising temperature range and carbides do not form. When the

equalisation temperature is higher than 850°C, carbon will completely dissolve into the austenite. The addition of titanium can greatly increase the solubility temperatures of VN. An addition of 0.005 wt.% Ti to Steel 1 will increase the solubility temperature of VN by about 100°C and it is predicted that the solubility temperature of VN in Steel 3 is almost 400°C higher than that in Steel 2. The addition of Ti slightly decreases the precipitation of AlN and reduces the solubility temperature of AlN by about 50°C but has no influence on the precipitation of MnS. For Steels 2 and 3, when the equalisation temperature is over 1430°C, liquid appears and the dissolution of elements in austenite decreases.

5.2 Precipitation in Steel 1 during the HDC process and tempering

5.2.1 The effect of stripping and water-quenching

The precipitation during the HDC process is determined by the temperature. When the steels were stripped from a mould, the temperatures dropped to 900°C~1000°C before the steels entered an equalisation furnace. Since the solubility of microalloying elements in ferrite is much less than that in austenite and the $\gamma \rightarrow \alpha$ phase transformation will promote the precipitation of the second phase particles, it is very important to ensure whether or not this phase transformation occurs during stripping. The criterion is whether the stripping temperature is greater than the Ac_3 temperature of the steels, which represents the minimum austenitising or solution treatment temperature. Since carbon is present as a principal element, the effect of other elements

could be allowed for on the basis of the Fe-C phase diagram. An equation for calculation of the Ac_3 temperature was derived by **Andrews (1965)**:

$$Ac_3 = 910 - 203\sqrt{C} - 15.2Ni + 44.7Si + 104V + 31.5Mo + 13.1W$$
$$- (30Mn + 11Cr + 20Cu - 700P - 400Al - 120As - 400Ti) \qquad 5.17$$

The calculated result shows that the Ac_3 temperature of Steel 1 is 869°C, lower than the possible lowest temperatures reached during the mould stripping mentioned above. This means that the phase transformation ($\gamma \rightarrow \alpha$) is most unlikely occur during stripping. Therefore, the possible precipitation of TiN, MnS, AlN, and VN discussed here are only related to austenite.

After equalisation, the steel was water-quenched to room temperature. In commercial steelmaking, the cooling rate of the continuously cast steel is not as fast as that due to water-quenching in the lab condition. Carbides, such as cementite, will precipitate in the ferrite matrix during the phase transformation, as in a low carbon microalloyed steel. In this research, the quenched microstructure was observed to be lower bainite and not martensite. This means that most of the carbide particles observed in the microstructure formed during quenching, and not during equalisation or stripping, and therefore, did not play a role in restricting the as-cast austenite grains from growing during the equalisation.

5.2.2 Precipitation during the HDC process

According to calculated solubility temperatures, MnS may be the first precipitate to form in Steel 1 during the processing and will appear during stripping (**Fig. 5.22**). Its solubility temperature can reach as high as 1400°C.

AlN is the other compound which could theoretically precipitate during stripping. However, since the complete precipitation of AlN would take at least 6 hours at about 1100°C (**Gladman, 1993**), AlN will be expected to precipitate to a greater extent during the equalisation treatment. AlN appears in the present work only in the steel ingots equalised at 1150°C for 1333 min, while MnS precipitates appear in the steel ingots for all three equalisation times. In fact, the EDX spectrum analysis shows that some AlN can precipitate with manganese sulphide, which may act as a nucleus for the AlN after 1333 min equalisation time (**Fig. 4.49**). This was also observed by **Li *et al.*** (**2001**).

Vanadium is the most soluble of the currently used microalloying elements and does not readily precipitate in austenite. VN was not found in the microstructures of the specimens which was equalised at 1150°C and water-quenched. A small amount of very fine $(Ti_xV_{1-x})N$ precipitates were found in the specimens equalised for both 53 min and 318 min (**Figs. 4.46~4.47**). Although no titanium was deliberately added into Steel 1, traces of titanium still exist in the steel as observed by **Wilson *et al.*** (**2001**). Titanium can significantly increase the solubility temperature of VN. Its effects will be

discussed later in a separate section. These types of $(Ti_xV_{1-x})N$ particles were found to be bigger and have fewer amount after 1333 min equalisation time. This may be because the titanium content in the steel is so low that the coarsened particles, which are well dispersed on the carbon replicas, were more difficult to find after the longer equalisation time.

5.2.3 The effect of tempering

The equilibrium solubility of vanadium and nitrogen in ferrite at 25°C can be calculated by the **Frohberg (1960)** equation.

$$\lg[V][N] = -\frac{7830}{T} + 2.45 \qquad 5.18$$

The calculated result is $[V][N]=1.54\times10^{-24}$. This means that neither vanadium nor nitrogen will be able to dissolve in ferrite under the equilibrium condition at room temperature. When the steel was water-quenched to room temperature, vanadium remained supersaturated in the ferrite matrix. However, the solute atoms at room temperature have a relatively low activity and do not have enough energy to overcome the nucleation energy barrier. In this case, it is very difficult for them to precipitate. Higher temperatures will provide the activation energy to the solute atoms and promote the precipitation of solute atoms, such as vanadium and nitrogen, from the ferrite matrix. When some previously precipitated particles can act as the heterogeneous nuclei for VN, the precipitation of VN will be much easier. As shown in **Fig. 4.50**, VN precipitates with AlN. When the steel was equalised at 1150°C for 1333 min, AlN has sufficient time to precipitate fully. These AlN particles can become the potential nuclei of VN. The electron diffraction

pattern shows that the orientation relationship of VN and AlN is: $(11\bar{1})_{VN}$ //$(011)_{AlN}$, $[101]_{VN}$ //$[31\bar{1}]_{AlN}$. We can also find that the interplanar spacing of these two planes is very close: $d_{11\bar{1}_{VN}} = 0.2361\,nm$ **(JCPDS-ICDD, 1978a)** and $d_{011_{AlN}} = 0.2371\,nm$ **(JCPDS-ICDD, 1978b)**. No significant lattice deformation is therefore required for their epitaxial relationship.

5.3 The effect of titanium on vanadium precipitation

5.3.1 Direct charging

It is well known that titanium, as a microalloying element, creates important changes in properties and microstructures of the steels through austenite grain refinement by TiN **(Kunishige 1989)**.

For Steel 1, during direct charging, some $(Ti_xV_{1-x})N$ particles were found although a specific titanium analysis was not included in the chemical composition supplied for the present steel, and the level is less than 0.005 wt.% titanium content. As the solubility temperature of $(Ti_xV_{1-x})N$ is as high as 1425°C, it will gradually precipitate on cooling during the process. The fine precipitates (<20 nm) form at the beginning of the process (**Figs. 4.46~4.47**).

As discussed in **5.1**, the solubility temperature of VN in Steel 1 is lower than 1150°C. Therefore it may not precipitate during equalisation at this temperature. However, since both TiN (a=0.42 nm) and VN (a=0.41 nm) **(Leslie, 1981)** have the same crystal structure – face-centred cubic and the

very similar lattice parameters, it becomes possible for VN to use titanium nitride as a nucleation site and form a precipitate $(Ti_xV_{1-x})N$. This can result in the precipitation of a complex vanadium-titanium nitride at relatively high temperatures.

In the early stage of equalisation, the particles will precipitate at sites where the activation energy is higher, such as dislocations, vacancies, and boundaries etc. The growth rate of particles is dependent on the element which has the slowest diffusion rate. The diffusion coefficient, *D*, at any given temperature is defined by

$$D = D_0 \exp(-Q_{diff} / RT) \qquad 5.19$$

where D_0 is a constant, Q_{diff} is the activation energy for diffusion, R is the gas constant and T is the temperature in Kelvin. The data are shown in **Table 5.7.** The calculated results show that titanium is the controlling factor because it has a much lower diffusion coefficient (1.73×10^{-14} m^2s^{-1}) than that of nitrogen ($9.13\times10^{-11}m^2s^{-1}$). More time is required for titanium to diffuse long distances in the austenite matrix. Therefore, $(Ti_xV_{1-x})N$ particles cannot grow fast. When the steel remains at a high temperature for a long time, the coarsening of the precipitates, known as Ostwald ripening, will occur. Some small TiN particles dissolve in the austenite matrix and then the dissolved titanium and nitrogen have plenty of time to travel a long distance in the austenite matrix and reach a larger particle.

Compared with Steel 2, Steel 3 has a similar chemical composition except the addition of titanium. With the addition of 0.009 wt.% Ti, the temperature at which vanadium exists in precipitates increases from 1075°C to 1444°C, 349°C higher, according to the calculation by ChemSage. When Steel 3 ingots were equalised at 1100°C, a large number of $(Ti_xV_{1-x})N$ particles were found in the cuboidal and cruciform shapes in the microstructure. The size of the cruciform particles is much larger than that of the cuboidal ones. The possible nucleation mechanism and the difference between these two types of particles will be discussed in **5.33**.

5.3.2 Conventional cold charging

With the conventional cold charging process route, the precipitation process of $(Ti_xV_{1-x})N$ is different from with the HDC process route. Because of the strong affinity of titanium for nitrogen, the dissolution of titanium nitride becomes almost impossible to achieve during reheating. Furthermore, the cooling to room temperature following continuous casting, and the reheating to 1150°C allows more time for $(Ti_xV_{1-x})N$ to grow. So, more coarse ineffective particles may precipitate after cold charging in comparison to direct charging (**Kaspar, 1994**). In conventionally cold charged Steel 2, no TiN or $(Ti_xV_{1-x})N$ was found at either reheating temperatures and for the three reheating times. This may be the reason for very few large $(Ti_xV_{1-x})N$ particles observed in the microstructures or because the titanium content in the steel

was too low, since the titanium content in Steel 2 is also shown to be less than 0.005%.

But in Steel 3, which contains 0.009% titanium and was also conventionally cold charged, a large number of cuboid $(Ti_xV_{1-x})N$ precipitates were found everywhere, but with a tendency to outline boundaries (**Fig. 5.23**). Many appear in rows. Most of the rows can cover hundreds of microns and are very difficult to follow from the beginning of the row to the end (**Fig. 5.24**). But, some small spheroid-shape rows can still be found in the microstructure (**Fig. 5.25**). Usually, these rows do not follow the austenite grain boundaries after reheating. They may follow the austenite grain boundaries which formed during solidification of the steel or the dendrites.

5.3.3 About cruciform precipitates

With the addition of 0.009 wt.% titanium, many cruciform particles were found in directly hot charged Steel 3. These particles are considered as nucleating and growing during cooling of the as-cast structure (**Prikryl *et al.*, 1996**). The composition of the precipitates nucleated in the austenite is determined by the thermodynamic conditions imposed by the local driving force, the theoretical equilibrium composition, and the diffusivities of solutes (**Zhou, 1991**)(**Zhou, 1992**). Some precipitates having a higher titanium content will nucleate at relatively high temperatures and consequently will have the opportunity to coarsen during cooling into the form of cruciform precipitates with a significant size range. The precipitates forming at lower temperatures

have a higher vanadium content. Because of the paucity of the nucleation sites at all temperatures, it is easier for precipitates to grow from an original Ti-rich core following some preferential planes in the surface of cuboidal particles where the growth rates are obviously higher than other planes. It seems likely that the growth of the arms of cruciform particles on the Ti-rich substrate is epitaxial in nature (**Feng *et al.*, 1989**). All these cruciform particles were found to be rich in both titanium and vanadium and they were reported to be nitrides of the form $(Ti_xV_{1-x})N$ (**Prikryl *et al.*, 1996**) (**Li *et al.*, 2000**). The mixed nitride $(Ti_xV_{1-x})N$ which formed on casting is a metastable phase that evolves to form a stable TiN. On reheating, the $(Ti_xV_{1-x})N$ particles diminish in size due to the dissolution of vanadium. The large difference in the equilibrium solubility of TiN and VN in austenite causes the partitioning of V to austenite, rendering TiN as the stable phase.

When the steel is processed by conventional charging, water-quenching provides a fast reduction in the temperatures of the steel and the Ti-rich cuboidal particles, formed during casting, will not be able to grow. During reheating, the phase transformation leads to the formation of much smaller austenite grains so that more nucleation sites for the precipitation are available on the grain boundaries. This may explain why no cruciform precipitates were found.

5.4 Normal grain growth and abnormal grain growth

It is well known that the structure of a cast slab consists of a thin layer of fine equiaxed austenite grains near the slab surface, a region of columnar grains and a region of coarse equiaxed grains near the slab mid-thickness position (**Crowther, 1997**). For microalloyed steels, the columnar grains and coarse equiaxed grains can be in the range of several hundred microns up to millimetres, because little precipitation occurs during the solidification of the steel to prevent the austenite grain boundaries from moving (**Priestner *et al.*, 1995**). The further equalisation (in direct charging) or cooling and reheating (in cold charging) will produce different grain growth processes, i.e. abnormal or normal, and influence the microstructures.

5.4.1 Direct charging

During stripping, the temperature of steels decreased from 1450~1500°C to 1000~1100°C. In this stage, MnS could precipitate in austenite (**Priestner *et al.*, 1995**) and provide a barrier to prohibit the austenite grains from growing (**Fig. 5.22**). In their research on low carbon manganese steels, **Eissa *et al.*** (**1998**) explained that with up to 1.5% Mn, the increase in Mn contents leads to more nucleation sites, reduces the diffusion rates of carbon and other alloying elements and results in a resistance to the movement of grain boundaries.

In the early time of the equalisation, MnS might be the only precipitate which could be effective to prohibit austenite grain growth due to too few $(Ti_xV_{1-x})N$

precipitates in the austenite matrix in Steel 1 to provide a similar effect. Gladman's equation (**Equation 2.10**) can be used to predict the pinning effect of MnS particles on the austenite grain size. If the sulphur in the steel is considered to combine completely with manganese, according to the data in **Table 5.8**, the calculated f of MnS is 1.039×10^{-4}. The calculated results are listed in **Table 5.9**. The measured average austenite grain sizes are almost equal to the calculated results by using Z =1.6, which is same as Z used in Gladman's paper (**Gladman, *et al.*, 1994**), when the equalisation times are 53 min and 318 min (**Fig. 5.26**). This result shows that MnS could be the main type of pinning particle in the early stage of the solidification.

It is well accepted that austenite grain growth may follow the parabolic law,

$$d^2 - d_o^2 = Kt \qquad 5.20$$

where d is the mean grain diameter at time t, d_o is the initial mean grain diameter and K is a rate constant. The present experimental result taken from **Fig. 4.5** shows that the austenite growth does not follow the parabolic law. Following the relatively fast austenite grain growth in the 53 min and 318 min equalisation times, the average austenite diameter equalised for 1333 min at 1150°C is much lower than the value predicted by **Equation 5.20**. This result indicates that the extra pinning force occurs in the longer equalisation time. Moreover, as the parabolic law uses the average grain diameters, it is unable to be used to identify abnormal grain growth.

In the columnar zone, the austenite grain diameters increase rapidly in the length direction and slowly in the width direction because during the solidification the temperature gradient is steep along the length direction and flatter along the width direction. During this stage, the main control factor for austenite grain growth is not the pinning force from the second particles, but is the temperature gradient. Then, during the equalisation period, columnar grains in the length direction are too big to be pinned by MnS and AlN particles. The radii of columnar grains in the width direction are almost same, so that the grain growth rate is very slow.

Furthermore, the precipitation of AlN takes a long time and it was only found in the microstructure of Steel 1 which was equalised for the longest time (1333 min) at 1150°C. The extra pinning force will build up by AlN to prevent the further growth of austenite grains, especially the smaller austenite grains. In this circumstance, the average diameters of austenite grains increase less than calculated data. This is the reason why the measured austenite grain diameter in 1333 min equalisation time is smaller than the calculated ones by using the Gladman equation (**Table. 5.9 and Fig. 5.26**)

The coarsening of MnS particles in the equalisation furnace would reduce the pinning effect on the austenite grain boundaries and bring about the sudden growth of some austenite grains. In this circumstance, abnormal austenite grain growth was encouraged. As the equalisation time increases, the increase of MnS particle size should result in the increase of austenite grain

size. However, the occurrence of smaller AlN particles (about 104nm) after the long equalisation time, produced the extra pinning force at the austenite grain boundaries and prevented the further significant austenite growth.

To sum up, a map (**Fig. 5.27**) is used to illustrate the precipitates which appear in austenite during equalisation at 1150°C for three different times.

5.4.2 Two attempts to evaluate the detailed and quantified effect of MnS and AlN particles

5.4.2.1 The effect of MnS with the different size groups on the austenite grain size

To evaluate the effect of MnS particles with different diameters, an attempt has been made to categorise the MnS particles into different size groups. A further extension of the Gladman equation has been the size grouping of particles which pin austenite grain up to a critical size. The average MnS particle diameter and volume fraction in each MnS diameter group are shown in the **Table 5.10** and the average measured austenite grain diameters used to calculate the volume fraction in each austenite diameter group are shown in the **Table. 5.11.**

The relationship of the pinning force per unit area of the grain boundary (P) and the second-phase particle size (r) was given by Zener as following

$$P = 3 f\gamma / 2 r \qquad 5.21$$

where γ is the surface energy of the boundary, f is the volume fraction of particles. This equation shows that the pinning force of the grain boundary is proportional to the volume fraction of particles and inversely proportional to the second-phase particle size, given that the surface energy of the boundary remains the same. The smaller the second-phase particle size and higher volume fraction of particles are, the higher the pinning force of the grain boundary is, and thus the smaller the austenite grain size is. Therefore, the size grouping may be a method to help understand which groups of the particle size have the major effect on pinning the austenite grain boundaries.

When the Gladman equation (**Equation 2.10**) is applied to the calculation of the average austenite grain volume fraction in each austenite diameter group, it must be modified and rewritten in the following form:

$$R = \frac{\pi r}{6 \frac{\alpha_{MnS}}{\alpha_{\gamma}} f} \left(\frac{3}{2} - \frac{2}{Z} \right) \qquad 5.22$$

where α_{MnS} is the percentage of MnS volume in each diameter group, α_{γ} is the percentage of austenite volume in each diameter group. As is mentioned above, Z = 1.6 was again considered to be suitable value and obtained from **Fig. 5.26.** The calculated austenite diameters are listed in **Table 5.12.**

It was pointed out (**Gawne, *et al.*, 1971**) (**Humphreys, *et al.*, 1995**) that when the diameters are greater than 0.8 μm, the particles may stimulate the nucleation of new grains. Therefore, considering that MnS particles with a greater diameter of 0.8 μm do not play a role in pinning the austenite grain

boundaries, the comparison between the calculated austenite grains from these MnS particles and the measured austenite grains is not listed in **Table 5.12**. However, the calculated austenite diameters compare well with the measured austenite diameters only for an equalisation time of 53 min and when the MnS particle size is less than 0.6 μm in diameter. Even though the different Z values from 1.0 to 2.0 were considered, the agreement of the measured austenite grain size with the calculated austenite grain size are still not satisfied in the longer equalisation times of 53 min and 1333 min. The reason could be due to the abnormal grain growth.

Comparing the distribution of MnS particle size (**Fig. 4.45**) and the equiaxed austenite grain size (**Fig. 4.15**), it can be found that when the steel was equalised for 53 min, the amount of coarse MnS particles with a size greater than 0.8 μm is only 2%. When the steel was equalised for 318 min and 1333 min, larger numbers of coarse MnS particles (> 0.8 μm) were observed. The percentages are 16% and 30%, respectively. In this circumstance, these particles will not play a role in pinning the austenite grains. The above analysis could be used to explain why the fitting extent in 53 min equalisation time is much better than those in 318 min and 1333 min equalisation times.

When the equalisation time is 1333 min, no MnS particles in the size smaller than 0.2 μm were observed which could pin the smaller austenite grains (<0.3 mm). Therefore, these smaller austenite grains in the microstructure could be pinned by AlN particles (**Fig. 4.49**) whose size is less than 0.2 μm.

These AlN particles were observed after 1333 min but, because of their slower precipitation kinetics, were not expected and indeed not observed after the shorter equalisation times.

5.4.2.2 The effect of MnS and AlN on the austenite grain size by using Gladman model

Gladman and Li (1994) explained the effect of mixtures of particles, such as oxides, sulphides, and nitrides, on austenite grain refinement. Separate *f/r* for TiO_2, MnS, and TiN were summarised linearly to give a value which was used to calculate the hypothetical pinned austenite grain size. An equation was given as follows:

$$R_G' = \frac{(1 - 4/3Z)}{\sum (f_i / r_i)} \qquad 5.23$$

where R_G' is the radius of austenite grains, f_i is the volume fraction of particle i, r_i is the radius of particle i, Z is same as the one used in **Equation 2.10**. However, the agreement between calculated and experimental data was not entirely satisfactory because of the onset of abnormal grain growth.

For the present work, there are two types of particles, MnS and AlN, and adopting the approach of **Gladman and Li (1994)**, the equation can be written as following

$$R_G' = \frac{(1 - 4/3Z)}{f_{MnS}/r_{MnS} + f_{AlN}/r_{AlN}} \qquad 5.24$$

where f_{AlN} is the volume fraction of AlN particles, r_{AlN} is the radius of AlN particles, f_{MnS} is the volume fraction of MnS particles, r_{MnS} is the radius of MnS particles. Data for MnS and AlN particles observed after 1333 min equalisation time have been calculated. It has been calculated (**Appendix 2**) that $f_{MnS} = 1.04\times10^{-4}$, $f_{AlN} = 9.78\times10^{-4}$, $r_{MnS} = 0.75$ μm, $r_{AlN} = 0.1$ μm, and using $Z = 1.6$, then $R_G' = 16.8$ μm. The calculated R_G' by **Equation 5.23** is much smaller than the measured austenite grain diameter (710 μm). The problem is that in **Equation 5.23**, two types of particles are supposed to take effect in the early stage of the austenite grain growth when the austenite grains are small. Actually, in the present research, before AlN takes effect, the austenite grain size is already very big (670 μm) when the steel is equalised for 318 min. In this circumstance, the main effect of AlN is to prevent the further growth of the small austenite grains. Therefore, this equation is unsuitable in the present work to calculate the effect of two types of particles on pinning austenite grains.

5.4.3 Conventional cold charging

After stripping, Steel 2 was water-quenched to the room temperature. A bainitic microstructure was obtained that involved a $\gamma\rightarrow\alpha$ phase transformation. **Militzer (1996)**, and **Enomoto & Aaronson (1986)** investigated ferrite nucleation at austenite grain boundaries and found that ferrite nucleation occurs only at a few preferred sites at the boundary, i.e., at grain corners or in the areas with a favourable crystallographic orientation. For small austenite grain size and slow cooling rate, only nucleation at grain

corners occurs. However, with increasing cooling rates, and/or with increasing austenite grain sizes, early growth of these nuclei has to be considered and the transformation start temperature decreases. The associated increase in undercooling encourages ferrite nucleation at the remaining sites of the austenite boundary. Furthermore, the austenite decomposition can be inhibited by adding Mn, with the delay being more pronounced at higher temperatures. The fine MnS particles precipitated during cooling could also prevent ferrite grains from growing.

When the steel was reheated, a reverse phase transformation of $\alpha \rightarrow \gamma$ occurs which could result in the further reduction of the austenite grain size. The nucleation of austenite at some preferential sites, where the activation energy is higher, such as the ferrite boundaries, areas of high-densities of dislocations, and inclusions (>0.8μm), etc., could result in the reduction of the average austenite grain size. These smaller austenite grains provide more preferential sites for the nucleation of AlN and avoid the longer migration of Al atoms and N atoms. Therefore the precipitation rate of AlN increased. Many AlN particles were found after all the three different reheating times at both 1050°C and 1150°C (**Figs. 5.28~5.30**).

After comparing the modified equations based on the Zener equation, it was clarified by **Gao et al. (1998)** that the Gladman and Rios equations were fairly close to the experimental results of V-microalloyed steels. Using both the Gladman (**Equation 2.10**) and Rios equations (**Equation 2.13**), the

calculated volume fractions of AlN, f, are shown in **Table 5.13**. Compared with the volume fraction calculated from the aluminium and nitrogen contents in Steel 2, these values are very close. This result can be considered to confirm that the austenite grain growth, in this case, is controlled mainly by AlN precipitates. During reheating it is the pinning effect of AlN, not manganese sulphide, that prevents the austenite from growing. Under these conditions, the austenite grain growth is normal.

When 0.009% titanium was added as in Steel 3, a large number of $(Ti_xV_{1-x})N$ particles precipitated during reheating. They become a dominant factor in pinning austenite because titanium has a stronger tendency to combine with nitrogen than most other elements. Most of the nitrogen in Steel 3 will be consumed by titanium instead of aluminium. The stronger pinning effect of TiN or $(Ti_xV_{1-x})N$ (**Tamehiro *et al.*, 1985**) results in the smaller austenite grains, which are about 20 μm smaller than those in Steel 2.

The calculated results are shown in **Table 5.6**. For Steel 3, the compositions of $(Ti_xV_{1-x})N$ particles are different with the change of reheating temperatures. x is 0.46 at 1050°C and 0.62 at 1150°C. The weight percentage of VN in $(Ti_xV_{1-x})N$ decreases by almost 50%. The increase of the x value and the reduction of VN show that much more vanadium will go into the solution as the holding temperature increases. In the present work, the temperature at which vanadium exists in the form of a precipitate is

dramatically increased by nearly 400°C from 1050°C in Steel 2 to 1425°C in Steel 3.

The addition of Ti not only affects the precipitation of V, but also the precipitation of Al. In Steel 2, the solubility temperature of AlN is 1300°C. When 0.009% Ti is added to the steel, the solubility temperature of AlN decreases to 1250°C. Furthermore, as some nitrogen combines with Ti and V, there is less nitrogen available for the formation of AlN. Therefore, when the steels are held at 1050°C and 1150°C, the amount of AlN precipitates also decreases from 0.028 wt.% and 0.019 wt.% to 0.020 wt.% and 0.013 wt.%, respectively.

A higher reheating temperature of 1150°C, increases the growth rates of both the $(Ti_xV_{1-x})N$ precipitates and the austenite grains. Even though the particle diameters did not show obvious differences in average values, the distribution of the particle size displayed significant coarsening, more than three times the average values, of a small number of particles, about 5%. The coarsening of these precipitates, which represent a significant volume fraction, will greatly reduce the local pinning force on the austenite grains. When the steel is reheated at such a high temperature for a long time, 318 min in the present experiment, some particles will coarsen to about the critical pinning diameter. In this situation, the pinning force on the austenite grain boundary will significantly decrease in some sites and a few austenite grains in these sites will grow much faster than other surrounding austenite

grains. This abnormal grain growth can only cease when the smaller grains are consumed and the big grains meet each other. So, another normal growth of austenite grains, in millimetres in diameter, can be seen in the 1333 min reheating specimens.

When the steel was reheated at 1150°C, it was found that vanadium could only precipitate with titanium. EDX analysis showed that the atomic ratio of titanium to vanadium in stoichiometric $(Ti_xV_{1-x})N$ is about 6:4, i.e. x=0.6. This result is consistent with the calculated result by using ChemSage and means that after combining with titanium and vanadium, there was about 0.013% nitrogen remaining in Steel 3 which was available to form AlN. A few large AlN particles can still be seen (**Fig. 5.31**), especially in the 318 min and 1333 min reheating microstructures.

5.5 Microstructure

5.5.1 Direct charging

In the present experiment, the cooling rate of 10 kg ingots of the Steel 1 should be much slower than that of the specimens with a smaller size heated in the laboratory simulation process, and a bainitic microstructure instead of martensitic one in this type of low carbon microalloyed steel is expected after the equalisation and water-quenching process.

The bainite transformation is considered as an incomplete reaction process, which indicates that the growth of bainitic ferrite is diffusionless, with any

excess carbon being rejected into the residual austenite subsequent to transformation. It is generally accepted that there is no long-range redistribution of substitutional alloying elements during the growth of bainitic ferrite in steels (**Stark *et al.*, 1990**). The bainitic microstructure is developed by the sympathetic nucleation of laths or plates of bainite within each austenite grain, and forms by a diffusion controlled shear process. The sympathetic nucleation process leads to the formation of 'packets' of laths, each lath being separated, within an packet, by a low angle boundary (**Pickering, 1967**). Several such packets may be formed within an austenite grain, depending upon the active variant of the orientation relationship between the austenite and bainitic ferrite, thereby providing a high angle boundary between the packets of bainitic ferrite. The basic structure of bainite thus consists of high angle boundaries between the laths in each bainitic ferrite (**Gladman, 1997**).

It is well accepted that the initial nucleation event is almost always confined to the austenite grain boundaries which presumably contain the most potent defects for nucleation, and intragranular nucleation of bainite can essentially be ignored (**Bhadeshia, 1992**). In the present experiment, the longer equalisation time can lead to the migration of defects, such as dislocations. Then a decrease of dislocation density will be caused by the annihilation and rearrangement of the dislocations (**Humphreys *et al.*, 1995**). In this situation, the nucleation sites of bainitic ferrite will decrease as the equalisation time increases. This can reduce the possibility of bainitic ferrite nucleation on the

austenite grain boundaries, leaving more spaces for the growth of bainitic ferrite, and resulting in a larger bainitic ferrite lath width. When the equalisation time increases further (in present case, to 1333 min), the austenite grains do not increase significantly. The coarsening of some second particles, e.g. manganese sulphide, can be still occurring. These non-metallic particles can also act as nucleation surfaces for the bainitic ferrite (**Bhadeshia, 1992**) and provide extra sites for the nucleation of bainitic ferrite laths. This may be the reason that the bainitic ferrite lath width increases at first and then decreases.

In the present work, the change of the lath width with equalisation times in the columnar zone is similar to that in the equiaxed zone. But the lath width in the equiaxed zone of the steel equalised for 318 min is wider than that in the columnar zone. This may be because the cooling rate in the centre of steel is lower.

Tempering a bainitic microstructure can double the lath width. However, in the microstructure of the steel equalised at 1150°C for 1333 min, tempering does not lead to any obvious change of the bainitic ferrite lath width. This may reveal a difference in the bainitic ferrite between (a) 53 and 318 min and (b)1333 min, in equalisation times.

5.5.2 Simulated conventional cold charging

For the simulated conventional cold charging process, the steels were quenched after reheating. The cooling rates are very high (greater than 200°C/s) because the specimens used in laboratory were very small. The microstructures are mainly martensitic, and the martensite lath width will be decided by different conditions.

5.5.2.1 Cooling rate

For Steel 2 in the present experiments, two different specimen sizes were used. The specimens in the non-encapsulated condition were five times thicker than those which were encapsulated. Also, non-encapsulated specimens can form a thick oxide layer after reheating because they were not isolated from oxygen. This oxide layer can act as a thermal barrier to reduce the heat loss. So, the cooling rate of the non-encapsulated specimens was about half that of encapsulated specimens. As the lath width of the martensite is more affected by cooling rate, a decrease of the lath width is obtained as the cooling rate increases. This result is also consistent with that reported by **Schreder (1976)**.

The cooling rate also affects the change of martensite lath width following the change of reheating times. When the cooling rate of the specimens was very high (about 600~700°C/s), this becomes the dominant factor which decides the martensite lath width. There are no obvious changes in the martenisite lath width observed in the present work when the reheating times increase.

5.5.2.2 Reheating temperature

As mentioned in **5.4**, the higher reheating temperatures can increase the austenite grain size which then produce fewer grain boundaries and defects in the microstructure available to produce the nucleation sites for the formation of martensite. This will lead to an increase of martensite lath width.

5.6 Strengthening

5.6.1 Direct charging of Steel 1

It has long been recognised that the influence of bainite on the mechanical behaviour of a steel is difficult to understand because of the inability to attain fully bainitic microstructures at all transformation temperatures, a consequence of the incomplete reaction phenomenon (**Hehemann *et al.*, 1957**). Isothermal transformation to bainite was considered impractical on a commercial scale, continuous cooling from austenitising temperature being the preferred heat-treatment.

The strength of bainite can in principle be factorised into components consisting of the intrinsic strength of pure annealed iron, substitutional solid solution, strengthening due to carbon in solid solution, and a variety of microstructural components including dislocation strengthening, particle effects and grain size effects (**Bhadeshia, 1992**).

This is not unexpected, given that the bainitic ferrite laths exert an overriding influence on strength, since they are much smaller than the austenite grain size. **Kamada, *et al.* (1976)** also found that the hardness of bainite is independent of the austenite grain size, even though the latter influences the bainite sheaf thickness.

This explains why the change of hardness values of Steel 1, equalised for three different times, follows the change of lath width values and does not follow the change of austenite grain sizes. This result is consistent with the observation that the hardness of fully bainitic microstructures is not sensitive to the austenitising temperature **(Irvine *et al.*, 1965) (Kamada *et al.*, 1976)**.

Using **Equation AlN-4**, the calculated weight of aluminium and nitrogen in solution in austenite at 1150°C is 0.0324 wt.% and 0.007 wt.%, respectively. This means that more than half of the aluminium and two thirds of the nitrogen in Steel 1 will be able to precipitate during the equalisation if equilibrium conditions are reached. The rest will remain in solution and lead to solid solution strengthening. However, it will take a relatively long time for aluminium and nitrogen to reach the equilibrium precipitation conditions **(Gladman, 1997)**, therefore, it is necessary that the steels remain in the equalisation furnace for a relatively long time for the precipitation of AlN.

As is discussed in the early parts of this Chapter, the increase of the equalisation time not only increases the ferrite lath width, but also promotes

the precipitation of AlN in austenite, which will reduce the supersaturation of aluminium in ferrite by two ways. The first way is to reduce the supersaturation of aluminium and nitrogen in austenite. The second way is to promote the further precipitation of AlN during cooling through the growth of AlN instead of the nucleation and growth of AlN. In this circumstance, the hardness of the steel decreases at the beginning of the equalisation (at times of less than 318 min). When the precipitation of AlN reaches equilibrium, the aluminium and nitrogen content in austenite remain constant. So, when the equalisation time increases further (more than 318 min), the hardness of the steel increases a little following the decrease of ferrite lath width during the time interval from 318 min to 1333 min (**Figs. 4.2 and 4.33**).

Tempering usually provides two reverse effects on the hardness of the quenched microstructure in Steel 1. First, the reduction of the supersaturation of vanadium and aluminium in bainitic ferrite and the increase of the carbide size and bainitic ferrite lath widths lead to a decrease of the hardness. But, in another way, the occurrence of fine VN and AlN particles strengthen the steel through dispersion strengthening mechanism and increase its hardness. So, the effect of tempering on the change of hardness is complex. The bainitic ferrite lath width cannot be considered as the only factor which influences the change of hardness of the steel, even though it is considered to be a very important factor. The precipitation of nitrides also contributes a share to the change of the hardness.

5.6.2 Conventional cold charging of Steel 2 and Steel 3

During conventional cold charging process, the cast steel was cooled to room temperature and reheated. After reheating it was water-quenched to examine the microstructures. In the present work, the samples used in the cold charging were much smaller than those in the direct charging. The reheating (austenitizing or solution) temperature was chosen to take carbides and nitrides which have precipitated during cooling from the casting processes into solid solution, and the required temperature can be calculated from the data given in **Table 5.1.**

Cooling rapidly into water from the reheating temperature results in the carbon and nitrogen, which have dissolved in austenite, being held in interstitial solid solution at room temperature. In addition, the equilibrium room temperature phase, ferrite, does not form, as the austenite/ferrite phase transformation is suppressed and a shear transformation to a distorted body centred tetragonal structure, called martensite occurs. At the lower carbon levels encountered in microalloyed steels (typically less than 0.15%C), the martensite is body-centred cubic in structure and usually comprises units which are lath shaped (**Baker, 1978**).

In Steel 2, the decrease of the hardness in both encapsulated and non-encapsulated specimens follows the increase of the lath width. Considering *d* as the martensite lath width because the lath width values, here, are much smaller than the austenite grain size values, this result complies with the

Hall-Petch equation (**Equation 2.1**) mentioned in Chapter 2. When equalised at 1150°C, the steel is slightly harder than at 1050°C. It is considered that at the higher equalisation temperature, there occurs a greater dissolution of precipitates in austenite.

When Steel 3 is reheated at 1050°C, it was observed that the lath width does not reduce significantly, and especially after 318 min equalisation, the lath width is almost constant. In this case, the hardness values of the steel in this condition do not have a noticeable reduction. However, in Steel 3, as abnormal grain growth occurs when reheated at 1150°C, the hardness has a significant decline after 318 min reheating time.

The results also show that the hardness values of the encapsulated specimens are much higher than those of the non-encapsulated specimens. When the specimens were water-quenched, the cooling rate of the encapsulated specimens was higher than the non-encapsulated specimens because of the larger specimen sizes. It is well understandable that the higher cooling rate can significantly decrease the martensite lath width (**Fig. 4.33**). This result is consistent with Naylor's result (**Naylor, 1976**).

5.6.3 Oxidation in the non-encapsulated specimens

When the specimens are reheated in air, their oxidation is inevitable. To estimate the diffusion distance, x, of oxygen in the steel, the equation given by **Swisher (1967)** can be used,

$$\log D = -\frac{8820}{T} + 0.76 \qquad 5.25$$

where D is diffusion coefficient, T is absolute temperature. Then starting with a constant composition of oxygen at the surface, the value of x, where the concentration falls to half the initial value is given by $x = \sqrt{Dt}$ **(Smallman, 1985)**, Thus knowing D at 1150°C and the reheating time, t, the depth of diffusion can be estimated. The calculated results show that when the reheating time are 53 min, 318 min, and 1333 min, the depth of diffusion of oxygen in the steel are 1.1 mm, 2.6 mm, and 5.4 mm, respectively. Therefore, even in the steel reheated at 1150°C for 1333 min, oxygen does not have enough time to diffuse to the centre of non-encapsulated specimens. The hardness values in the central part of the non-encapsulated specimens are therefore not affected by the oxidation. This is also the case in the encapsulated specimens where the experimental results showed a similar trend in the hardness values.

5.7 The expectation of the austenite grain growth control in specimens which have undergone the HDC process

Using Equations VN-4 and VN-5, for Steel 1, it is predicted that neither VN nor vanadium carbide will precipitate during equalisation at 1150°C. Only a small amount of fine vanadium titanium nitride, where the titanium to vanadium ratio is from 5:5 to 6:4, can be found in the austenite microstructure. However, this type of nitride does not play a great role in

pinning austenite grains because the amount of titanium in Steel 1 is very small and the volume fraction is therefore also small.

It is considered practically impossible to prevent the occurrence of large austenite grains by using only vanadium as a grain refining element. During the casting, the solidification temperature is as high as 1450~1500°C. The growth rate of austenite grains at such a high temperature can be much higher than that at the lower temperatures, such as at 1000~1150°C (**Gladman, 1997**). As was discussed above, in the solidification temperature range, only titanium nitride and MnS can precipitate and retard the move of the austenite grain boundaries. If VN is required to play the same role, then according to **Equation VN-4**, more than 2 wt.% vanadium is needed in the steel, since the nitrogen content in the steel is normally less than 0.022 wt.%. Such a content of vanadium is far too high for a microalloyed steel.

MnS can be used to provide a pinning effect on the austenite grain growth during the solidification of the steel. 1~2 wt.% manganese is usually present in a microalloyed steel. To use all the manganese in the form of sulphides, about 0.9 wt.% sulphur would be required in the steel. Actually, there is only between 0.01 wt.% to 0.2 wt.% sulphur in the microalloyed steels. Manganese is greatly excess for the formation of sulphide. So, an increase of sulphur content in the steel can result in the increase of the MnS precipitates. However, lower sulphur steels usually produce smaller inclusions in a given cooling/solidification rate, whereas high sulphur steels have a reverse effect

(**Gladman, 1997**). However, a further increase in the volume fraction of sulphides in the steels will result in the formation of bigger inclusions and may not produce the expected increase of pinning force.

Titanium nitride is another type of the precipitate which can act as a strong pinning particle for decreasing austenite grain growth. Since titanium nitride precipitation can occur at a very high temperature, and nucleate even in the molten steel, these particles will be able to retard the growth of grains in both the δ- and the γ-phases and increase the nucleation sites for the δ→γ transformation. A titanium addition to the steel can also promote the precipitation of VN at a higher temperature which will create further pinning forces opposing the austenite grain growth. All these effects from titanium nitride can result in much smaller austenite grain size.

However, although titanium nitride can provide the pinning force for retarding the austenite grain growth and reduce the austenite grain size, it may lose this pinning effect if it is present at a high temperature for a long time. In this circumstance, an abnormal austenite grain growth will occur.

The solubility temperature of AlN is a little higher than that of VN, but much lower than the solidification temperatures of the steel. AlN precipitation occurs only during equalisation. As the kinetic process for the AlN precipitation is quite slow during the equalisation (**Gladman, 1997**), this

compound is helpful to prevent the austenite grains from growing if the steel is held in the furnace for a longer time, for example over 10 hours.

From the above discussion, it can be understood that it is very difficult to get a small austenite grain size (~100 μm) during solidification and equalisation through a direct charging process. In certain instances, titanium nitride and MnS can retard the austenite grain growth during solidification. VN and AlN do not play great role on the pinning austenite grain boundaries during solidification and stripping. But, it is possible for them to precipitate from the austenite matrix and to act as the pinning particles to retard the further growth of austenite grains when the steel is held in the furnace for a long time.

CHAPTER 6 CONCLUSIONS

In the study of low carbon and high nitrogen V- and V-Ti-microalloyed steels in the simulated direct charging of the TSDR process and cold charging of the CCR process, the following conclusions can be reached:

1 The equations created in the binary alloys provided good tools for estimating the precipitation of carbides, nitrides, carbonitrides, and sulphides. However, the use of thermodynamics analysis software such as ChemSage is more helpful for doing the detailed analysis. It can be used with the complete composition of the steels to improve the understanding of microstructural evolution under equilibrium conditions.

2 Among the equations modified from the Zener Equation, those derived by Gladman and Rios are suitable for use to predict the austenite grain growth in microalloyed steels in both the direct charging and the cold charging.

3 At shorter equalisation times of 53 min and 318 min at 1150°C, the austenite grain growth of V-microalloyed steels in the direct charging is controlled by the pinning effect of MnS particles precipitated during the stripping of the ingots from the mould. The grain growth is usually abnormal because the enlarged MnS particles do not provide a strong pinning effect on the austenite grain growth.

4 The gradual precipitation of AlN particles, when the steel was equalised for longer than 318 min, produces the extra pinning force for the smallest of grains and is the main factor which prevents the further growth of the smallest austenite grains after 1333 min equalisation time. Therefore, there is only a slight increase of the austenite grain growth of V-microalloyed steels when the equalisation time increases from 318 min to 1333 min.

5 VN does not precipitate during equalisation at 1150°C and it will remain supersaturated in bainite after water-quenching. Tempering can promote the precipitation of VN when AlN acts as a nucleus for VN precipitation.

6 When MnS particles are categorised into different size groups, the calculated and measured austenite grain size have a more satisfactory agreement after 53 min equalisation time than after 318 min and 1333 min equalisation times. This is because of the weak pinning force on the movement of austenite grain boundaries from the larger MnS particles (>0.8μm), which are present but in small numbers after 53 min equalisation time.

7 The cruciform $(Ti_xV_{1-x})N$ precipitates occur in the directly charged Ti-V-microalloyed steels but do not occur in the reheated Ti-V-microalloyed steels. This is considered to be due to the preferential growth directions of

$(Ti_xV_{1-x})N$ precipitates because only a few nucleation sites for $(Ti_xV_{1-x})N$ are available in the austenite grain and/or grain boundaries during the equalisation stage.

8 The austenite grain growth of V-microalloyed steels in the cold charging is well controlled by the pinning effect of AlN particles. When reheated at 1050°C and 1150°C, AlN particles remain effective in pinning austenite grain boundaries. The austenite grain growth is normal. In this case MnS particles are too large to play a major pinning role.

9 With the cold charging, the addition of Ti to V-microalloyed steels results in the formation of fine austenite grains during reheating at 1050°C due to a stronger pinning effect from the fine $(Ti_xV_{1-x})N$ particles. However, abnormal austenite grain growth will occur at 1150°C when this type of steels remains in the furnace for more than 53 min.

10 From a practical perspective, in the present work, it can be concluded that a delay in the rolling or coiling of the TSDR process, which results in significantly longer equalisation time, has no major effect on the austenite grain size in the V-microalloyed steel but will lead to the complete precipitation of AlN prior to rolling. The latter factor should have a beneficial effect on he properties of the final products.

REFERENCES

Abad R., López B., Gutierrez I., *Materials Science Forum*, **284-286**(1998), 167

Adrian H., Pickering F.B., *Mater. Sci. Technol.*, **7**(1991), 176

Andrews, K.W., *J. Iron Steel Inst. Japan*, **203**(1965), 721

Ardell A.J., *Acta Metall.*, **20**(1972), 601

Baker T.N., *Science Progress*, **65**(1978), 508

Banks K., Koursaris A., Verdoorn F., Tuling A., *Mater. Sci. Technol.*, **17**(2001), 1596

Brozzo P., Buzzichelli G., Mascanzoni A., Mirabile M., *Metal Science*, **11**(1977), 123

Burke, J.E., *Trans. Metall. Soc. A.I.M.E.*, **180**(1949), 73

Burke, J.E., Turnbull D., *Prog. Metal Phys.* , **3**(1952), 220

Cabrera J.M., Al Omar A., Prado J.M., *Jour. Mater. Sci.*, **31**(1996), 1303

Cabrera J.M., Omar A.A., Prado J.M., *Z. Metallkd*. **89**(1998), 47

Carney D.J., *Trans. ASM*, **46**(1954), 882

Chen Z., loretto M.H., Cochrane R.C., *Mater. Sci. Tech.*, **3**(1987), 836

Cheng L.M., Hawbolt E.B., Meadowcroft T.R., *Canadian Metall.* Quarterly, **39**(2000), 73

Cracknell A., Petch N.J., *Acta Met.* **3**(1955), 186

Crowther D.N., Mitchell P.S., Morrison W.B., *Proc. 39th MWSP Conf.*, 1997 Indianapolis, 112

DeArdo A.J. *Materials Science Forum*, **284-286**(1998), 15

Drian A., *Mat. Sci. Tech.*, **8**(1993), 406

Dunn C.G., and Walter J.L., *Recrystallization, grain growth and Textures.* ASM, Ohio, 1966, 461

Eckstein,H.J., Fennert,M., Ohser, J., *Steel Research*, **64** (1993), 143

Edington J., *Ironmaking and Steelmaking*, 24(1997), 23

Eissa M., El-Fawakhry K., Mekkawy M., Hussein A.H., Tawfik A., *Steel Research*, **69**(1998), 334

Elst R., Humbeeck J.V., and Delaey L., *Acta Metall.*, **36**(1988), 1733

Enomoto, M., Aaronson, H.I., *Metall. Trans. A*, **17A**(1986), 1381

Erasmus, L.A., *J.Iron Steel Inst. Japan,* **202**(1964), 32

Erasmus, L.A., *J.Iron Steel Inst. Japan,* **202**(1964), 128

Essadiqi E., Collins L.E., Ruddle G.E., *Proc. of Met. Soc. Can. Inst. Mining, Metall. 34th Ann. Conf.* 1995, 341

Feng B., Chandra T., Dunne D.P., *Materials Forum*, **13**(1989), 139

Feppon J.M., Hutchinson W.B., *Acta Materialia,* **50**(2002), 3293

Flemming G., Hofmann F., Rohde W., Rosenthal D., *Metallurgical Plant and Technology International* 2, 1993, 84

Flores O., Martinez L., *Jour. Mater. Sci.*, **32**(1997), 5985

Frawley L.D., Priestner R., *Materials Science Forum*, **284-286**(1998), 485

Frohberg, M.G., *Stahl und Eisen*, **80**(1960), 539

Gao N., Baker T.N., *ISIJ International*, **39**(1998), 744

Gao N., Baker T.N., *The Metallurgical Industry Press*, 2000, 187

Gawne, D.T. and Higgins, R.A., *J. Mats. Sci.*, **6**(1971), 403

Garbarz B., Pickering E.B., *Mater. Sci. Tech.*, **2**(1986), 1106

Gibbs P.K., Peterson R., Parker B.A., *Proc. Conf. of Microstructures and Properties of Microalloyed Steels,* 1992, 201

Gladman T., *Proc. Roy.Soc.*, **294A**(1966), 298

Gladman T., Pickering F.B., *I.S.I.J.*, **205**(1967), 653

Gladman T., Li Q., *35th MWSP Conf. Proc.* ISS-AIME, **31**(1994), 453

Gladman T., *Physical Metallurgy of Microalloyed Steels*, The Institute of Materials, 1997

Goodenow R.H., *Trans. ASM*, **59**(1966), 804

Grossmann M.A., *Trans. AIME*, **150**(1942), 227

Hale G., Preston S., Nutting J., *Mater. Sci. Tech.*, **2**(1986), 571

Hall E.O., *Proc. Phys. Soc.*, **B64**(1951), 747

Hall D., Bennet G.H.J., *I.S.I.J.*, **205**(1967), 309

Hehemann R.F., Luhan V.J., Troiano A.R., *Trans. ASM.*, **49**(1957), 409

Hellman P., *Scan. J. Met.*, 4(1975), 211

Heslop J., and Petch N.J., *Phil. Mag.*, **3**(1958), 1128

Hillert M., *Acta Metall.*, **13**(1965), 227

Hillert M., *Acta Metall.*, **36**(1988), 1377

Honer, K.E., Baliktay, S., in '*Proc. 44th Int. Foundry Cong.*', Florence,

Honeycombe R.W.K., Bhadeshia H.K.D.H., *Steels*, Arnold, 1995

Houdremont, E. and Schrader, H. *Stahl und Eisen*, **56**(1936), 1412

Humphreys F.J., Hatherly M., *Recrystallization and Related Annealing Phenomena,* Pergmon, 1998, 283

Ikegami K., Yasunaga S., *AIIE-Transactions*, **13**(1981), 164

Irvine K.J., Pickering F.B., *J.Iron Steel Inst.*, **201**(1963), 944

Irvine,K.J., *J.Iron Steel Inst.,* **205**(1967), 106

Irvine K.J., Pickering F.B., Gladman T., *J.Iron Steel Inst.,* **205**(1967), 161

JCPDS-ICDD File Card No 25-1133, Selected Powder Diffraction Data, 1601, Park Lane, Swarthmore. Penn. 19801, USA, 1978

JCPDS-ICDD File Card No 25-1252, Selected Powder Diffraction Data, 1601, Park Lane, Swarthmore. Penn. 19801, USA, 1978

Jominy W.E., Boegehold A.L., *Trans. ASM*, **26**(1938), 574

Kaspar R., Zentara N., Herman J.C., *Steel Research,* **65**(1994), 279

Kirk-Othmer Encyclopedia of Chemical Technology, **1991**

Konig P., Scholz W., Ulmer H., *Archs Eisenhutt*, **32**(1961), 541

Koo J.B., Yoon D.Y., *Metall. Mater. Trans. A*. **32A**(2001), 1911

Kronberg M.L., Wilson F.H., *Trans. TMS-AIME*, **185**(1949), 501

Kunishige K., Nagao N., *I.S.I.J.*, **25**(1985), 315

Kunishige K., *ISIJ International*, **29**(1989), 940

Lagneborg R., Siwecki T., Zajac S., Hutchinson B., *Scand. Jour. Metall.,* 28(1999), 185

Leroy V., *Microalloying '95,* 1995, 213

Leslie, W.C., Rickett, R.L., Walton, C.S., *Trans. ASM,* **46**(1954), 1470

Li Y., Crowther D.N., Mitchell P.S., Baker T.N., *HSLA Steels '2000, Xi'an, China*, 326

Li Y., Crowther D.N., Wilson J.A., Craven A.J., Baker T.N., *Proc. of Electron Microscopy & Analysis Group Conf.*, EMAG2001, Dundee, 2001, 183

Lubensky P.J., Wigman S.L., Johnson D.J., *Proc. Microalloying '95 conf.*, 225

Mårtensson, H., *Scan. J. Metall.*, 1(1972), 319

Matsuda, S., Okumura, N., *Tran. Iron and Steel Inst., Japan,* **18**(1978), 198

Matsuo S., Ando T., Grant N.J., *Mater. Sci. Eng.,* **A34**(2000), 34

Militzer, M., Pandi, R., Howbolt, E.B., *Met. Mat. Trans. A*, **27A**(1996), 1547

Morrison W.B., Woodhead, J.H., *J. I.S.I.*, **201**(1963), 43

Morrison W.B., *I.S.I.J.*, **201**(1963), 317

Narita, K., *Tran. Iron and Steel Inst., Japen,* **15**(1975), 145

Naylor J.P., Blondeau R., *Metall. Trans. A*, **7A**(1976), 891

Naylor J.P., *Metall. Trans. A*, **10A**(1979), 861

Norström L.Å., *Scan. J. Metall.,* **5**(1976), 159

Ouchi C., Sampei T., Kozasu I., *Trans. ISIJ,* **22**(1982), 215

Peñalba F., Andres C.G., Carsi M., Zapirain F., *Journal of Materials Science*, **31**(1996), 3847

Petch N.J., *I.S.I.J.*, **174**(1953), 25

Pickering F.B., Transformation and hardenibility in steels, climax Molybdenum, Ann Arbor, 1967, 109

Priestner R., Ajmal M., *Mater. Sci. Tech.*, **3**(1987), 360

Priestner R., Zhou C., *Ironmaking and Steelmaking*, **22**(1995), 326

Priestner R., *Materials Science Forum*, **284-286**(1998), 95

Prikryl M., Kroupa A., Weatherly G.C., Subramanian S.V., *Metallurgical and Materials Transaction A,* **27A**(1996), 1149

Ralph B. R., *Mater. Sci. Technol.*, **6**(1990), 1139.

Richter J., Guth A., Kothe A., Backmann G., *Steel Research*, **64**(1993), 267

Rickett R.L., Kalin S.H., Mackenzie J.T., *Trans. AIME*, **185**(1949), 242

Rios P.R., *Acta Metall.*, **35**(1987), 2805

Rios P.R., *Mater, Sci. Eng.*, **A156**(1992), L5

Roberts M.J., *Metall. Trans.*, **1**(1970), 3287

Roberts,I.M., *Mat. Sci. Tech.*, **9** (1993), 1031,

Robertson Z.M., *Mat. Sci. Tech.*, 9(1993), 1031

Rose A.J., Personal Communication, 2002

Schreder T.A., *Metall. Trans. A*, **7A**(1976), 535

Singh A.P., Prasad A., Prakash K., Sengupta D., Murty G.M.D., Jha S., *Mater. Sci. Technol.*, **15**(1999), 121

Smallman R.E., *Modern Physical Metallurgy*, Butterworth & Co Ltd, 1985

Smith C.S., *Trans. A.I.M.E.*,**175**(1948),15

Solter R.L., Beattie C.W., *Trans. AIME*, **191**(1951), 721

Speich G.R., *Trans. TMS-AIME*, **245**(1969), 2553

Stark I., Smith G.D.W., Bhadeshia H.K.D.H., *Metall. Trans.A*, **21A**(1990), 837

Starratt, F.W., *J. of Metals*, **10**(1959), 799

Swisher J.H., Turkogan E.T., *Trans. Met. Soc. AIME*, **239**(1967), 426

Stuart H and Jones B. L. *Journal of Metals*, **35**(1983), No.4, 17

Tamehiro H., Nakasugi H., *Transaction of ISIJ*, **25**(1985), 311

Thompson C.V., Frost H.J., Spaepen F., *Acta Metall.*, 35(1987), 887

Turkdogan E.T., Ignatowicz S., Pearson J., *ISIJ*, **180**(1955), 349

Wada T., Tsukamoto H., Suga B.A., *I.S.I.J.*, **74**(1988), 1438

Wang S., *Journ. Mater. Sci.*, **25**(1990), 187

Wang S.C., Yang J.R., *Mater. Sci. Eng.*, **A154**(1992), 43

Wang S.C., Kao P.W., *Jour. Mater. Sci.*, **28**(1993), 5169

Wiester, H-J., Bading, W., Riedel, H., Scholz, W., *Stahl und Eisen*, **77**(1957), 773

Wilson F.G., Gladman T., *Intern. Mater. Rev.,* **33**(1988), 221

Woodhead, H., *HSLA Steels Technology & Application, AIM International* 1985, 15

Wriedt H., Hsun H., *Metall. Trans. A*, **7A**(1976), No.5, 711

Zajac S., Siwecki T., Hutchinson B., *Swed. Inst. Metals Res.,* Dec., 1996, 44

Zentara N., Kaspar R., *Stahl und Eisen*, **116**(1996), 98

Zhou H., Kirkaldy J.S., *Metall. Trans. A*, **22A**(1991), 1511

Zhou H., Kirkaldy J.S., *Metall. Trans. A*, **23A**(1992), 651

Appendix 1 The C-program for the calculation of precipitation of VCN in Steels 1 and 2 or 3

1 Steel 1

```
#include <stdio.h>

#include <math.h>

main()

{

  int i, k;

  float Kvn, Kvc, Kaln, T, Faln, Fc, Fn, Fp, A0, As, C, C0, Cs, N0, N, Ns,

V0,

        V, Vs;

printf("Enter a temperature value");

scanf("%f", &t);

T=t+273.15

for(i=0; i<=19999; i++)

{

  Kvn=pow(10, 3.03-7840/T)*(55.8/(100*14))*(55.8/(100*50.9));

  Kvc=pow(10, 6.72-9500/T)*(55.8/(100*50.9))*(55.8/(100*12));

 Kaln=pow(10, 1.8-7750/T)*(55.8/(100*14))*(55.8/(100*27));

 C0=(0.073*55.8)/(100*12);

 N0=(0.021*55.8)/(100*14);

 A0=(0.027*55.8)/(100*27);
```

```
V0=(0.16*55.8)/(100*50.9);
C=C0*(1-0.00005*i);
for(k=1; k<=19999; k++)
 {
  N=N0*(1-0.00005*k);
  Fp=(C0+N0-C-N)/(1-2*(C+N));
  Fc=(C0-(1-2*Fp)*C)/Fp;
  Fn=(N0-(1-2*Fp)*N)/Fp;
  Faln=A0-(Kaln/N)*(1-2*(C0+N0-C-N)/(1-2*(C+N)));
  Cs=Fc/((V0/Kvc)/(1-2*Fp-2*Faln+Fp*(C/Kvc+N/Kvn)));
  Ns=Fn/((V0/Kvn)/(1-2*Fp-2*Faln+Fp*(C/Kvc+N/Kvn)));
  Vs=V0/(1-2*Fp-2*Faln+Fp*(C/Kvc+N/Kvn));
  As=A0/(1-2*Fp-2*Faln+Fp*(N/Kaln));
if(((N/Ns>0.95)&&(N/Ns<1.05))&&((C/Cs>0.95)&&(C/Cs<1.05)))
{
printf("C=%f, Cs=%f, N=%f, Ns=%f, Vs=%f, As=%f\n",
        C*12*100/55.8, Cs*12*100/55.8, N*14*100/55.8,
        Ns*14*100/55.8, Vs*50.9*100/55.8, As*27*100/55.8);
}
}
}
```

2 Steel 2 or 3

```
#include <stdio.h>
#include <math.h>
main()
{
  int i, k;
float Kvn, Kvc, Kaln, t, T, Faln, Fc, Fn, Fp, A0, As, C, C0, Cs, N0, N, Ns,
      V0, V, Vs;
printf("Enter a temperature value");
scanf("%f", &t);
T=t+273.15
for(i=0; i<=19999; i++)
{
Kvn=pow(10, 3.03-7840/T)*(55.8/(100*14))*(55.8/(100*50.9));
Kvc=pow(10, 6.72-9500/T)*(55.8/(100*50.9))*(55.8/(100*12));
Kaln=pow(10, 1.8-7750/T)*(55.8/(100*14))*(55.8/(100*27));
 C0=(0.067*55.8)/(100*12);
 N0=(0.017*55.8)/(100*14);
 A0=(0.03*55.8)/(100*27);
 V0=(0.10*55.8)/(100*50.9);
C=C0*(1-0.00005*i);
for(k=1; k<=19999; k++)
 {
 N=N0*(1-0.00005*k);
```

```
Fp=(C0+N0-C-N)/(1-2*(C+N));

Fc=(C0-(1-2*Fp)*C)/Fp;

Fn=(N0-(1-2*Fp)*N)/Fp;

Faln=A0-(Kaln/N)*(1-2*(C0+N0-C-N)/(1-2*(C+N)));

Cs=Fc/((V0/Kvc)/(1-2*Fp-2*Faln+Fp*(C/Kvc+N/Kvn)));

Ns=Fn/((V0/Kvn)/(1-2*Fp-2*Faln+Fp*(C/Kvc+N/Kvn)));

Vs=V0/(1-2*Fp-2*Faln+Fp*(C/Kvc+N/Kvn));

As=A0/(1-2*Fp-2*Faln+Fp*(N/Kaln));

if(((N/Ns>0.95)&&(N/Ns<1.05))&&((C/Cs>0.95)&&(C/Cs<1.05)))

{

printf("C=%f, Cs=%f, N=%f, Ns=%f, Vs=%f, As=%f\n",

        C*12*100/55.8, Cs*12*100/55.8, N*14*100/55.8,

        Ns*14*100/55.8, Vs*50.9*100/55.8, As*27*100/55.8);

    }

    }

  }

}
```

Appendix 2 The calculated volume fraction of AlN and MnS particles from the chemical compositions of steels

1 AlN

In Steel 1, the contents of nitrogen and aluminium are 0.021 wt.% and 0.027 wt.%, respectively. According the chemical reaction formula of nitrogen and aluminium,

$$Al + N = AlN$$

0.027g Al can produce 0.041g MnS because nitrogen is in slight stoichiometric excess. The densities of AlN and Fe are 3.261 g/cm^3 and 7.8 g/cm^3, respectively. The volume of 0.041g AlN and 100g Fe is 0.041 / 3.261 = 0.0126 cm^3 and 100 / 7.8 = 12.82 cm^3. Therefore, the volume fraction, f, of AlN in Steel 2 is 0.014 /12.82 = 9.8×10^{-4}.

Similarly, the volume fraction of AlN in Steel 2 is 1.1×10^{-3}.

2 MnS

In Steel 1, the contents of sulphur and manganese are 0.002 wt.% and 1.83 wt.%, respectively. According the chemical reaction formula of sulphur and manganese,

$$Mn + S = MnS$$

0.002g S can produce 0.0054g MnS because manganese is in stoichiometric excess. The densities of MnS and Fe are 4.053 g/cm^3 and 7.8 g/cm^3, respectively. The volume of 0.0054g MnS and 100g Fe is 0.0054 / 4.053 =

0.00133 cm^3 and 100 / 7.8 = 12.82 cm^3, respectively. Therefore, the volume fraction, f, of MnS in Steel 1 is 0.00133 /12.82 = 1.039×10^{-4}.

Similarly, the volume fraction of MnS in Steel 2 is 2.078×10^{-4}.

FIGURES IN CHAPTER TWO

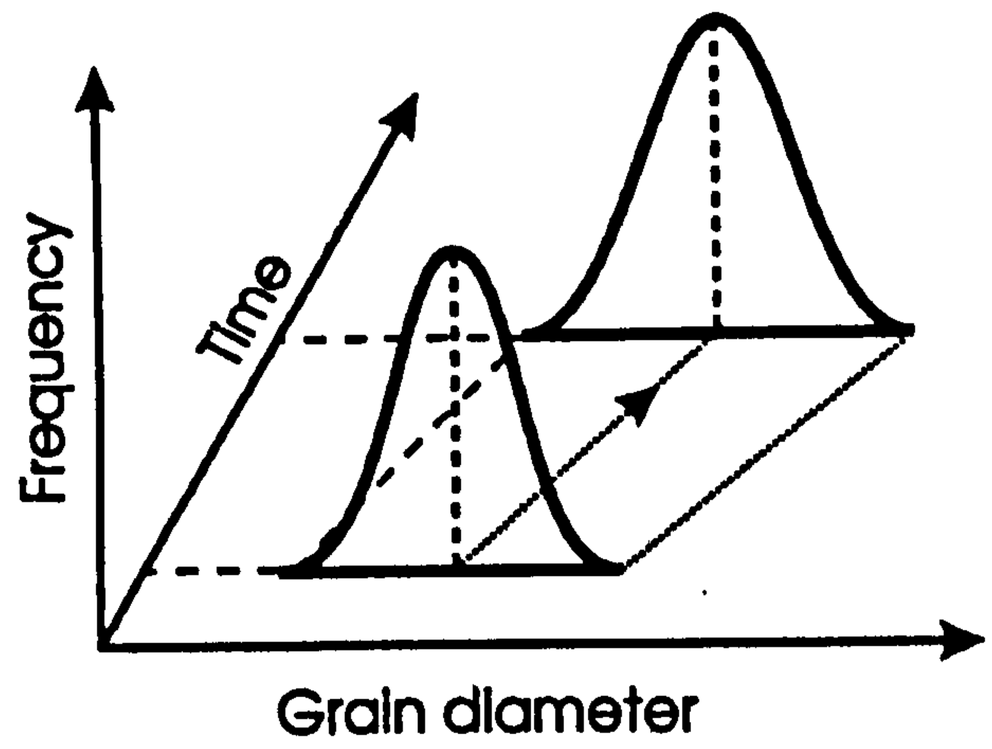

(a)

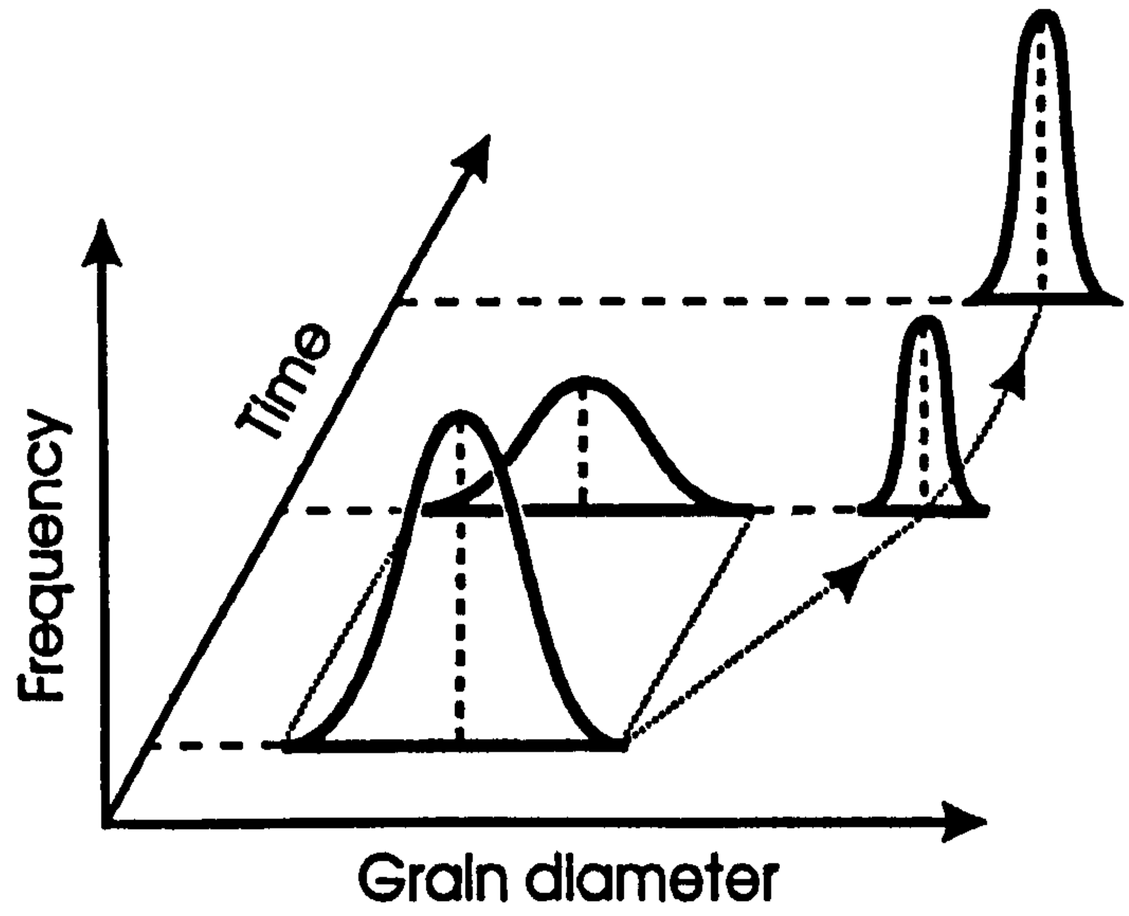

(b)

Fig. 2.1 Schematic representation of the change in grain size distribution during
(a) Normal grain growth and
(b) Abnormal grain growth

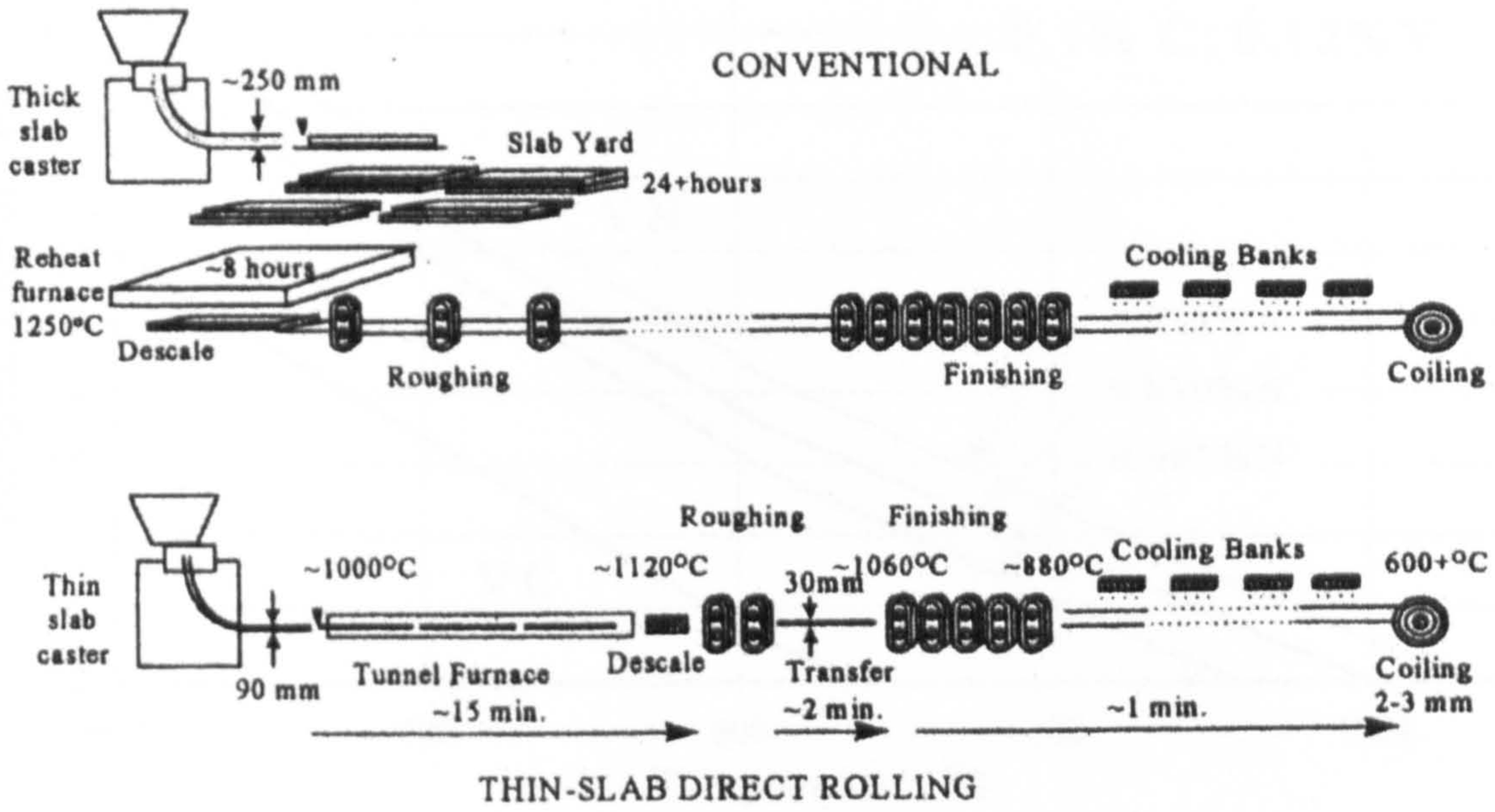

Fig. 2.2 Comparison of conventional rolling and thin-slab direct rolling

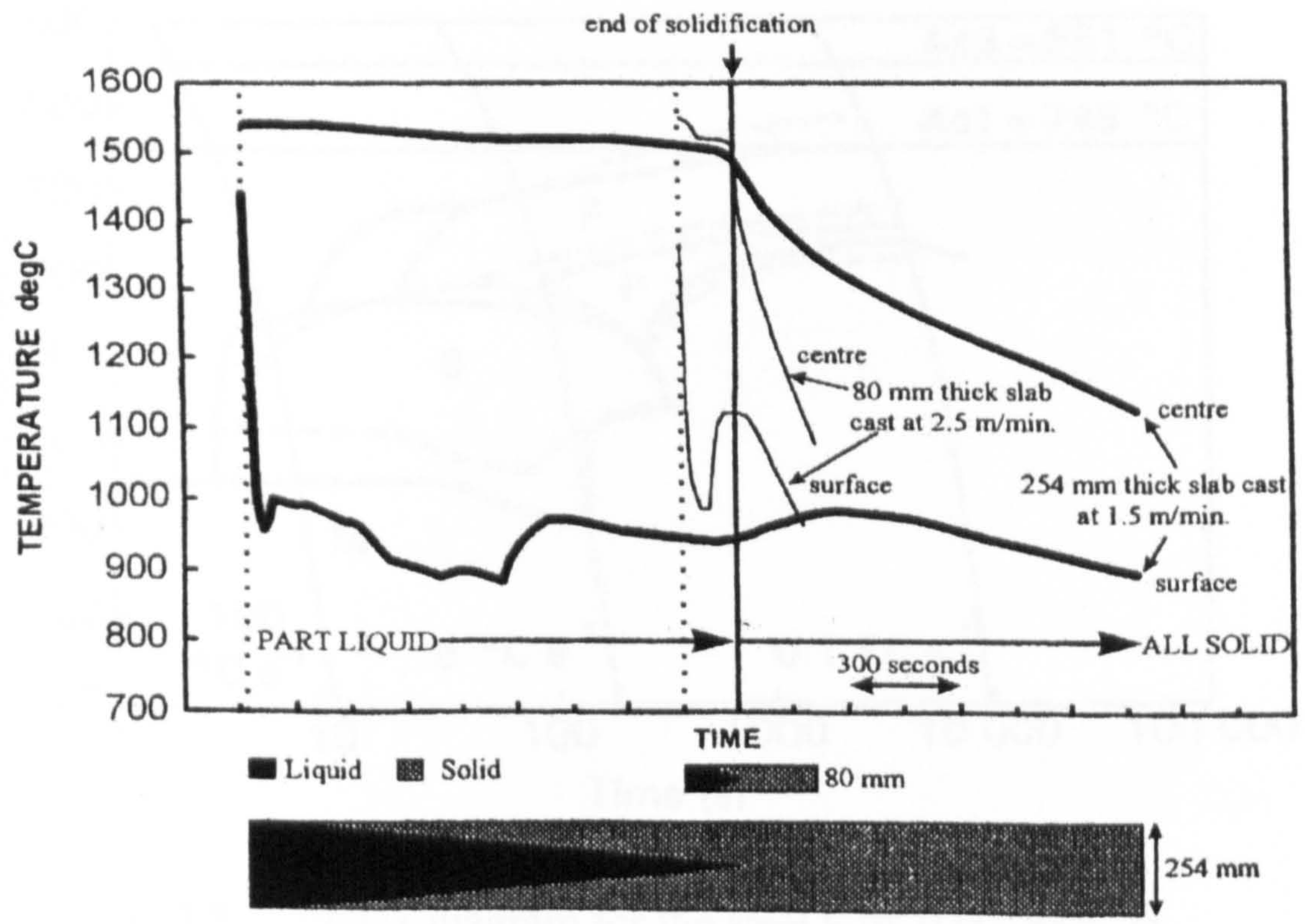

Fig. 2.3 Thermal histories of thick (conventional) and thin slab during casting

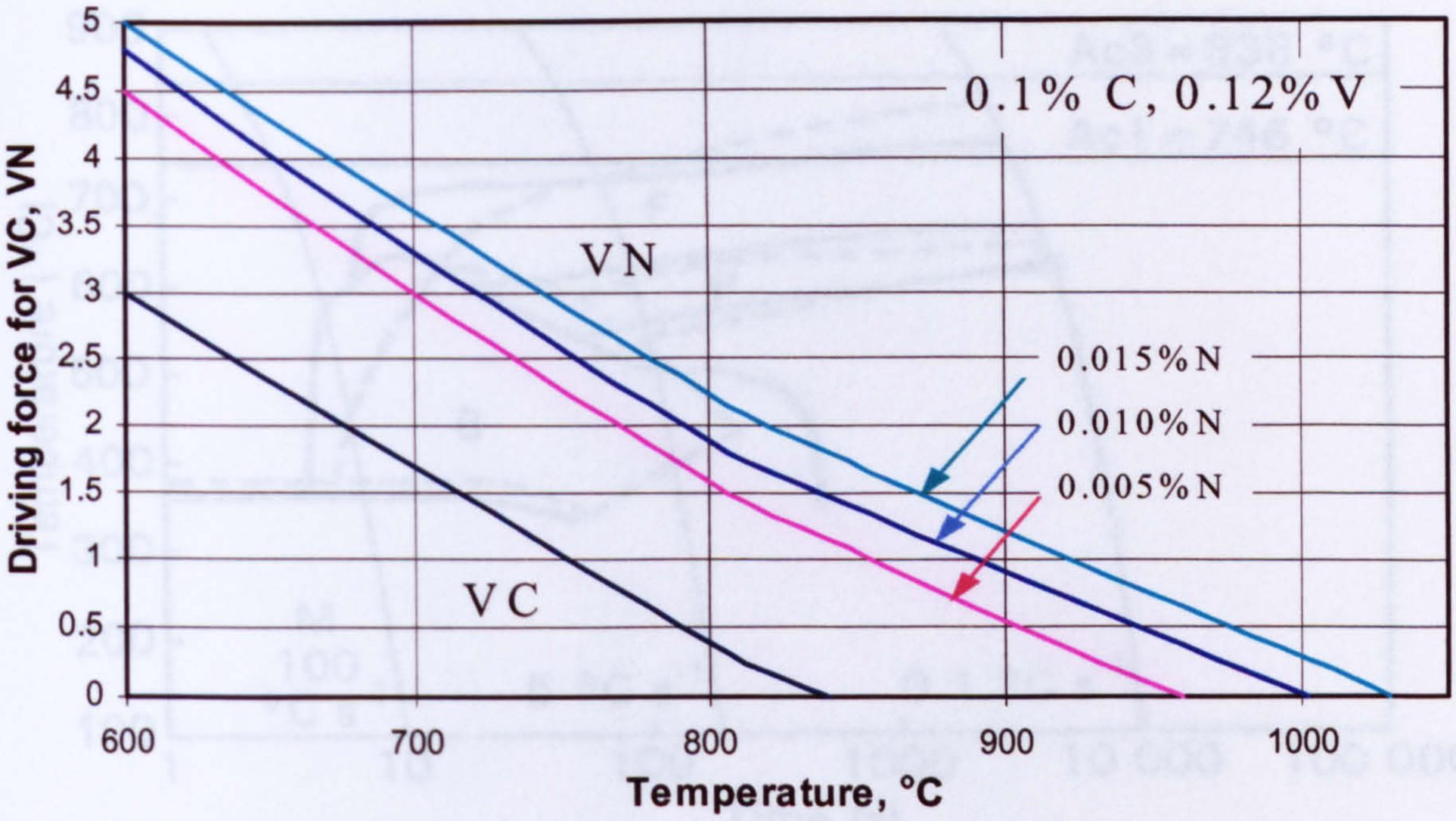

Fig. 2.4 Chemical driving force, $\Delta G_m/RT$, for precipitation of VC and VN

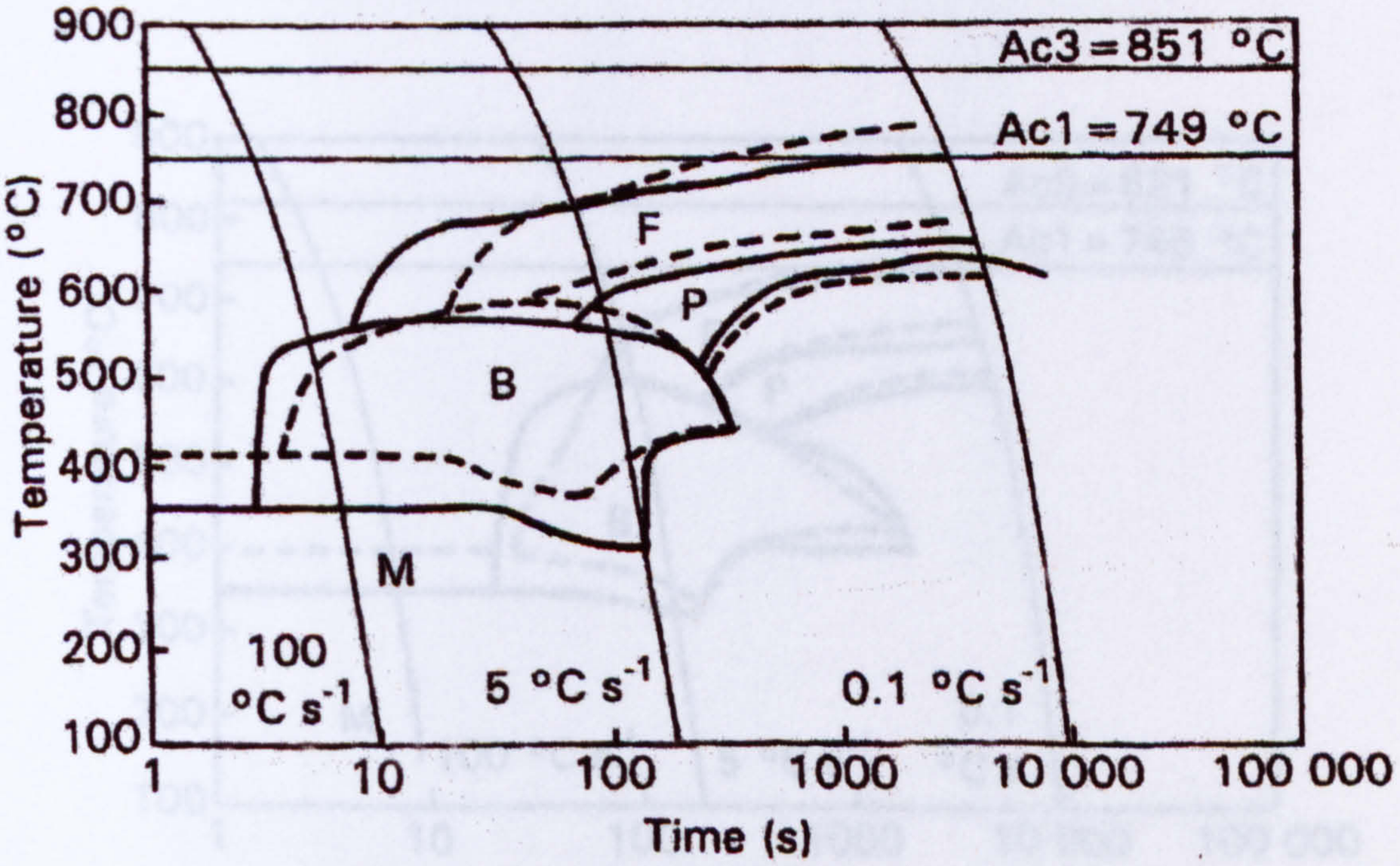

Fig. 2.5 CCT diagram for the steel with 0.007wt% Ti
a. The unbroken line represents T = 1050°C
b. The dashed line represents T = 1250°C

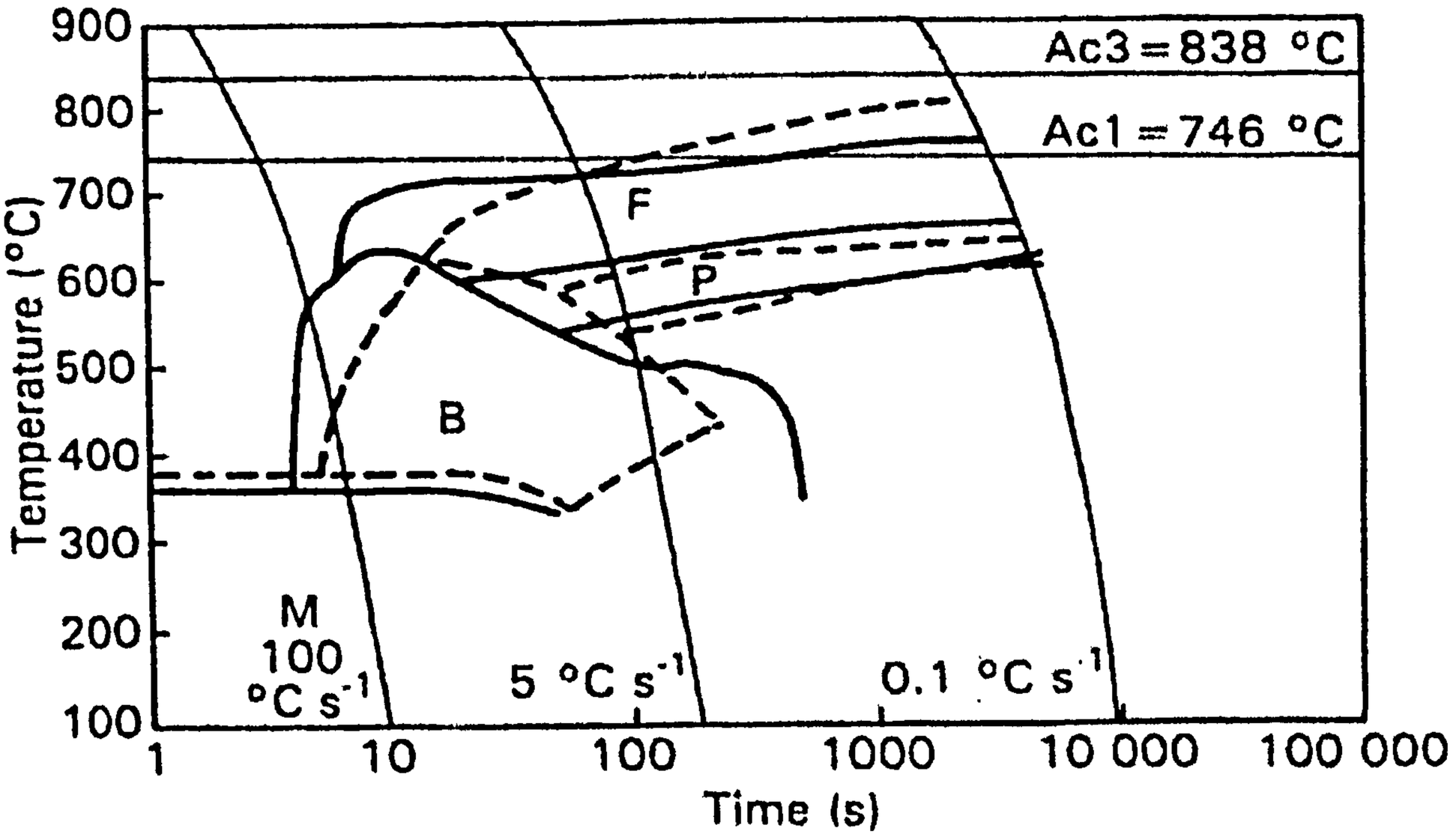

Fig. 2.6 CCT diagram for the steel with 0.019wt% Ti
a. The unbroken line represents T = 1050°C
b. The dashed line represents T = 1250°C

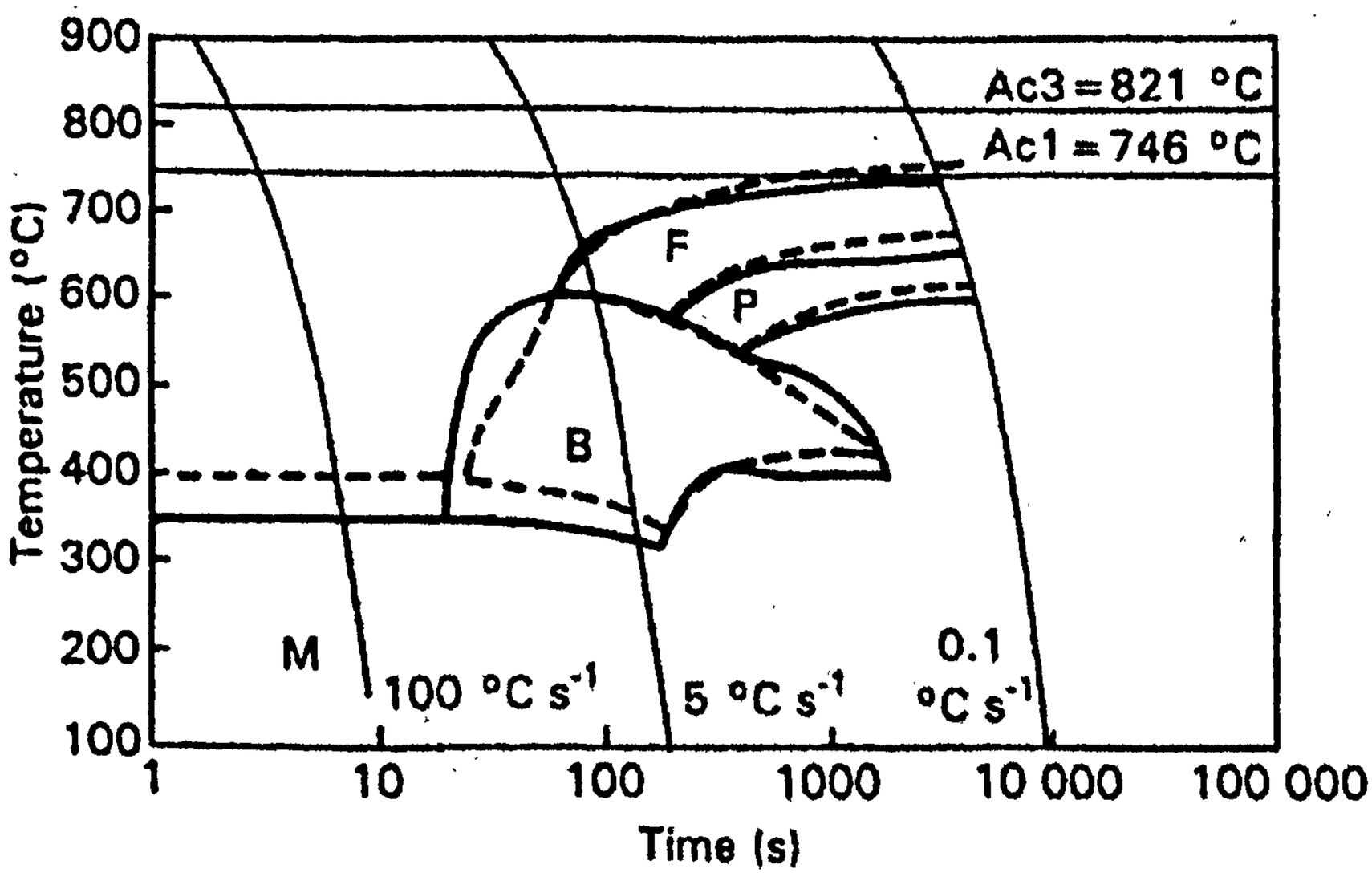

Fig. 2.7 CCT diagram for the steel with 0.039wt% Ti
a. The unbroken line represents T = 1050°C
b. The dashed line represents T = 1250°C

FIGURES IN CHAPTER THREE

Fig. 3.1 Simulated TSDR process

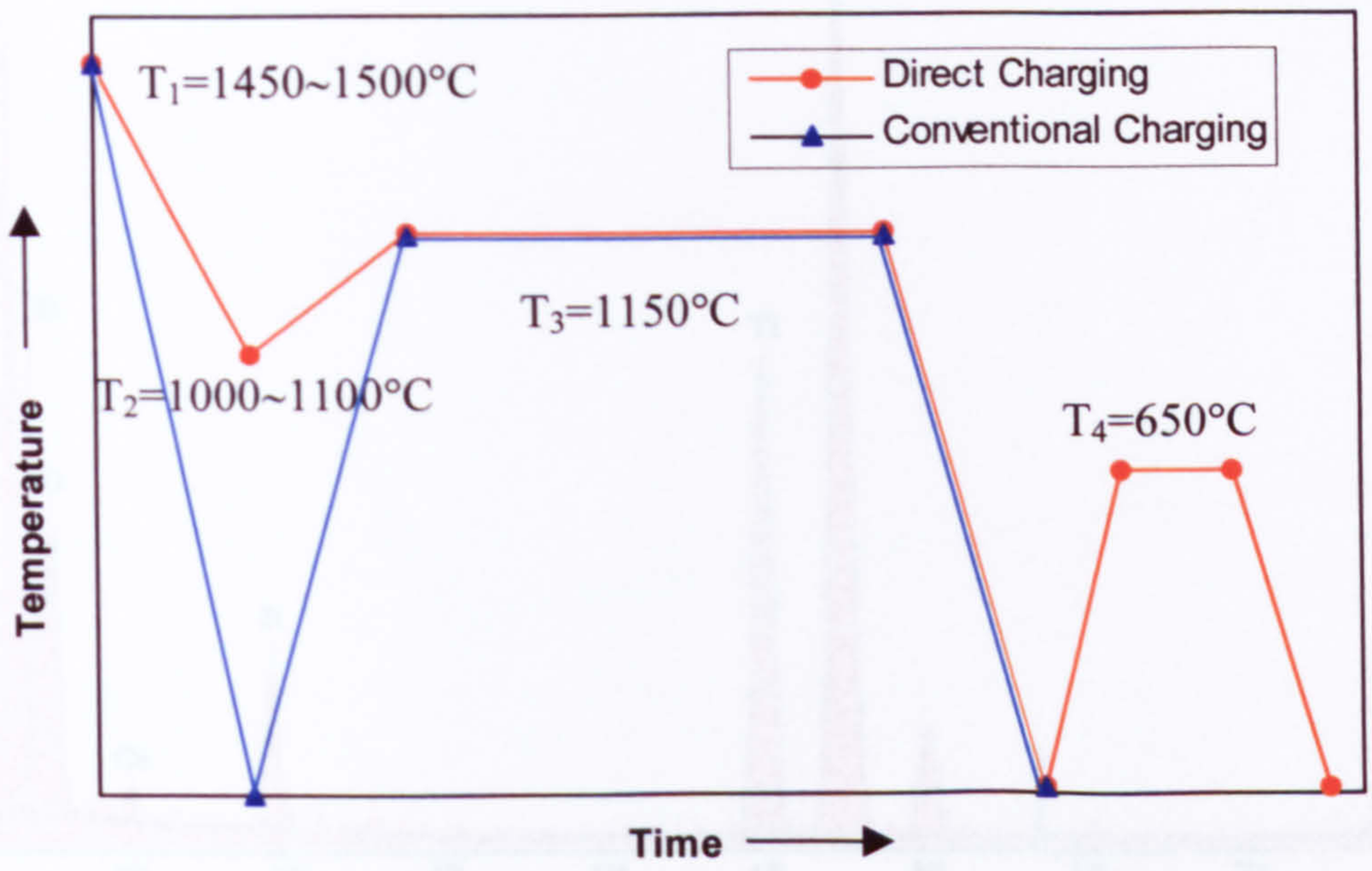

Fig. 3.2 Diagram of the charging processes

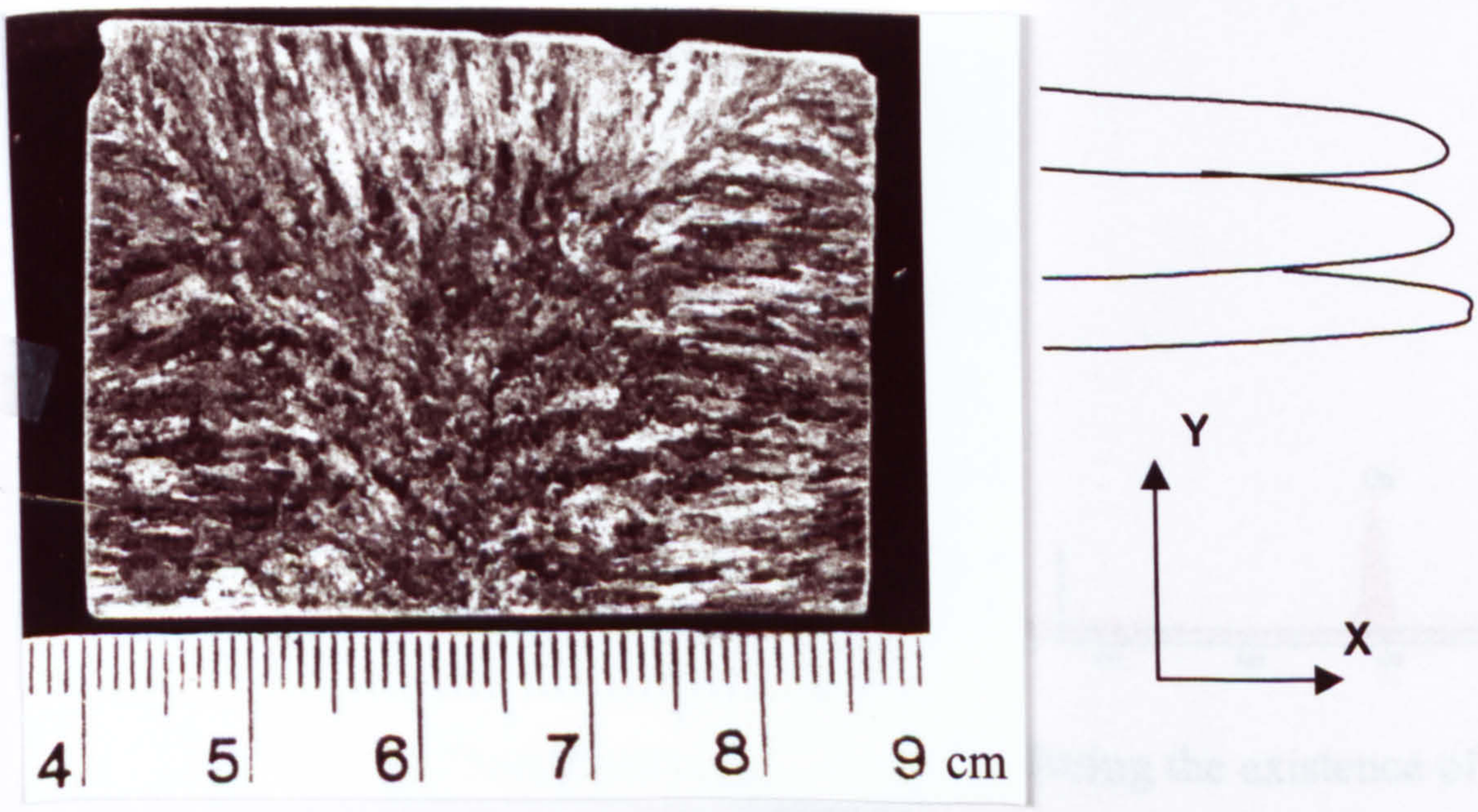

Fig. 3.3 The cast structure of Steel 1 after equalisation at 1150°C

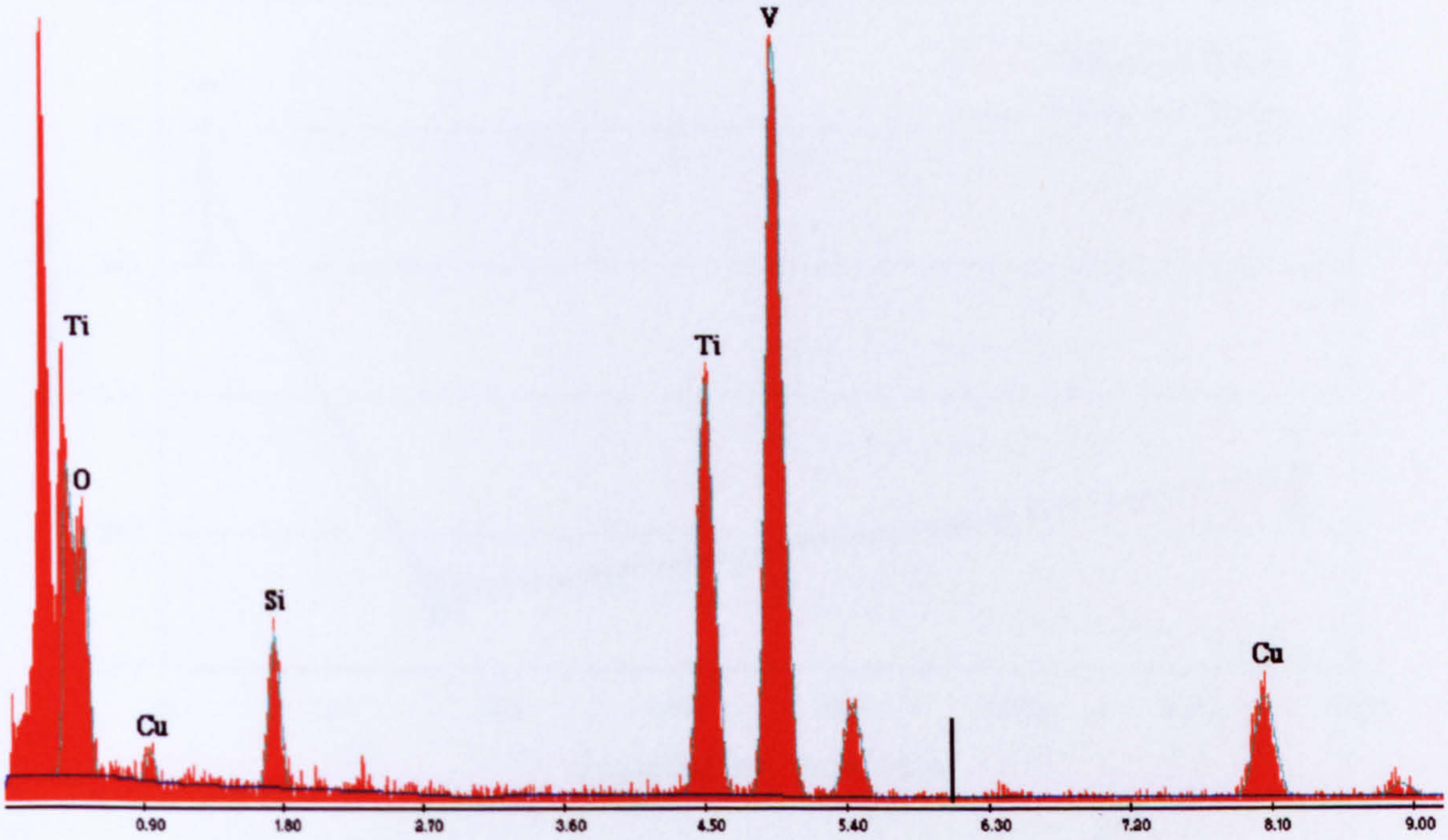

Fig. 3.4 Theoretical result when ignoring the existence of nitrogen

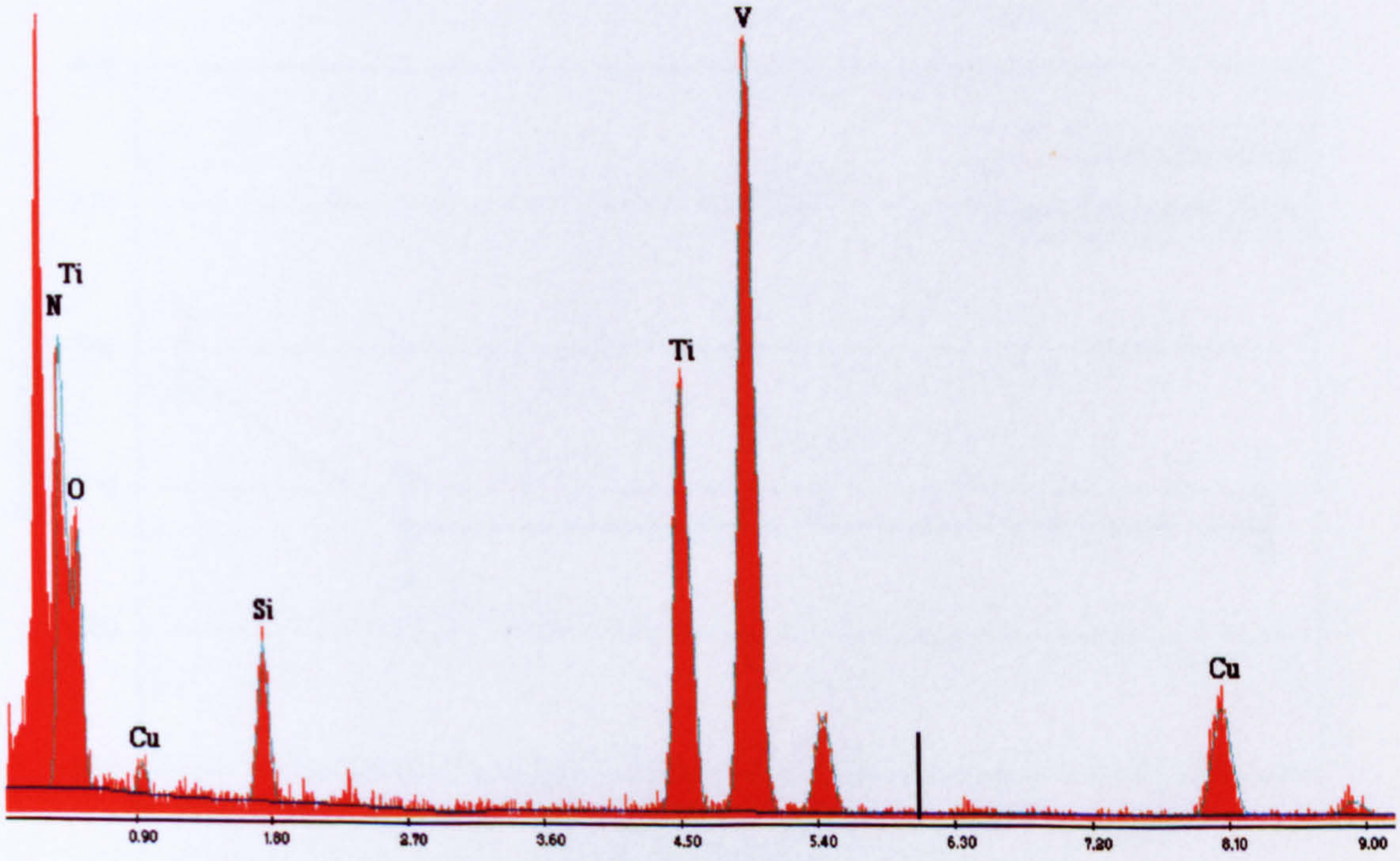

Fig. 3.5 Theoretical result when considering the existence of nitrogen

FIGURES IN CHAPTER FOUR

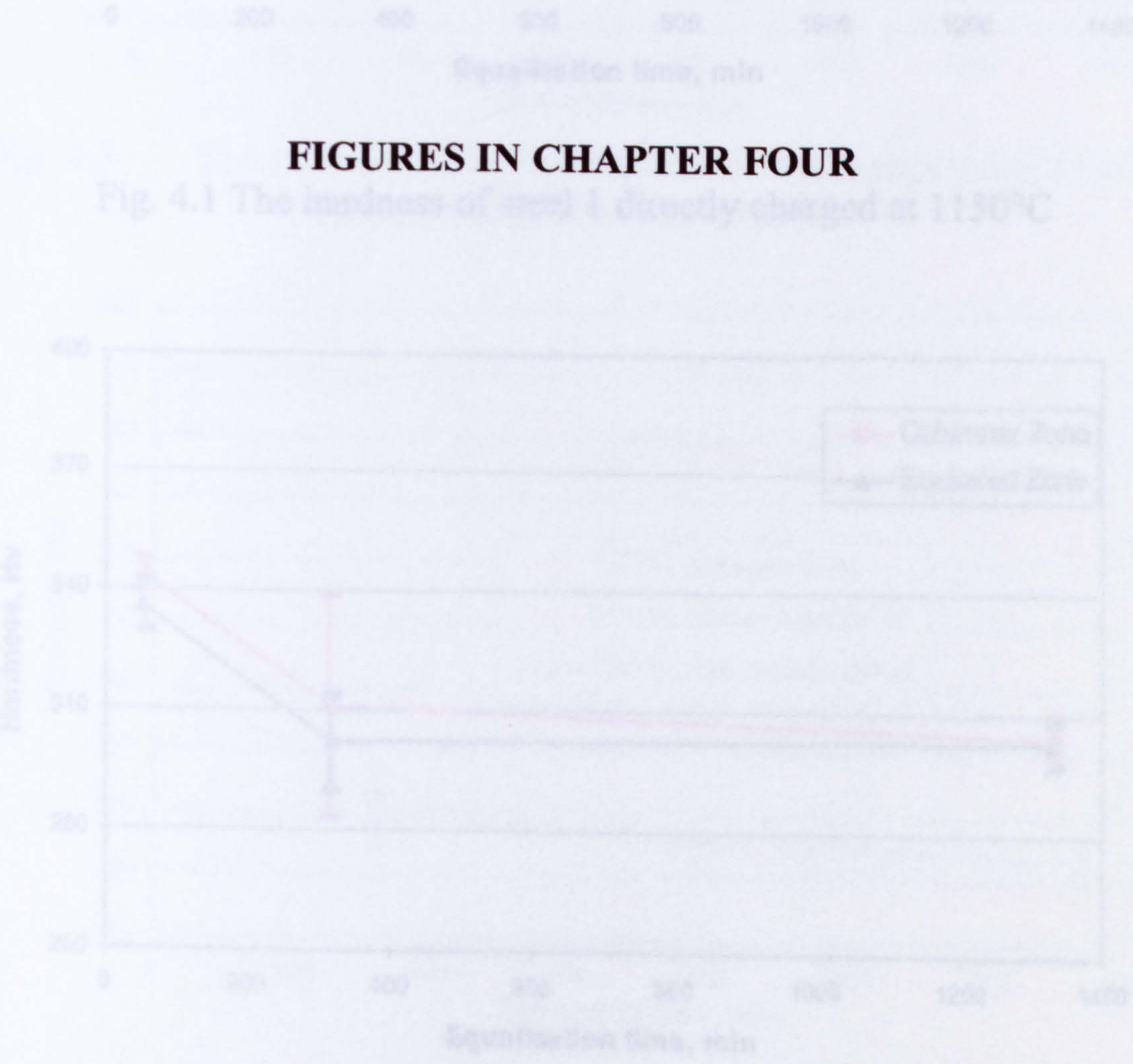

Fig. 4.1 The hardness of steel 1 directly charged at 1130°C and tempered at 650°C

Fig. 4.2 The hardness of steel 1 directly charged at 1150°C and tempered at 650°C

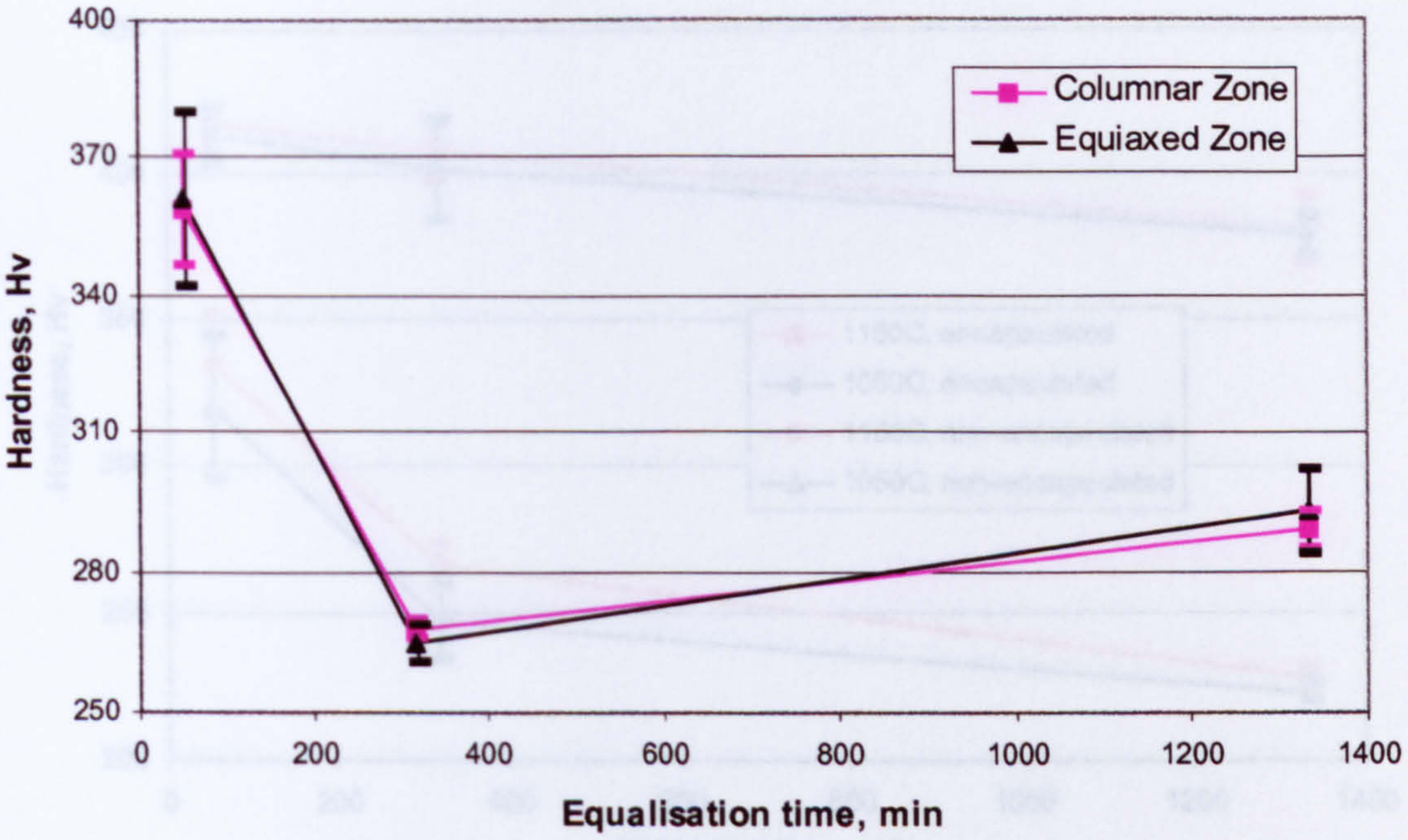

Fig. 4.1 The hardness of steel 1 directly charged at 1150°C

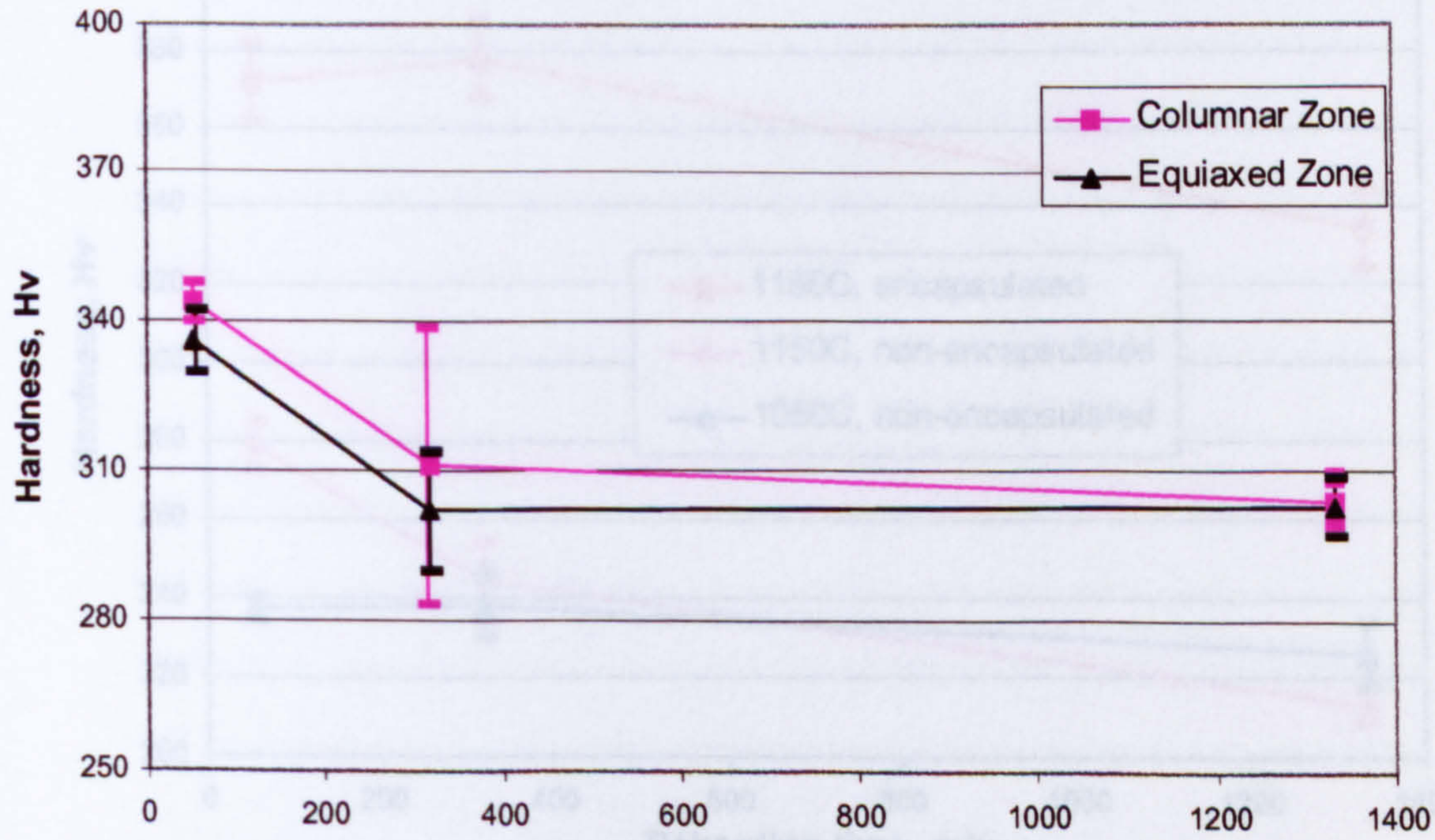

Fig. 4.2 The hardness of steel 1 directly charged at 1150°C and tempered at 650°C

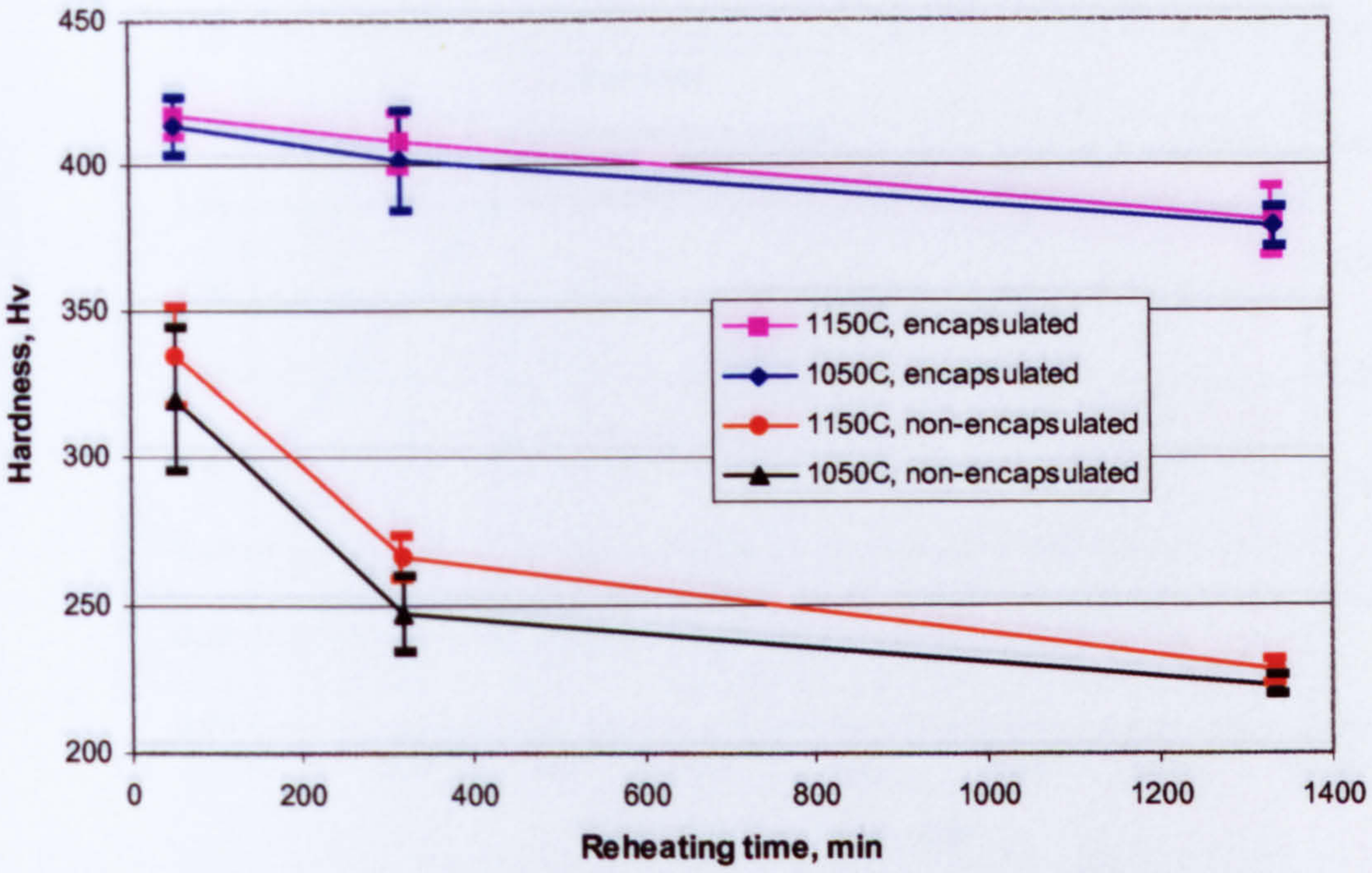

Fig. 4.3 The hardness of non-encapsulated and encapsulated Steel 2 reheated at 1050°C and 1150°C

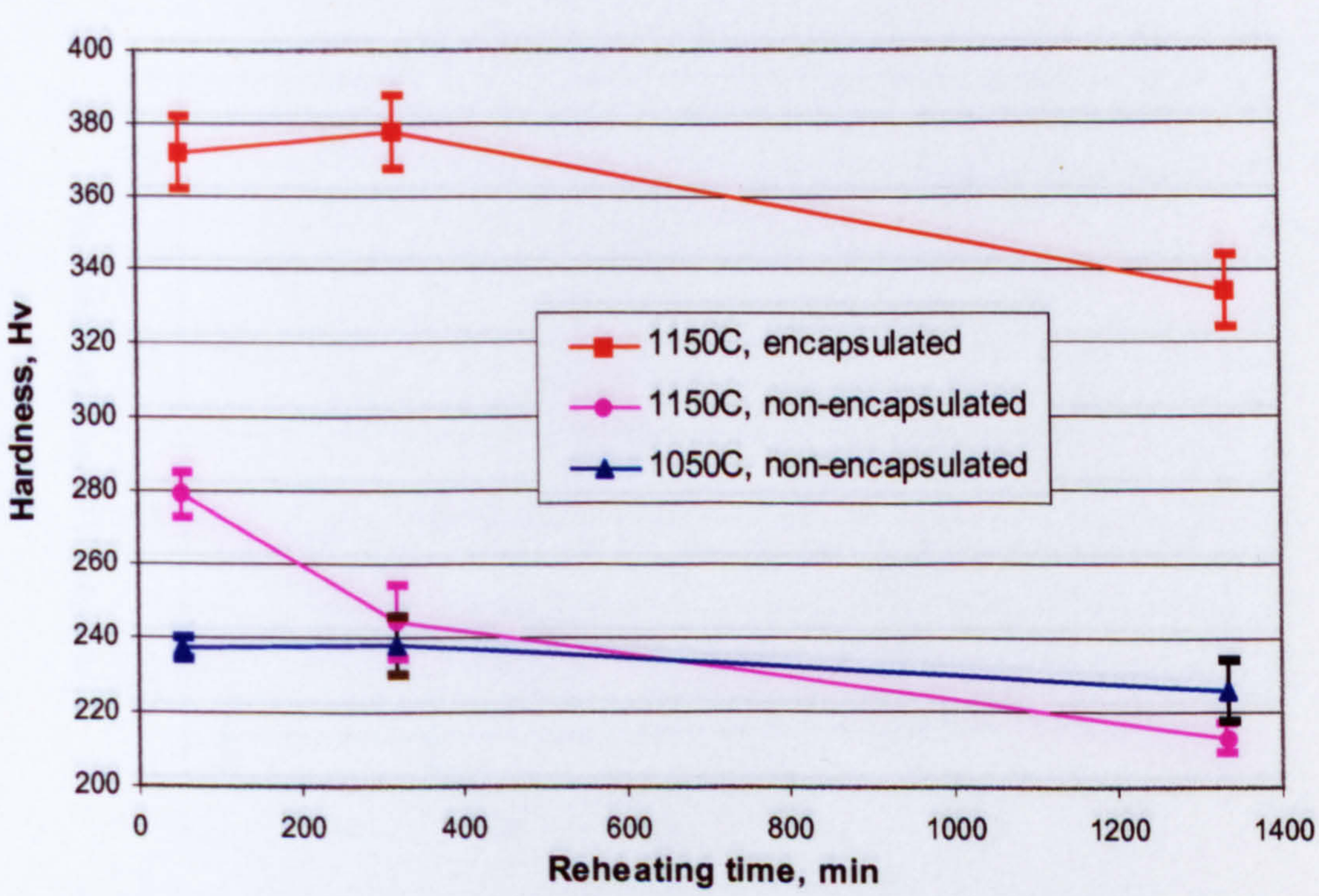

Fig. 4.4 The hardness of non-encapsulated and encapsulated Steel 3 reheated at 1050°C and 1150°C

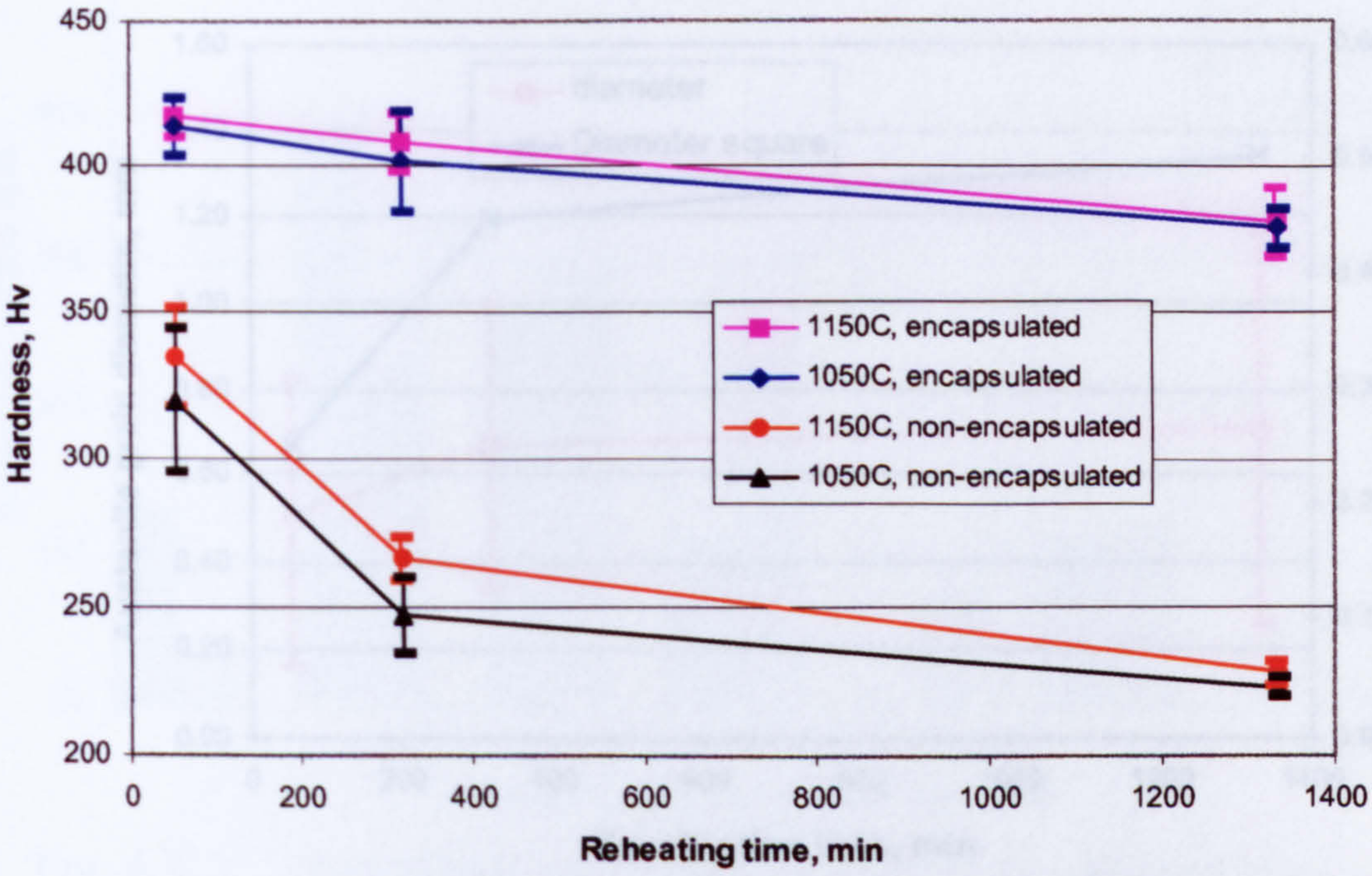

Fig. 4.3 The hardness of non-encapsulated and encapsulated Steel 2 reheated at 1050°C and 1150°C

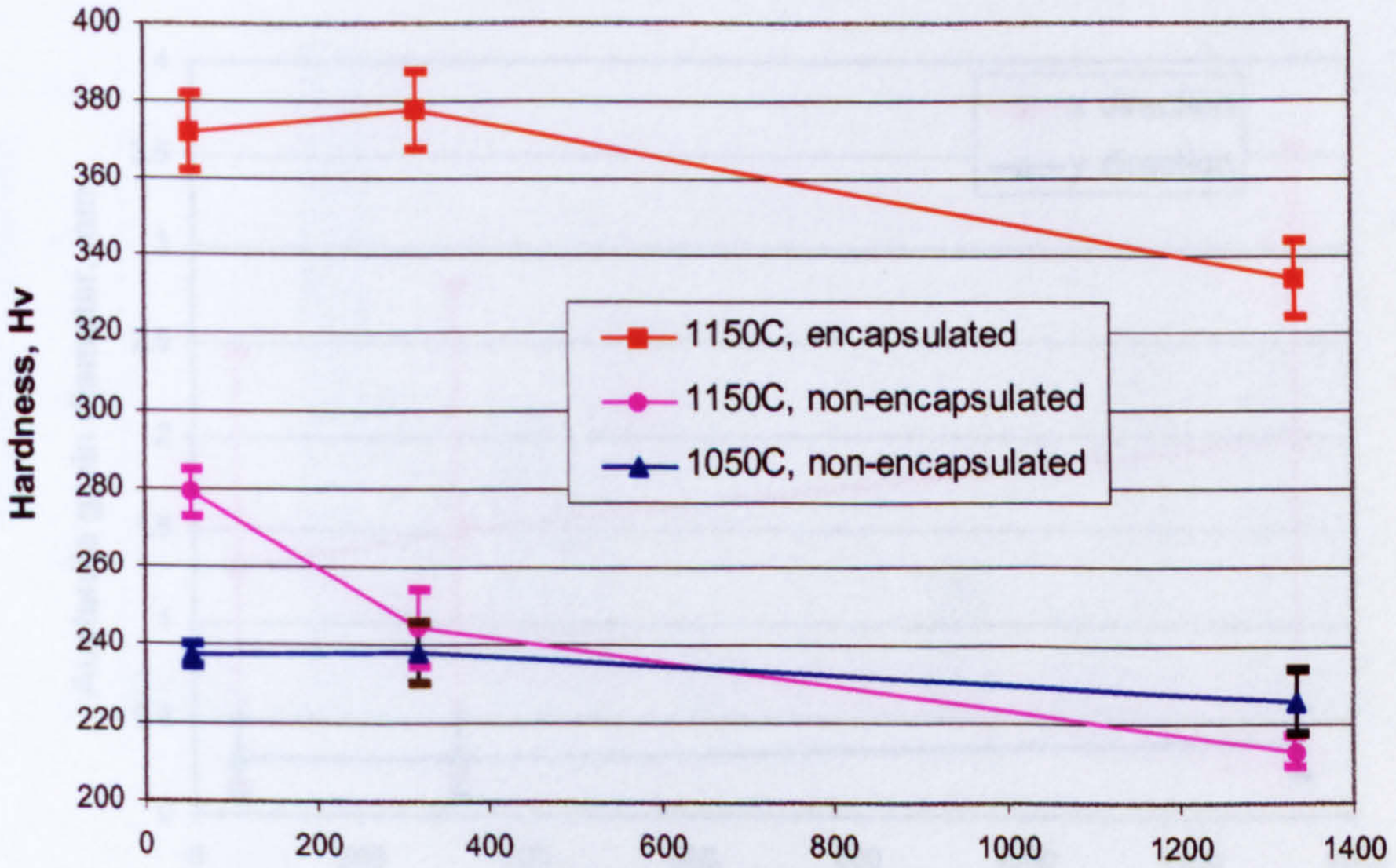

Fig. 4.4 The hardness of non-encapsulated and encapsulated Steel 3 reheated at 1050°C and 1150°C

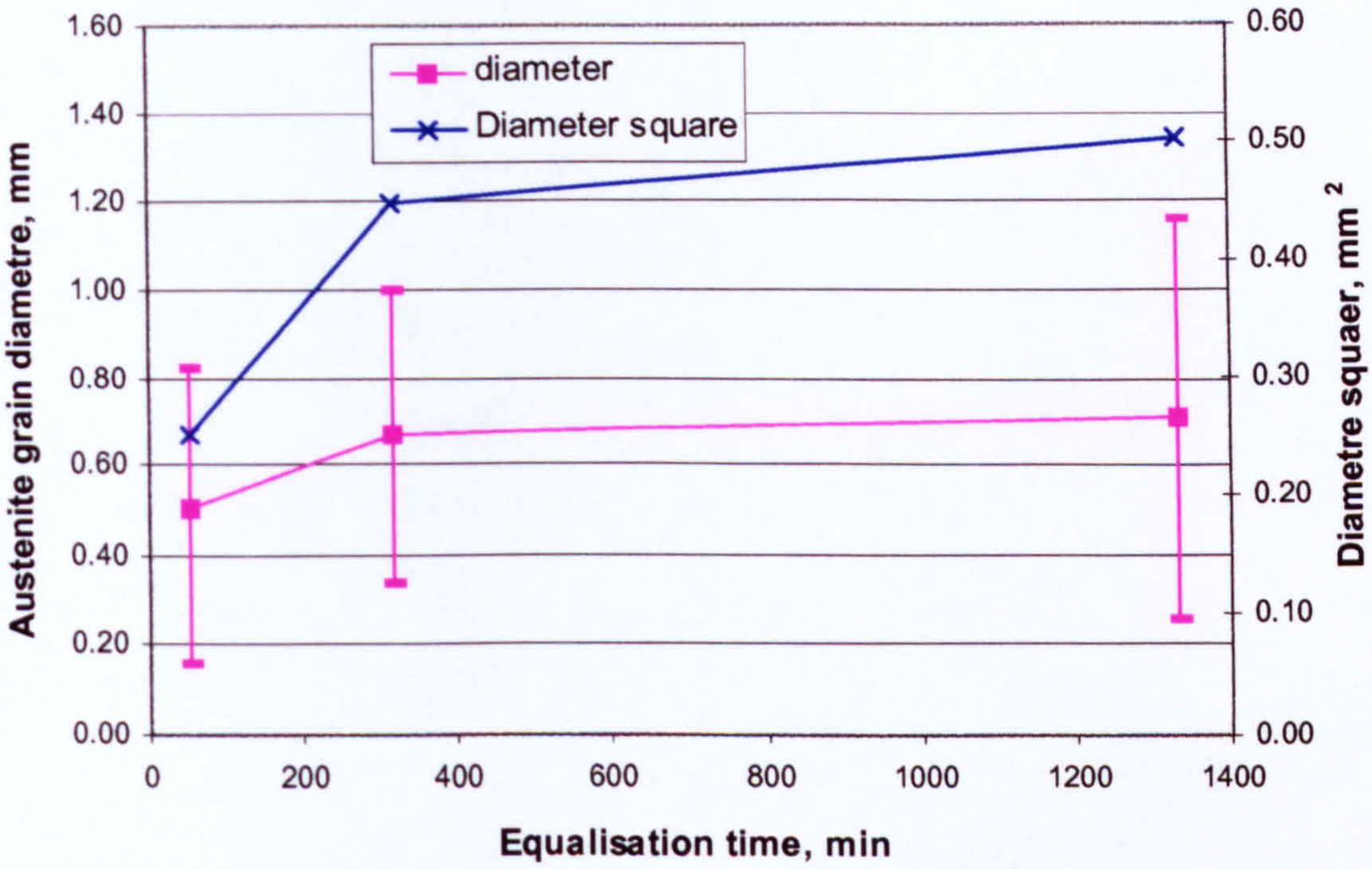

Fig. 4.5 Austenite grain size in the equiaxed zone of Steel 1 equalised at 1150°C

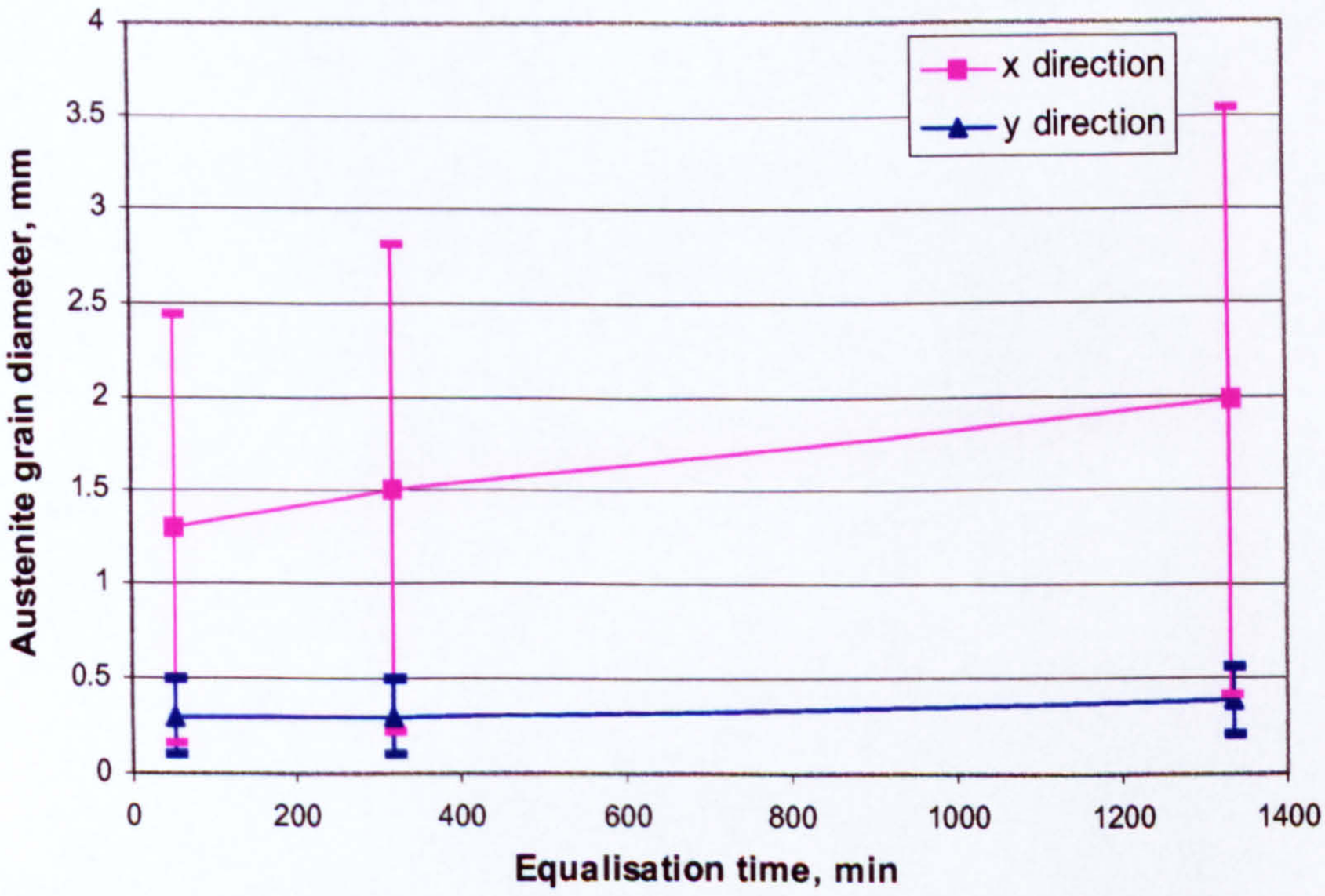

Fig. 4.6 Austenite grain size in the columnar zone of Steel 1 equalised at 1150°C

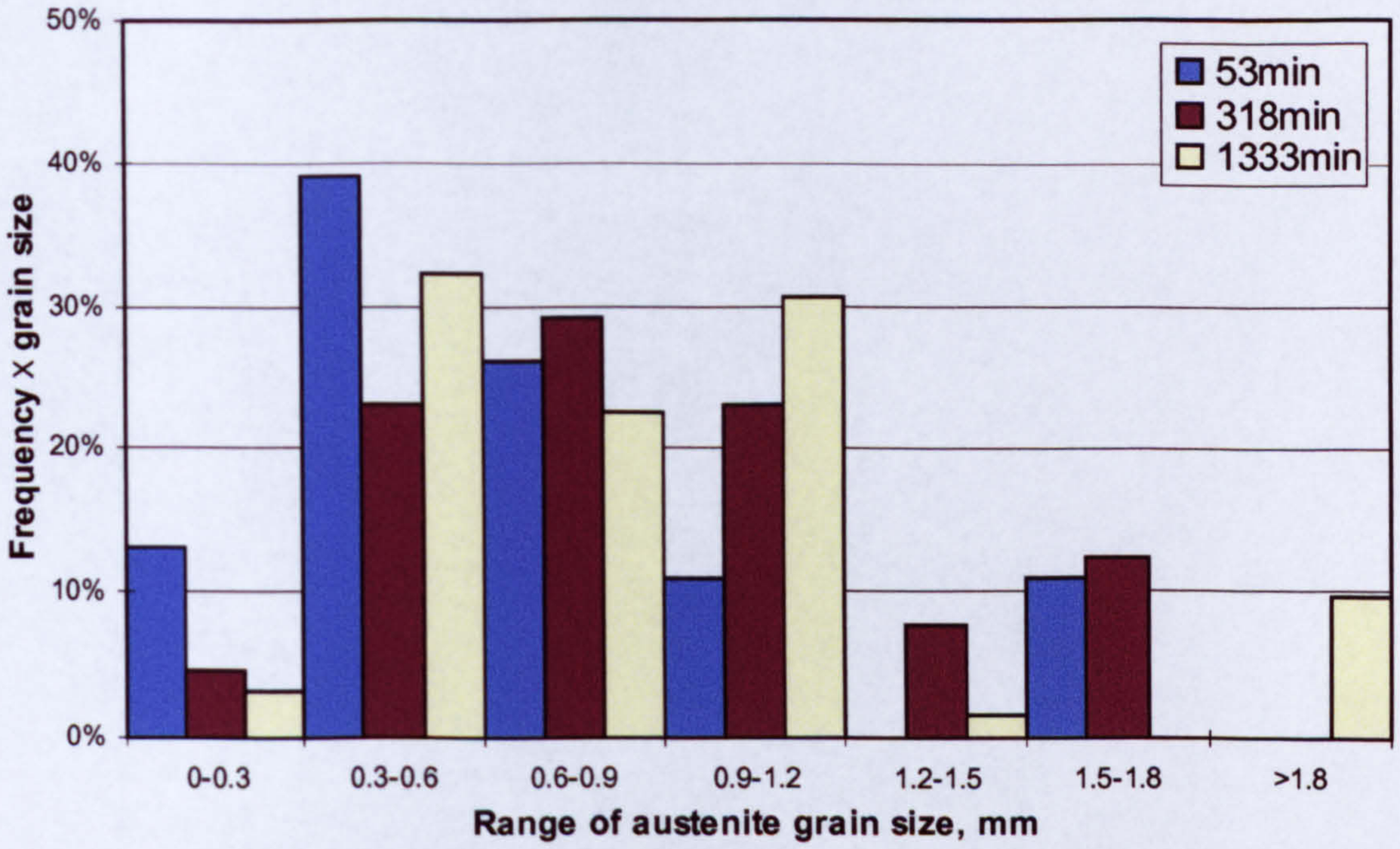

Fig. 4.7 Distribution of austenite grain size in equiaxed zone of Steel 1 at 1150°C for different equalisation time

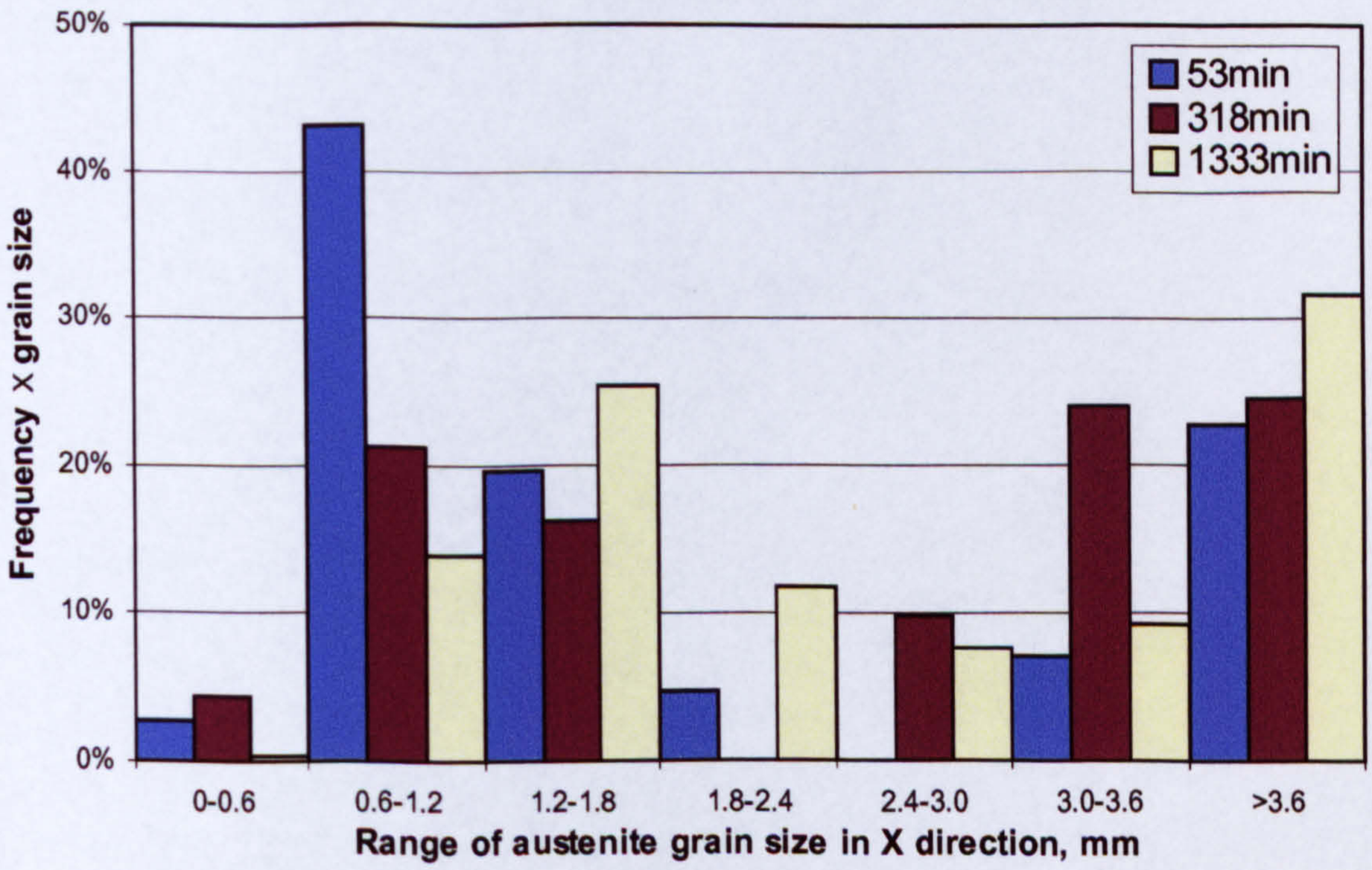

Fig. 4.8 Distribution of austenite grain size in X direction of columnar zone of Steel 1

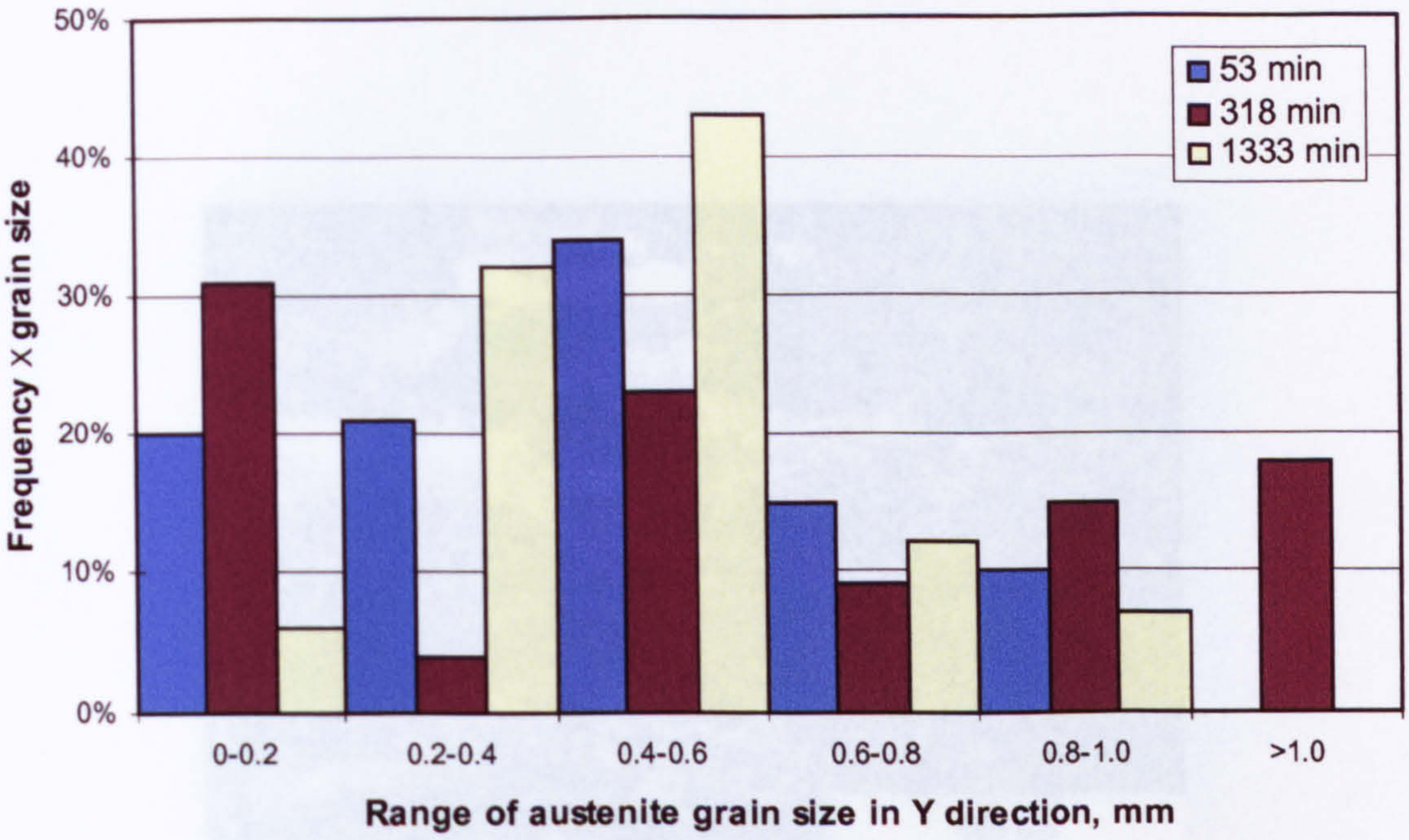

Fig. 4.9 Distribution of austenite grain size in Y direction of columnar zone of Steel 1

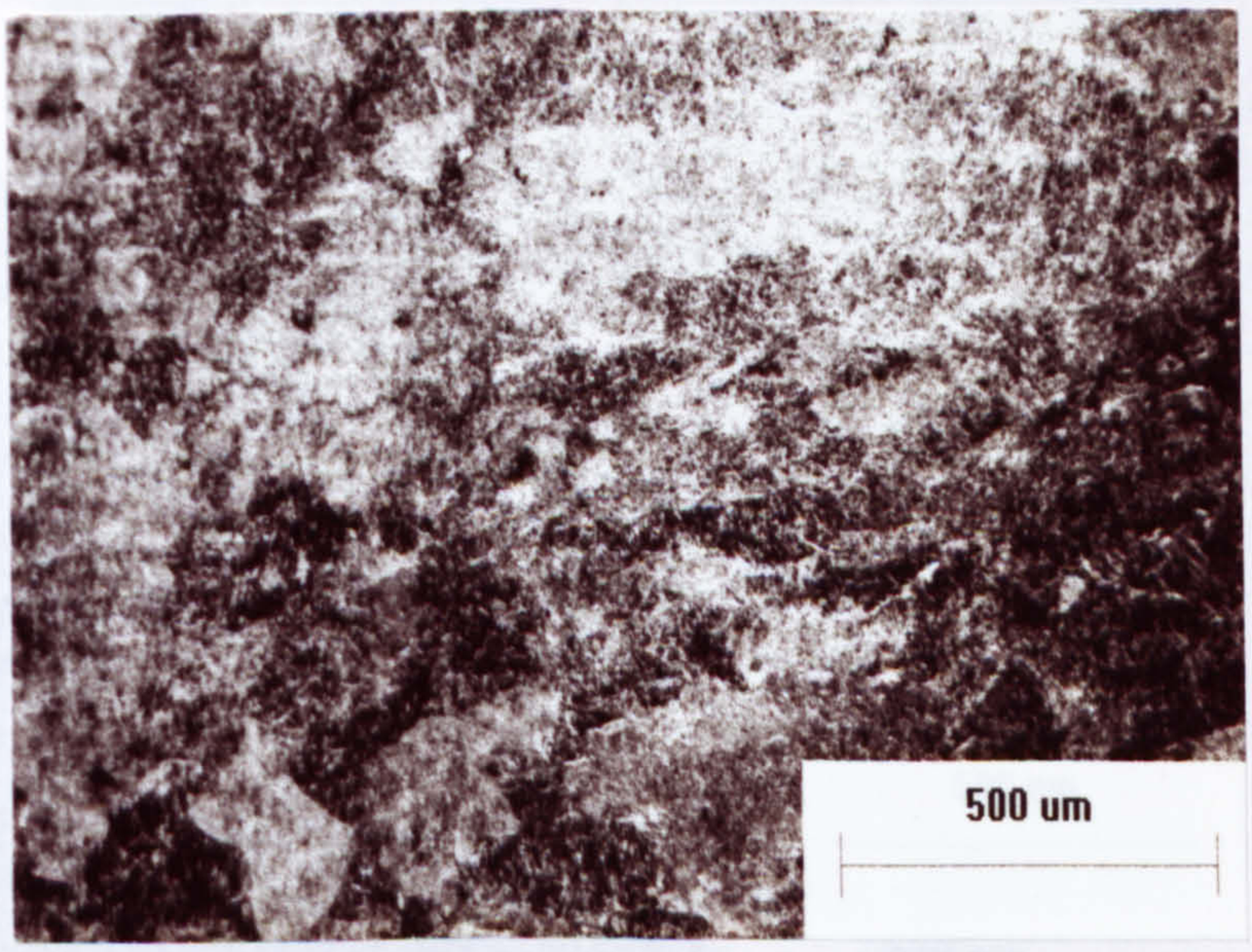

Fig. 4.10 Microstructure in equiaxed zone of Steel 1

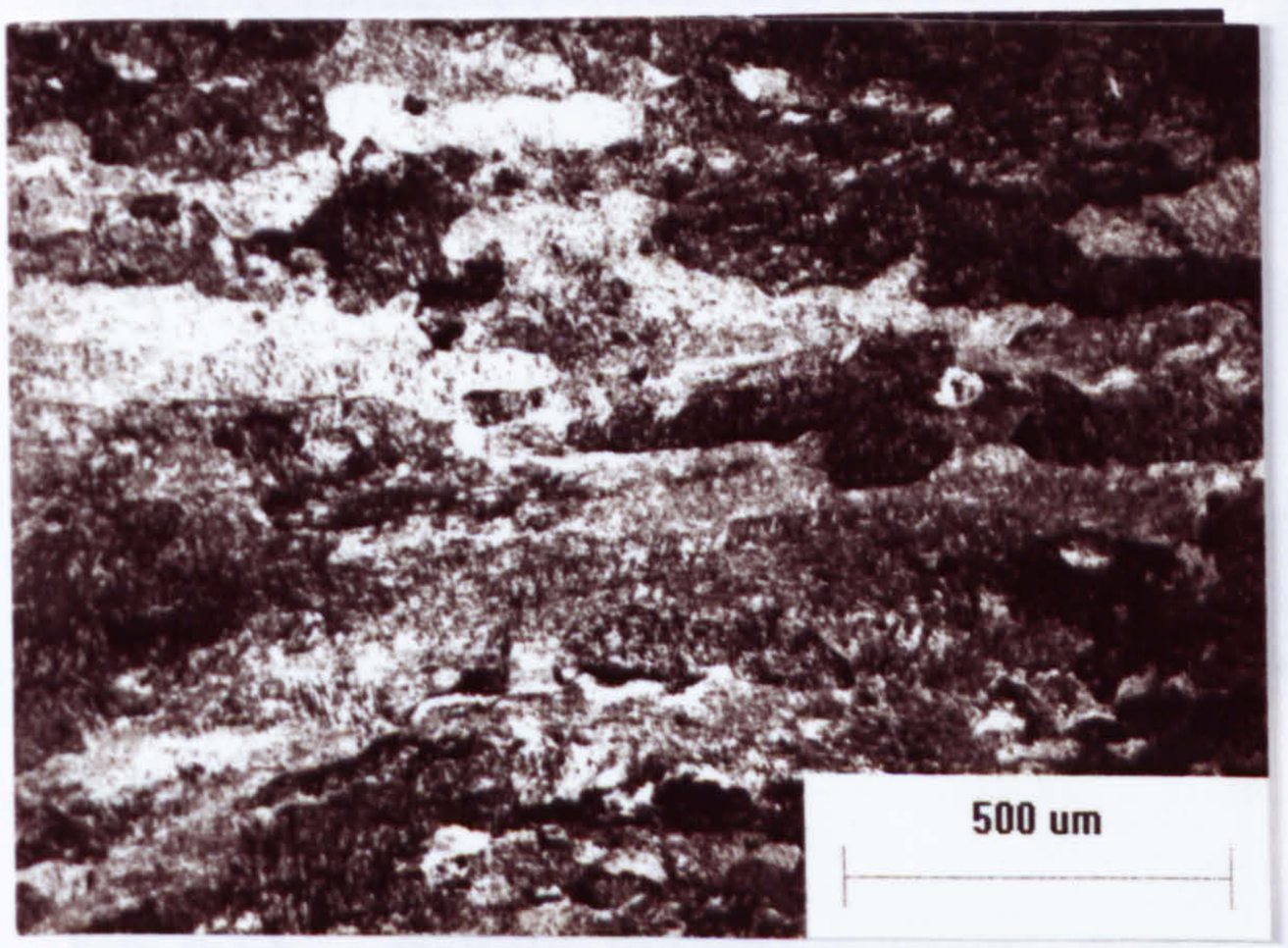

Fig. 4.11 Microstructure in columnar zone of Steel 1

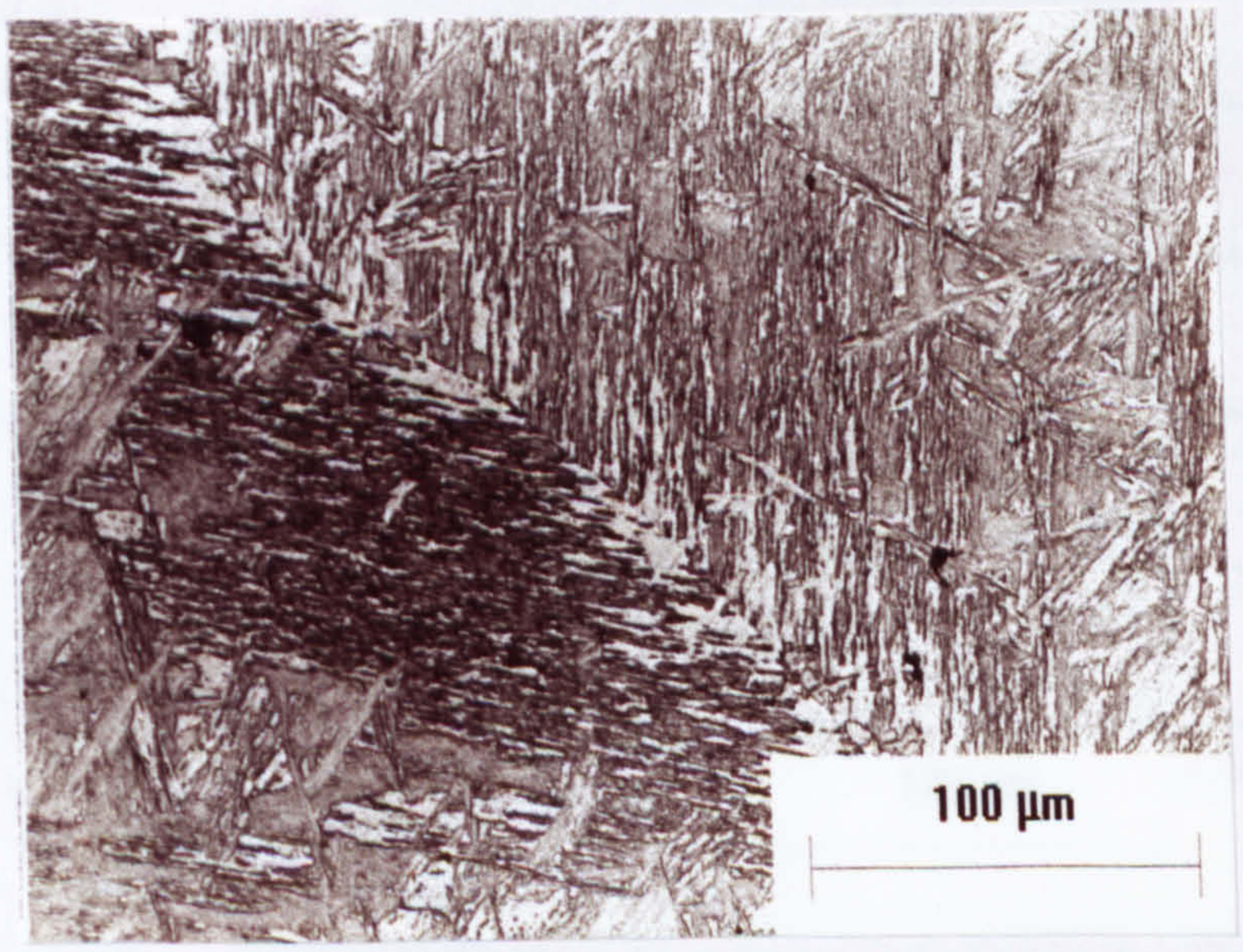

Fig. 4.12 Bainitic microstructure beside grain boundary

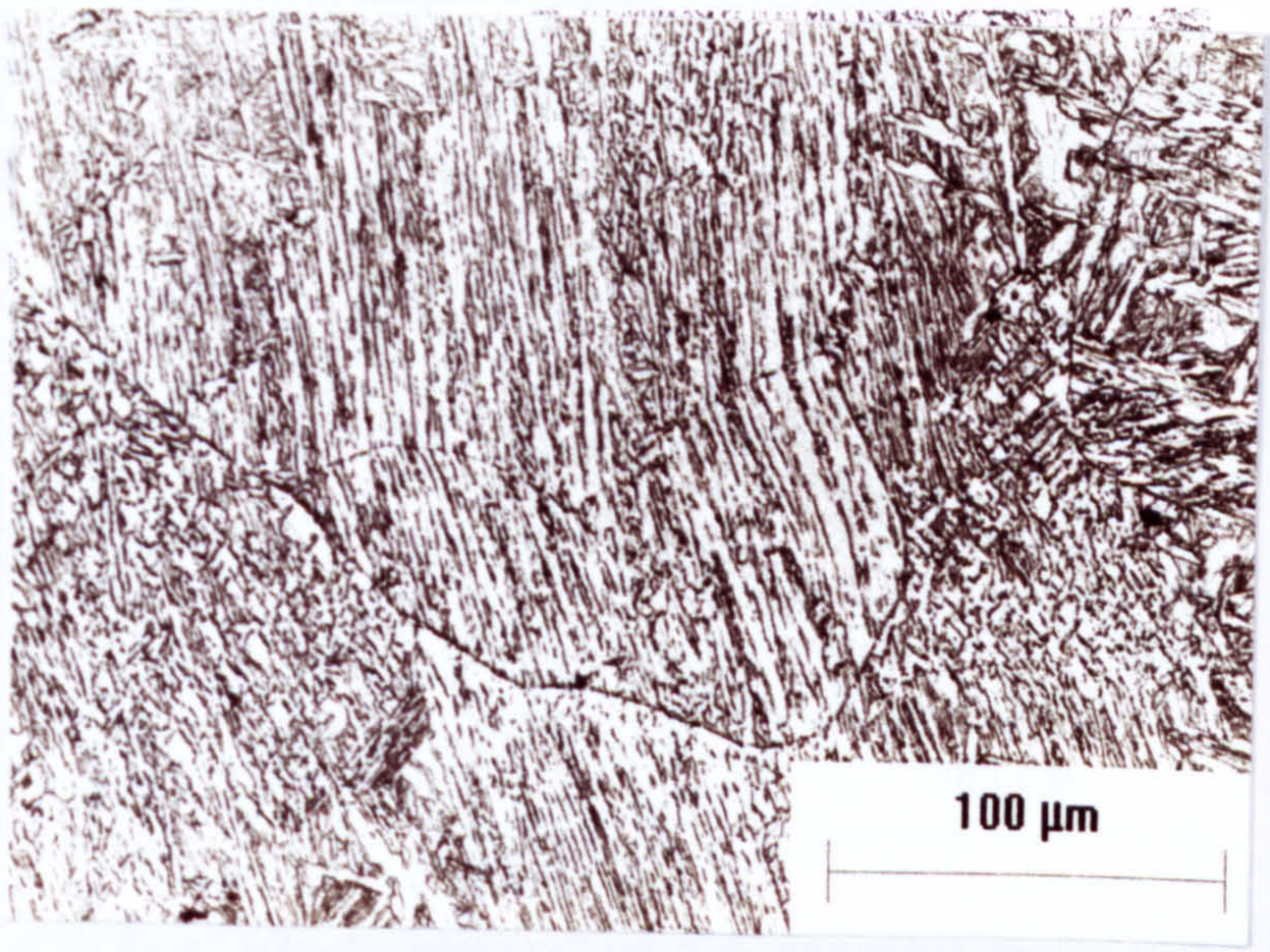

Fig. 4.13 Bainitic microstructure of Steel 1

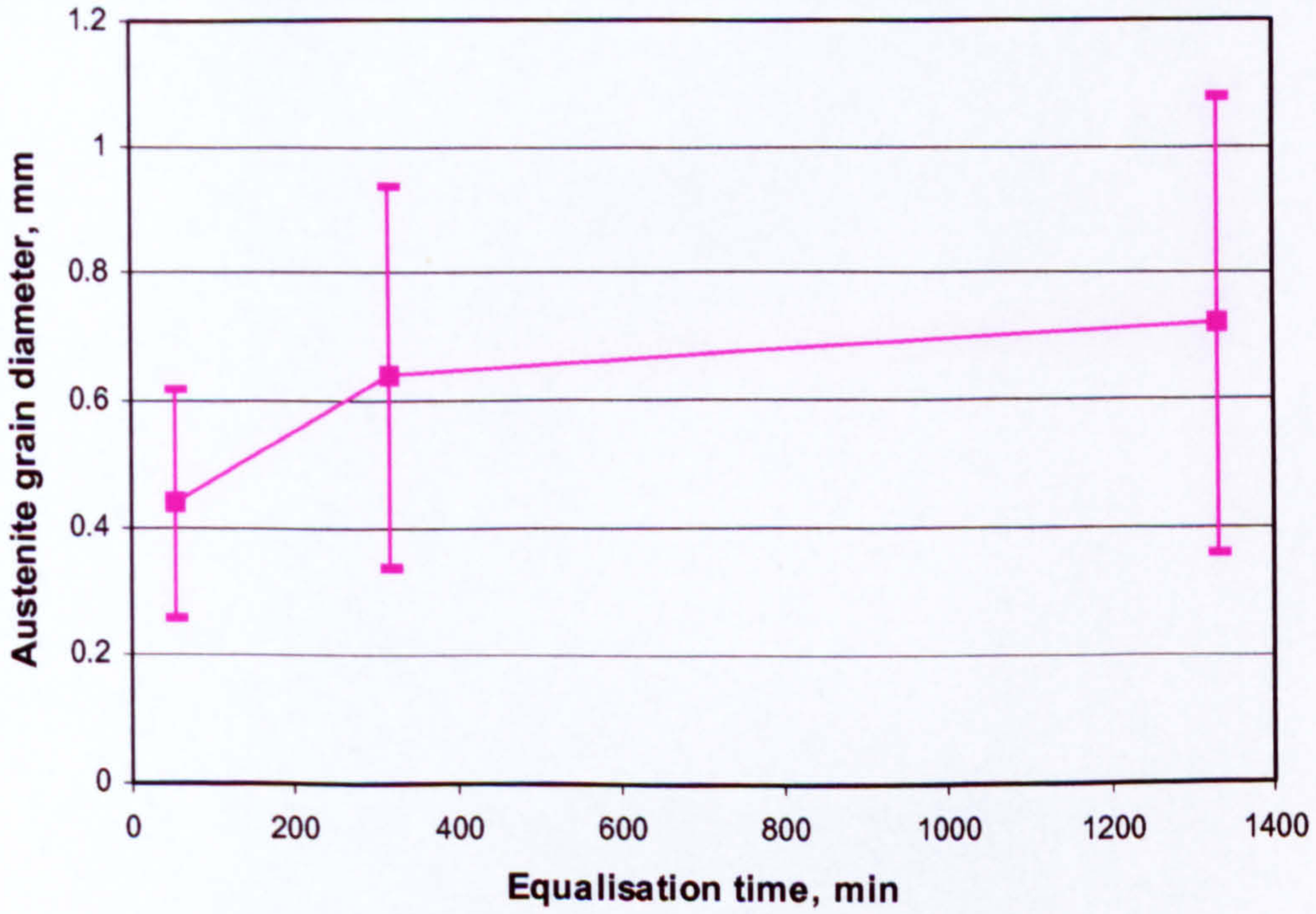

Fig 4.14 Austenite grain size in equiaxed zone of Steel 1 in the different equalisation times after tempering

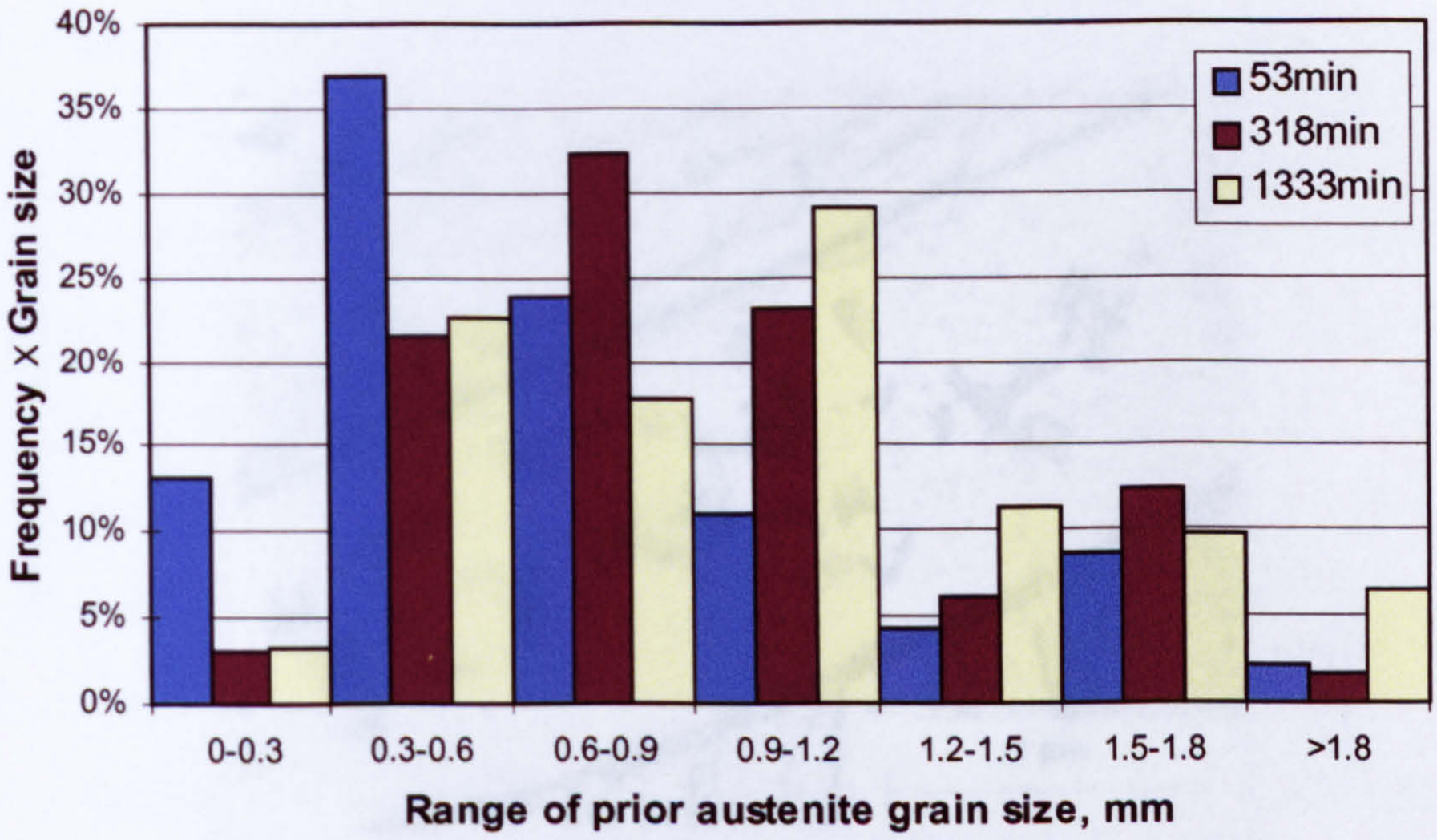

Fig 4.15 Distribution of austenite grain size in equiaxed zone of Steel 1 in the different equalisation times after tempering

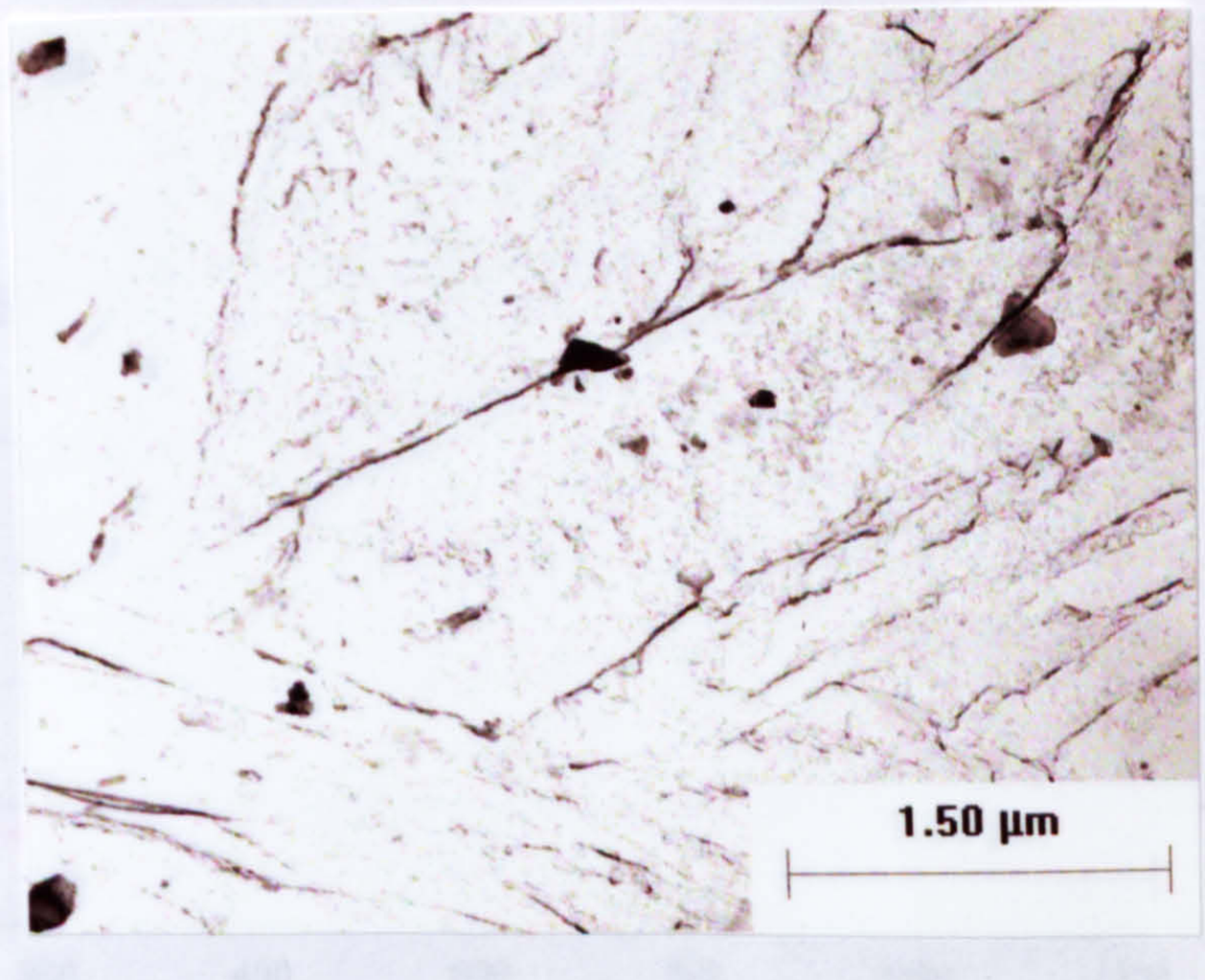

Fig. 4.16 Martensite lath of Steel 2 reheated at 1150°C

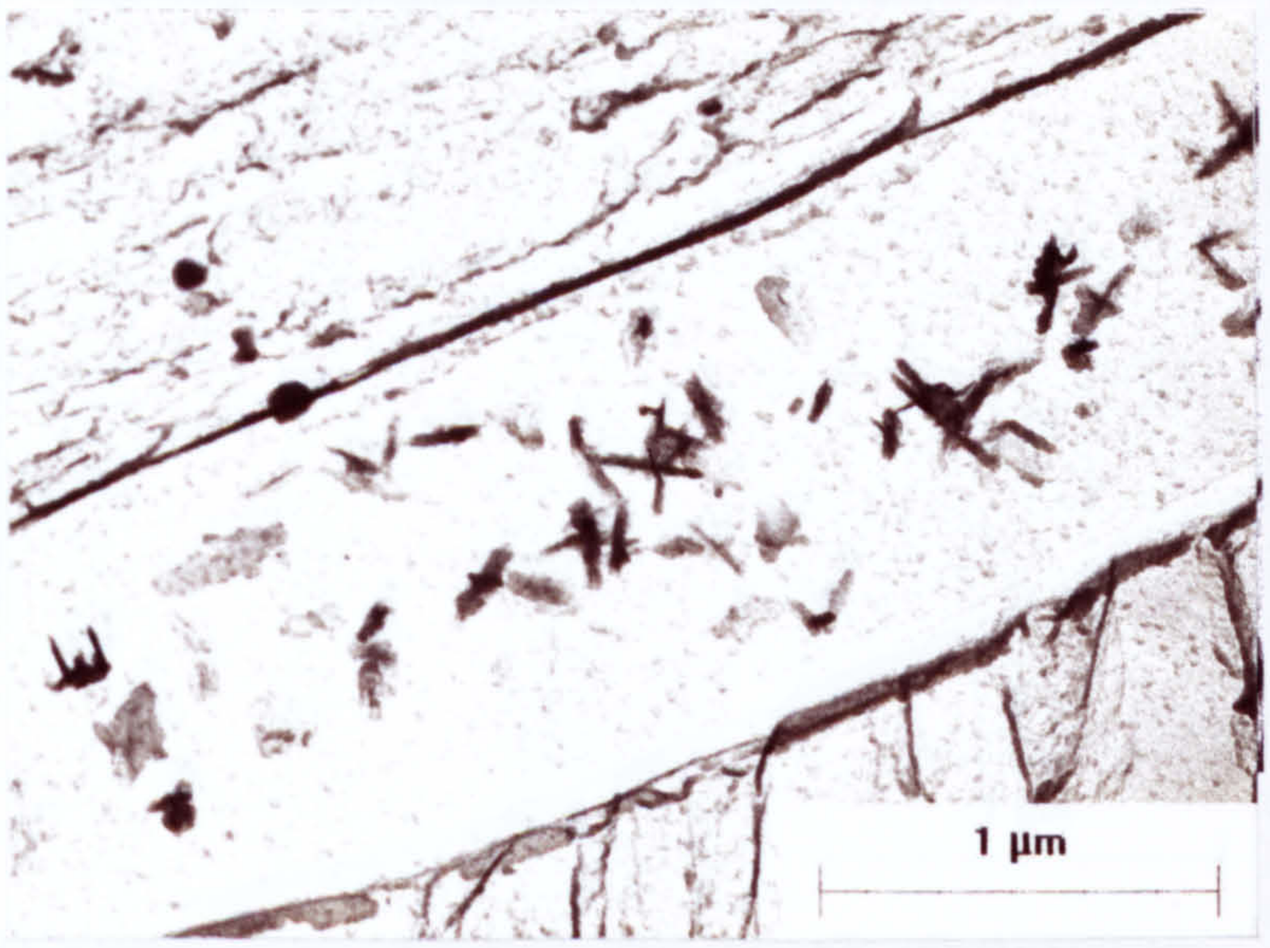

Fig. 4.17 Fe_3C in bainitic ferrite lath of Steel 2 reheated at 1150°C

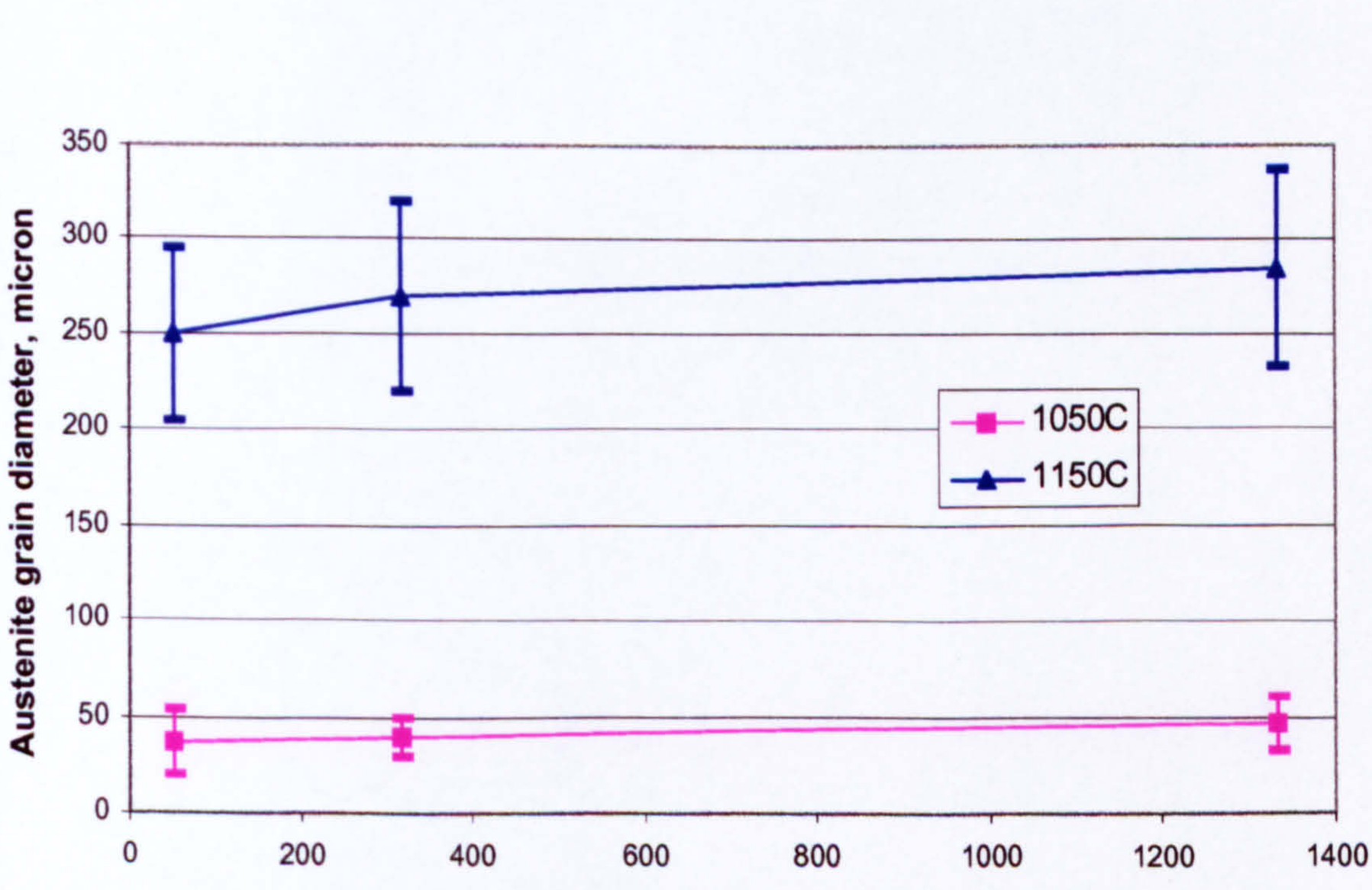

Fig. 4.18 Austenite grain size in non-encapsulated Steel 2 specimens reheated at 1050°C and 1150°C

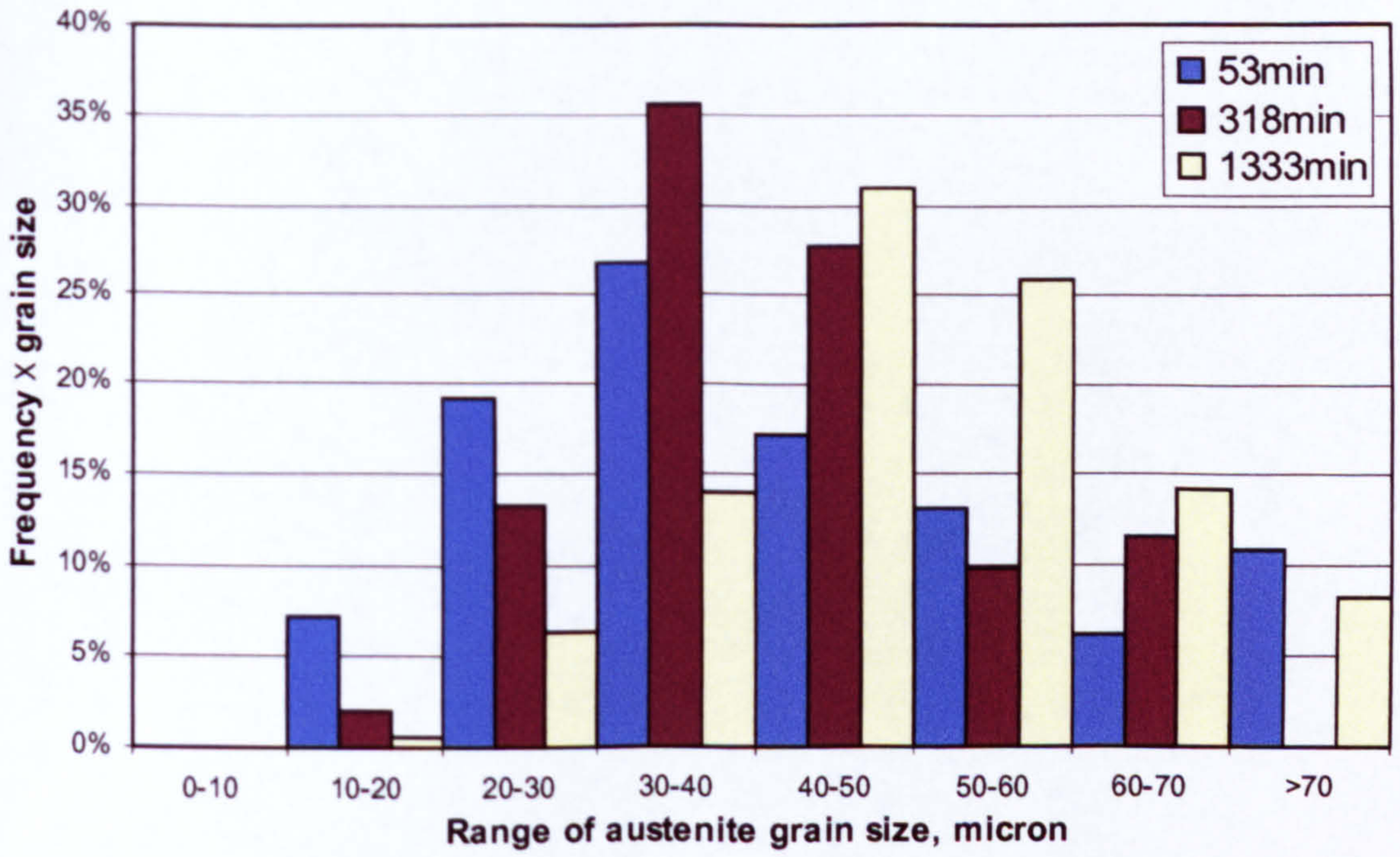

Fig. 4.19 Distribution of austenite grain size in non-encapsulated specimens Steel 2 at 1050°C

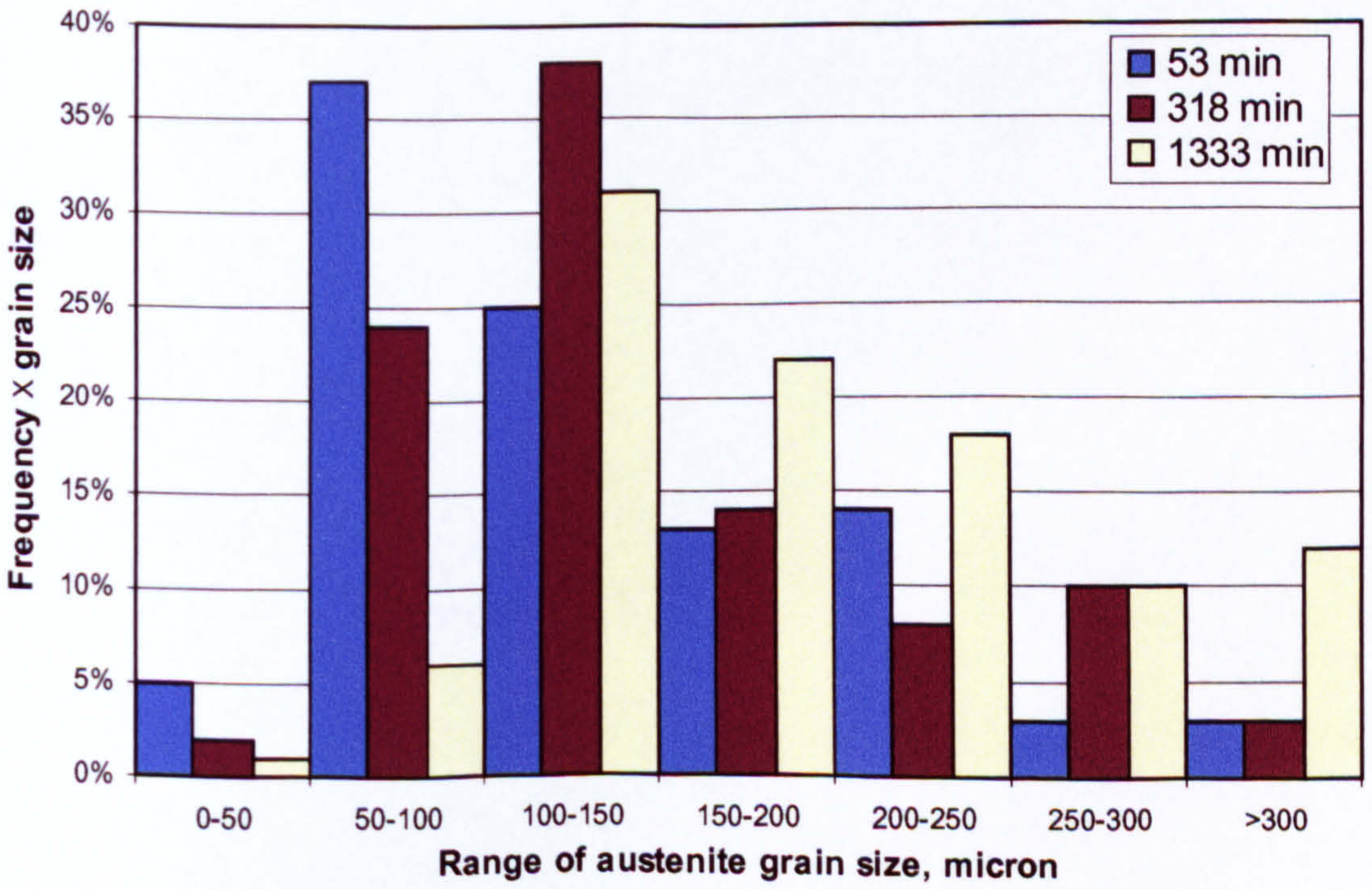

Fig. 4.20 Distribution of austenite grain size in non-encapsulated Steel 2 specimens at 1150°C

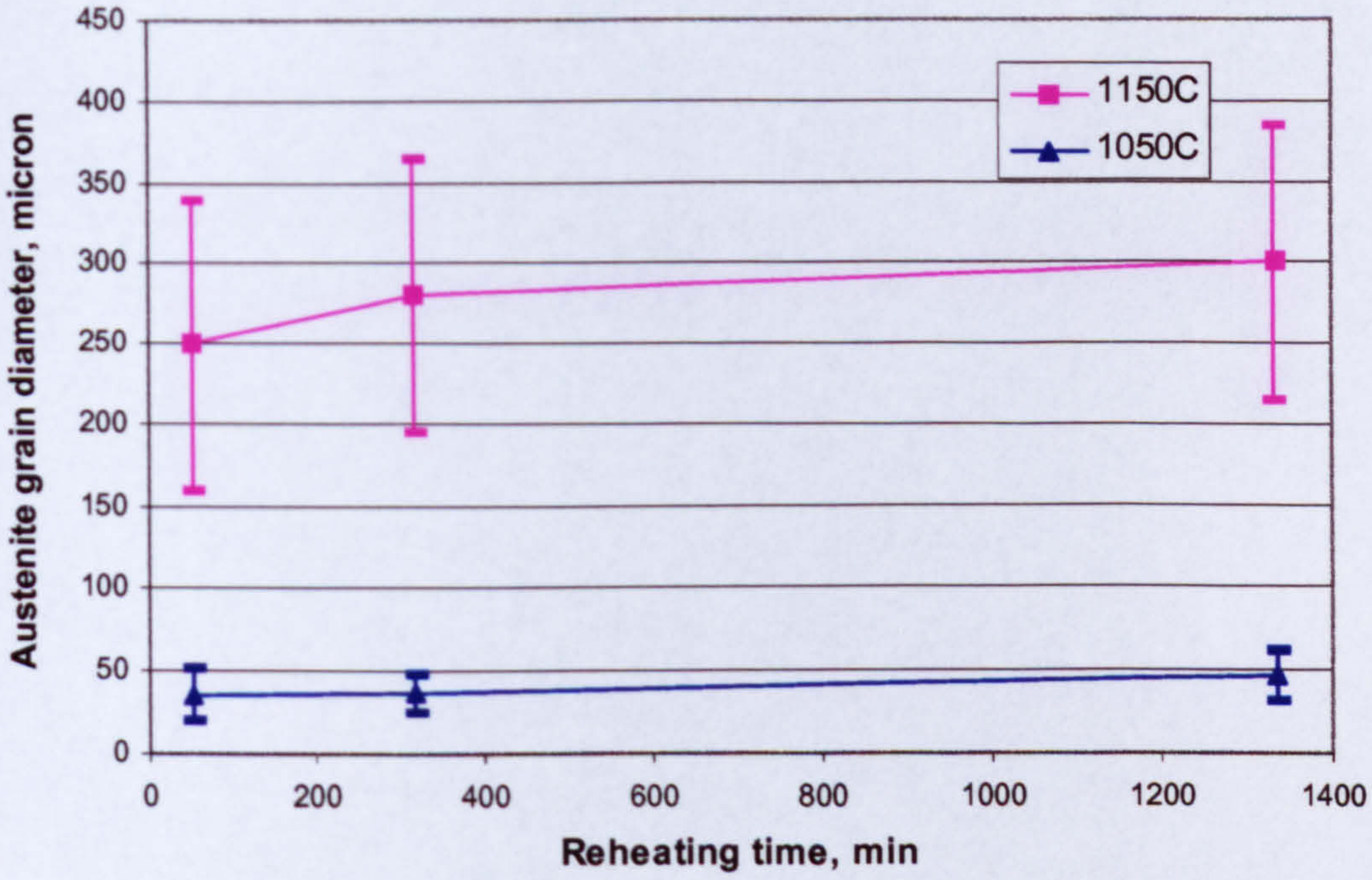

Fig. 4.21 Austenite grain size in encapsulated Steel 2 specimens reheated at 1050°C and 1150°C

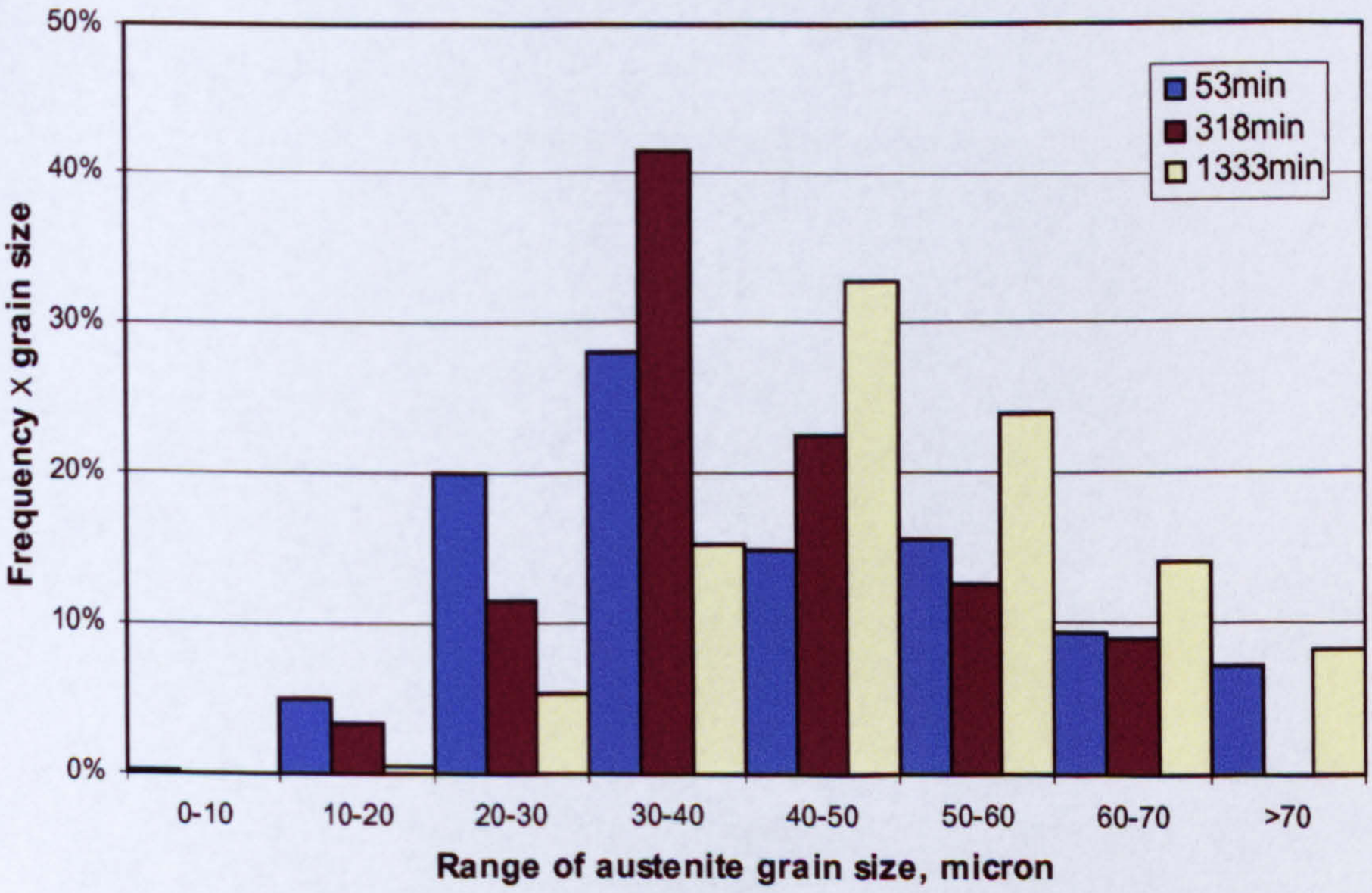

Fig. 4.22 Distribution of austenite grain size in encapsulated Steel 2 specimens at 1050°C

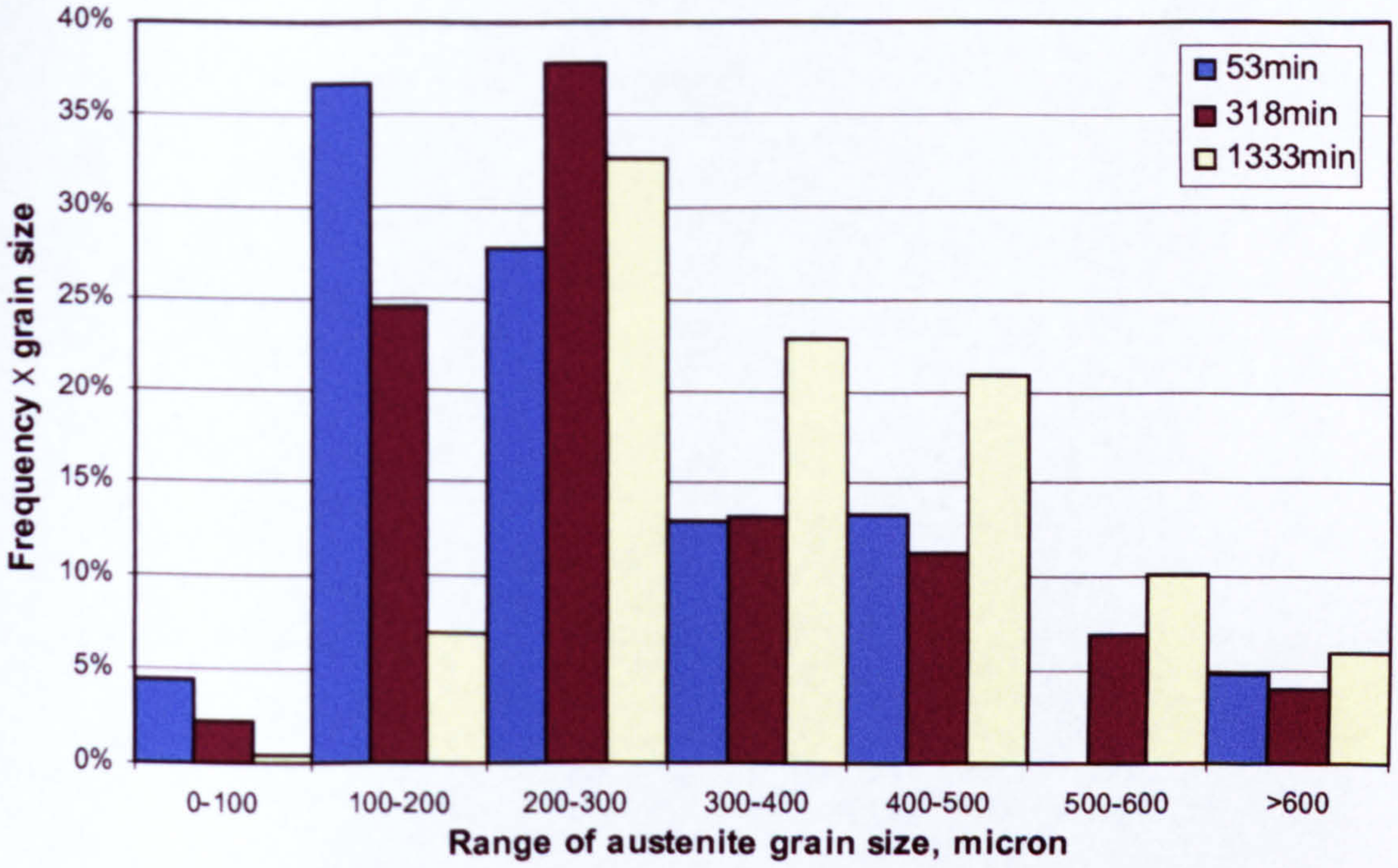

Fig. 4.23 Distribution of austenite grain size in encapsulated Steel 2 specimens at 1150°C

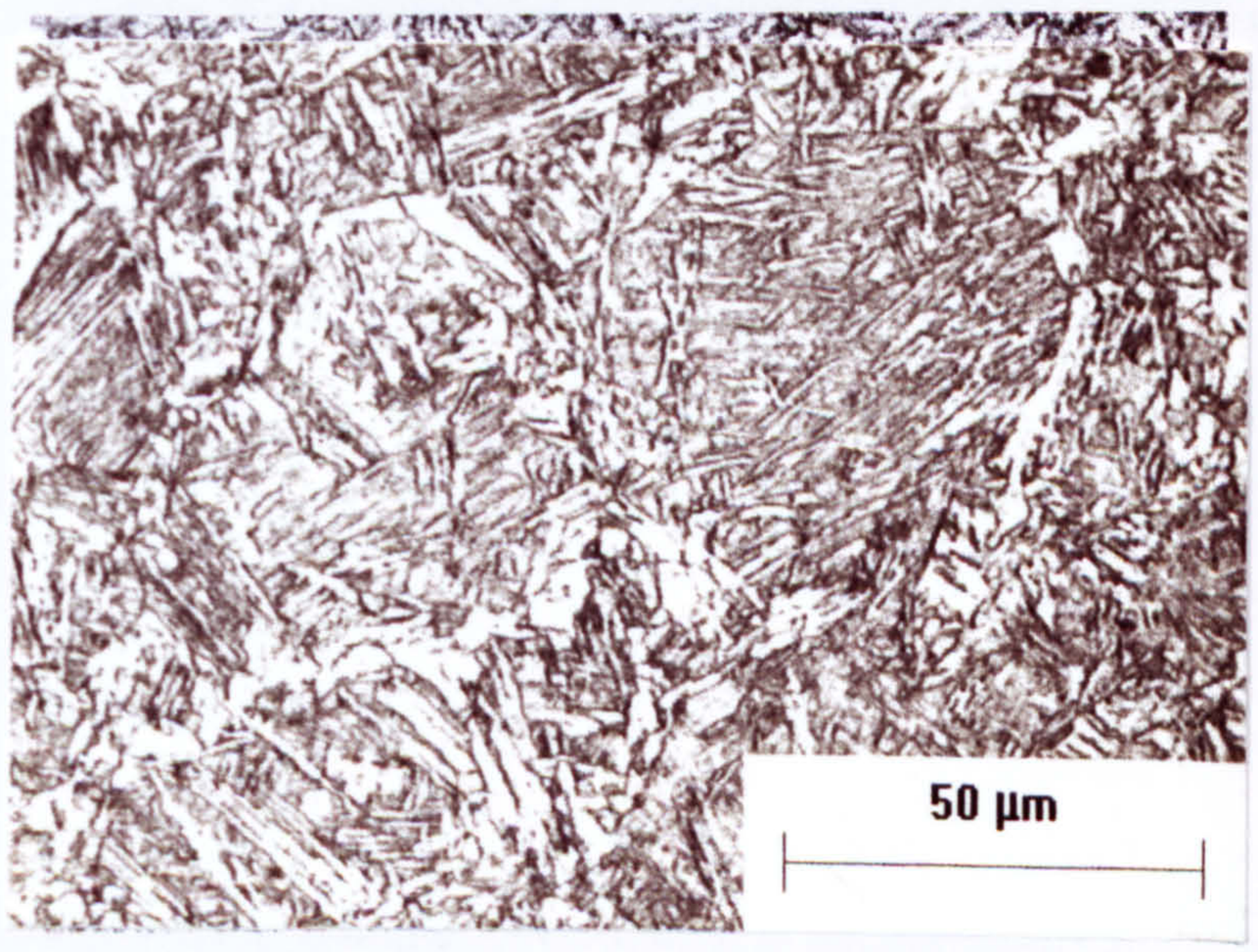

Fig. 4.24 Austenite grain microstructure in encapsulated Steel 2 specimens at 1150°C

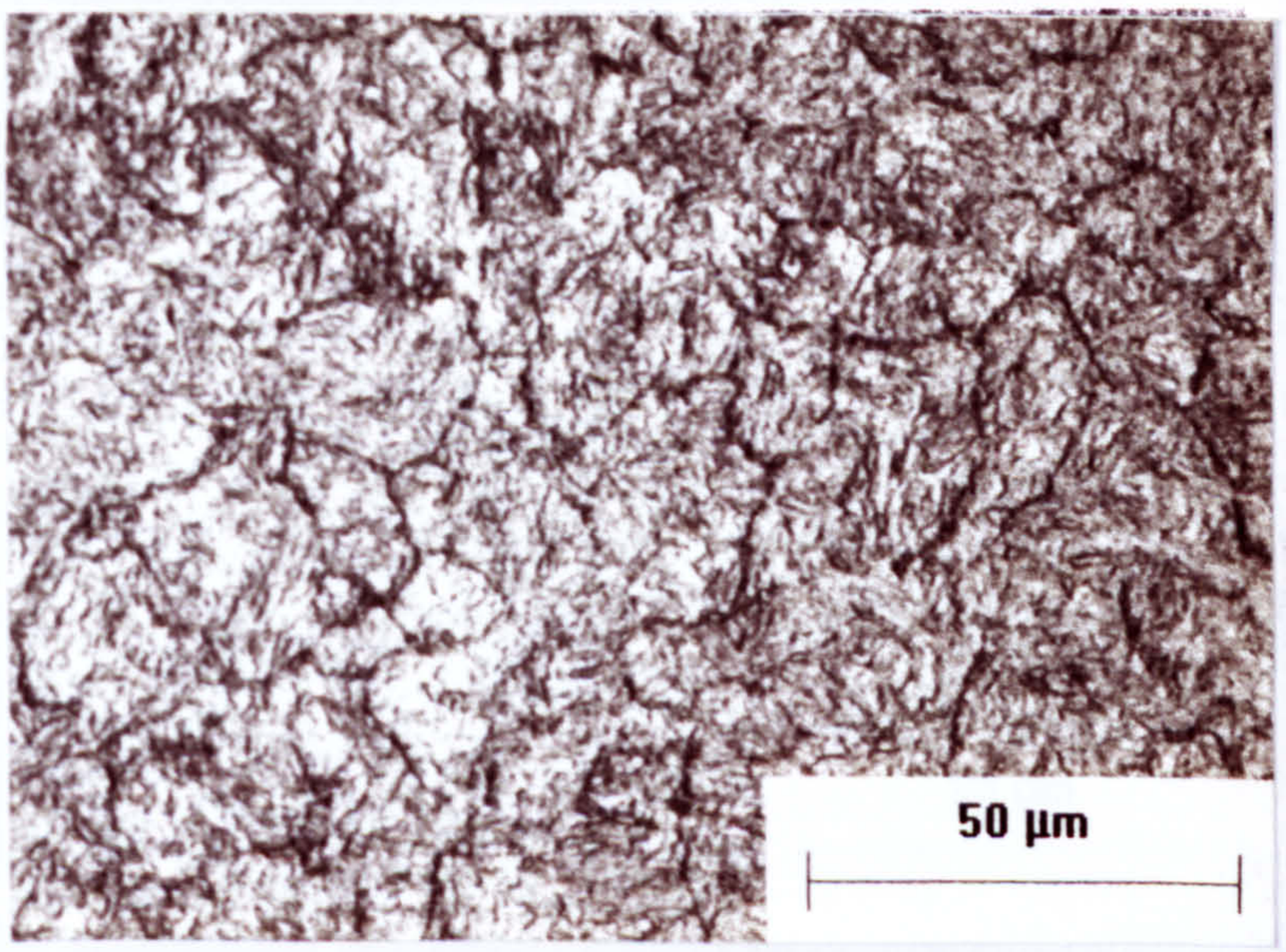

Fig. 4.25 Austenite grain microstructure in encapsulated Steel 3 specimens at 1050°C

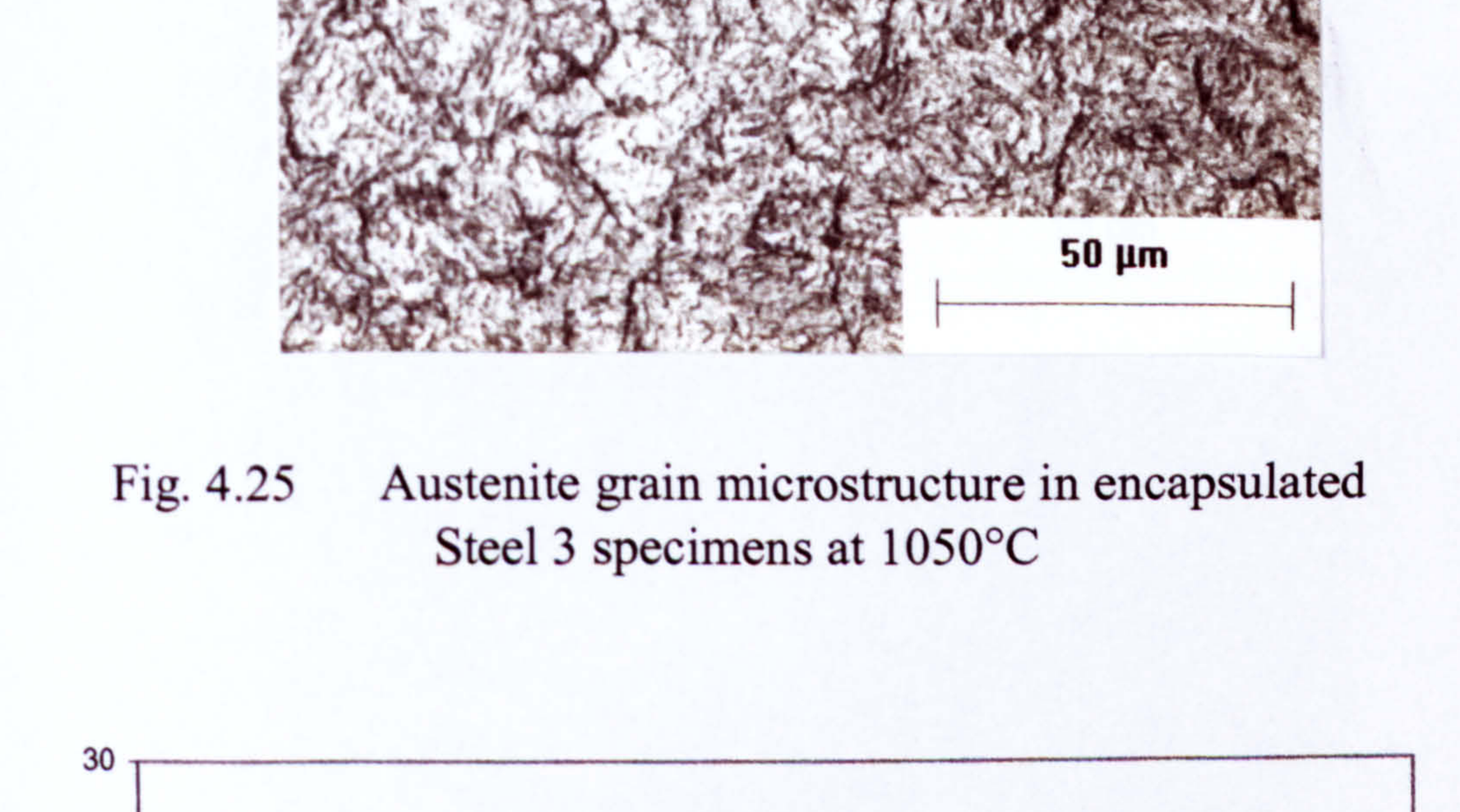

Fig. 4.26 Austenite grain size in encapsulated Steel 3 specimens reheated at 1050°C

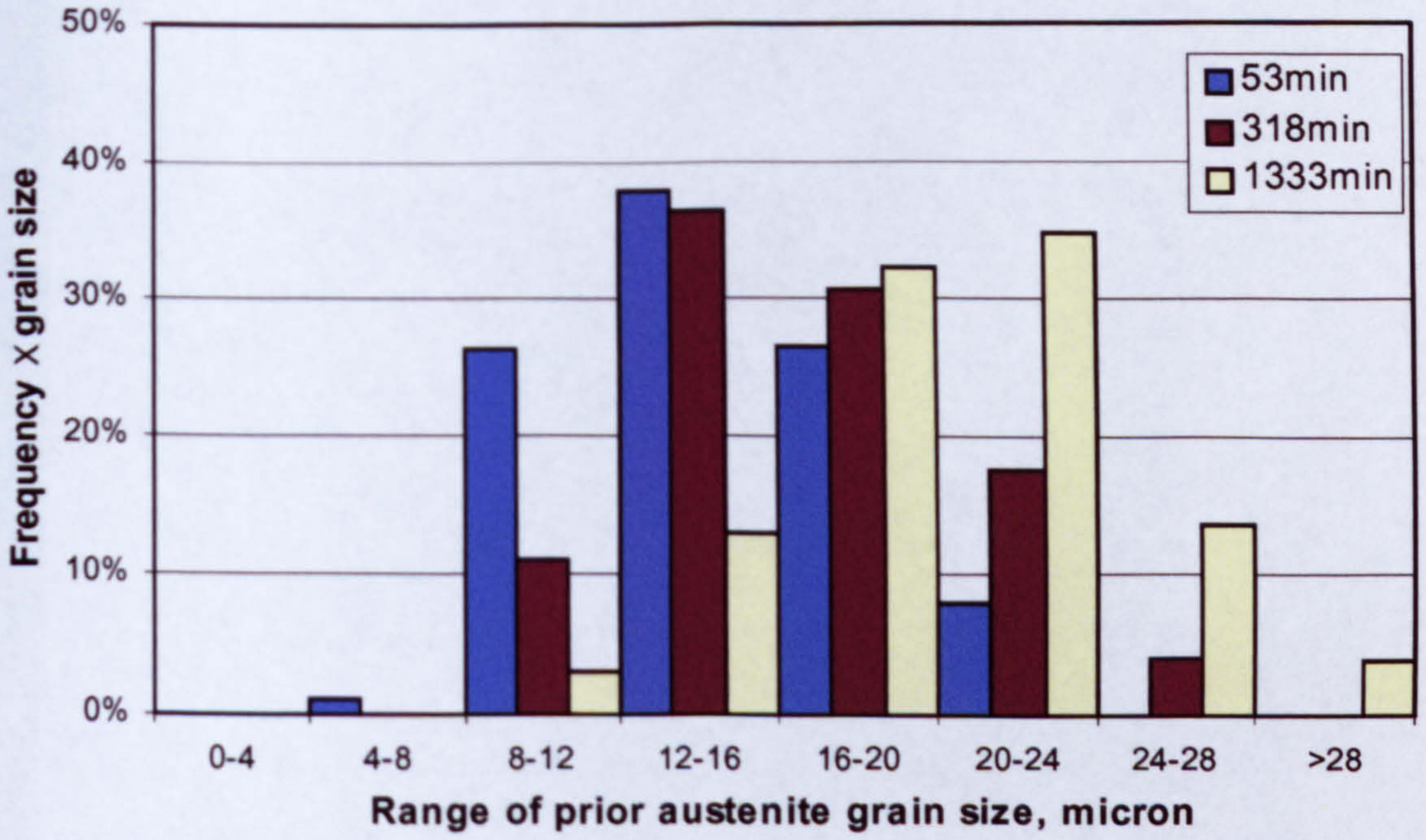

Fig. 4.27 Distribution of austenite grain size in encapsulated Steel 3 specimens at 1050°C

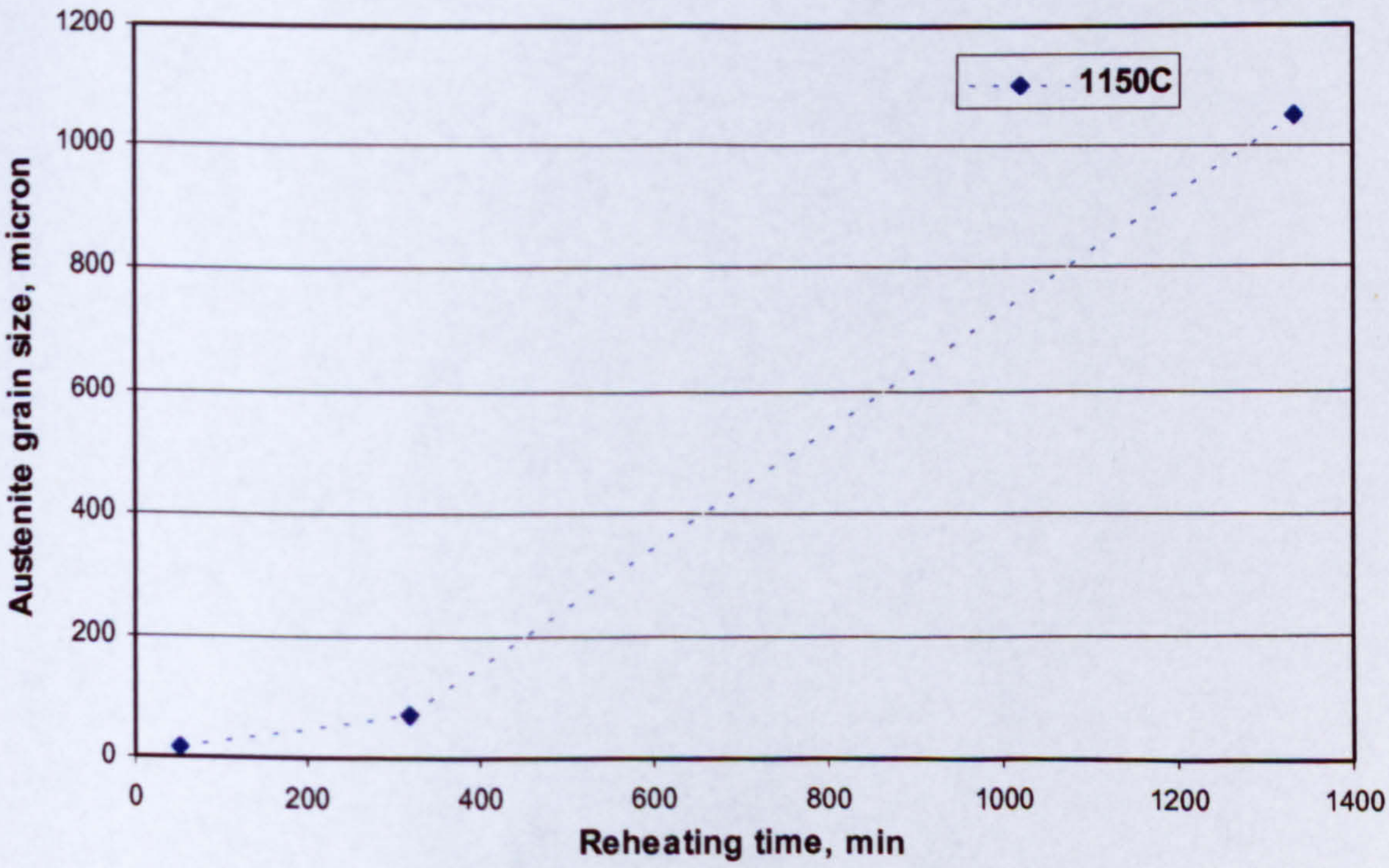

Fig. 4.28 Austenite grain size in encapsulated Steel 3 specimens reheated at 1150°C

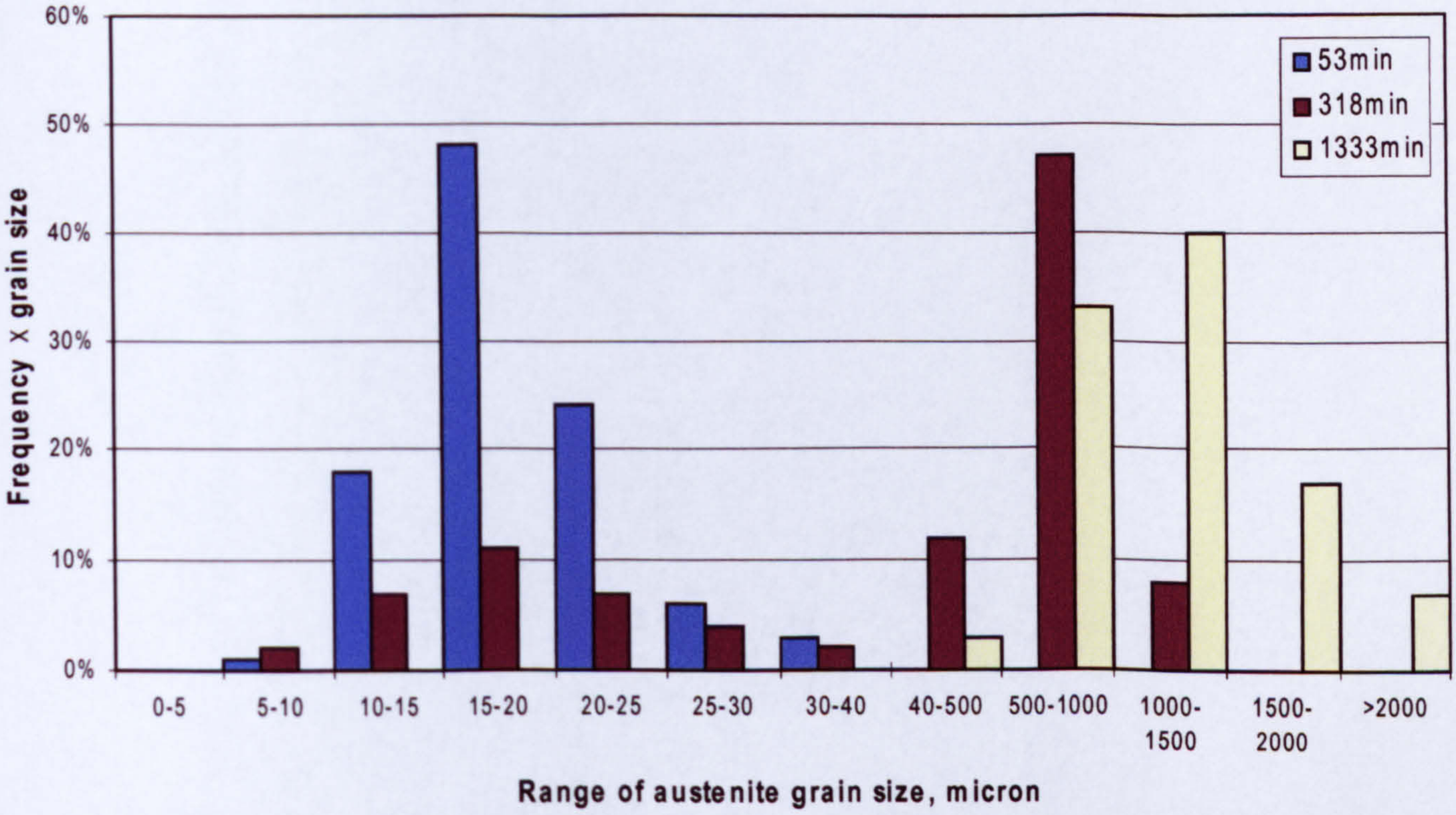

Fig. 4.29 Distribution of austenite grain size non-encapsulated Steel 3 specimens at 1150°C

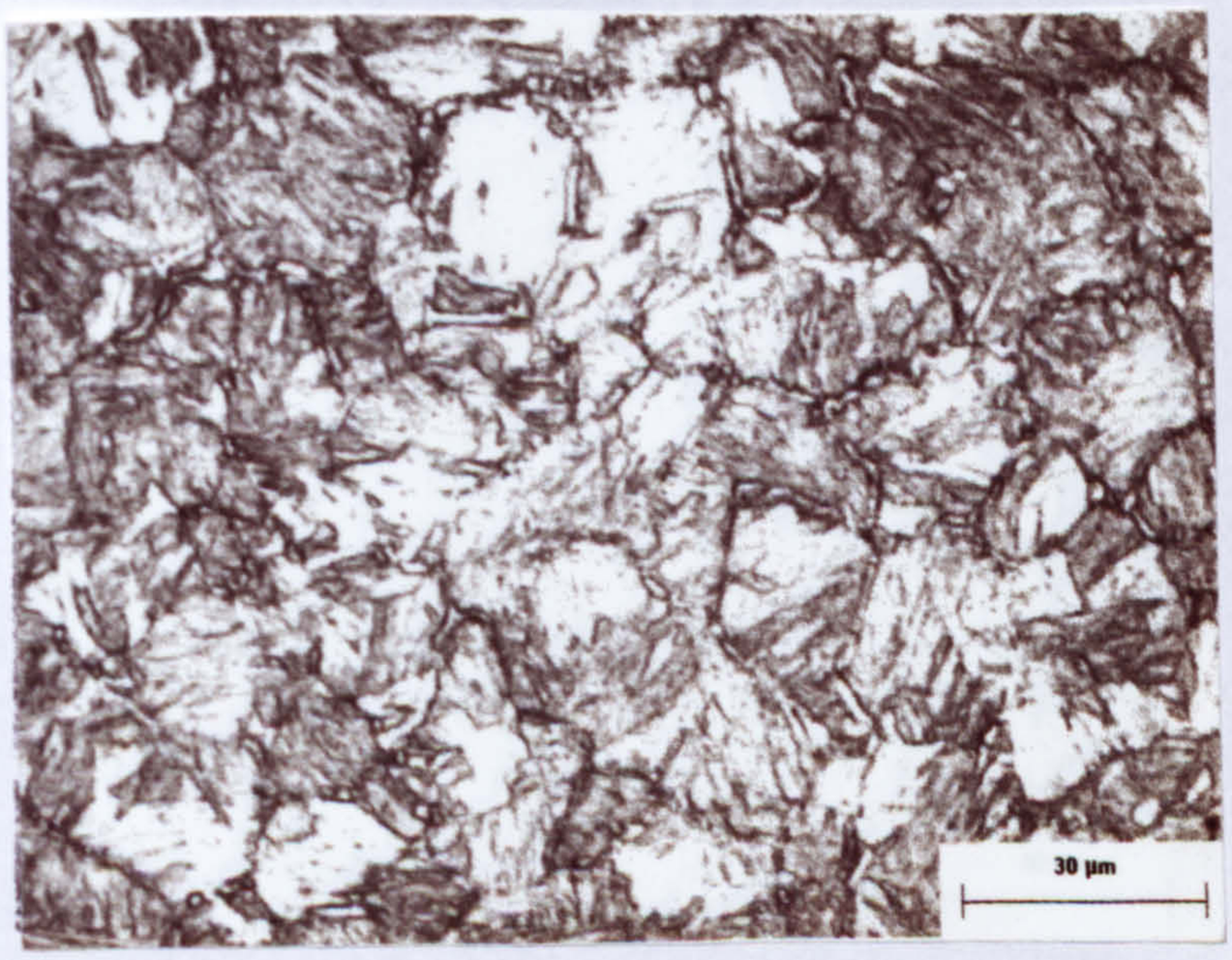

Fig. 4.30 Austenite grain microstructure in encapsulated Steel 3 specimens at 1150°C for 53min

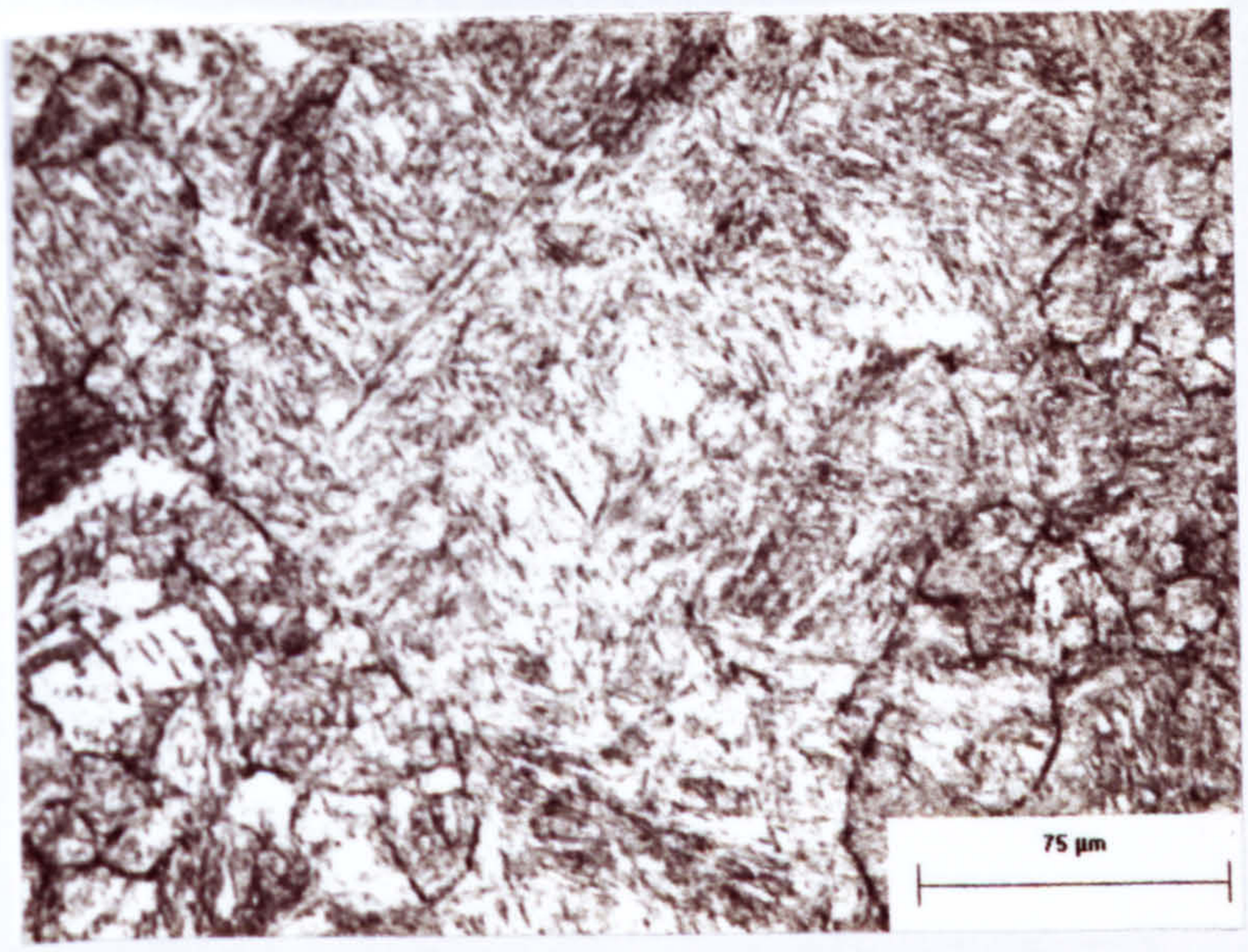

Fig. 4.31 Austenite grain microstructure in encapsulated Steel 3 specimens at 1150°C for 318min

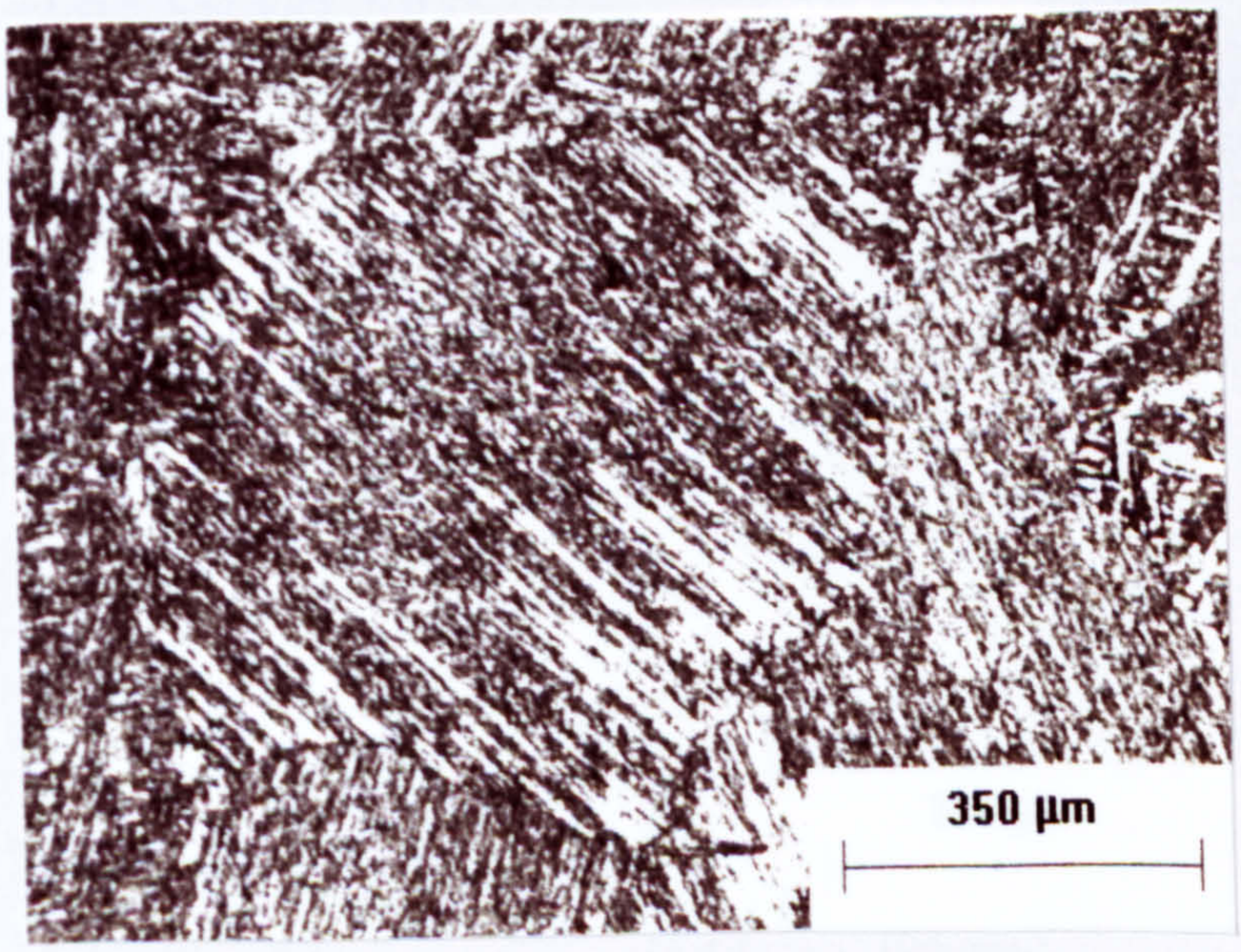

Fig. 4.32 Austenite grain microstructure in encapsulated Steel 3 specimens at 1150°C for 1333min

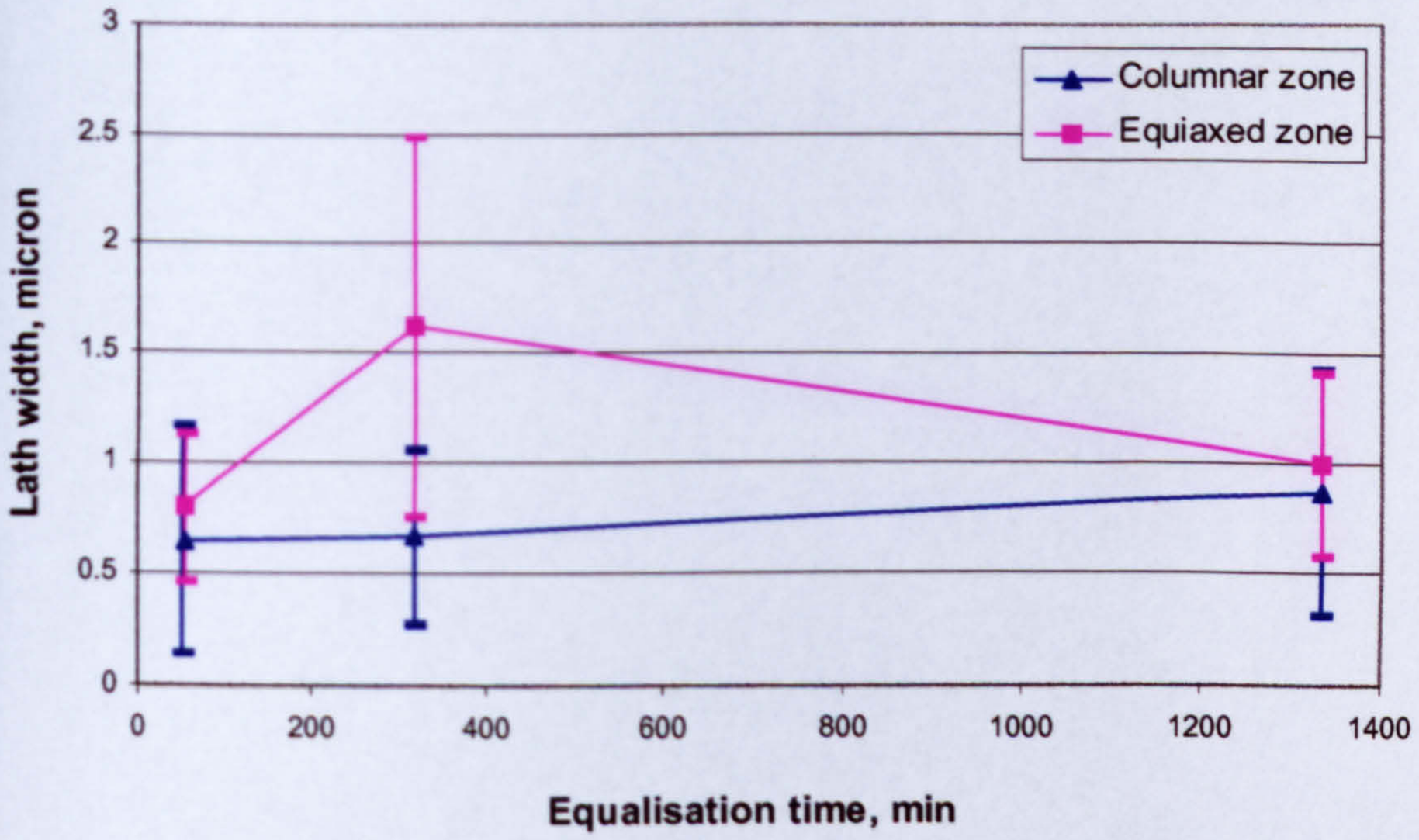

Fig. 4.33 Lath width in Steel 1 equalised at 1150°C before tempering

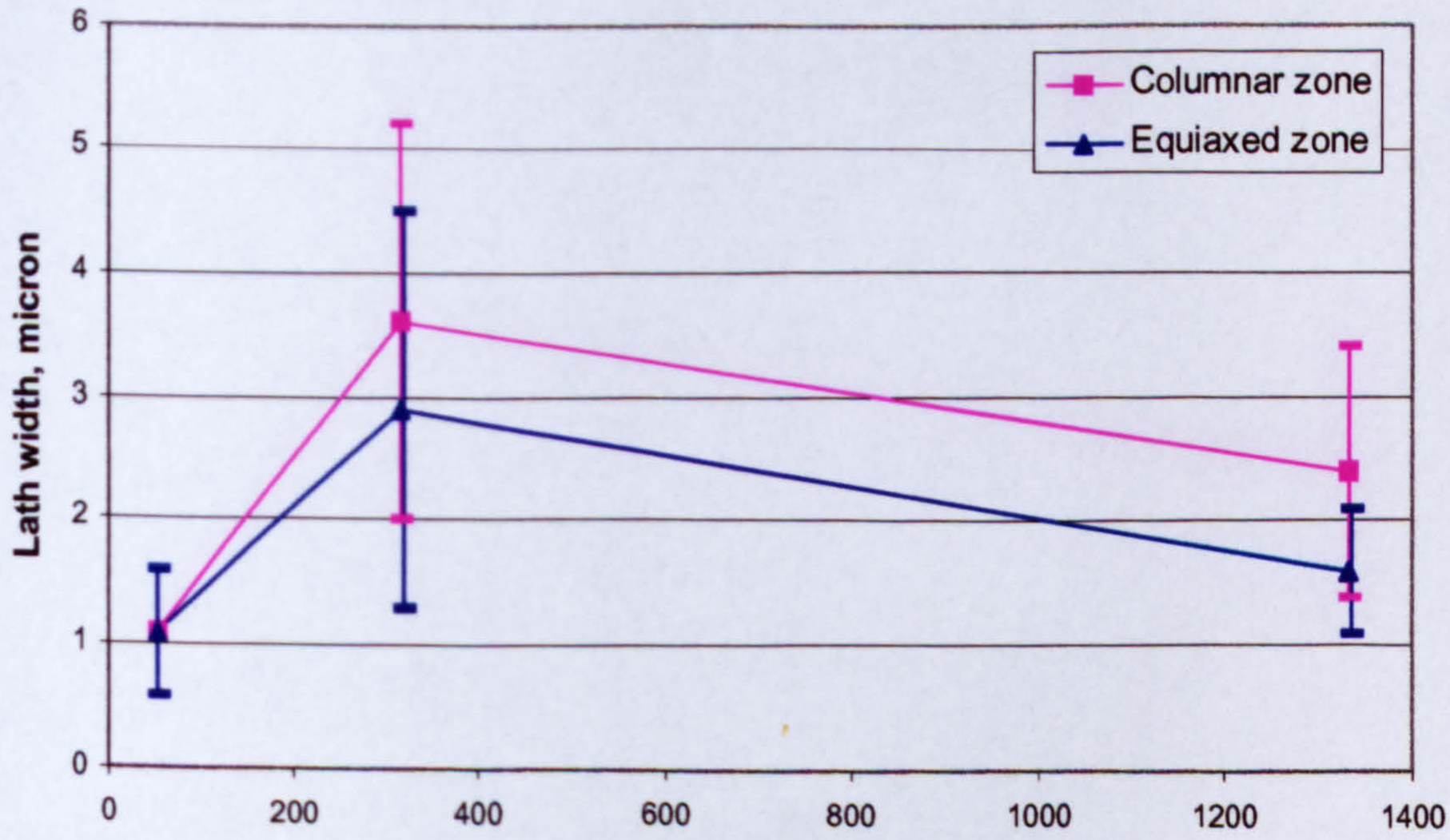

Fig. 4.34 Lath width in Steel 1 equalised at 1150°C after tempering

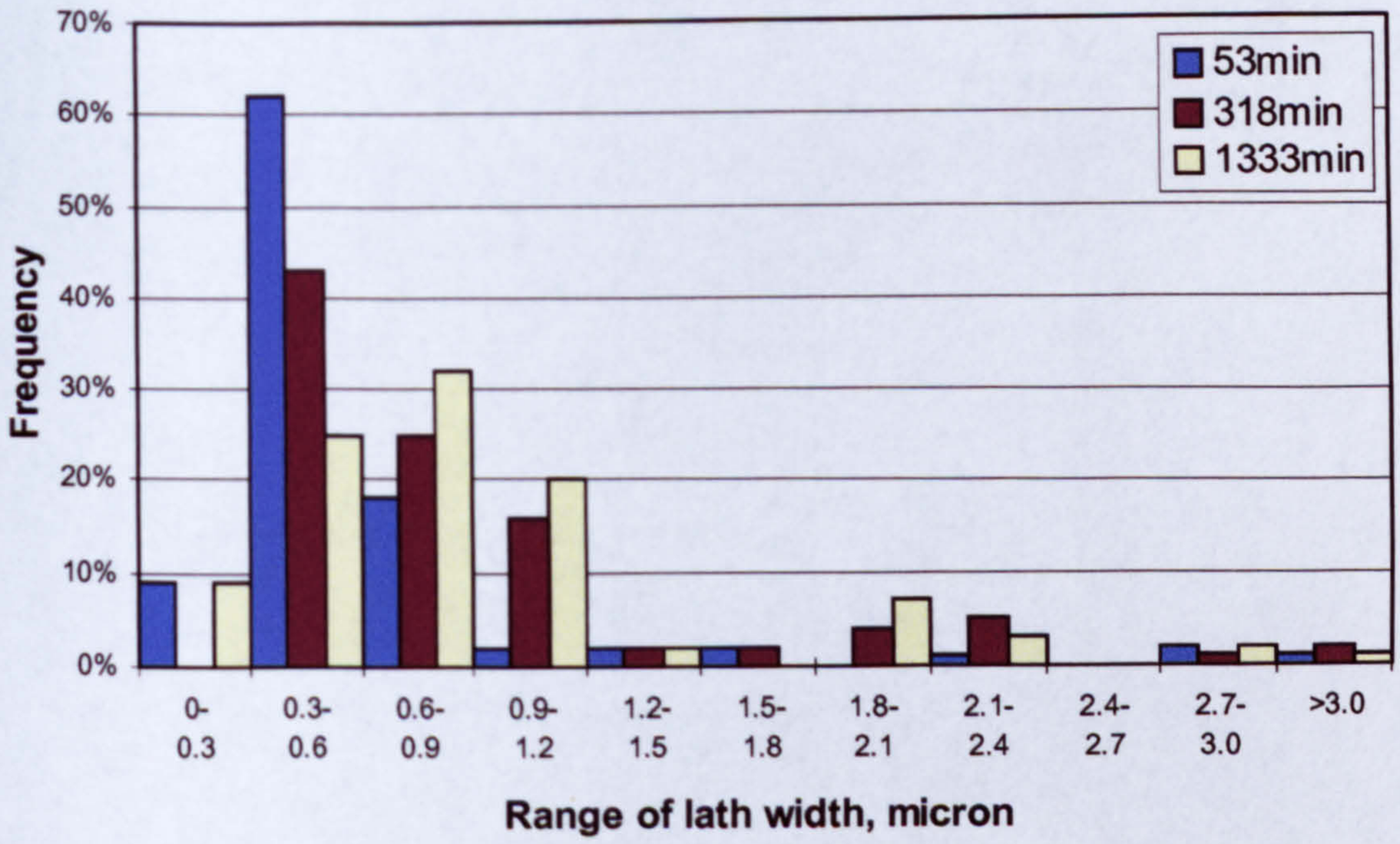

Fig. 4.35 Distribution of lath width in the columnar zone of Steel 1 equalised at 1150°C before tempering

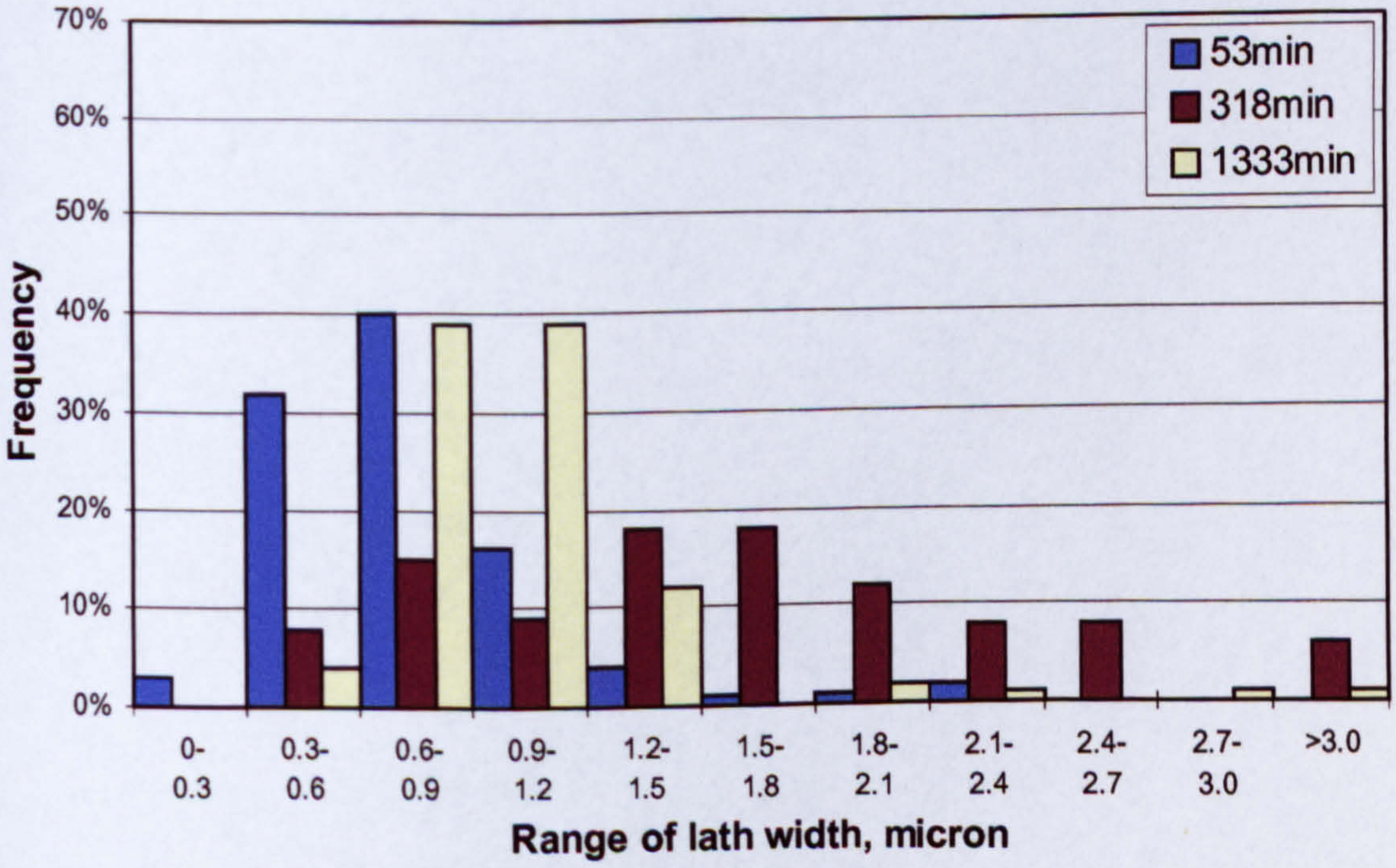

Fig. 4.36 Distribution of lath width in the equiaxed zone of Steel 1 equalised at 1150°C before tempering

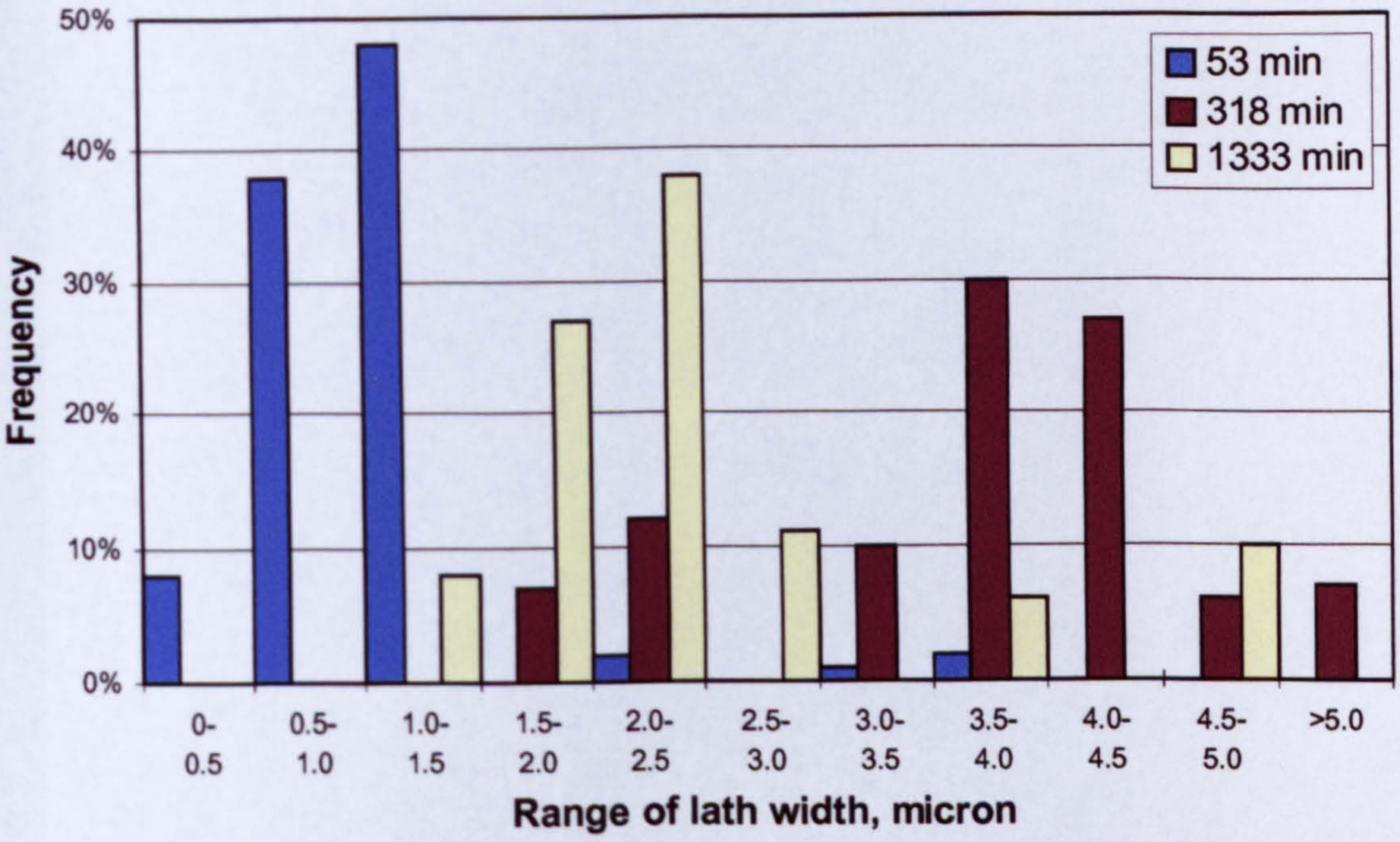

Fig. 4.37 Distribution of lath width in the columnar zone of Steel 1 equalised at 1150°C after tempering

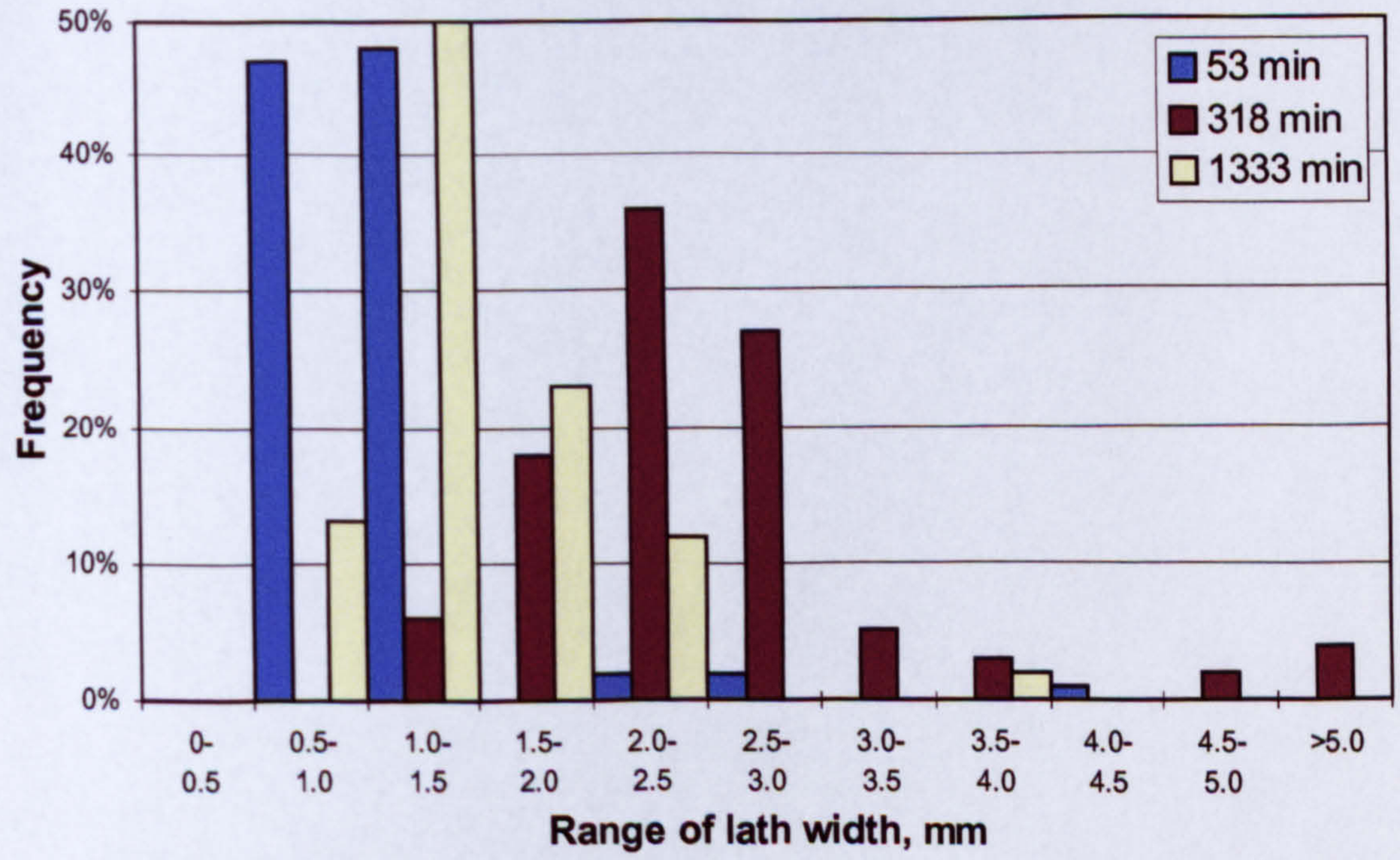

Fig. 4.38 Distribution of lath width in the equiaxed zone of Steel 1 equalised at 1150°C after tempering

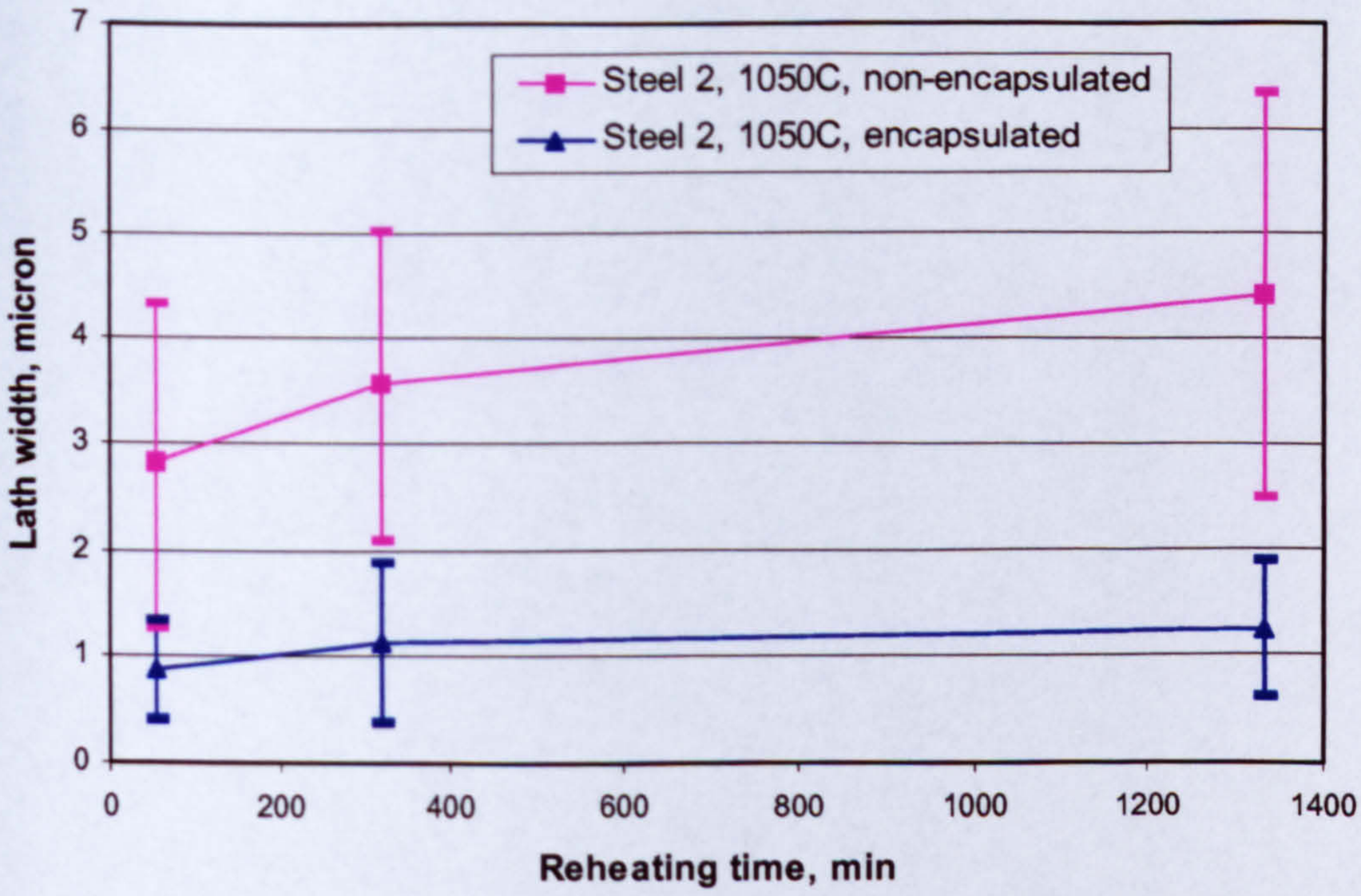

Fig. 4.39 Lath width in Steel 2 reheated at 1050°C

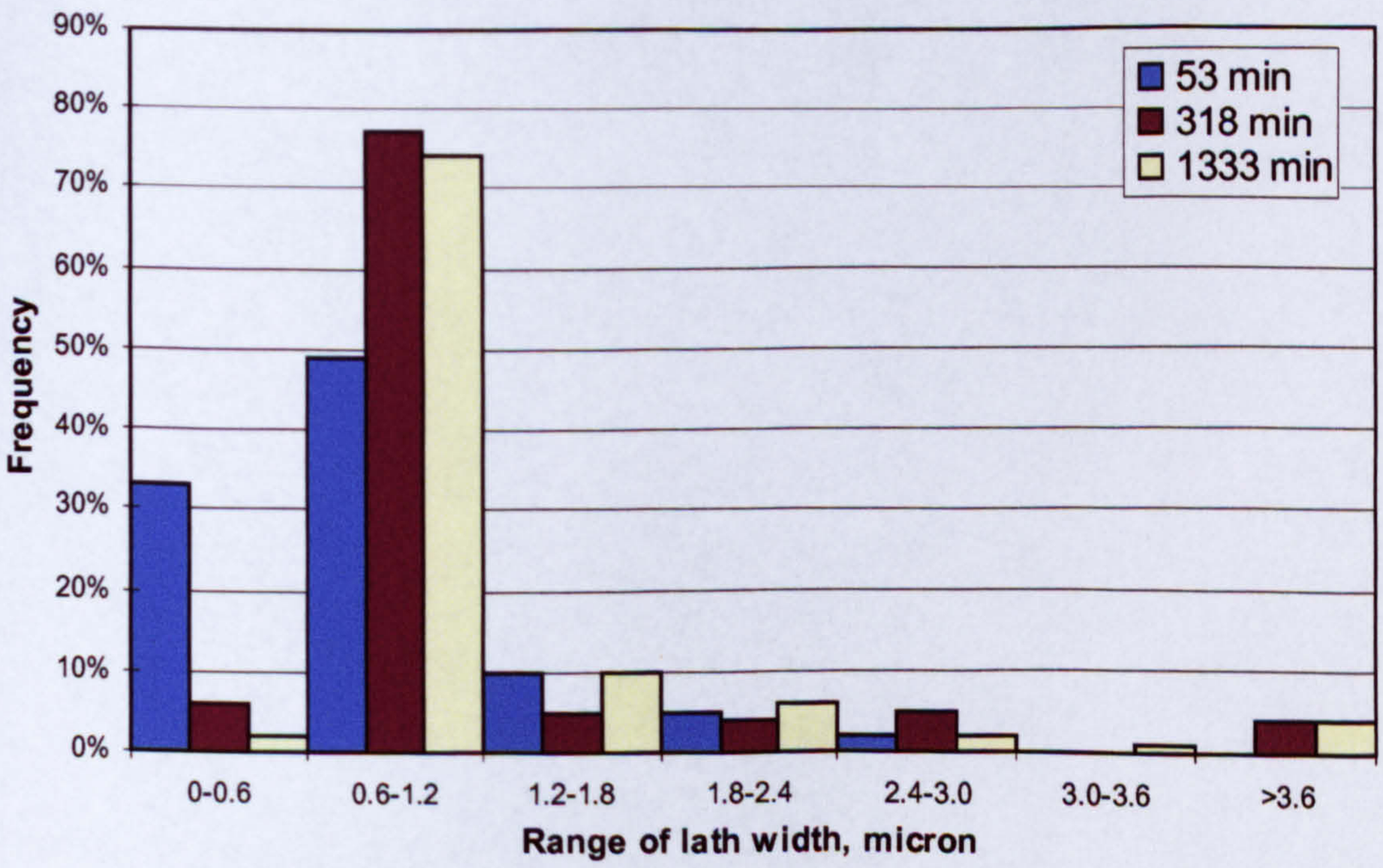

Fig. 4.40 Distribution of lath width in non-encapsulated Steel 2 reheated at 1050°C

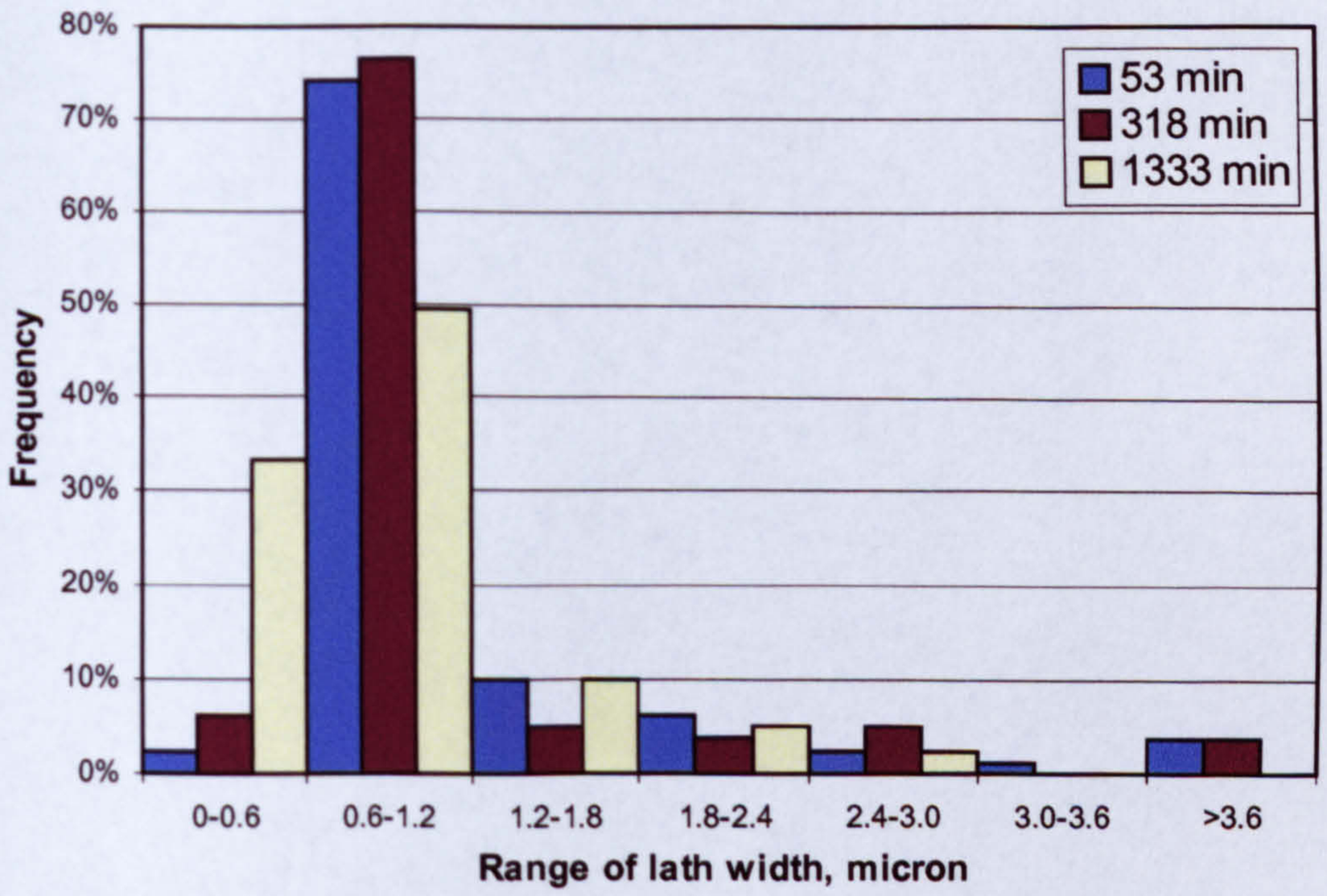

Fig. 4.41 Distribution of lath width in encapsulated Steel 2 reheated at 1050°C

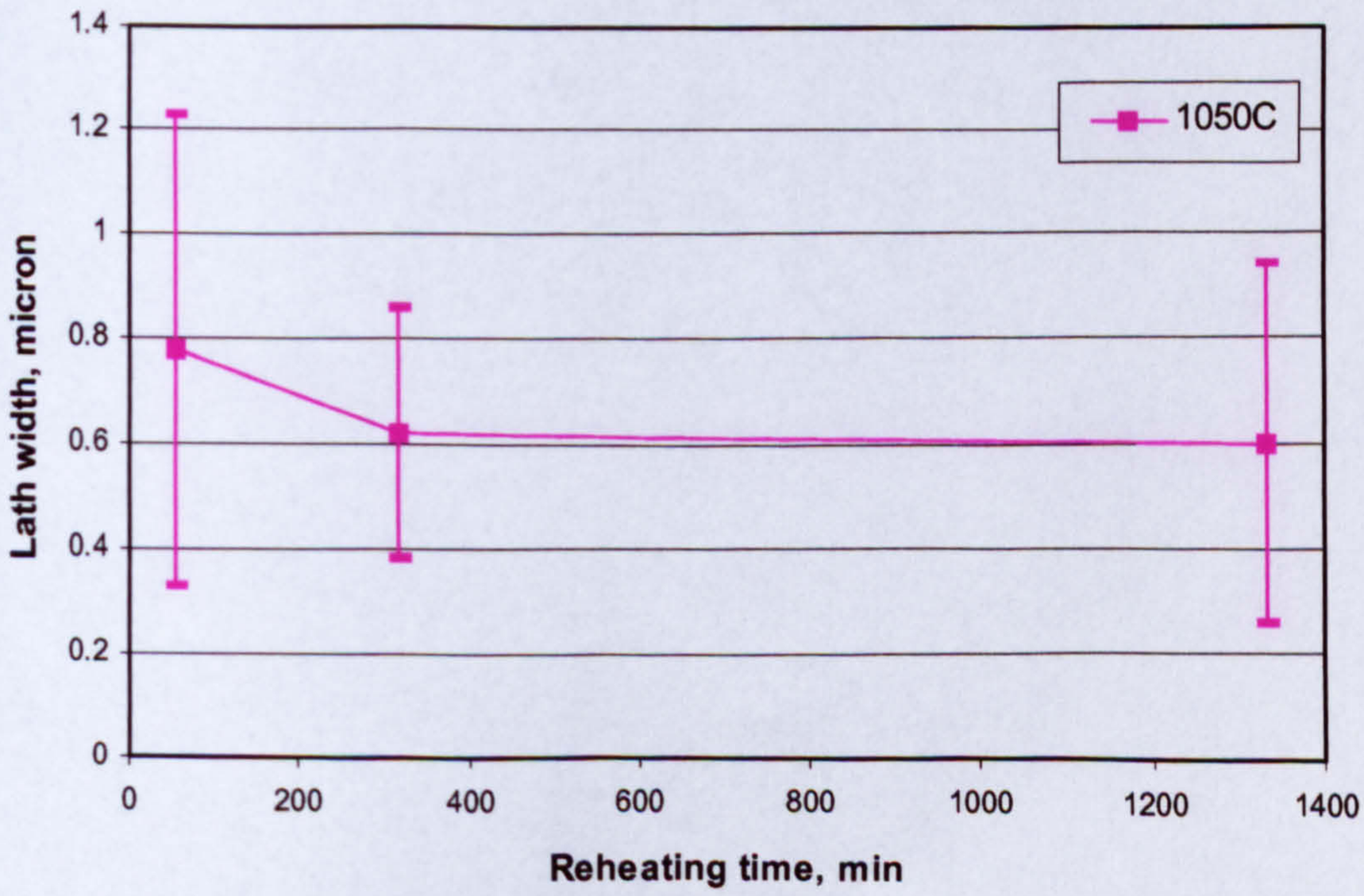

Fig. 4.42 Lath width in encapsulated Steel 3 reheated at 1050°C

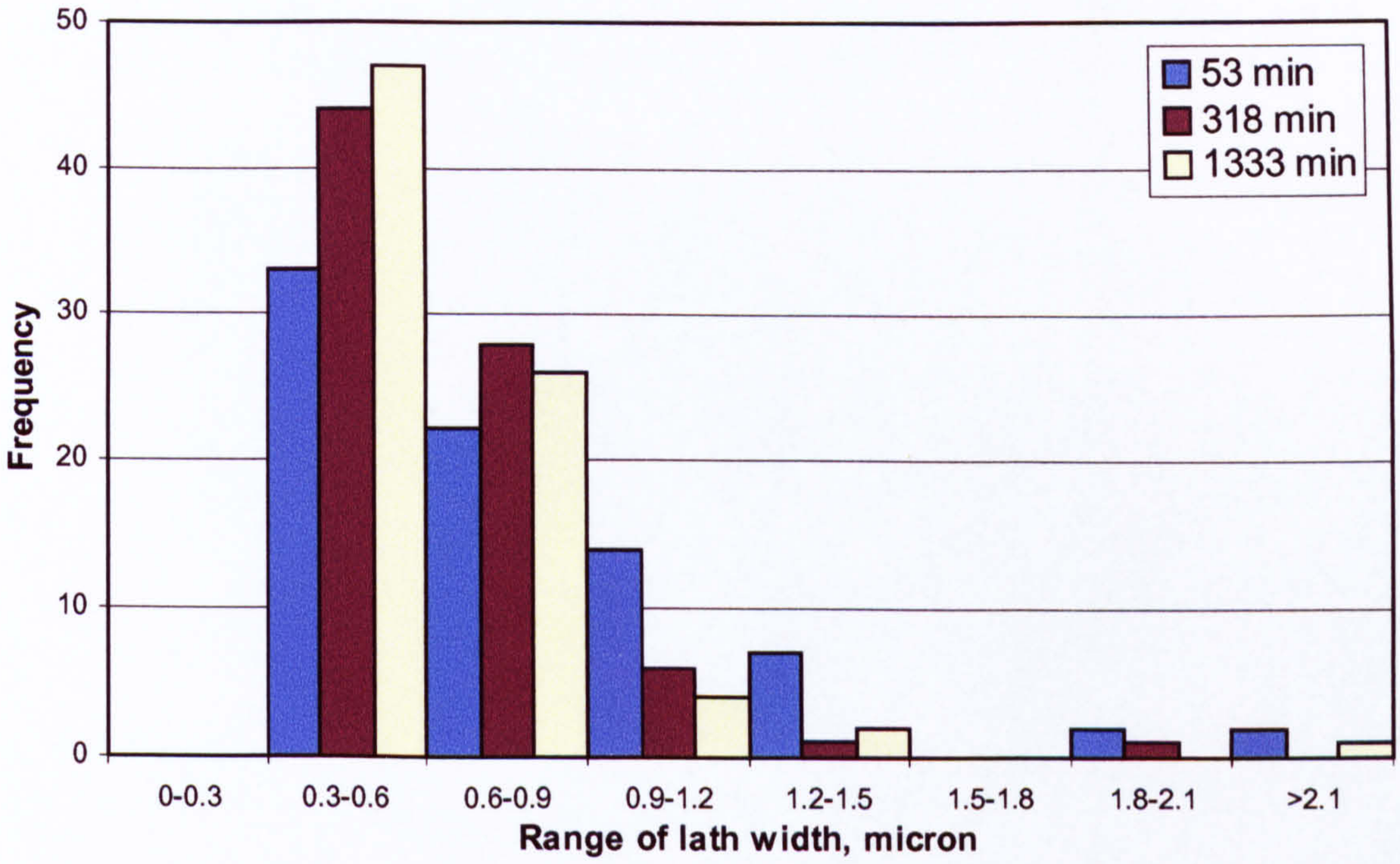

Fig. 4.43 Distribution of lath width in encapsulated Steel 3 reheated at 1050°C

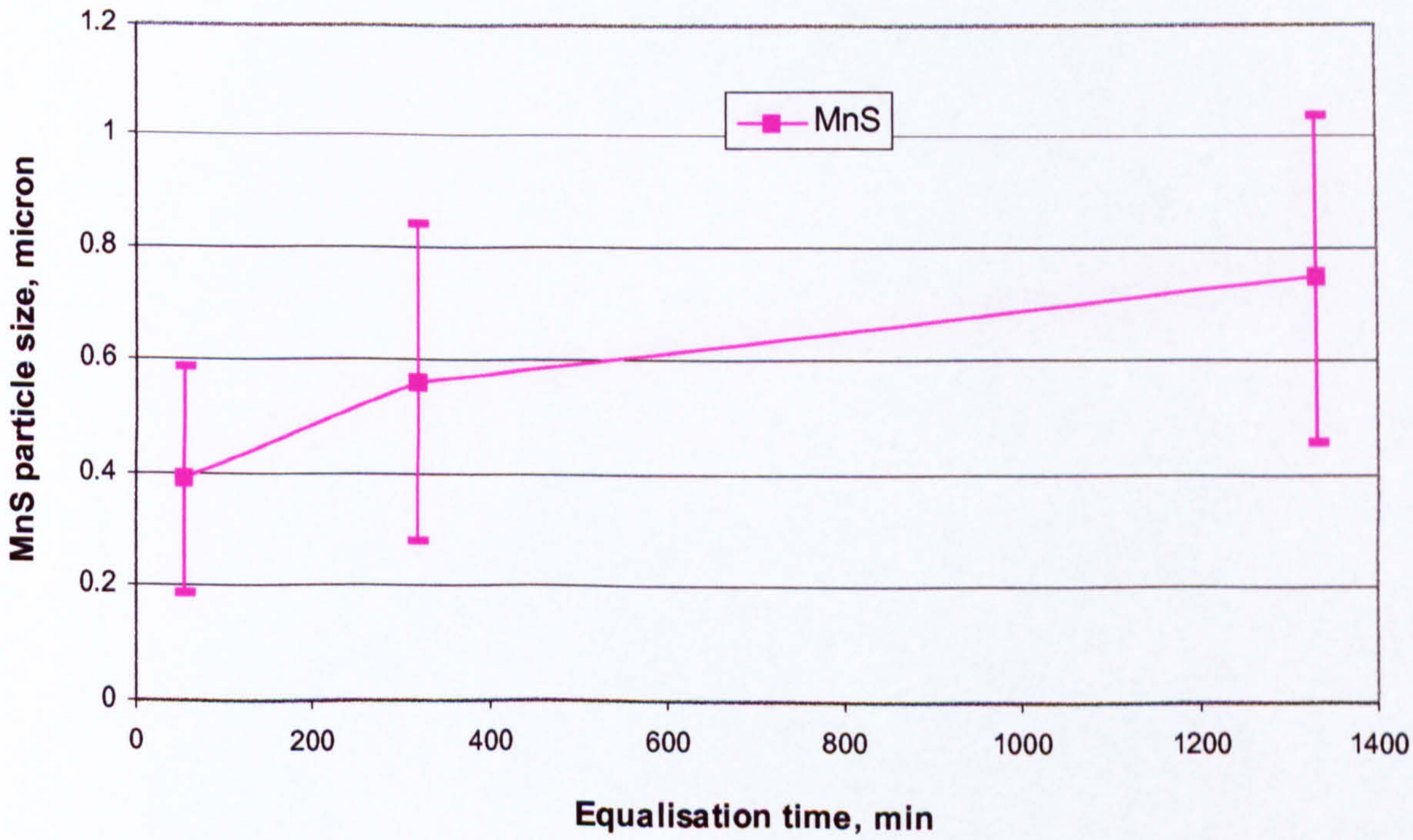

Fig. 4.44 MnS particle size in Steel 1 when equalised at different times

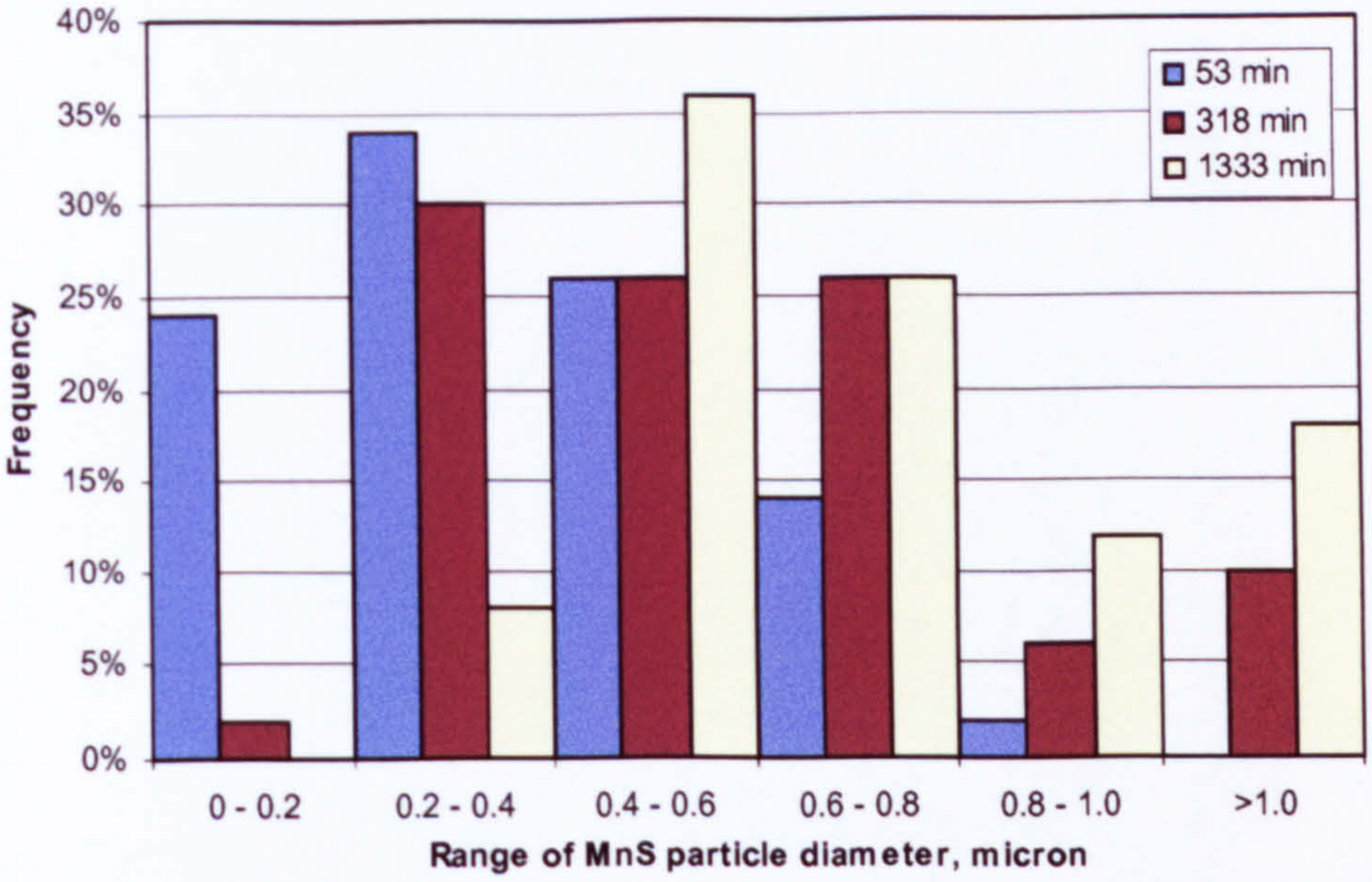

Fig. 4.45 MnS particle size distribution when equalised at different times

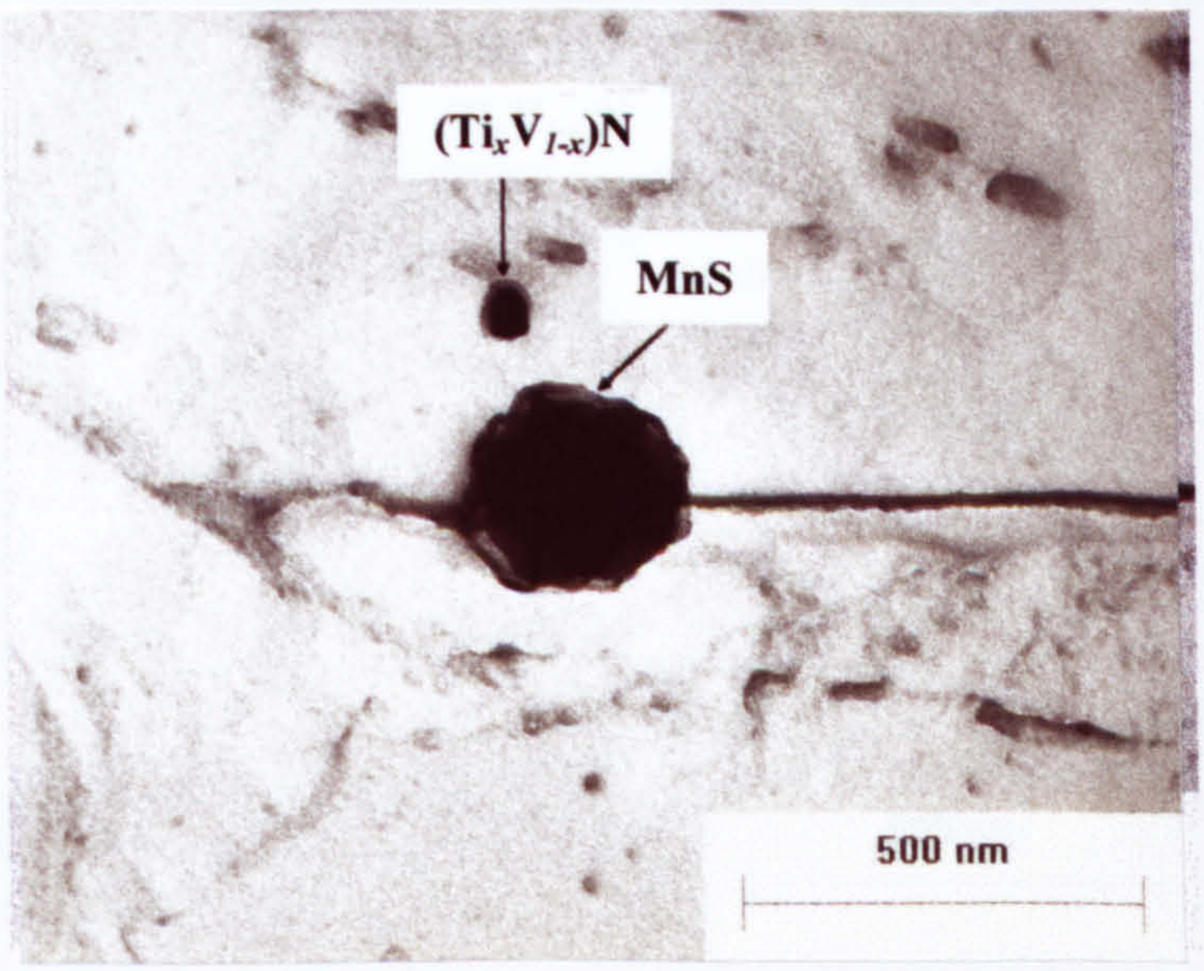

Fig. 4.46 $(Ti_xV_{1-x})N$ and MnS in Steel 1 equalised at 1150°C for 53 min

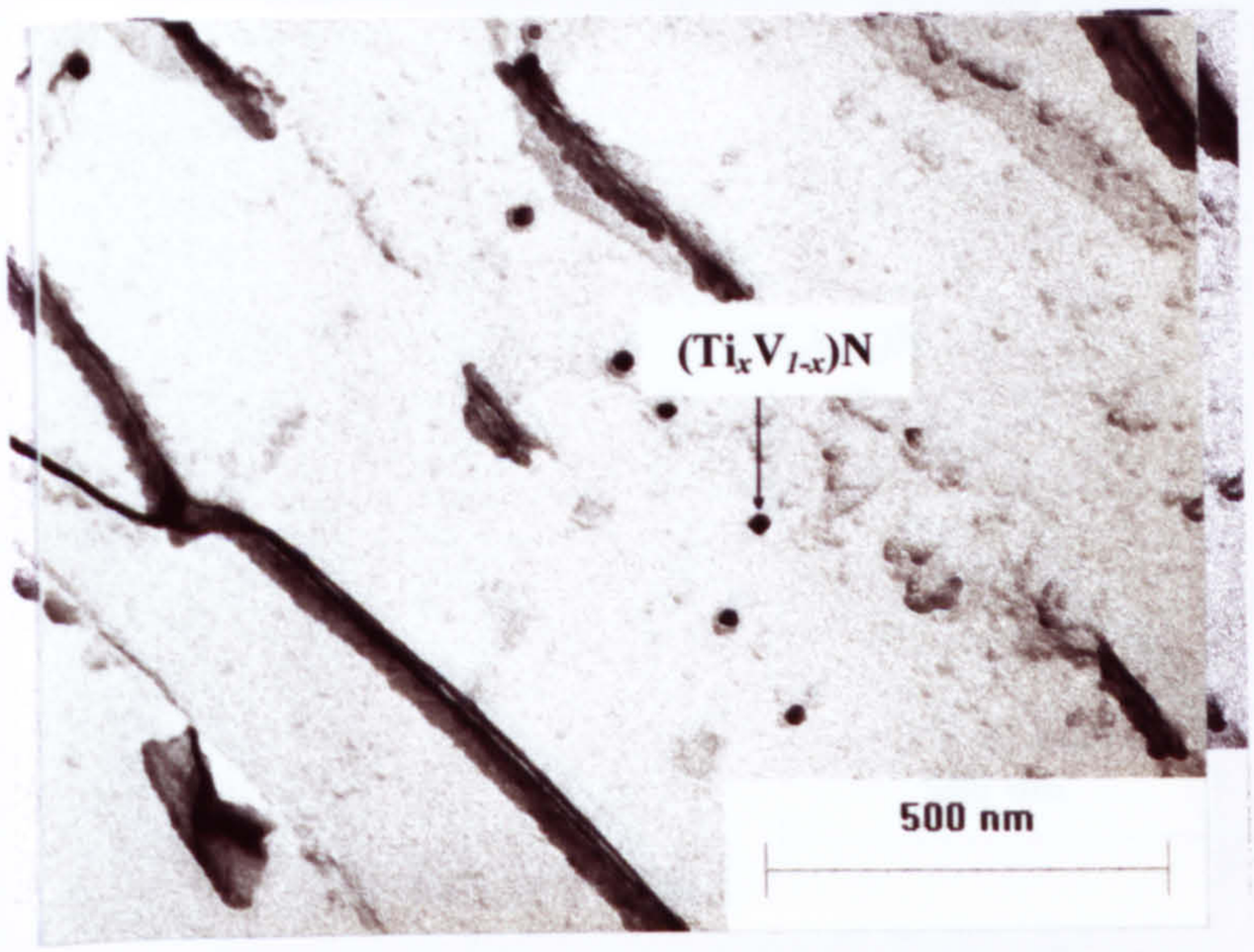

Fig. 4.47 Cuboid $(Ti_xV_{1-x})N$ in Steel 1 equalised at 1150°C for 318 min

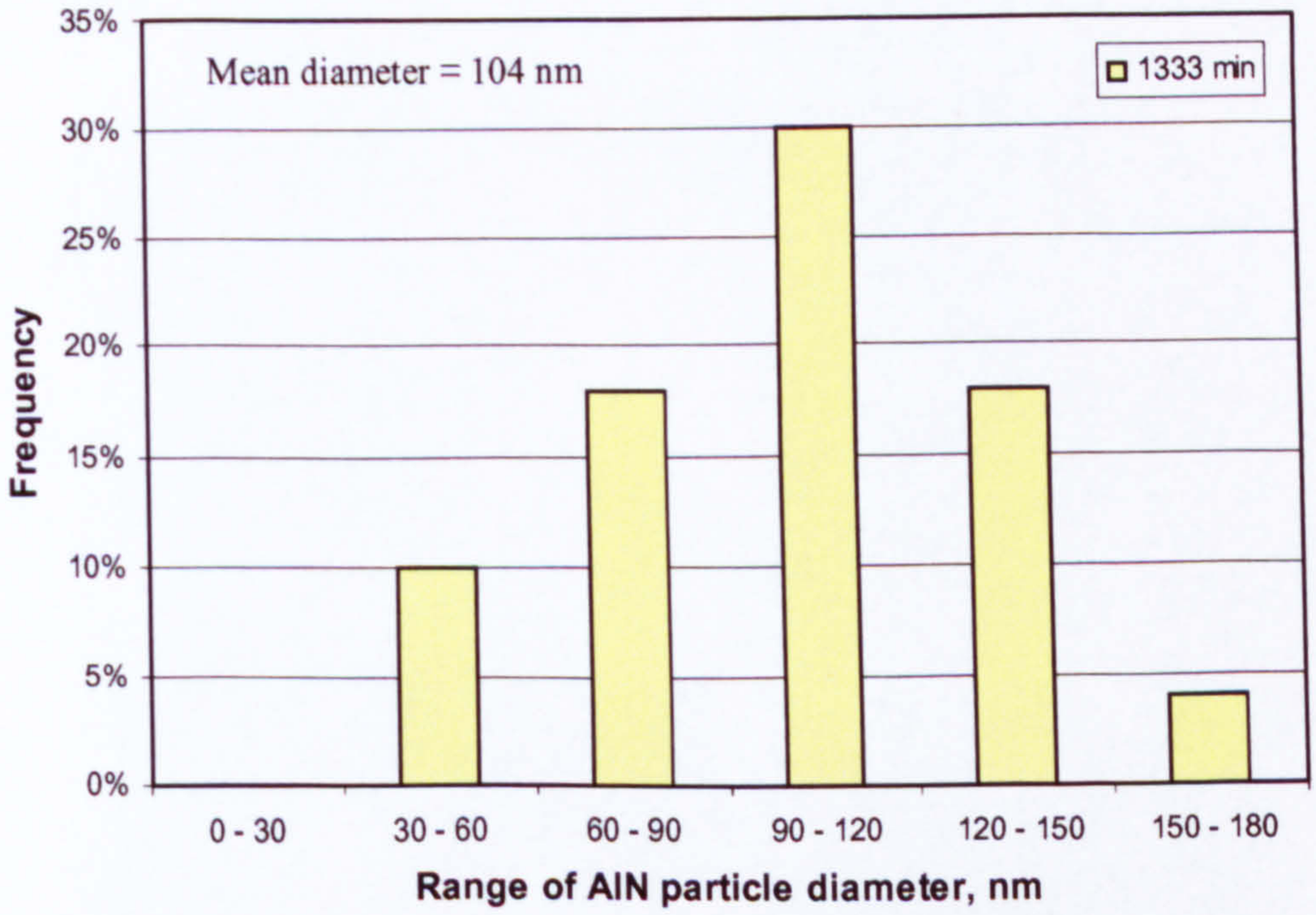

Fig. 4.48 AlN particle size distribution in Steel 1 when equalised at 1333 min

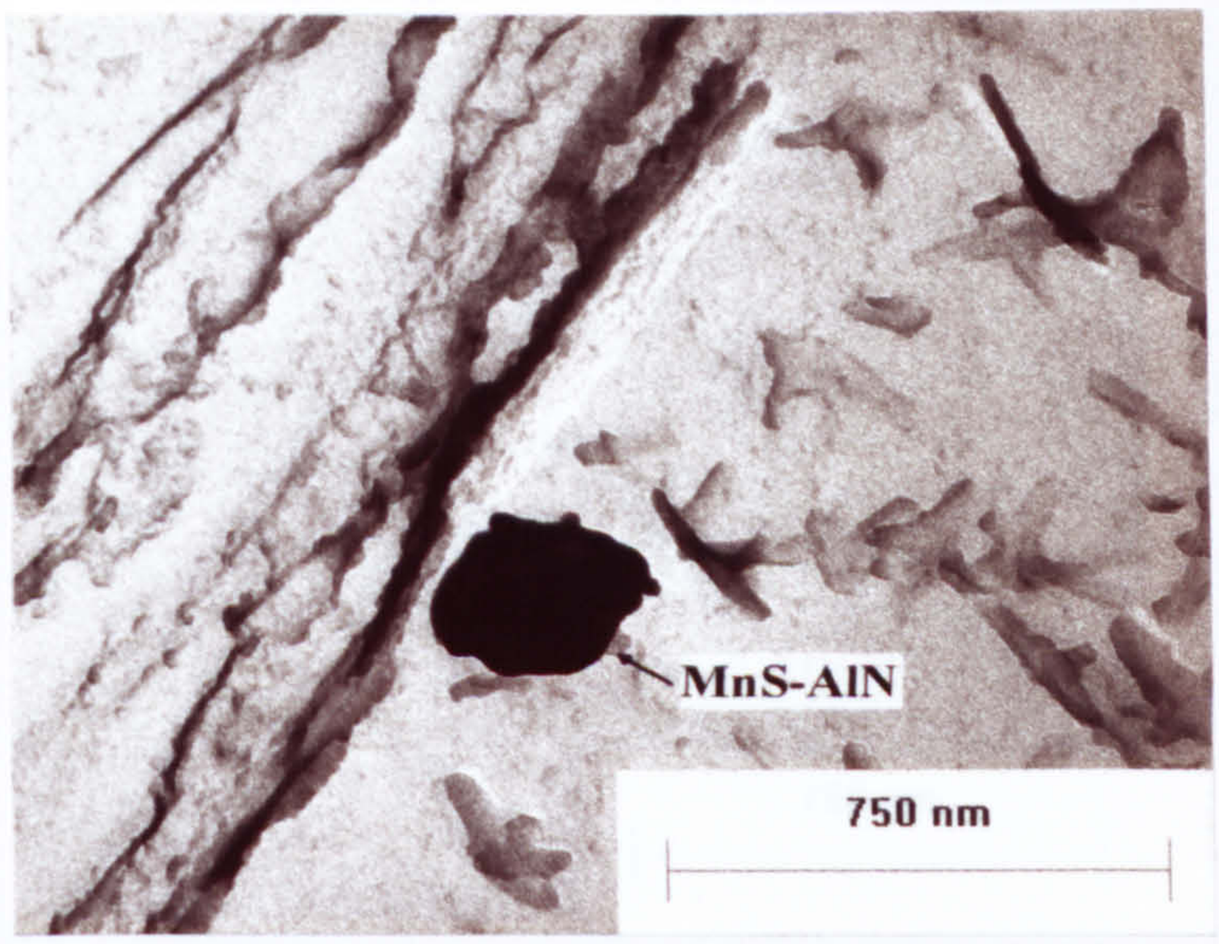

Fig. 4.49 AlN-MnS in Steel 1 equalised at 1150°C for 1333 min

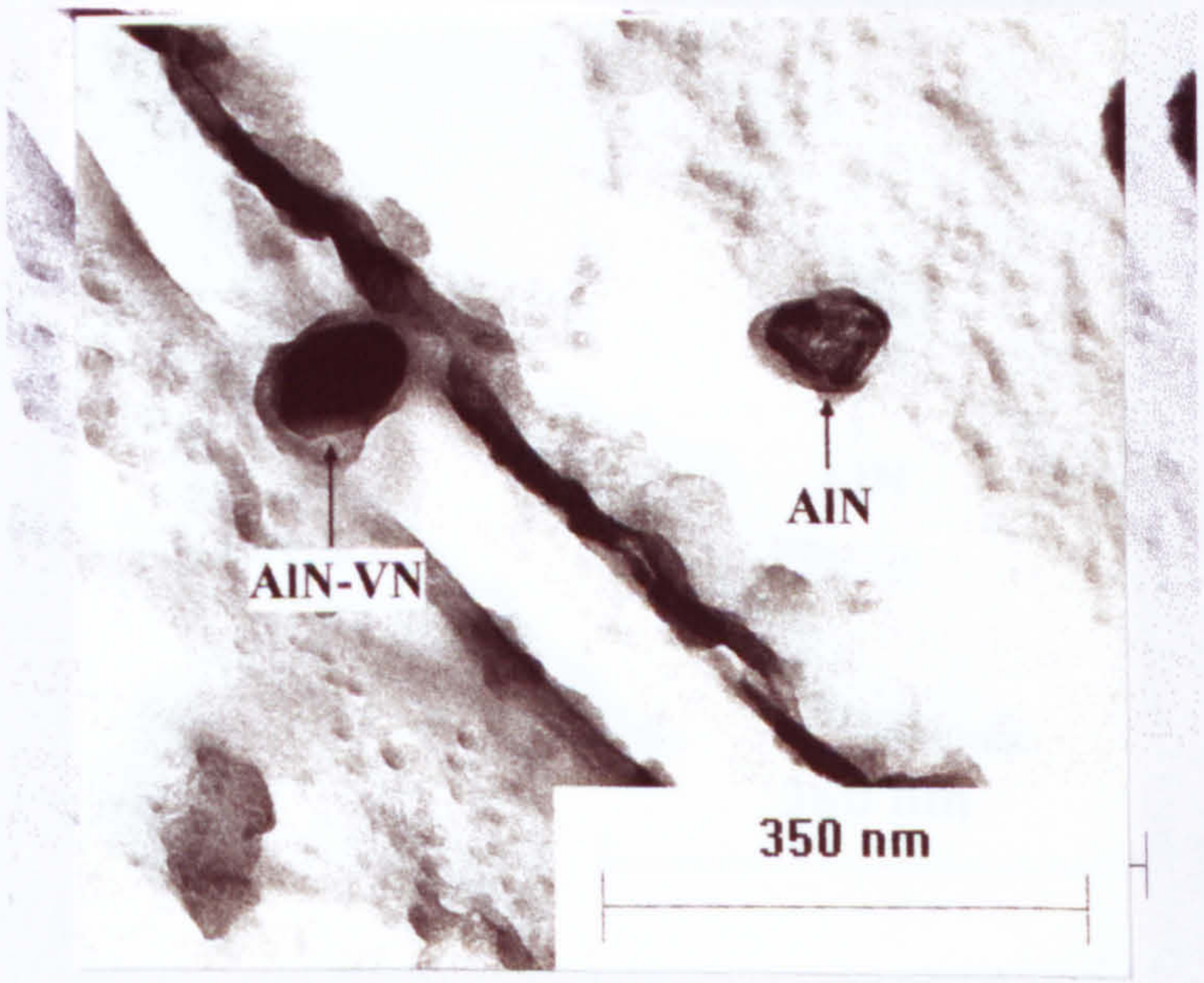

a

b

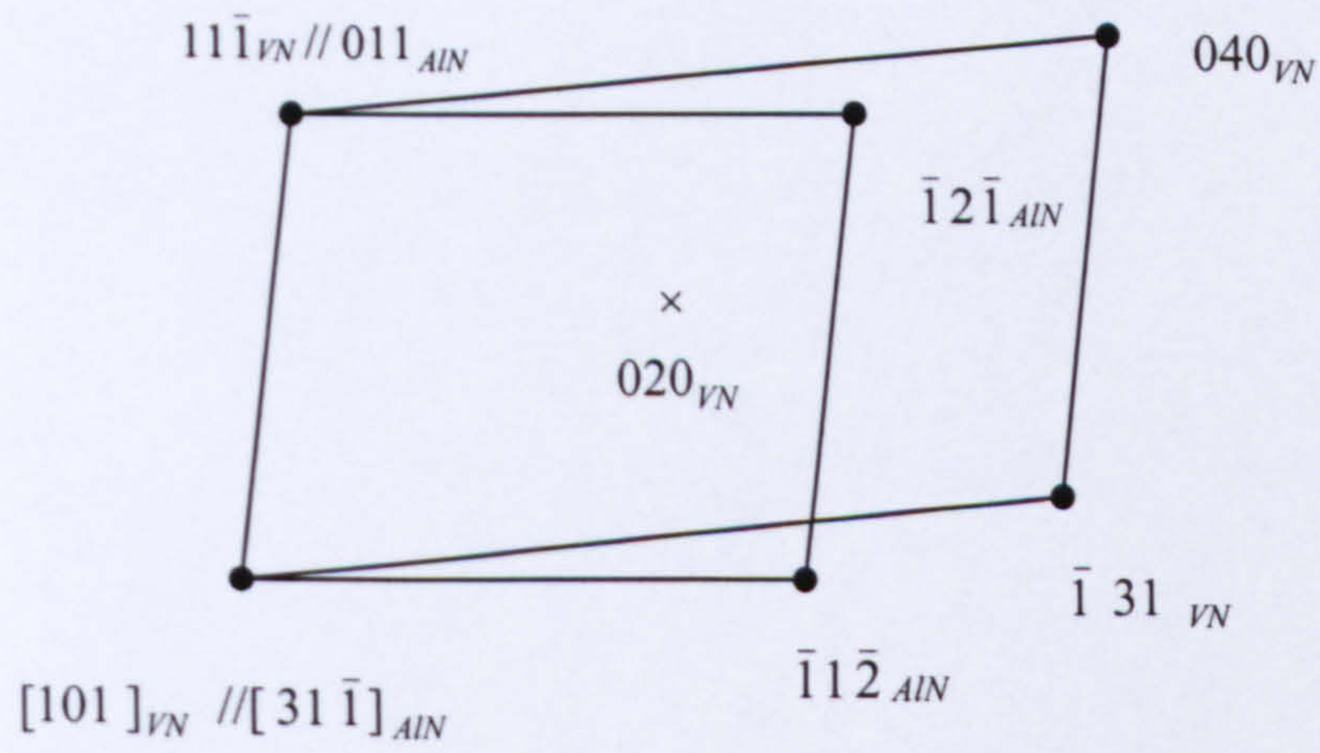

c

Fig. 4.50 AlN-VN in Steel 1 equalised at 1150°C for 1333 min after tempering

a. Microstructure
b. Diffraction pattern of VN and AlN
c. The plate spacing relationship of VN and AlN

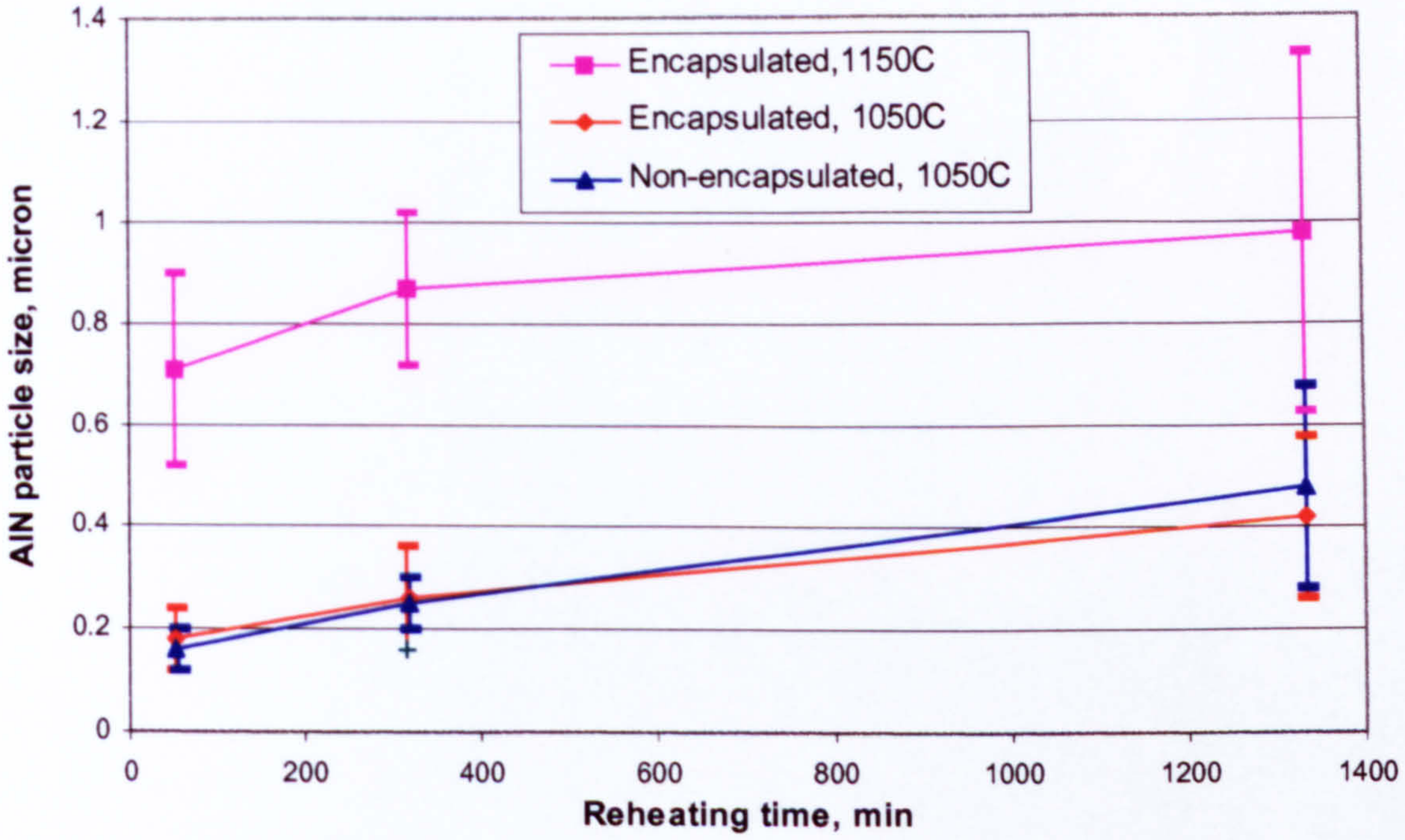

Fig. 4.51 AlN size in the microstructure of encapsulated and non-encapsulated Steel 2 reheated at 1050°C and 1150°C

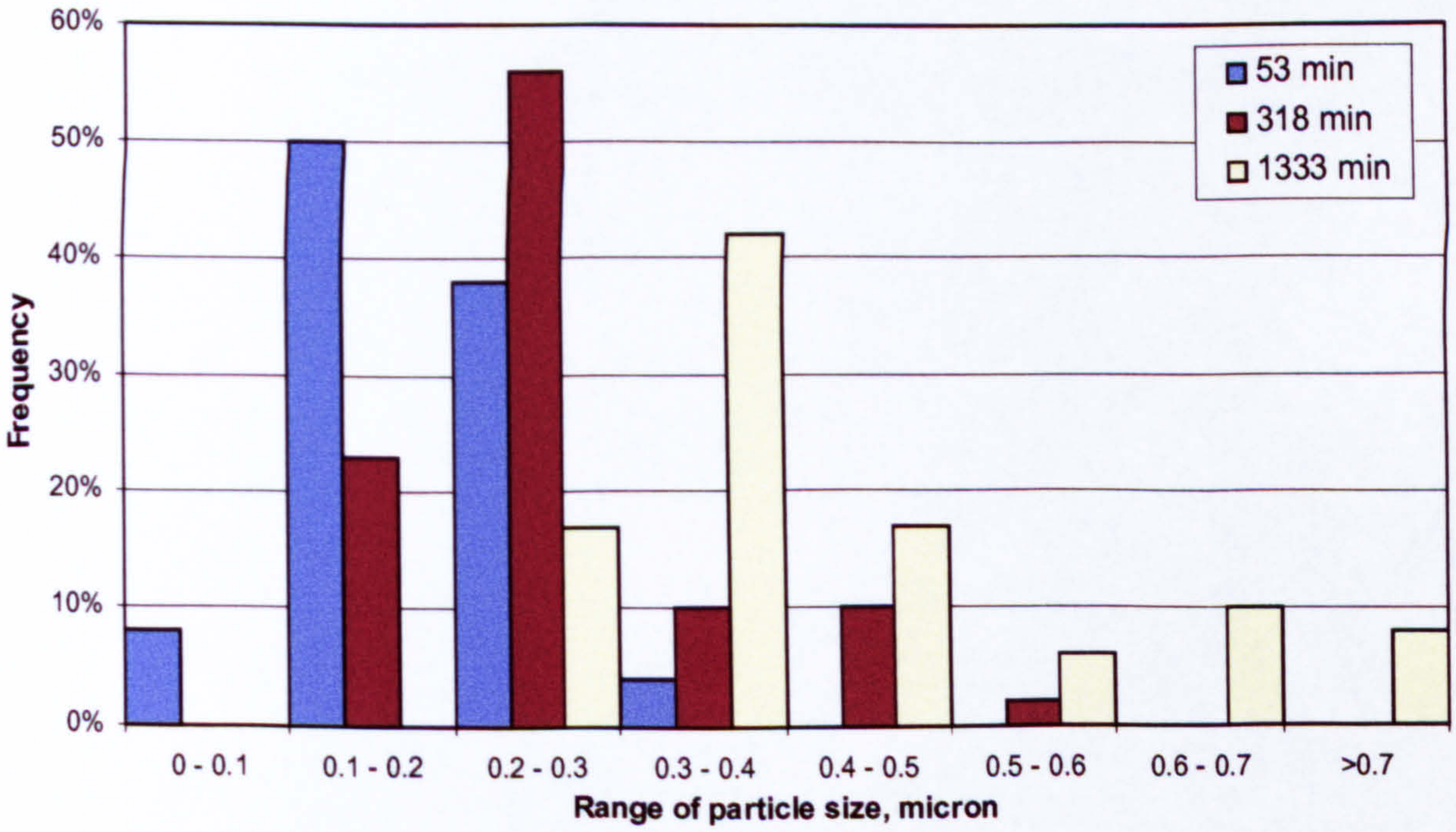

Fig. 4.52 Distribution of AlN particle size in the microstructure of non-encapsulated Steel 2 reheated at 1050°C

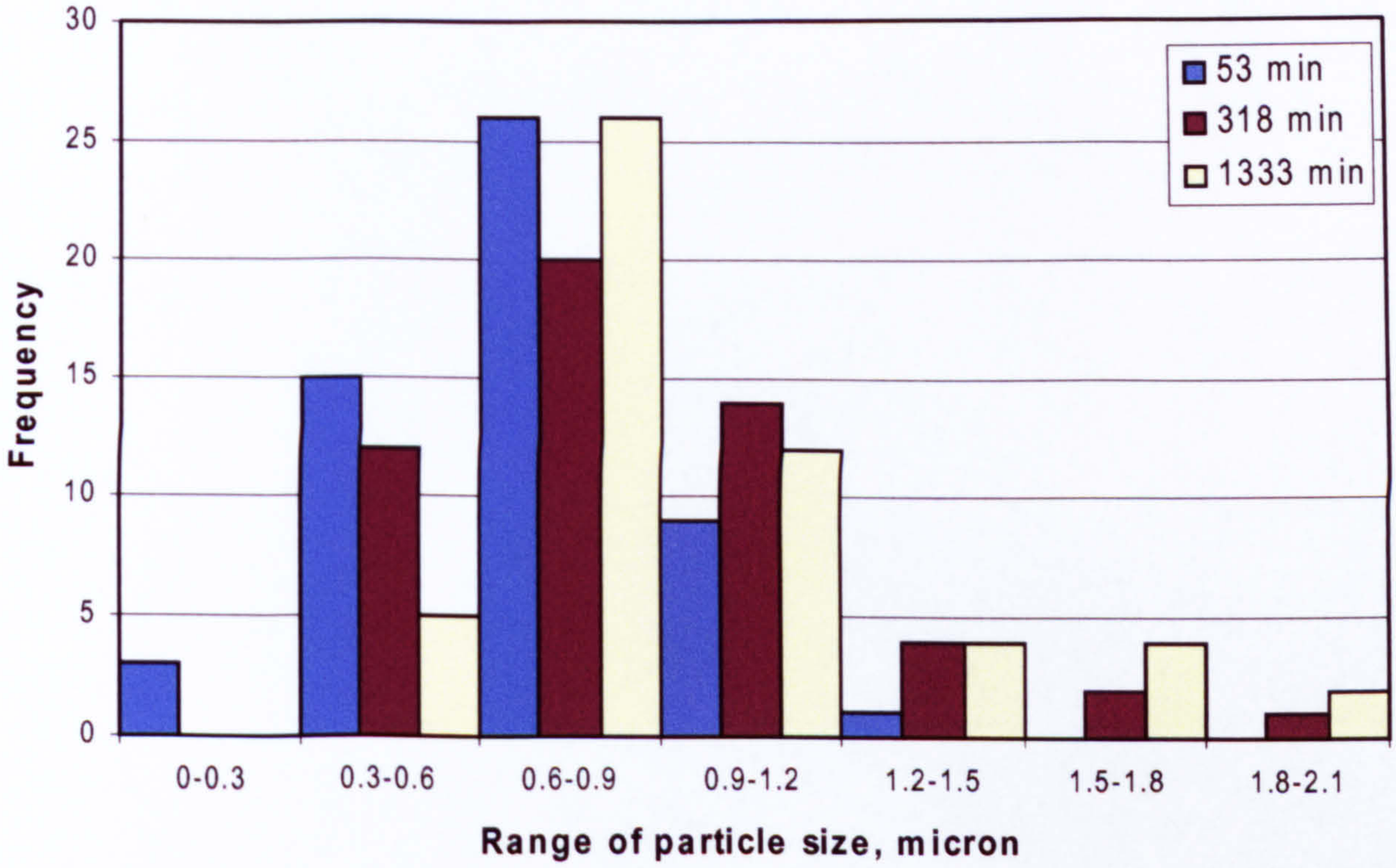

Fig. 4.53 Distribution of AlN particle size in the microstructure of encapsulated Steel 2 reheated at 1150°C

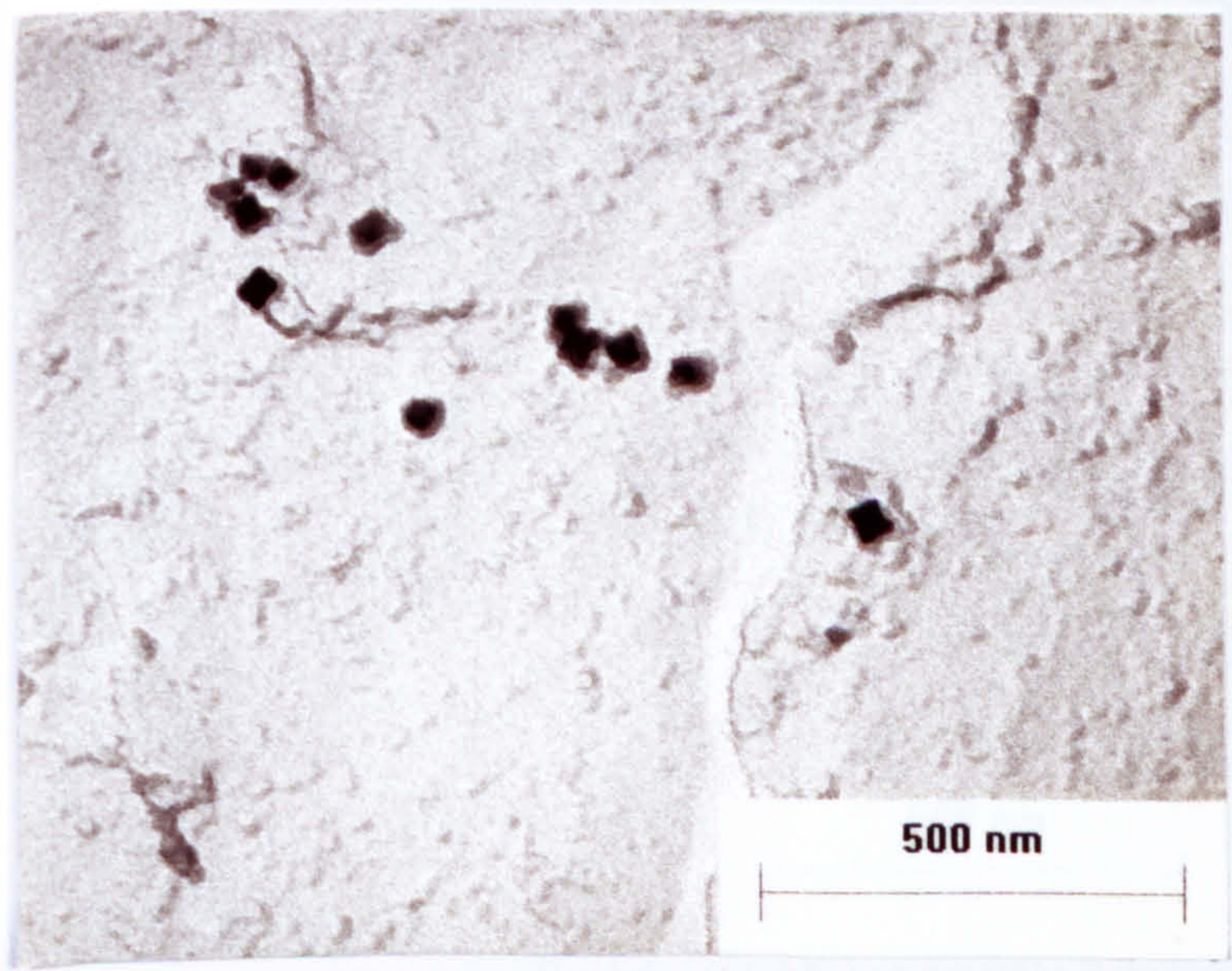

Fig. 4.54 Cuboidal particles in directly charged Steel 3

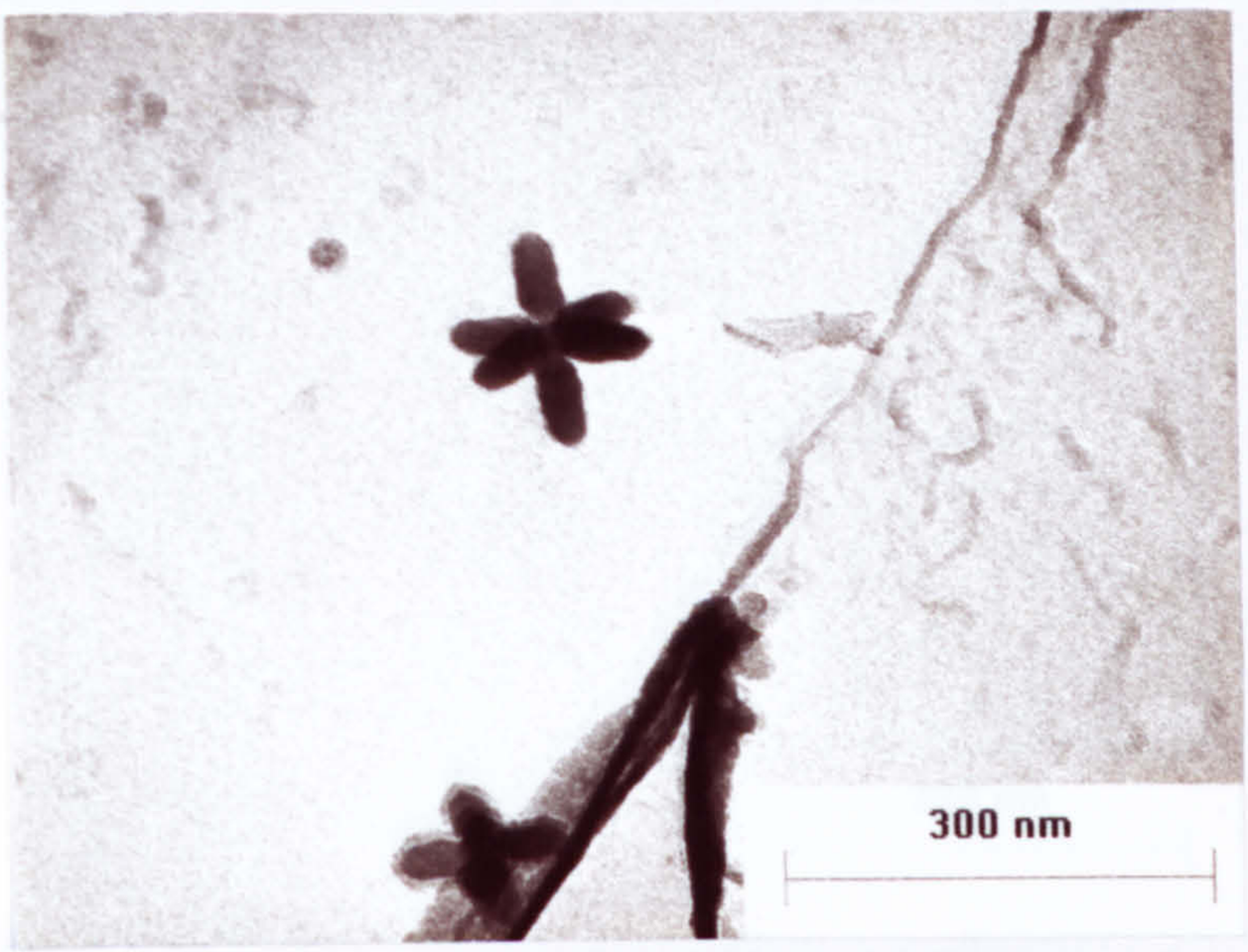

Fig. 4.55 Cruciform particles in directly charged Steel 3

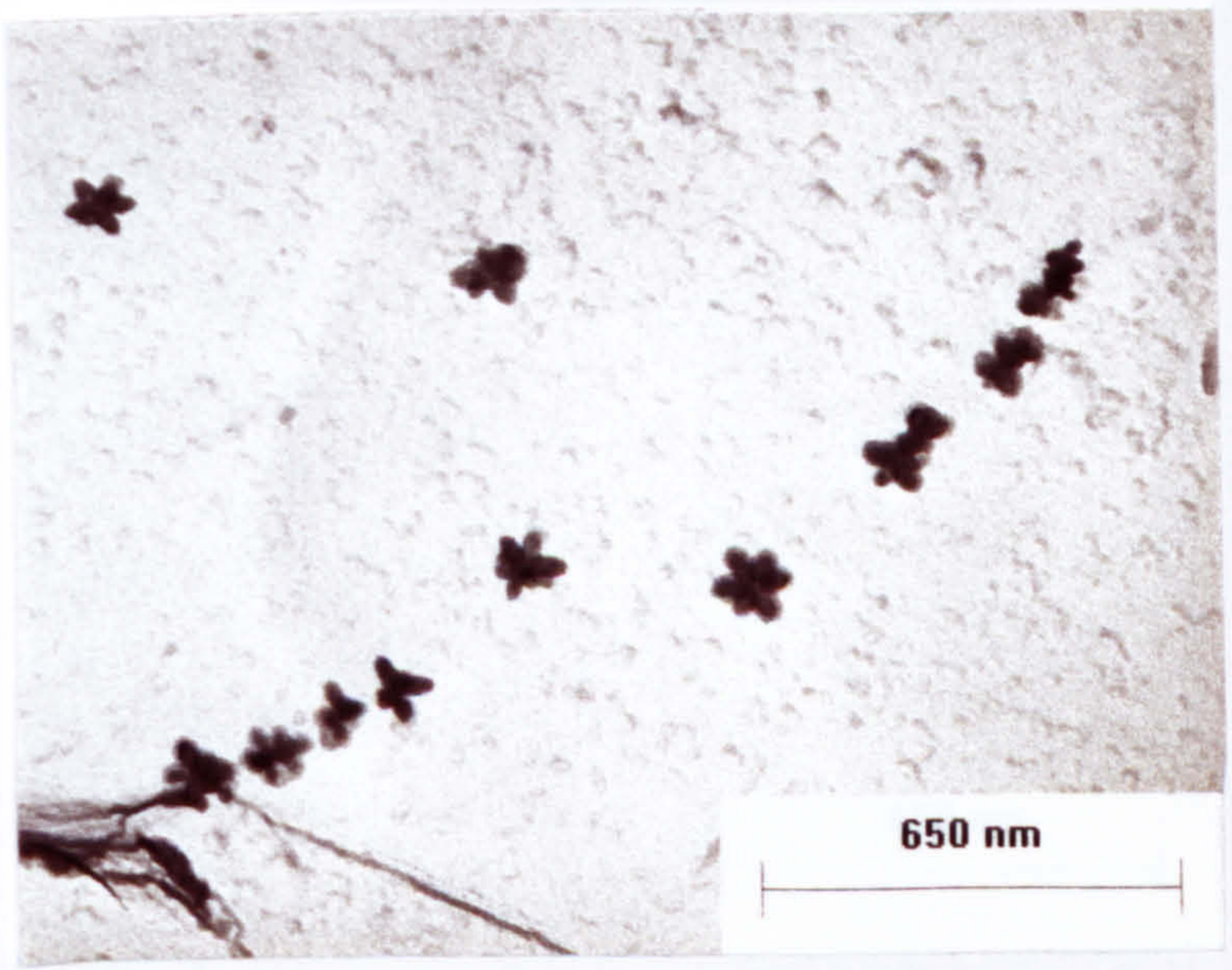

Fig. 4.56 Cruciform particles in rows in directly charged Steel 3

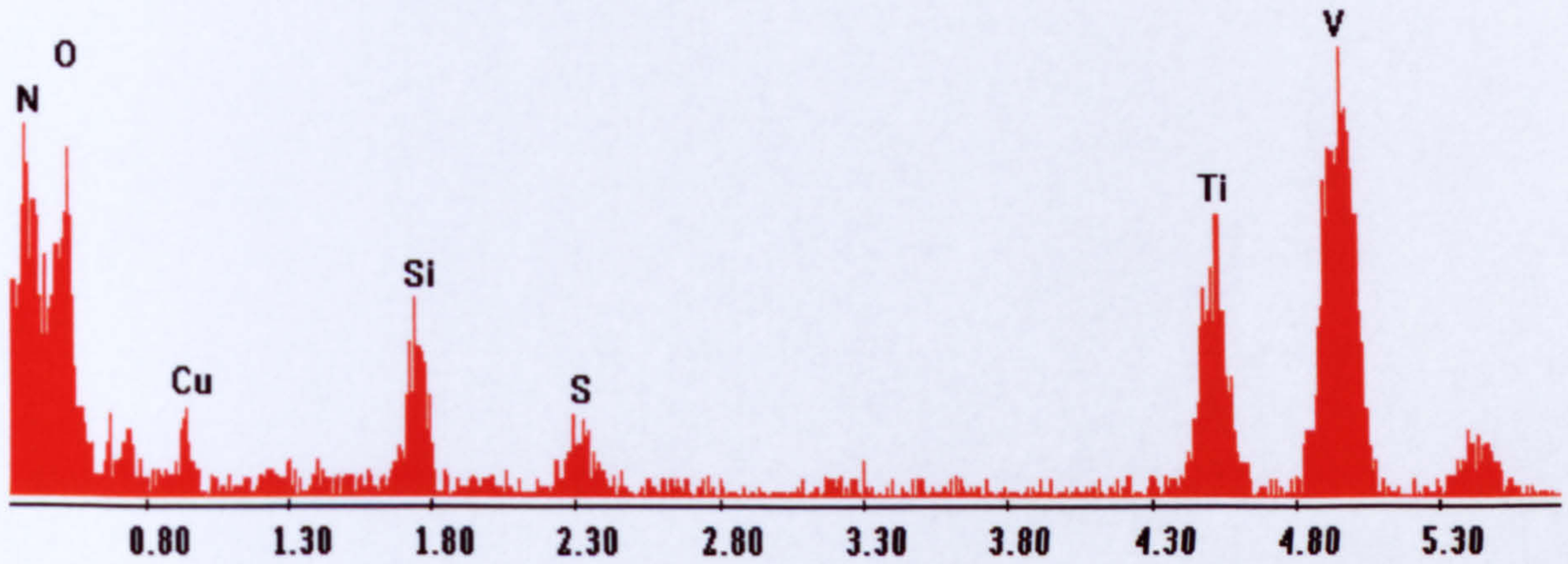

Fig. 4.57 The spectrum from the core of cruciform particles in directly charged Steel 3

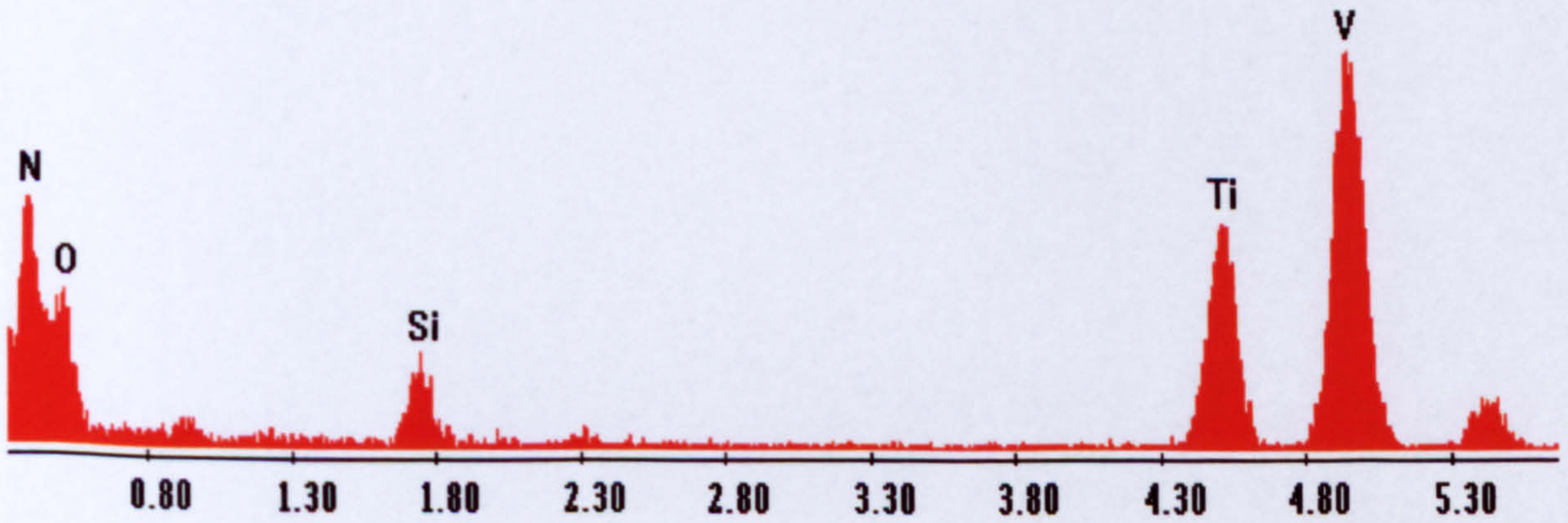

Fig. 4.58 The spectrum from the arm of cruciform particles in directly charged Steel 3

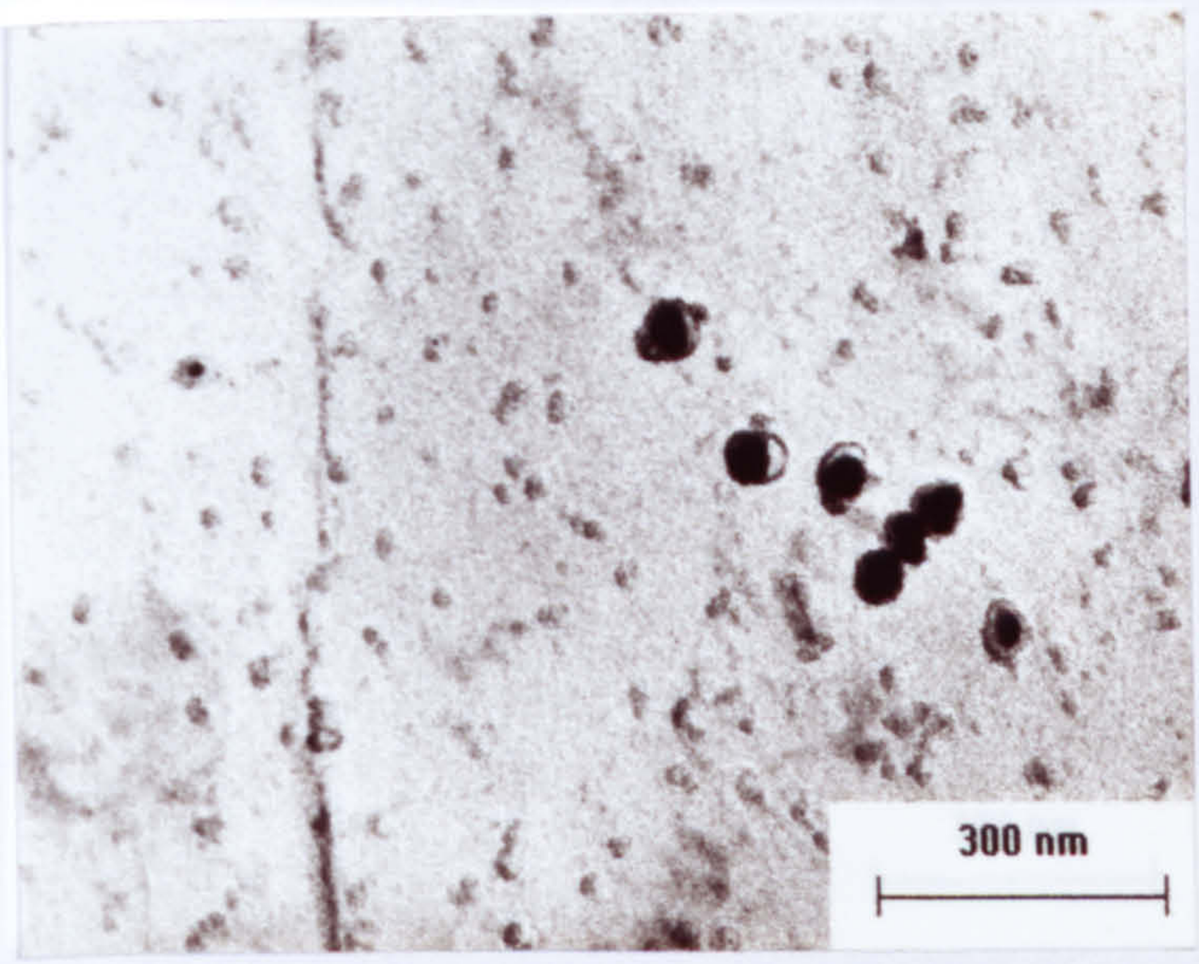

Fig. 4.59 Spheroidal $(Ti_xV_{1-x})N$ particles in cast Steel 3

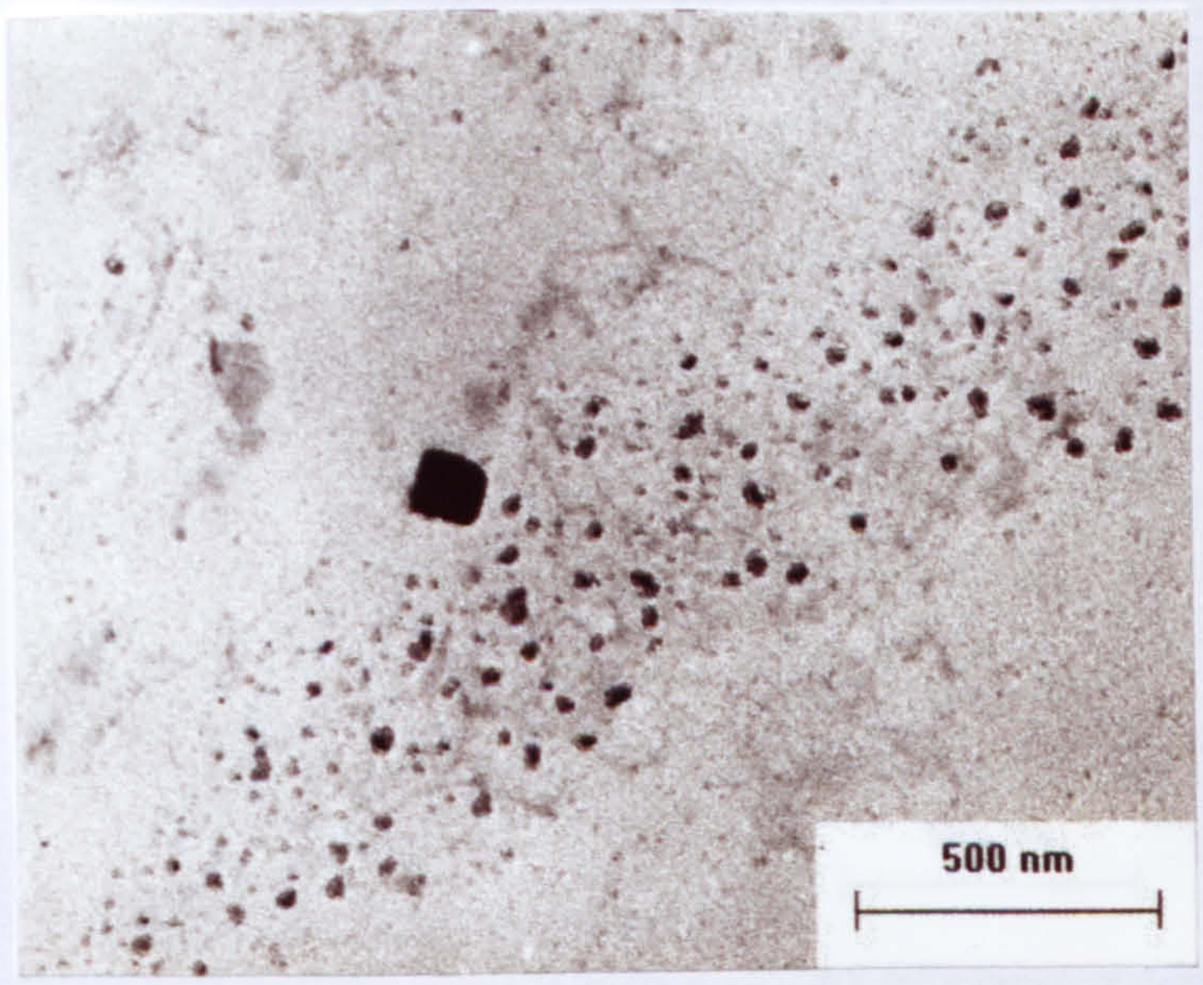

Fig. 4.60 Spheroidal $(Ti_xV_{1-x})N$ particles and cuboidal MnS particle in cast Steel 3

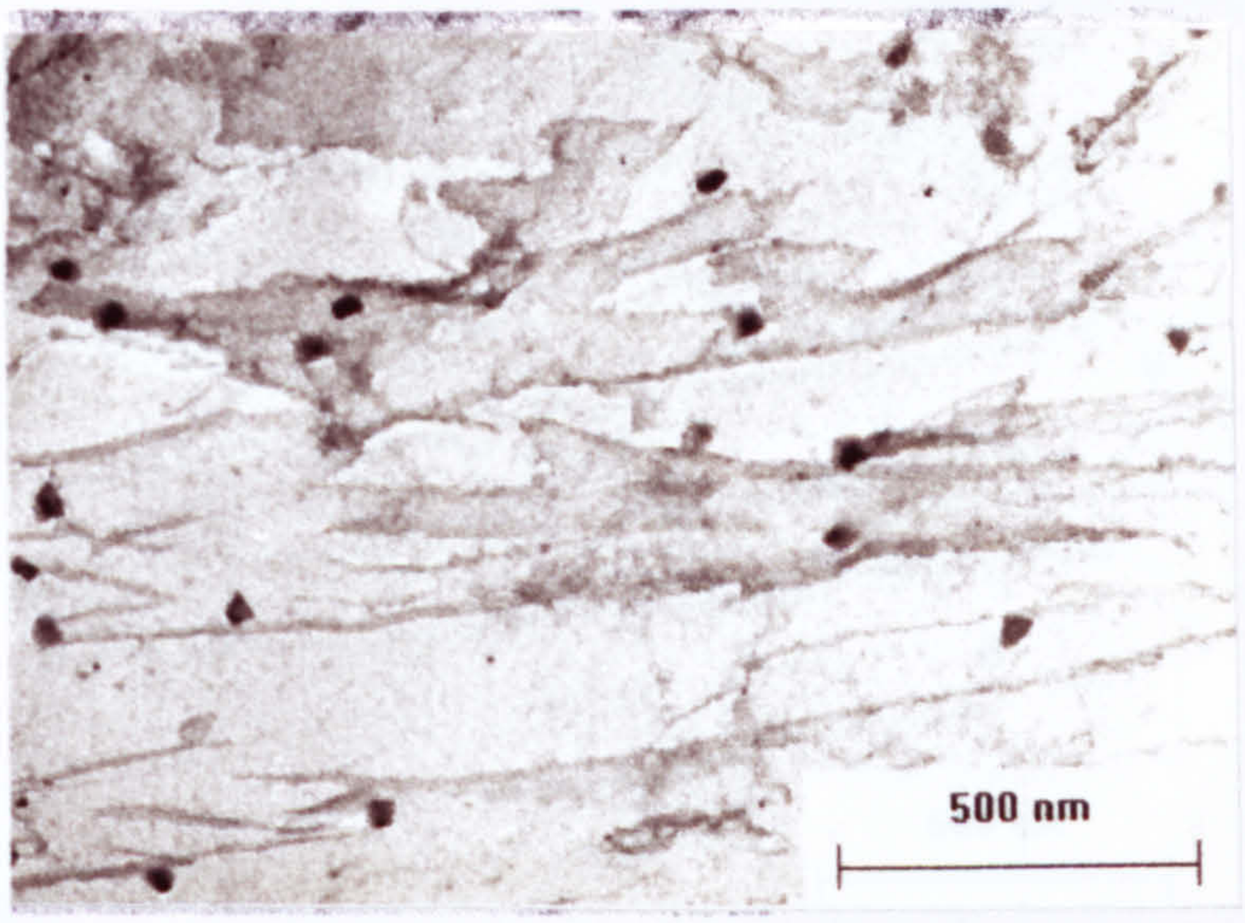

Fig. 4.61 Cuboidal $(Ti_xV_{1-x})N$ particles in conventional cold charged Steel 3 reheated at 1050°C

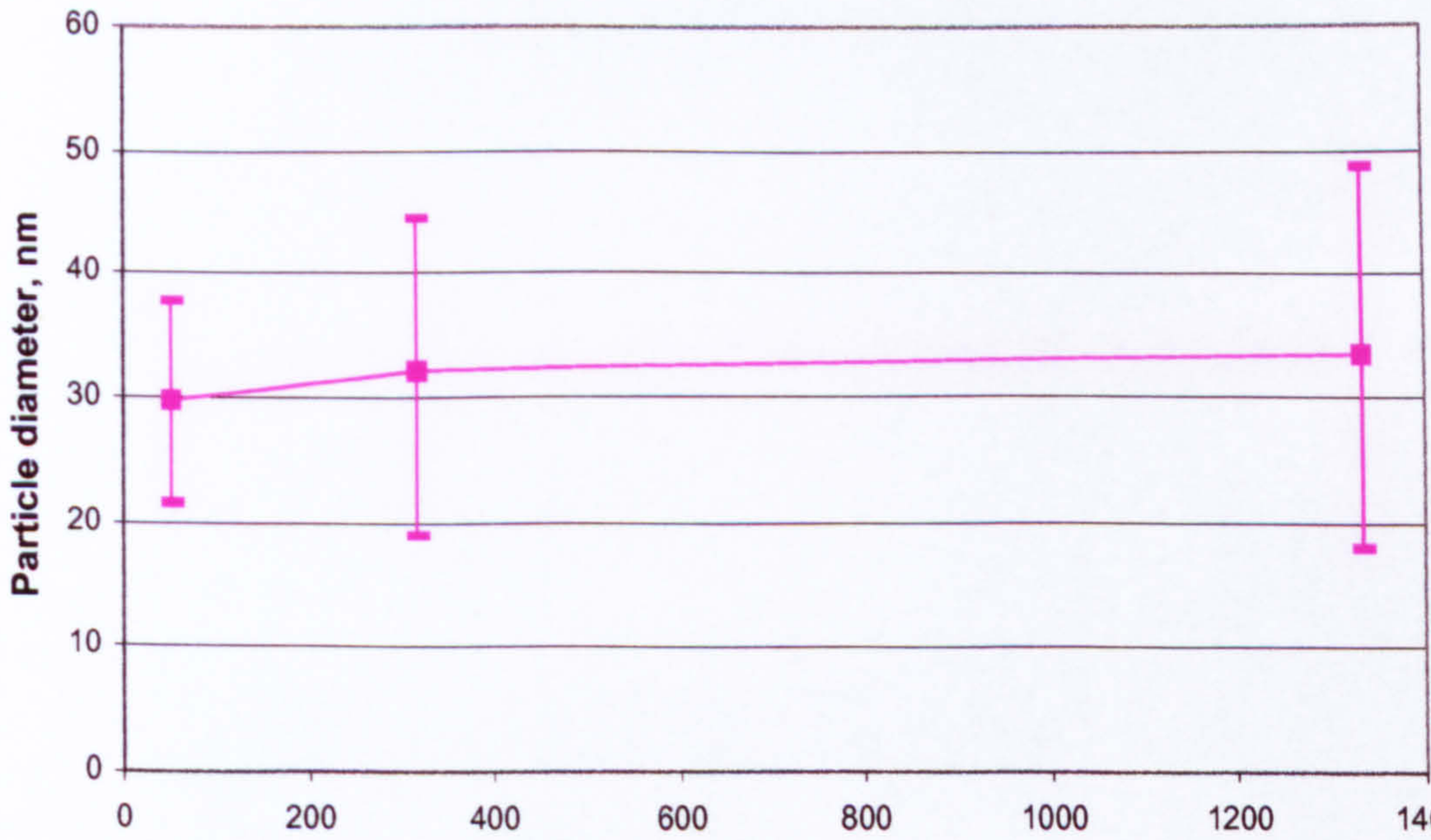

Fig. 4.62 $(Ti_xV_{1-x})N$ particle size in Steel 3 during reheating at 1150°C

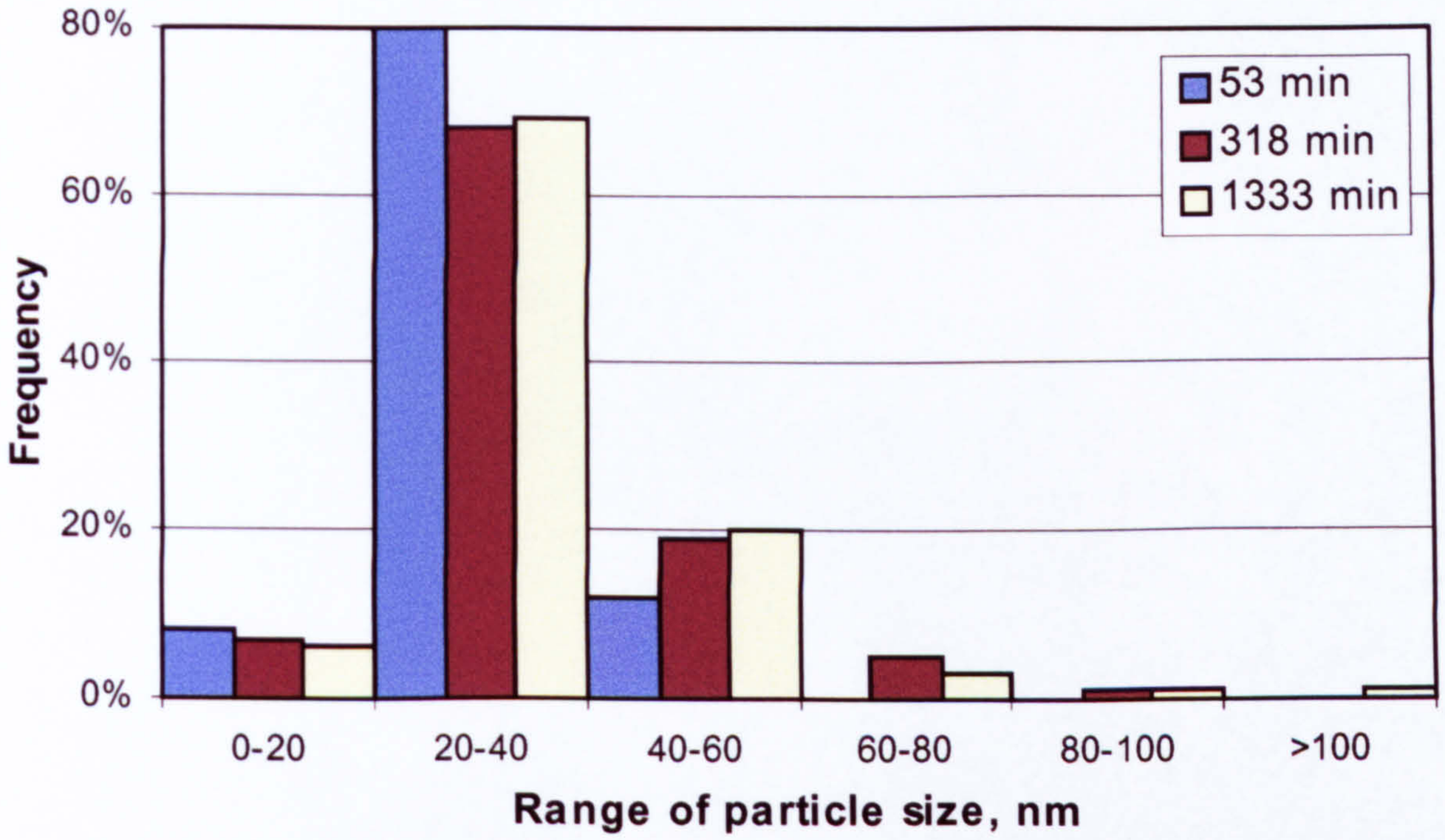

Fig. 4.63 The distribution of $(Ti_xV_{1-x})N$ particle size in Steel 3 during reheating at 1150°C

FIGURES IN CHAPTER FIVE

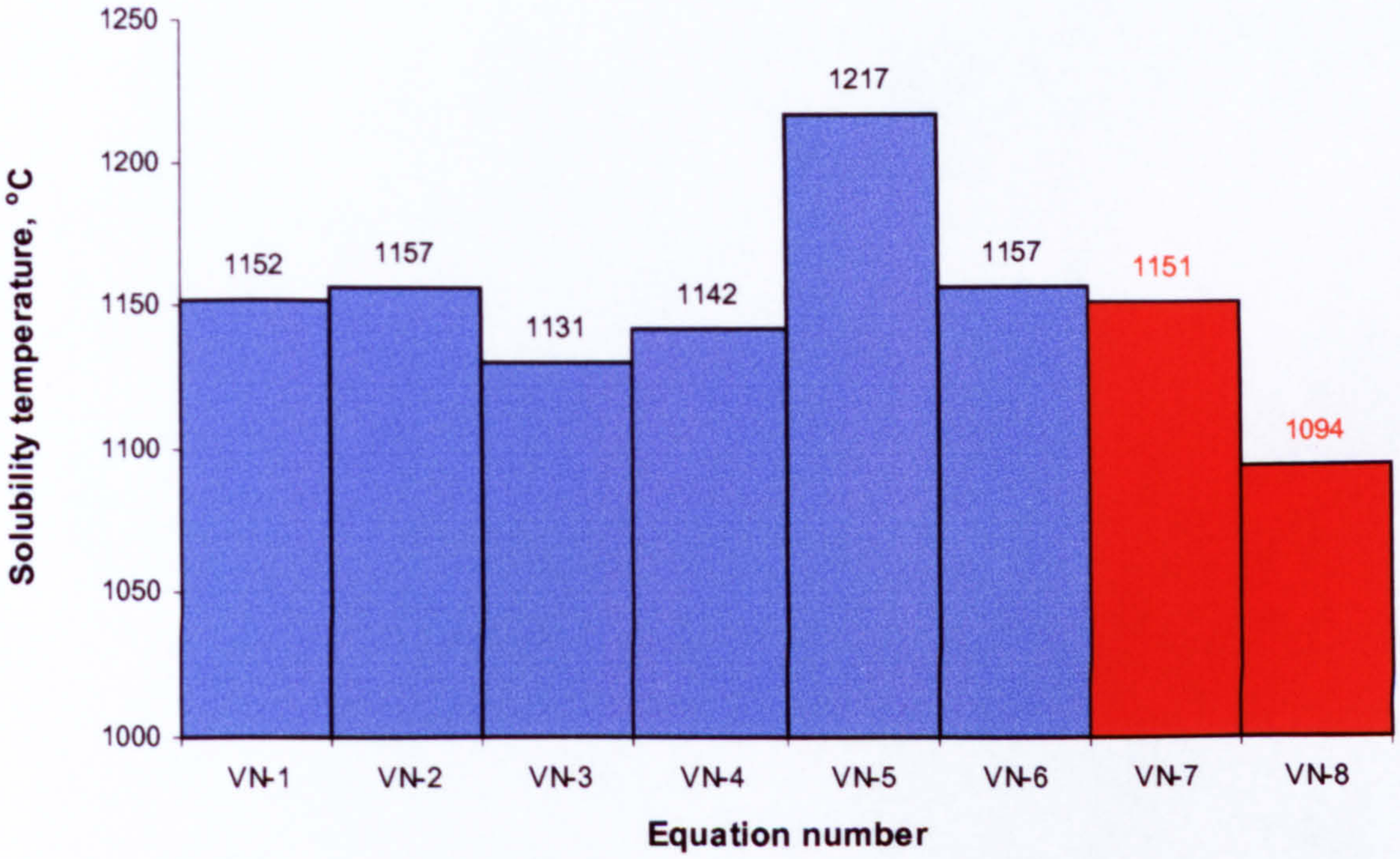

Fig. 5.1 Solubility temperatures of VN in Steel 1 calculated by several equations

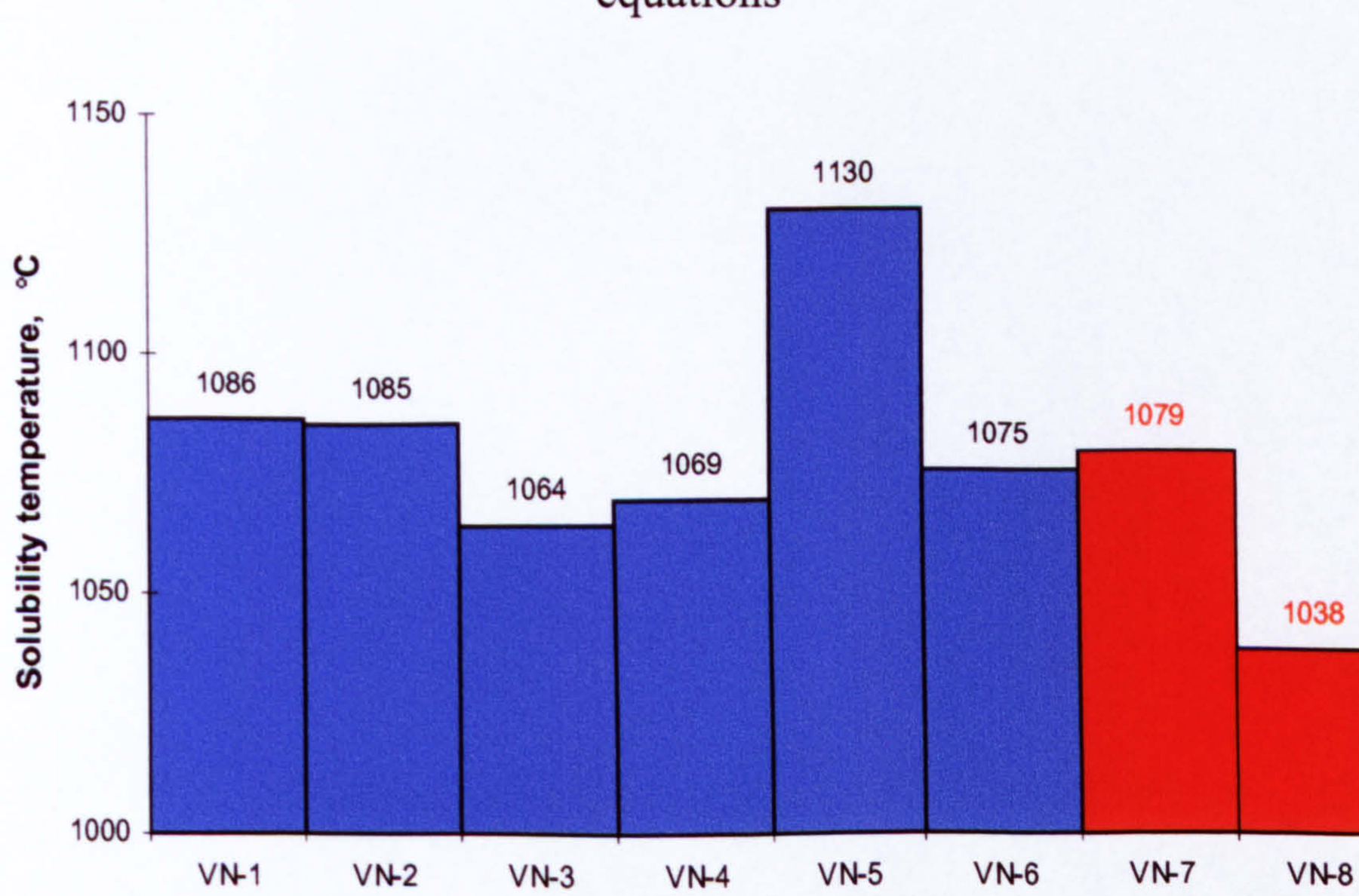

Fig. 5.2 Solubility temperatures of VN in Steel 2 and Steel 3 calculated by several equations

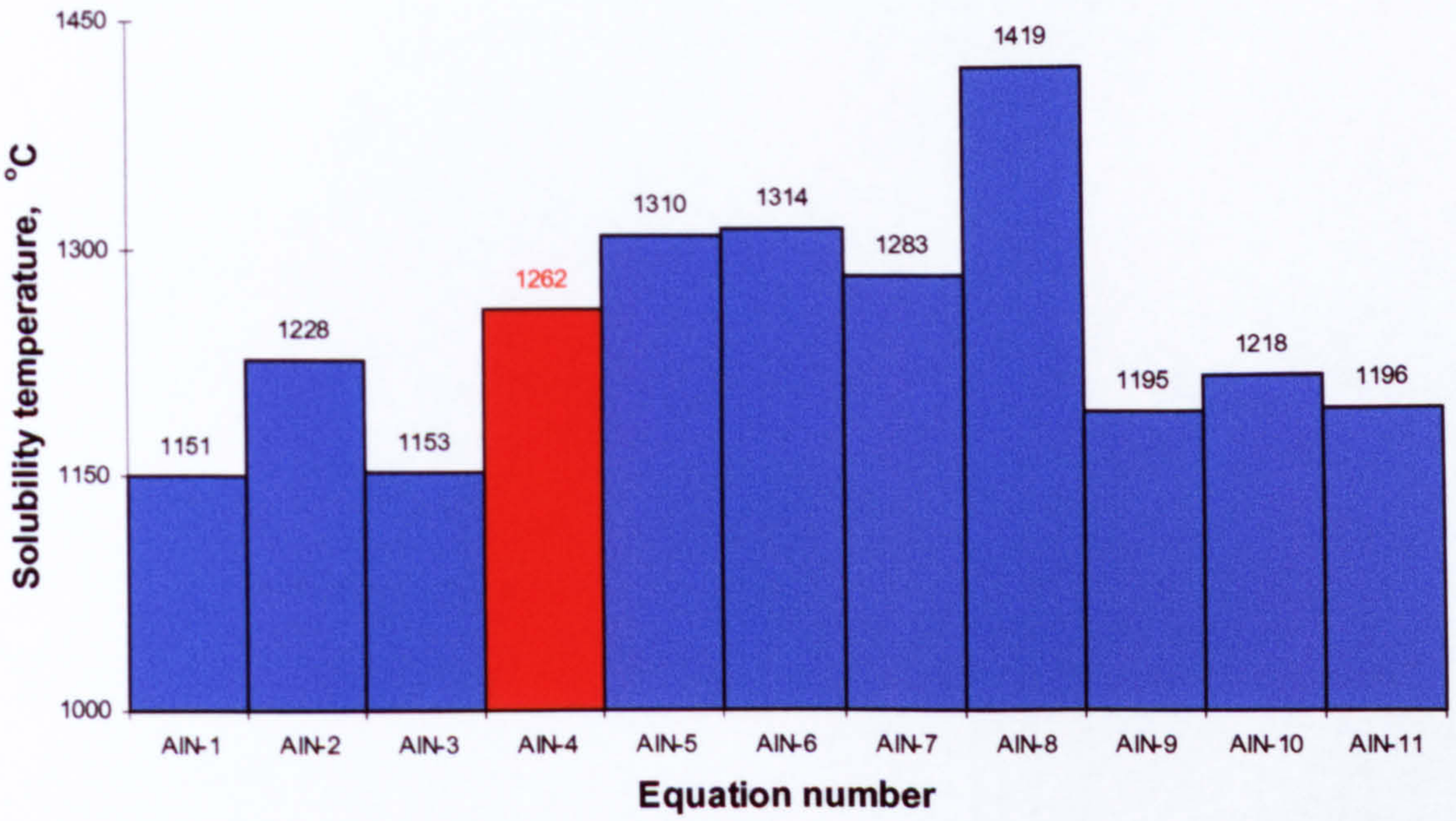

Fig. 5.3 Solubility temperatures of AlN in Steel 1 calculated by several equations

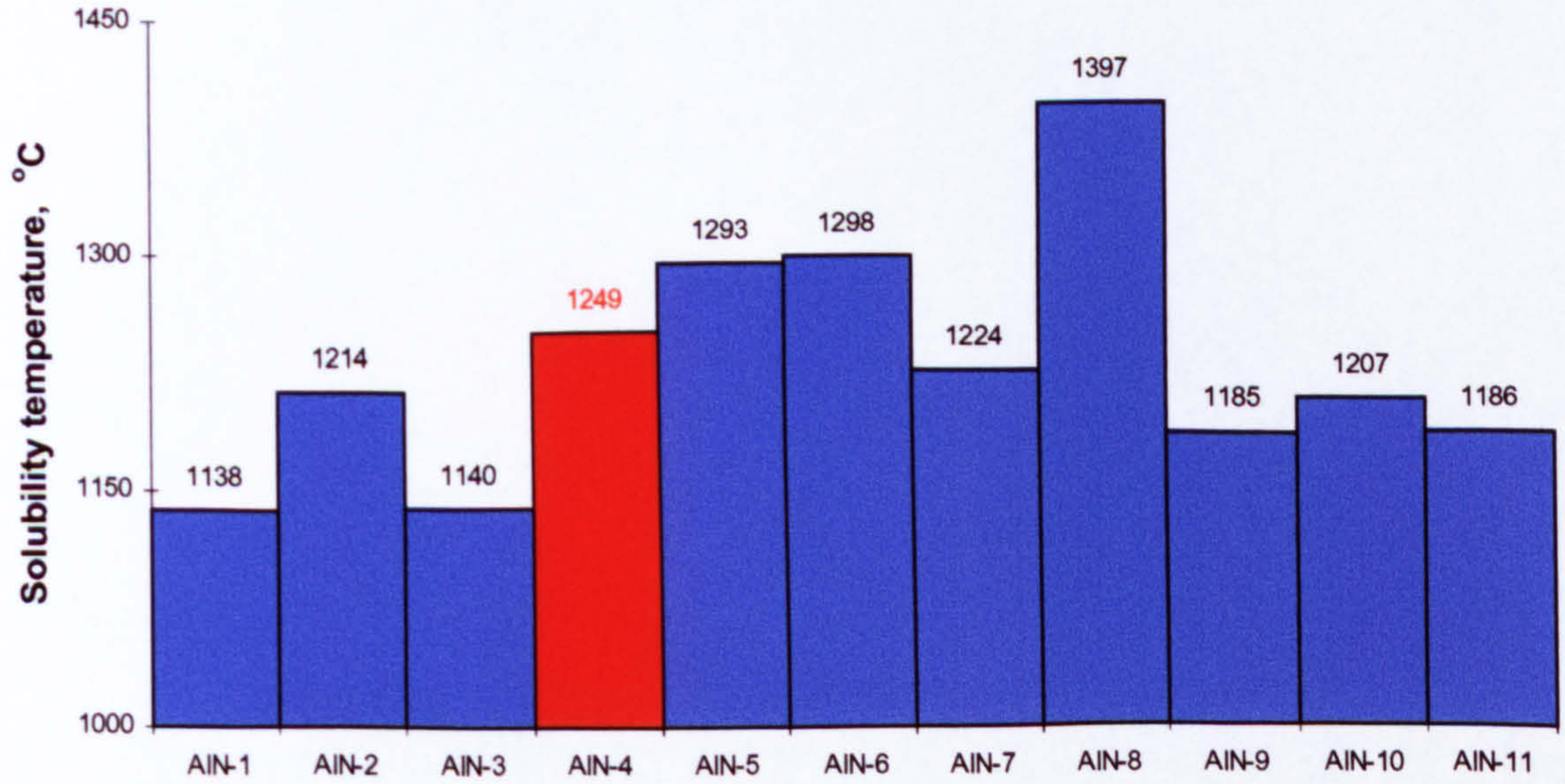

Fig. 5.4 Solubility temperatures of AlN in Steel 2 and Steel 3 calculated by several equations

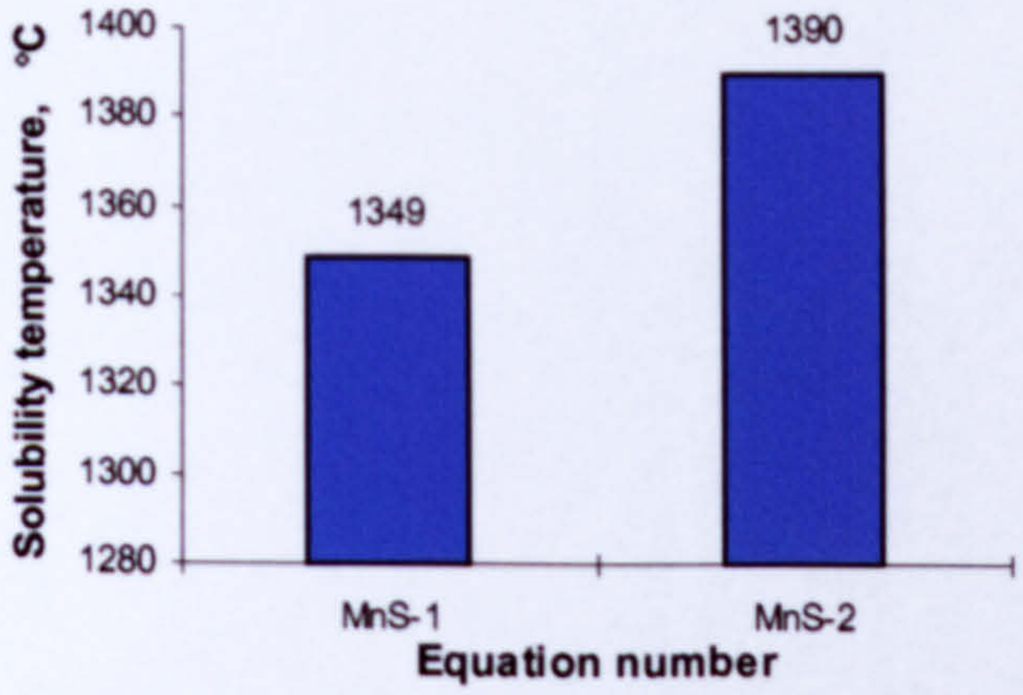

Fig. 5.5 Solubility temperatures of MnS in Steel 1 calculated by two equations

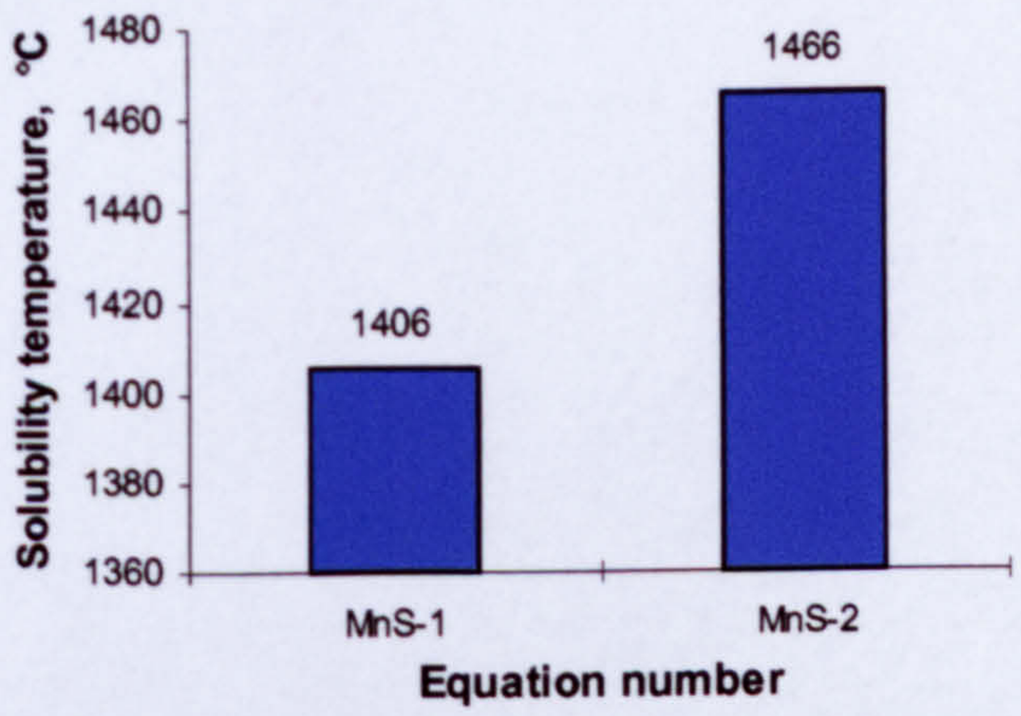

Fig. 5.6 Solubility temperatures of MnS in Steel 2 and Steel 3 calculated by two equations

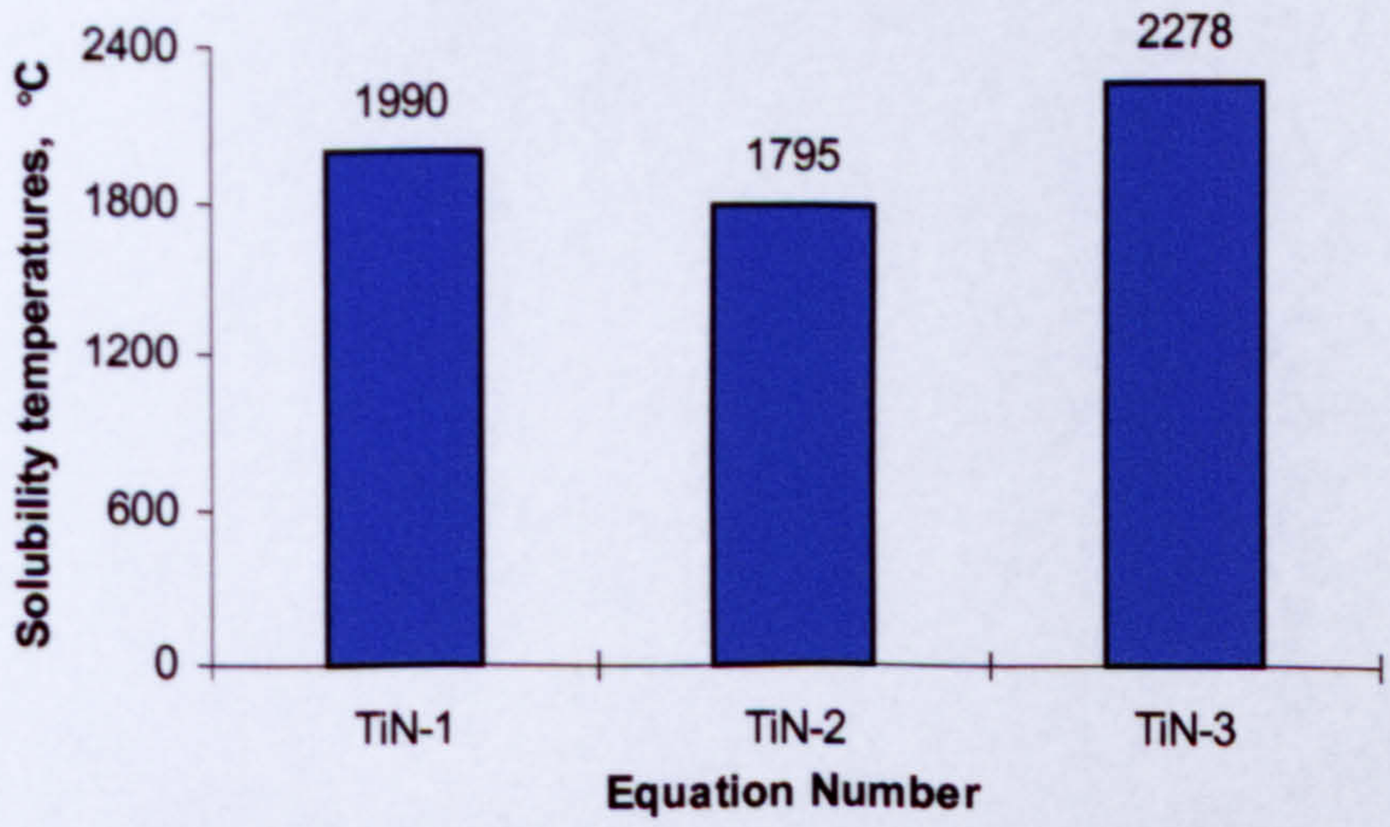

Fig. 5.7 Solubility temperatures of TiN in Steel 3 calculated by three equations

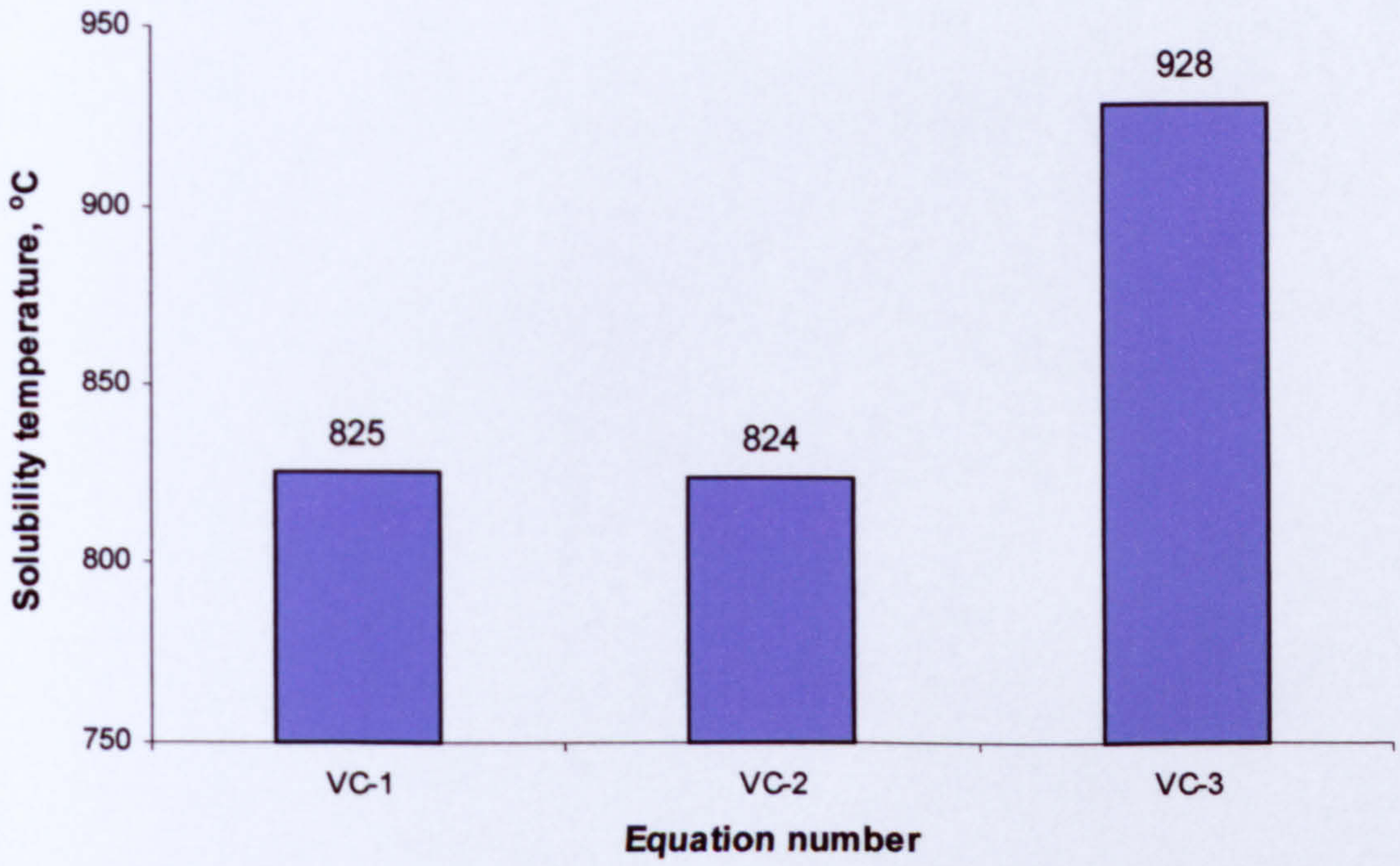

Fig. 5.8 Solubility temperature of VC in Steel 1 calculated by three equations

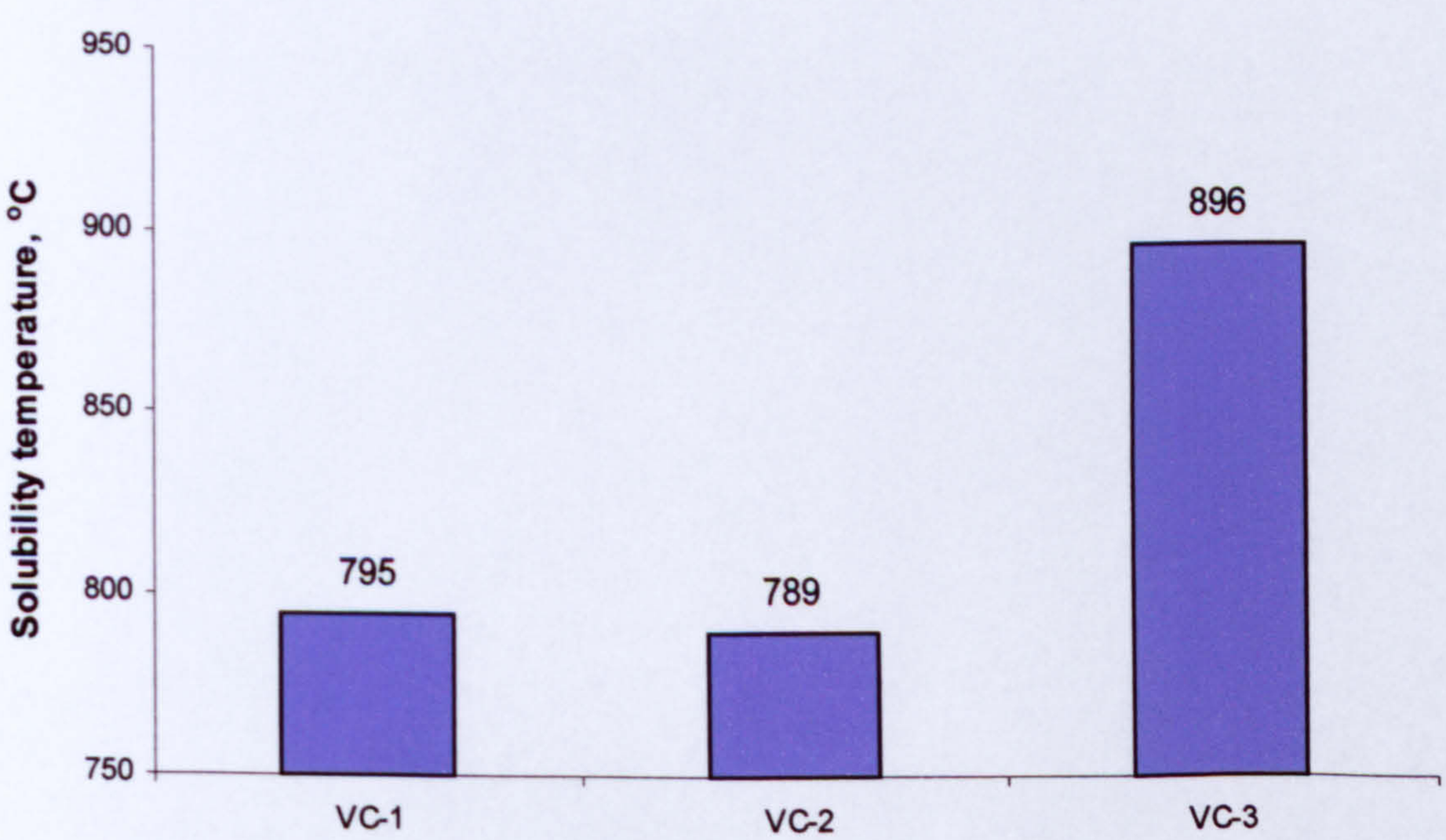

Fig. 5.9 Solubility temperature of VC in Steel 2& 3 calculated by three equations

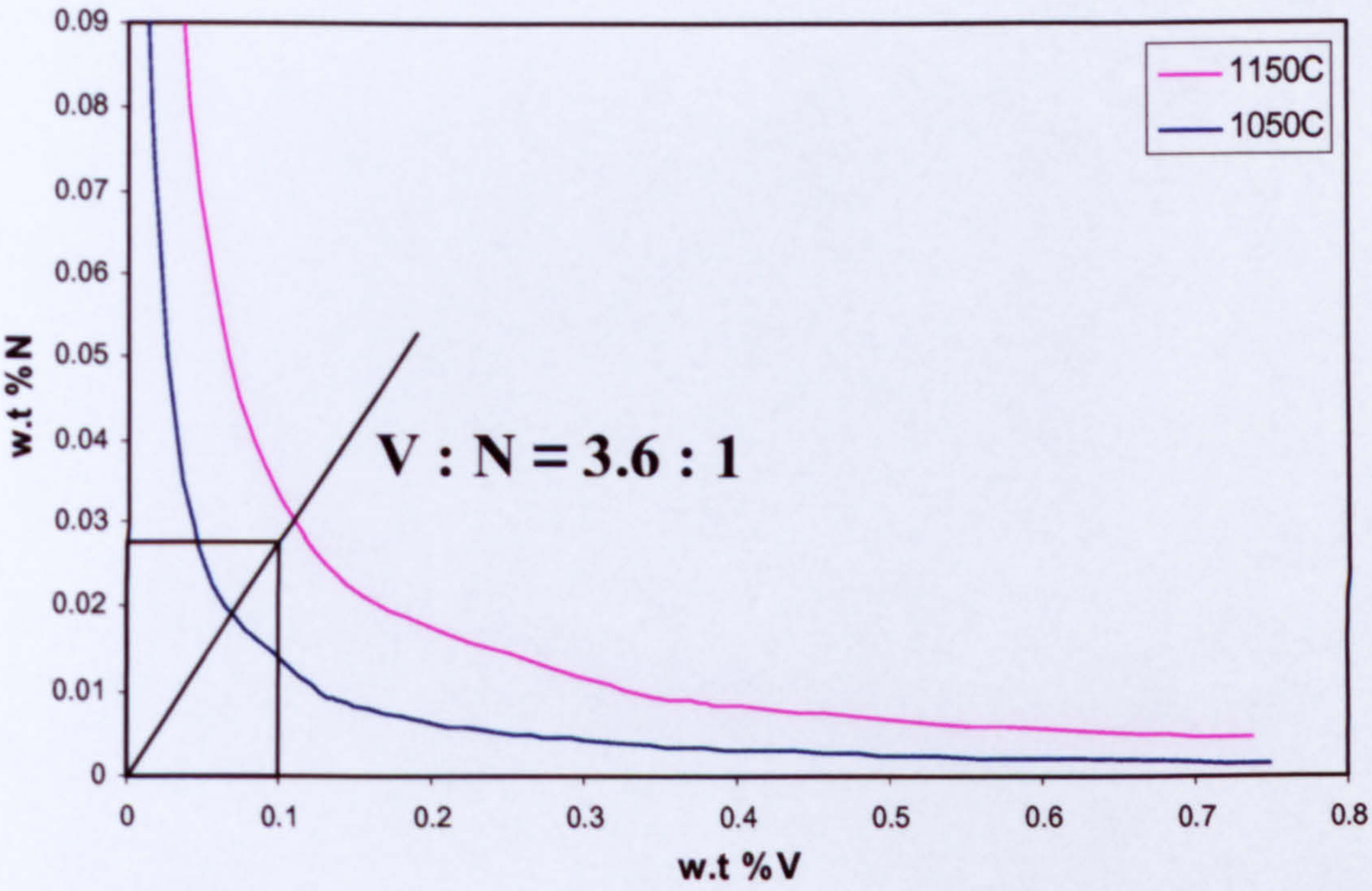

Fig. 5.10 Equilibrium solubility of VN calculated from Eq. VN-7

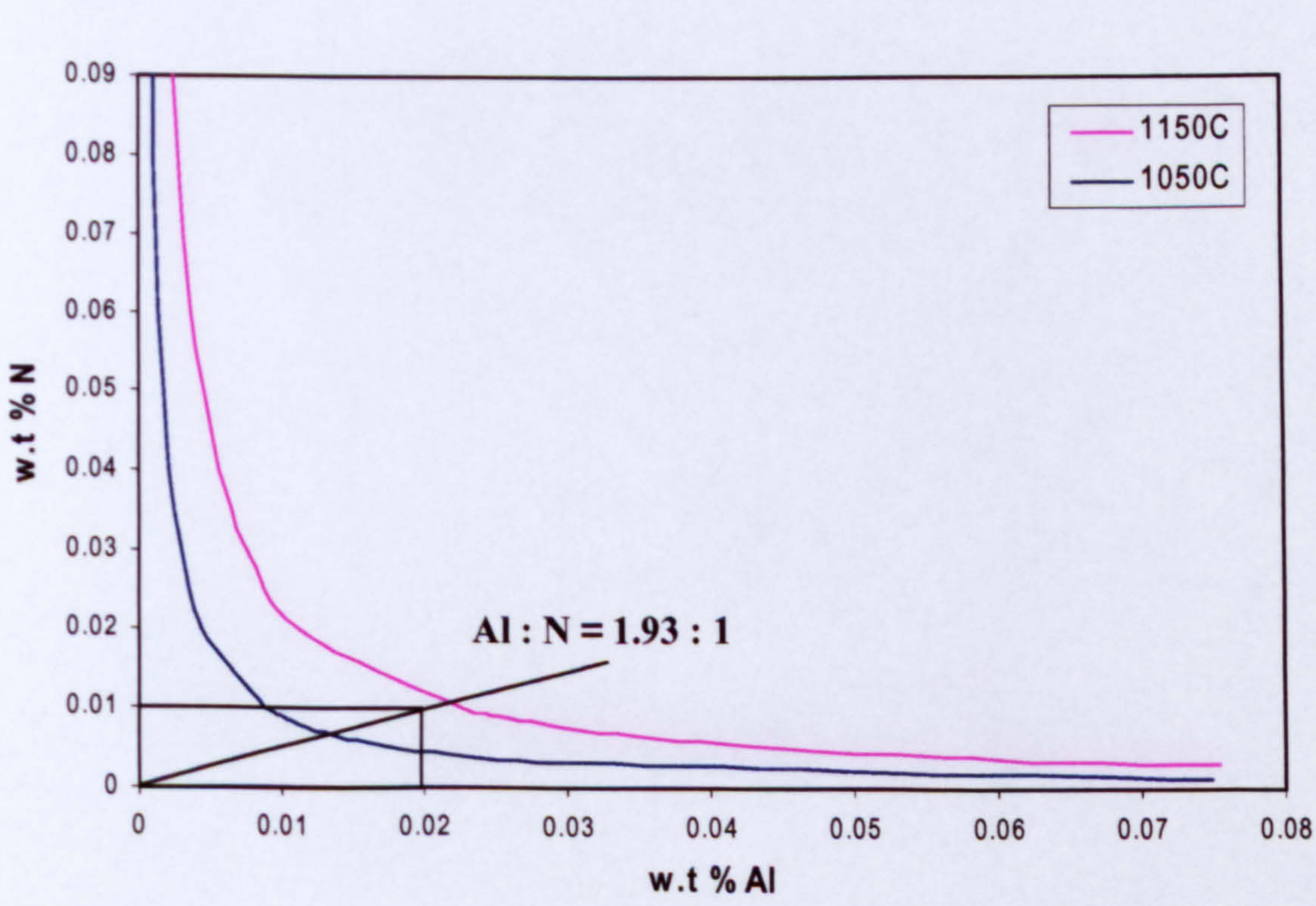

Fig. 5.11 Equilibrium solubility of AlN calculated by Eq. AlN-4

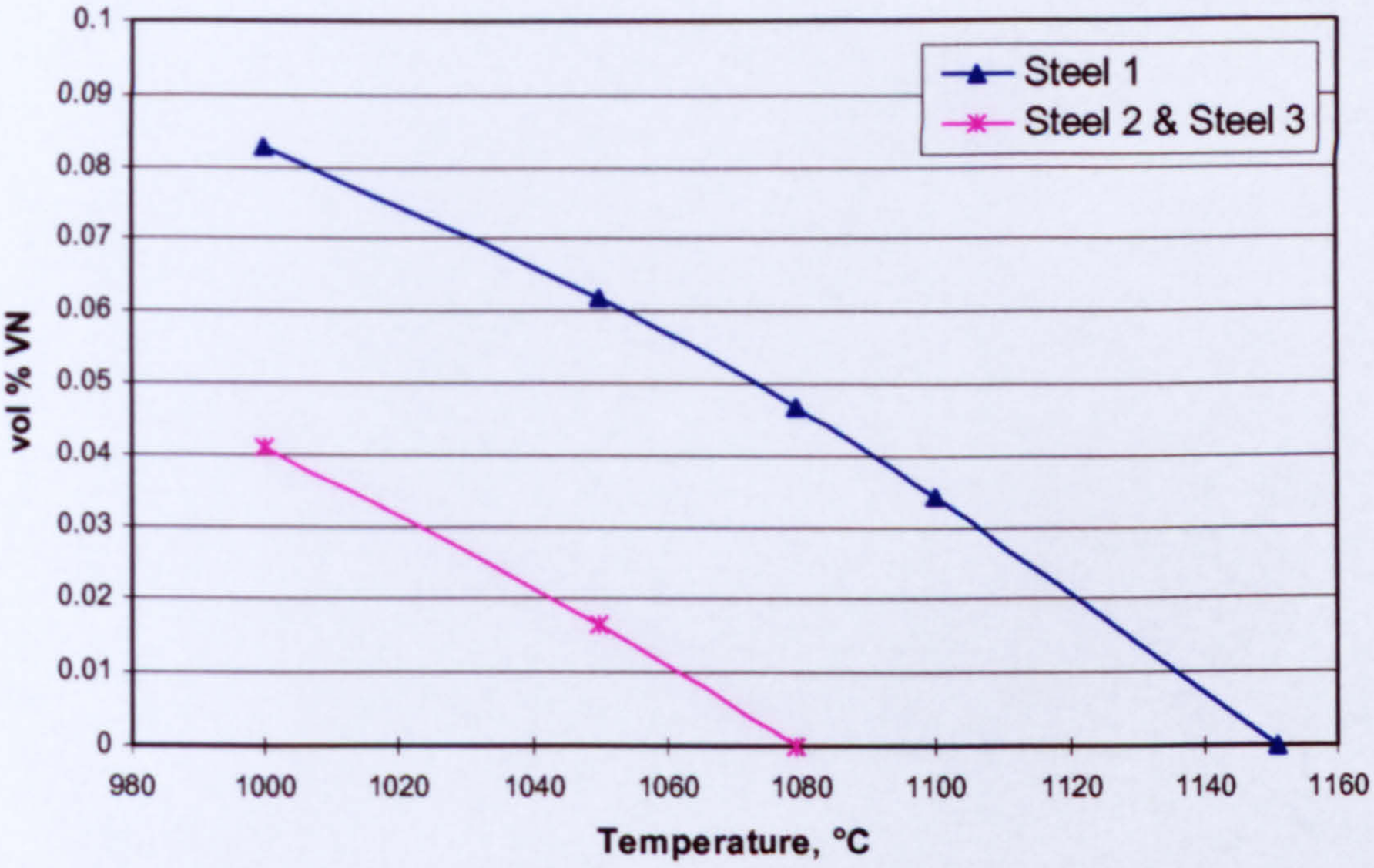

Fig. 5.12 Volume fraction of VN in austenite as a function of temperature

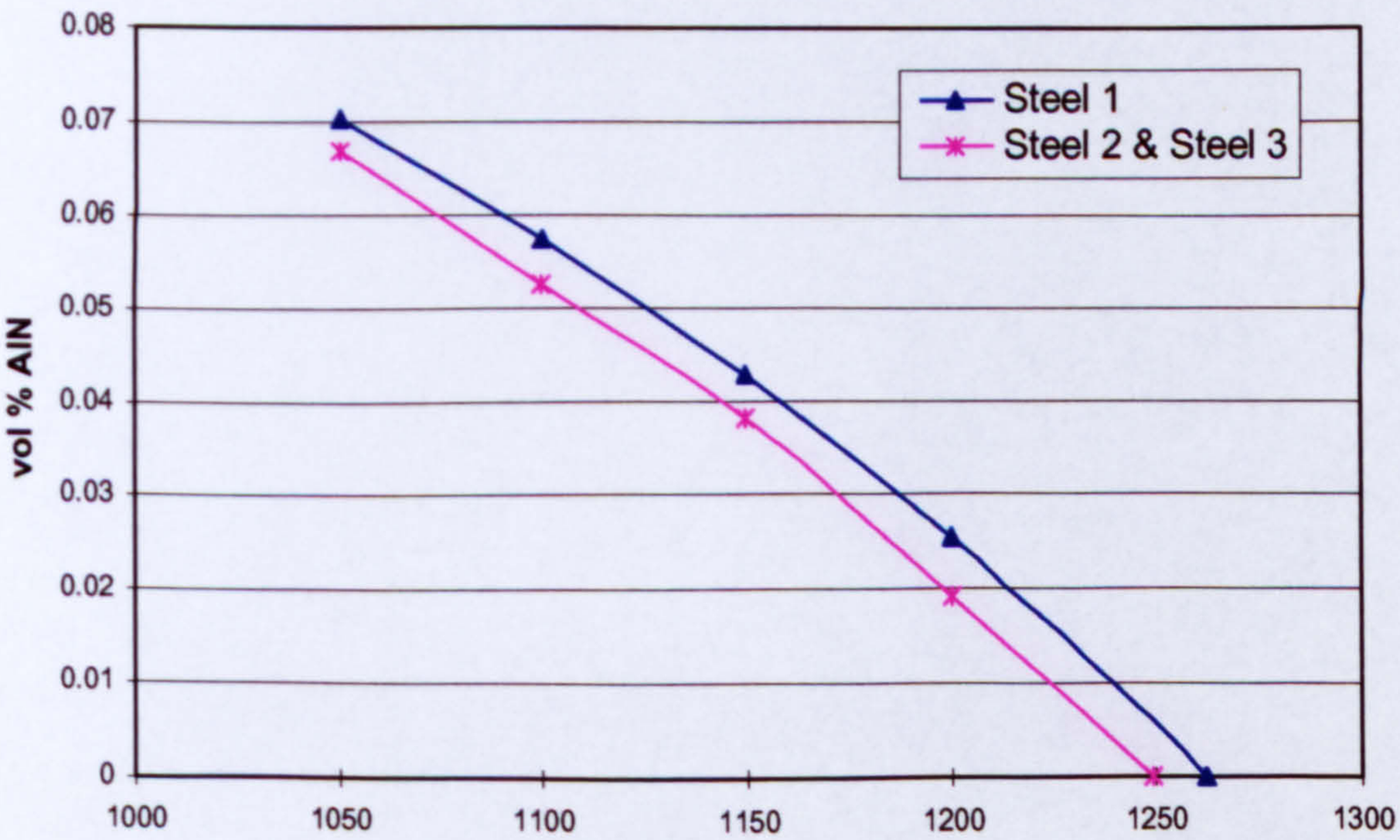

Fig. 5.13 Volume fraction of AlN in austenite as a function of temperature

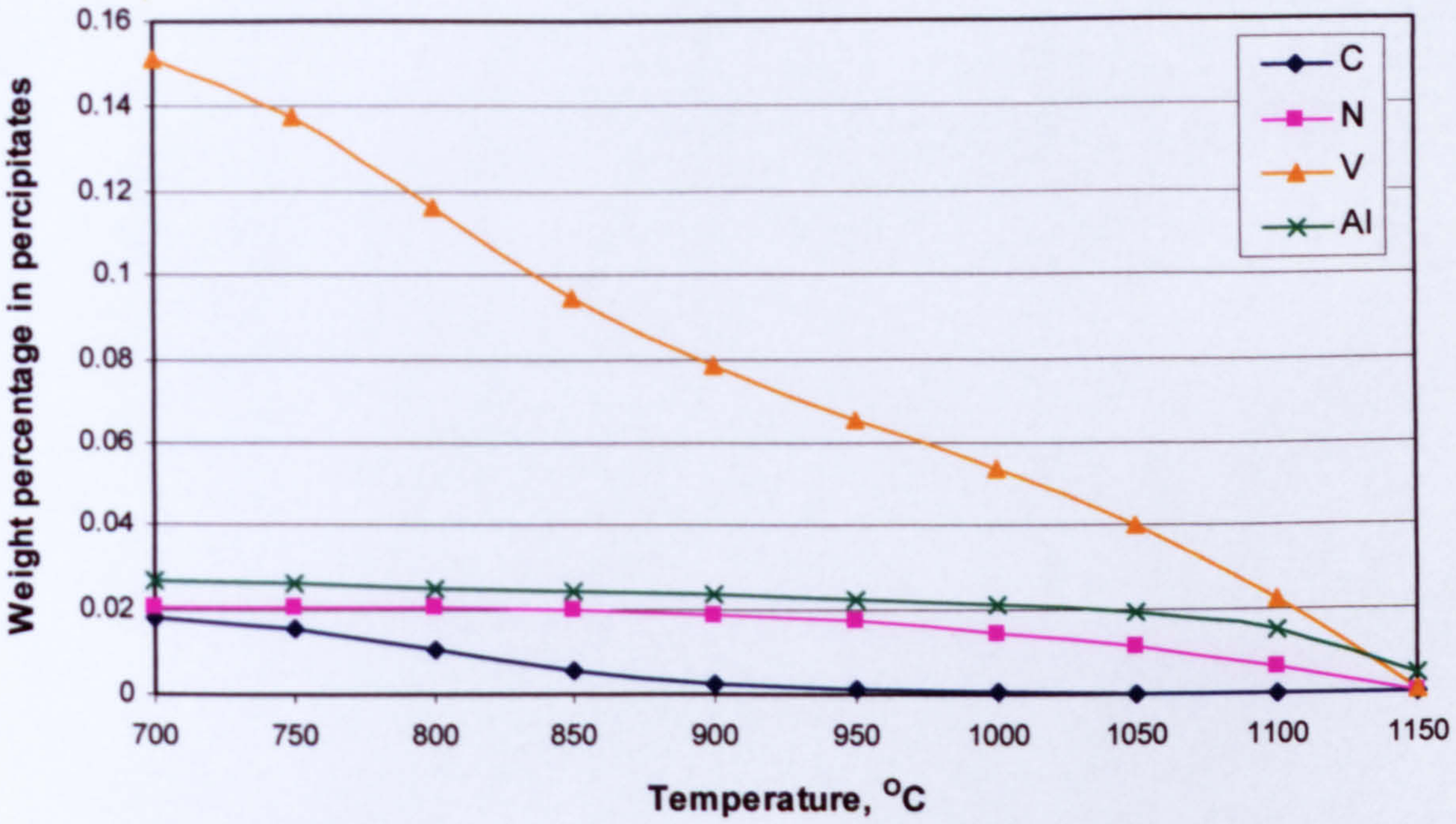

Fig. 5.14 The solubility of carbonitrides in Steel 1 as solution temperatures increase when considering the effect of Al

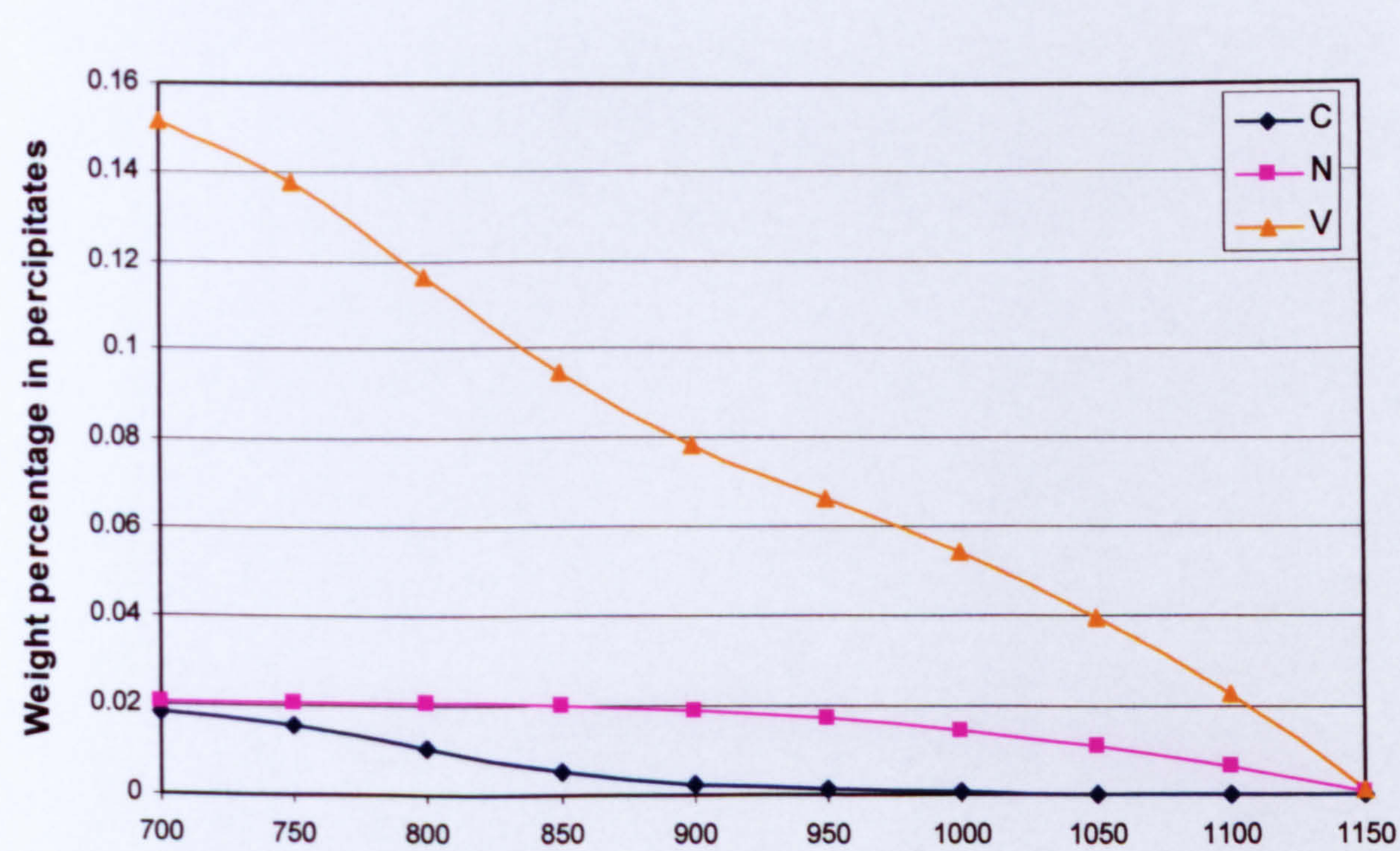

Fig. 5.15 The solubility of carbonitrides in Steel 1 as solution temperatures increase when neglecting the effect of Al

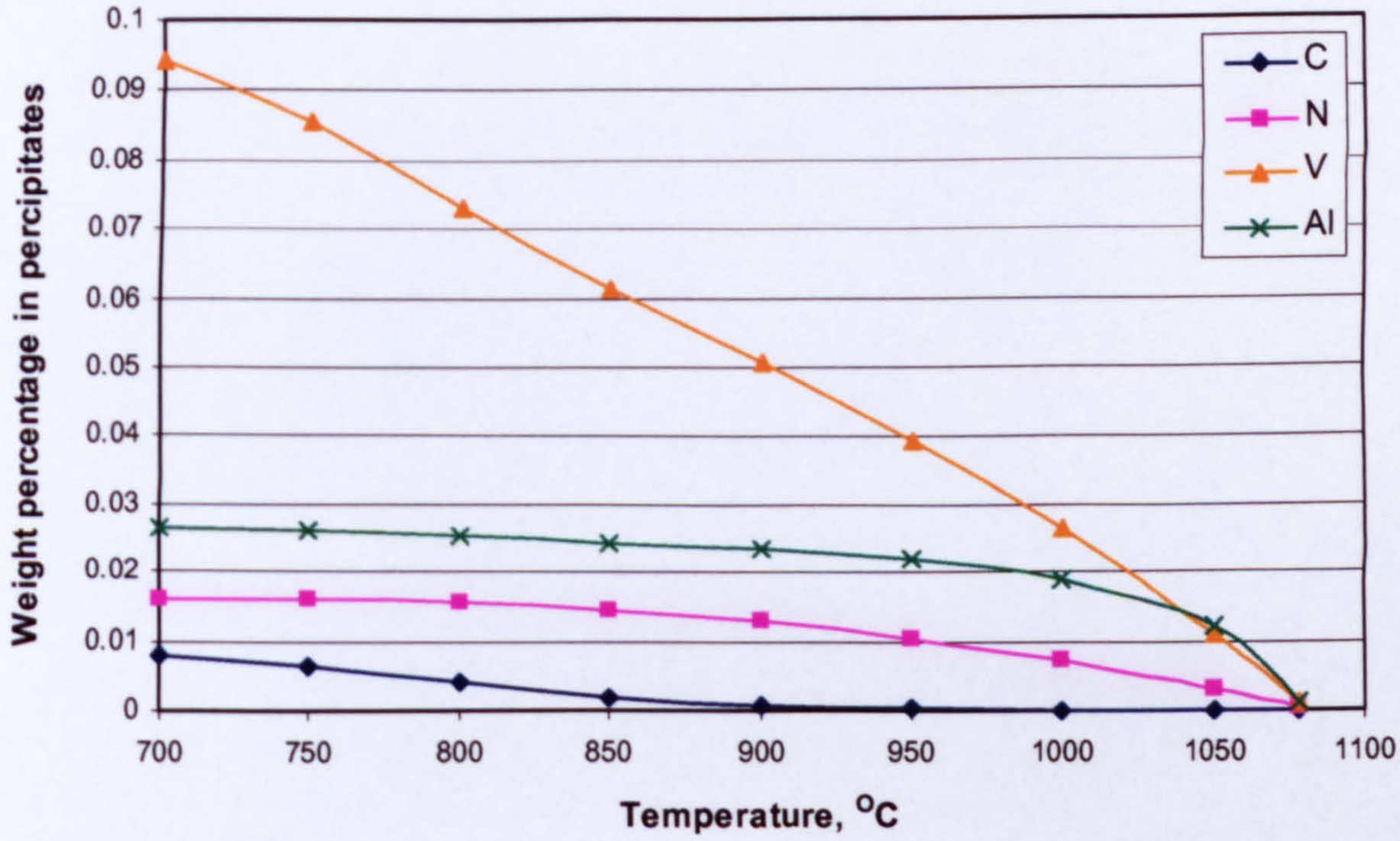

Fig. 5.16 The solubility of carbonitrides in Steel 2 as solution temperatures increase when considering the effect of Al

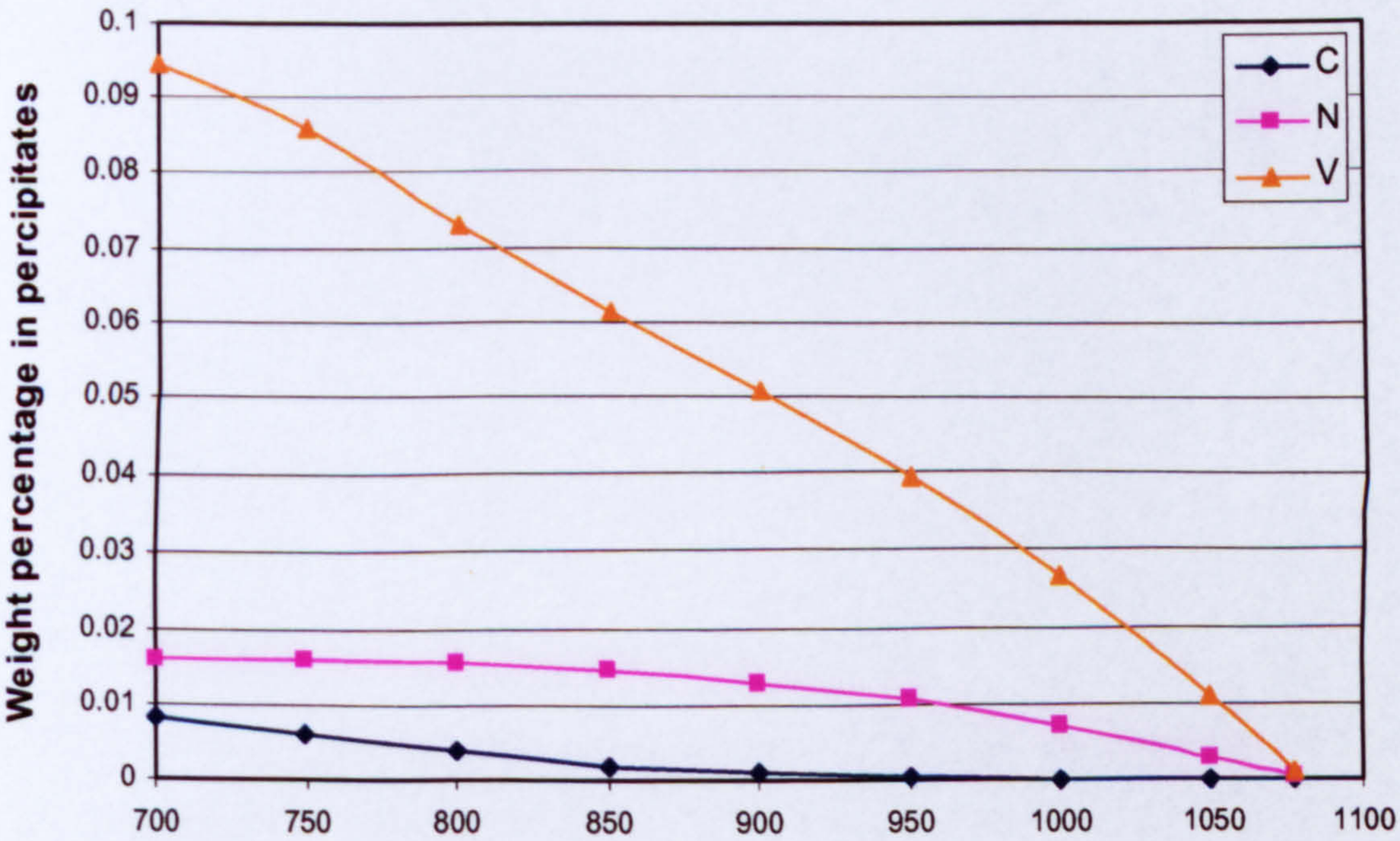

Fig. 5.17 The solubility of carbonitrides in Steel 2 as solution temperatures increase when neglecting the effect of Al

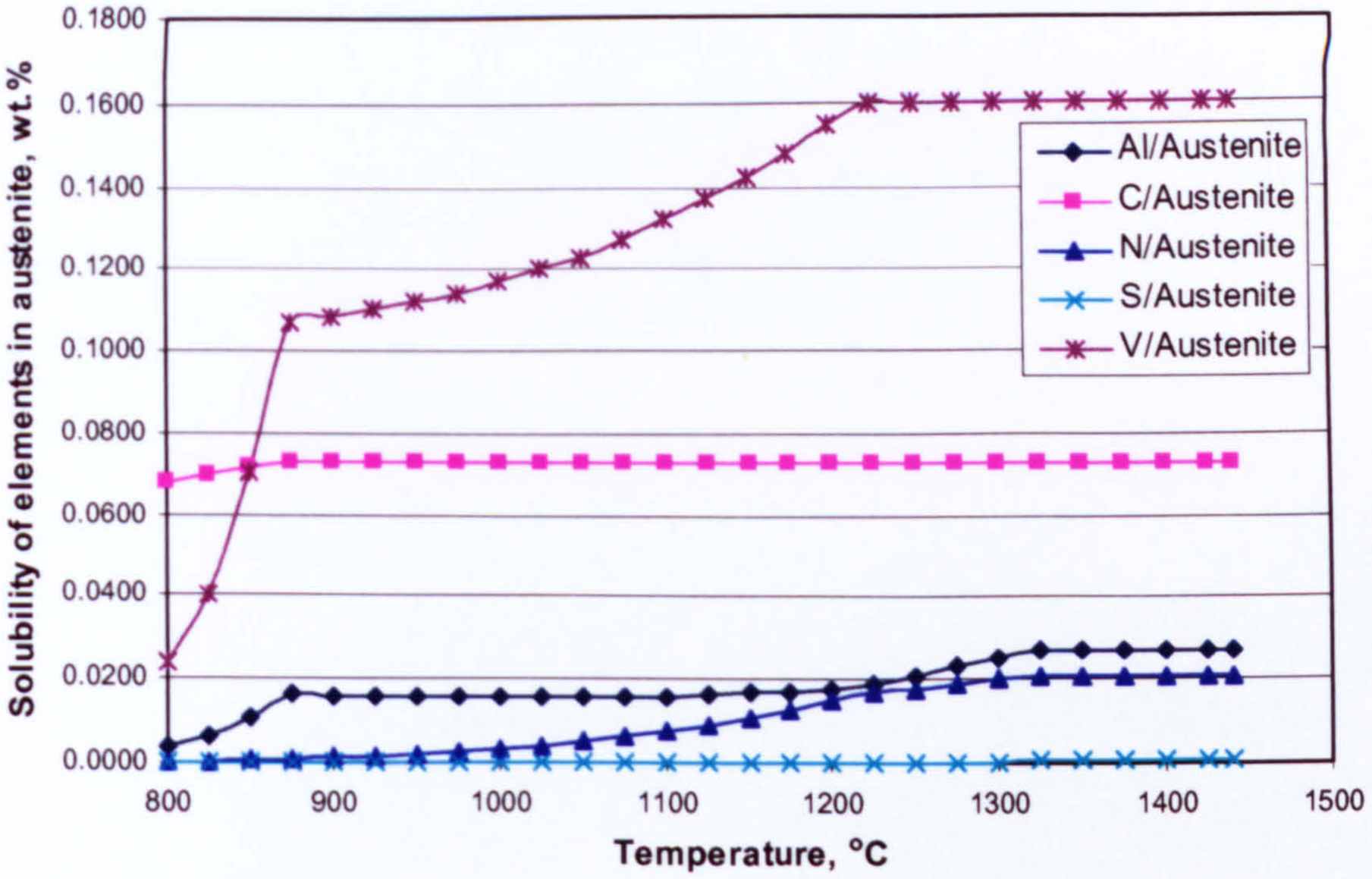

Fig. 5.18 Calculated solubility of elements in austenite of Steel 1 without Ti in calculation by using Chemsage

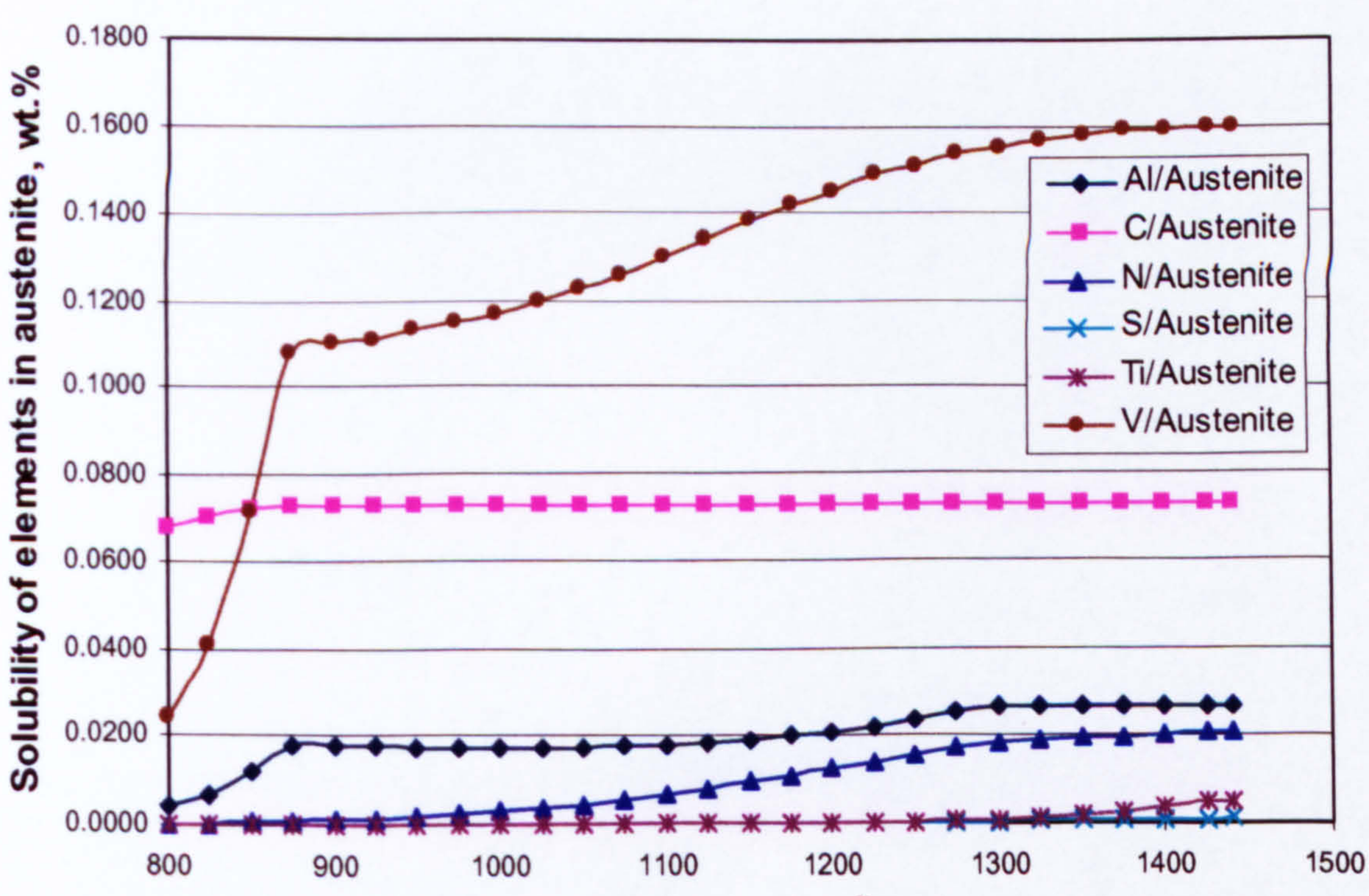

Fig. 5.19 Calculated solubility of elements in austenite of Steel 1 with 0.005 wt.% Ti in calculation

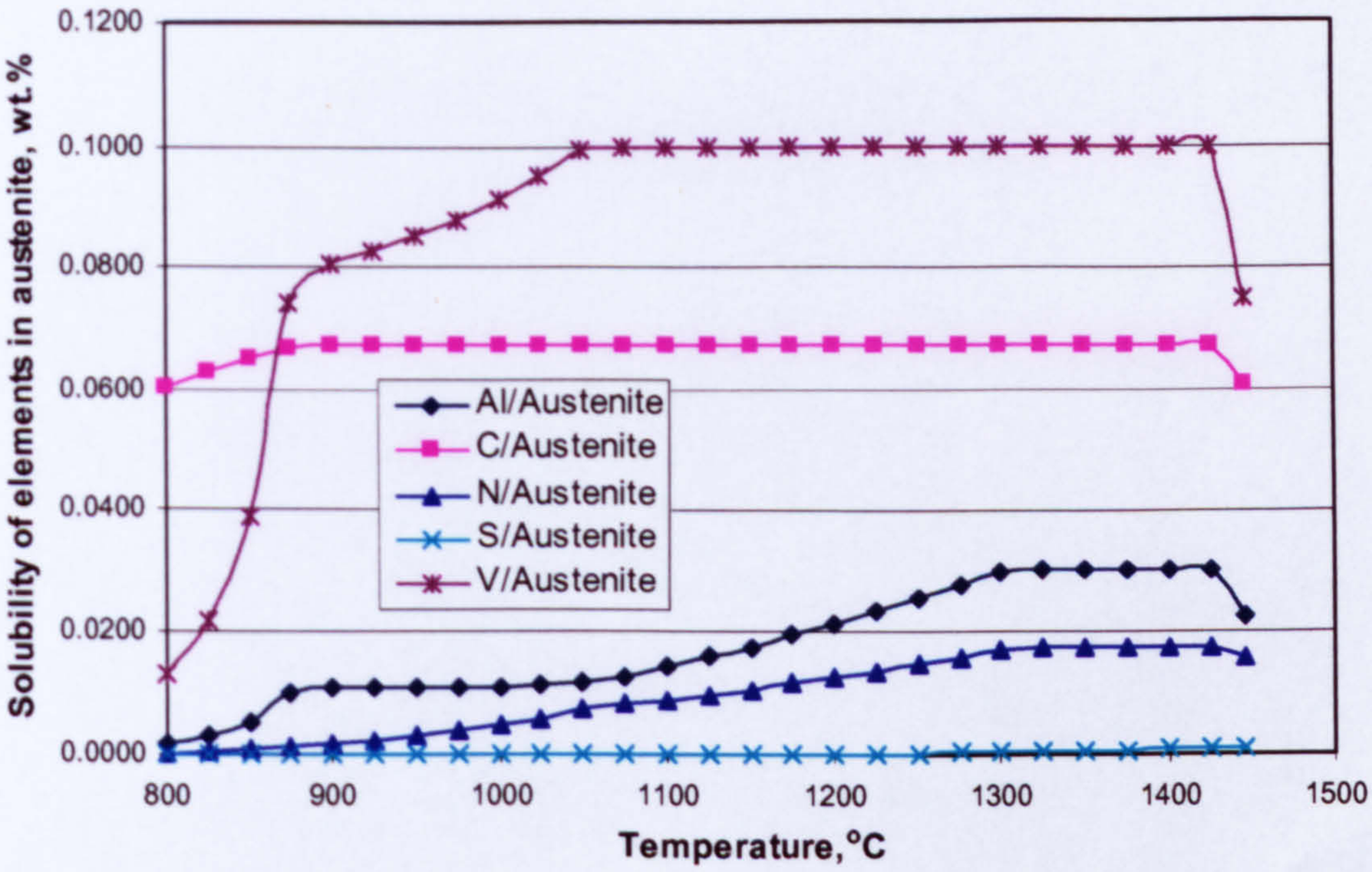

Fig. 5.20 Calculated solubility of elements in austenite of Steel 2

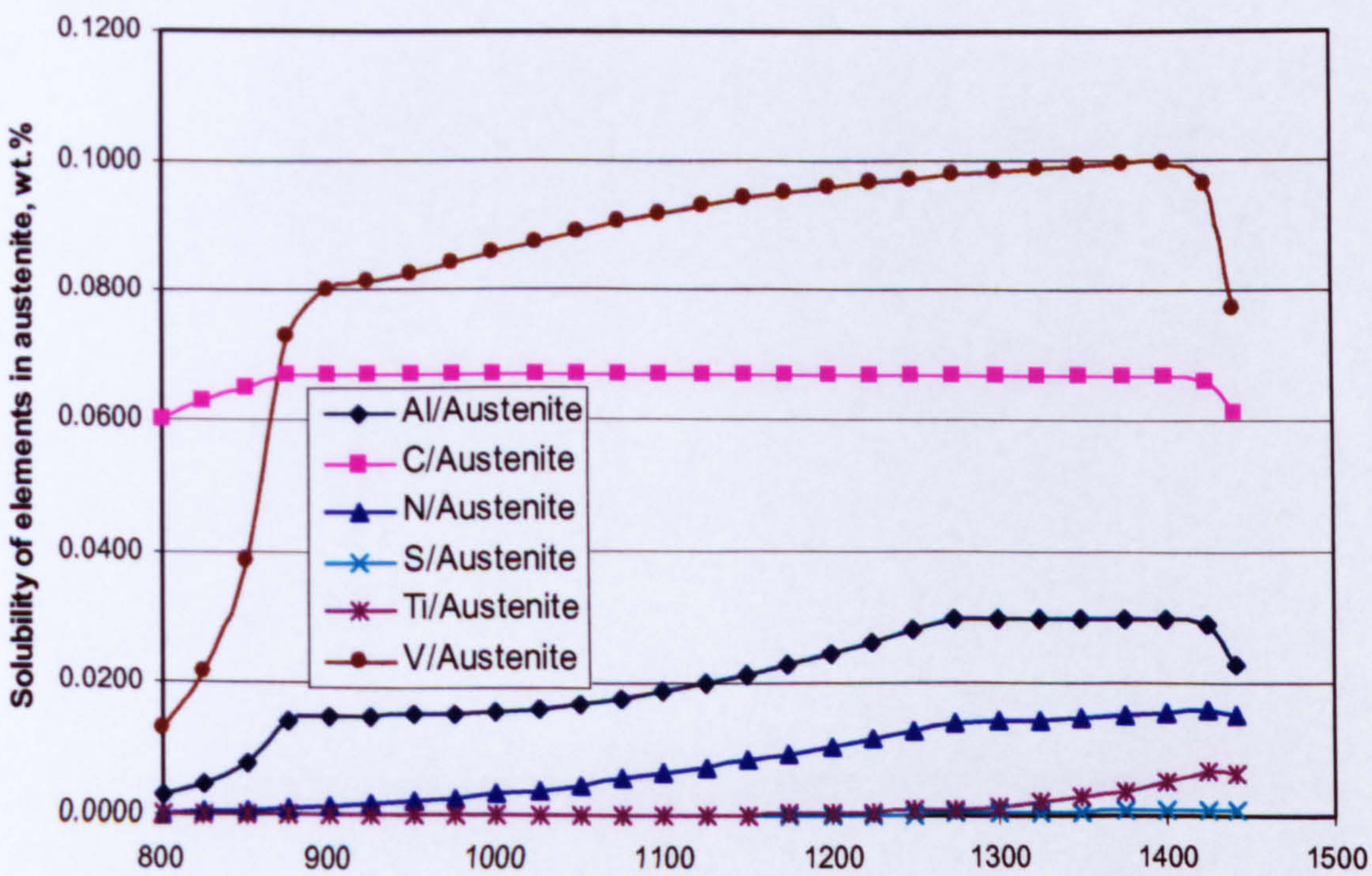

Fig. 5.21 Calculated solubility of elements in austenite of Steel 3 by using ChemSage

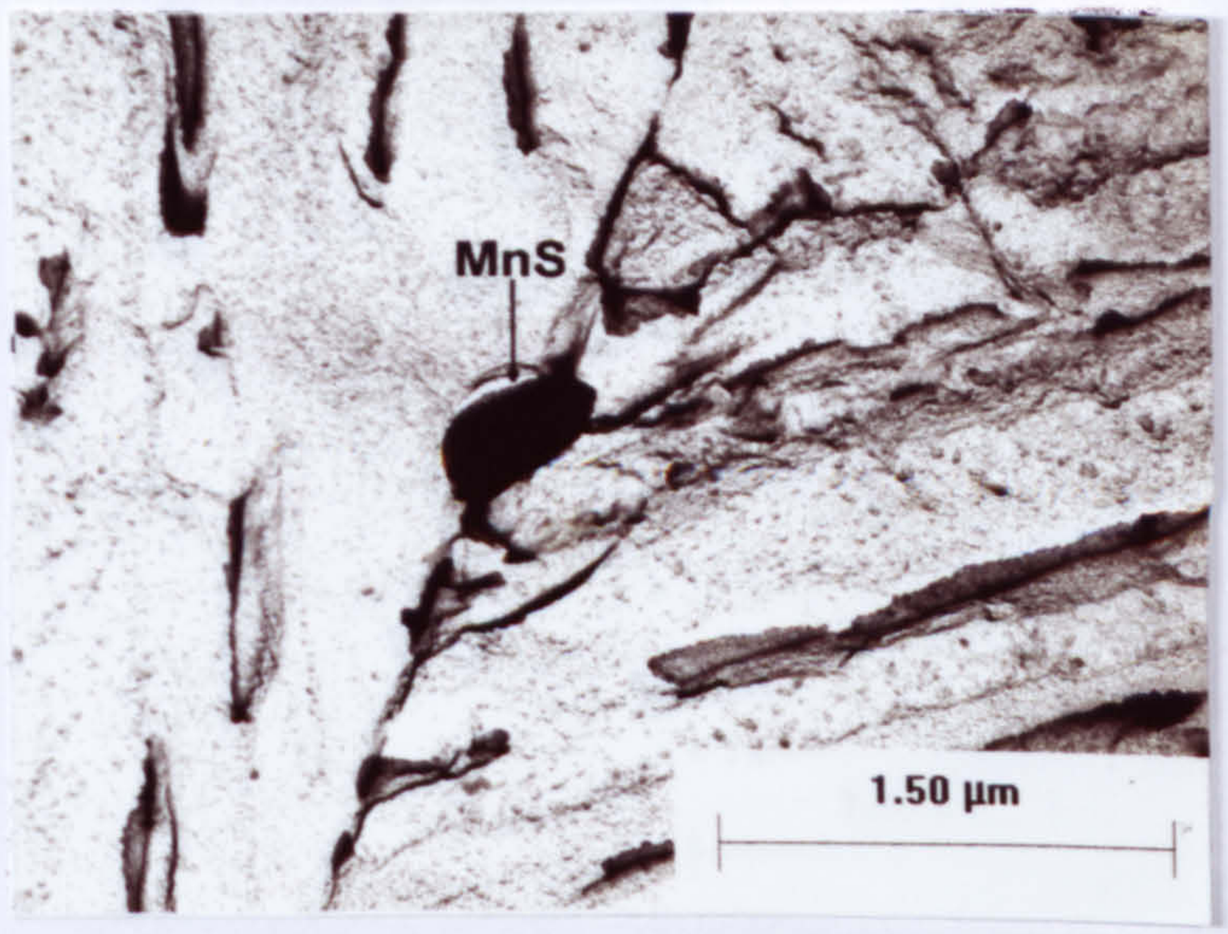

Fig. 5.22 MnS on austenite grain boundary in Steel 1 equalised at 1150°C for 53 min

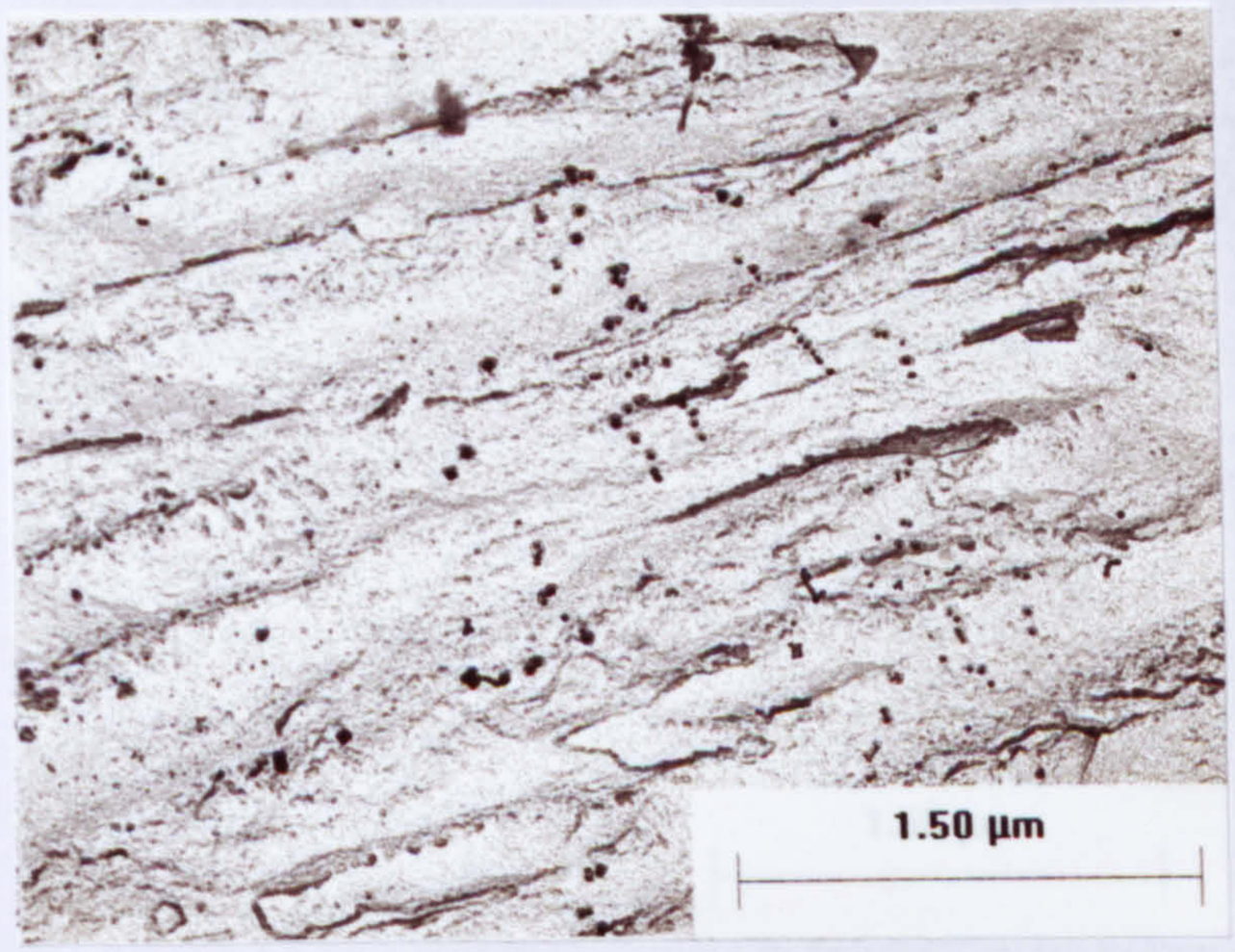

Fig. 5.23 $(Ti_xV_{1-x})N$ in Steel 3 reheated at 1150°C for 53 min

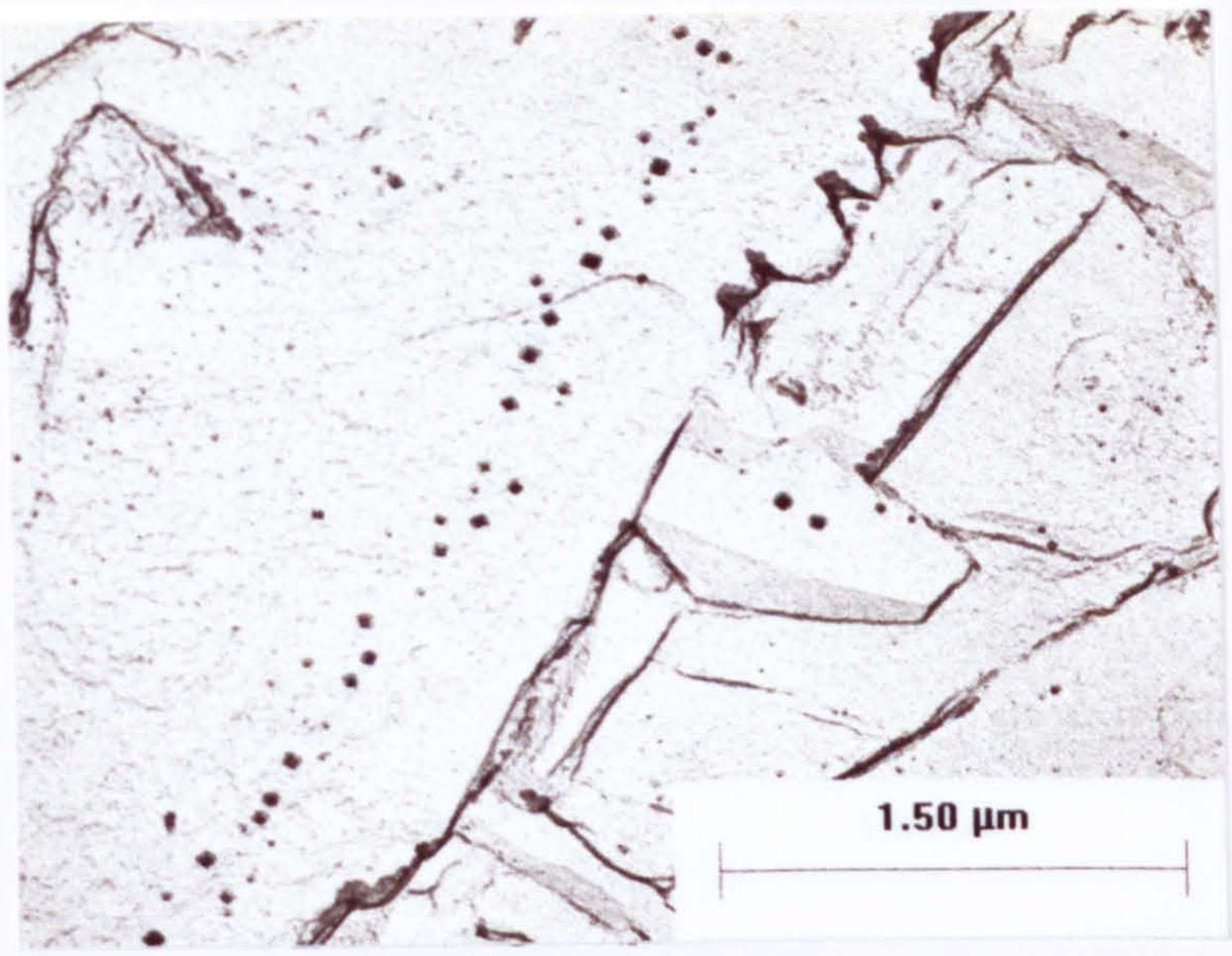

Fig. 5.24 Long $(Ti_xV_{1-x})N$ row in Steel 3 reheated at 1150°C for 53 min

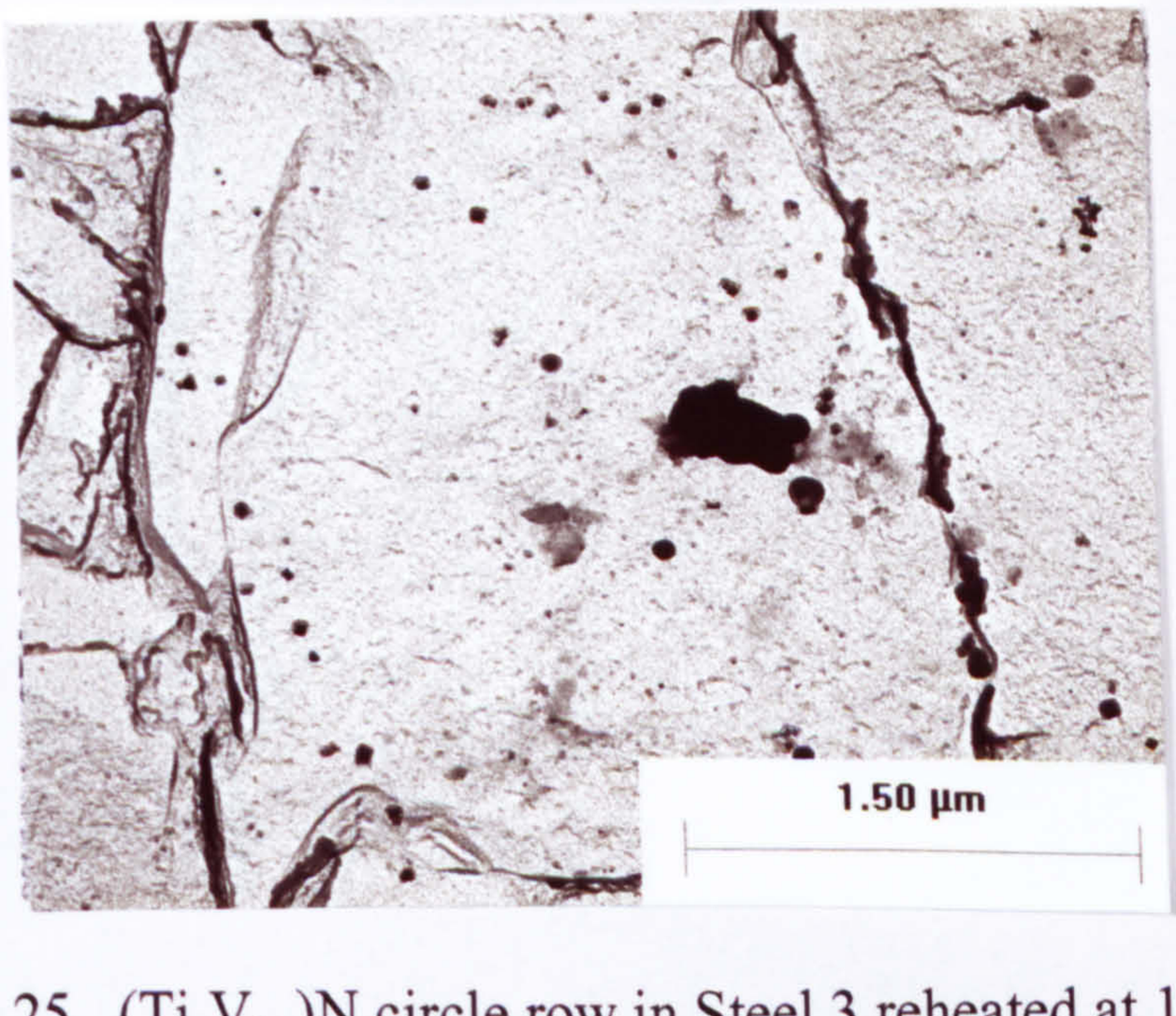

Fig. 5.25 $(Ti_xV_{1-x})N$ circle row in Steel 3 reheated at 1150°C for 53 min

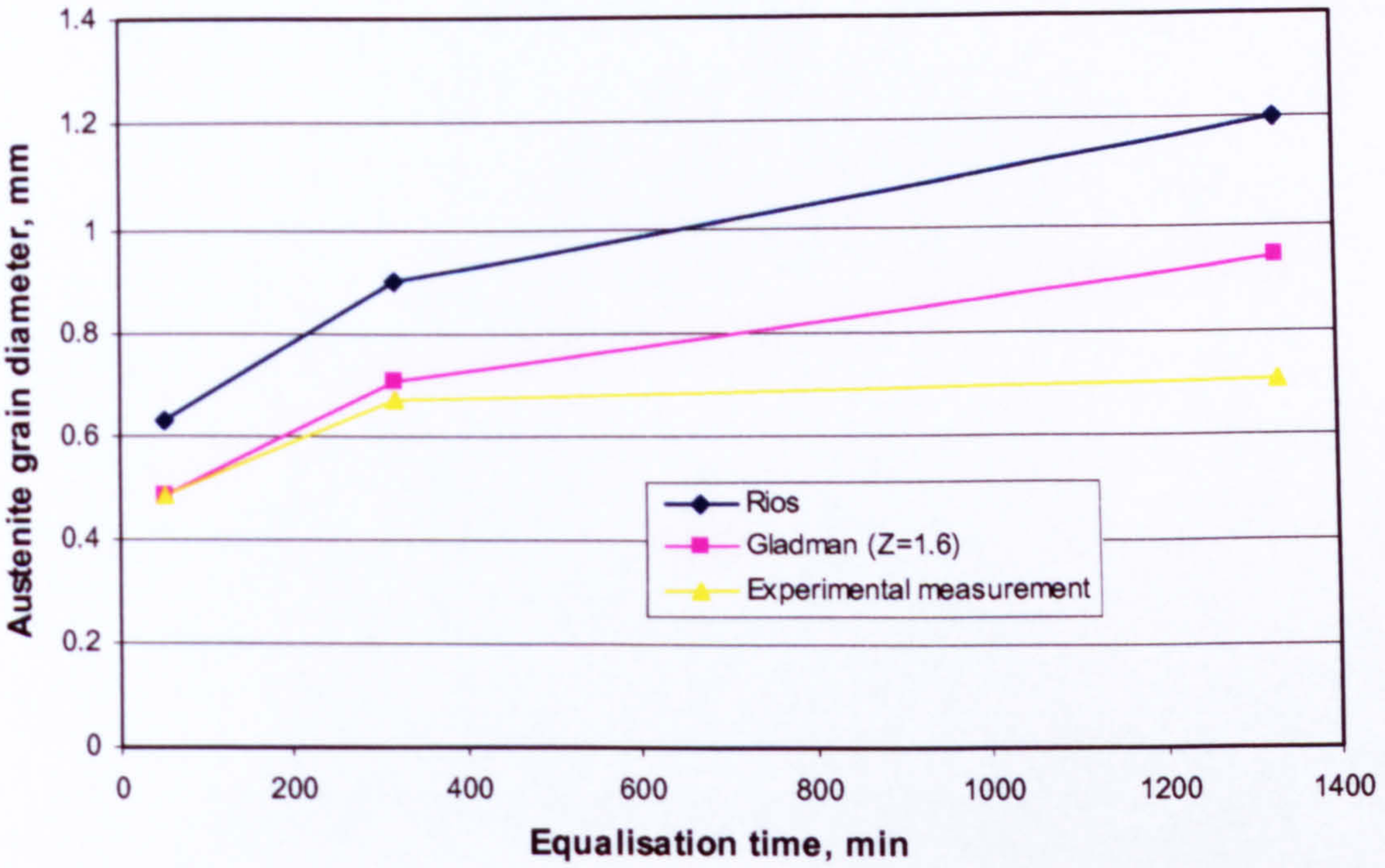

Fig. 5.26 The calculated and measured austenite grain size at different equalisation time by using Gladman and Rios equation

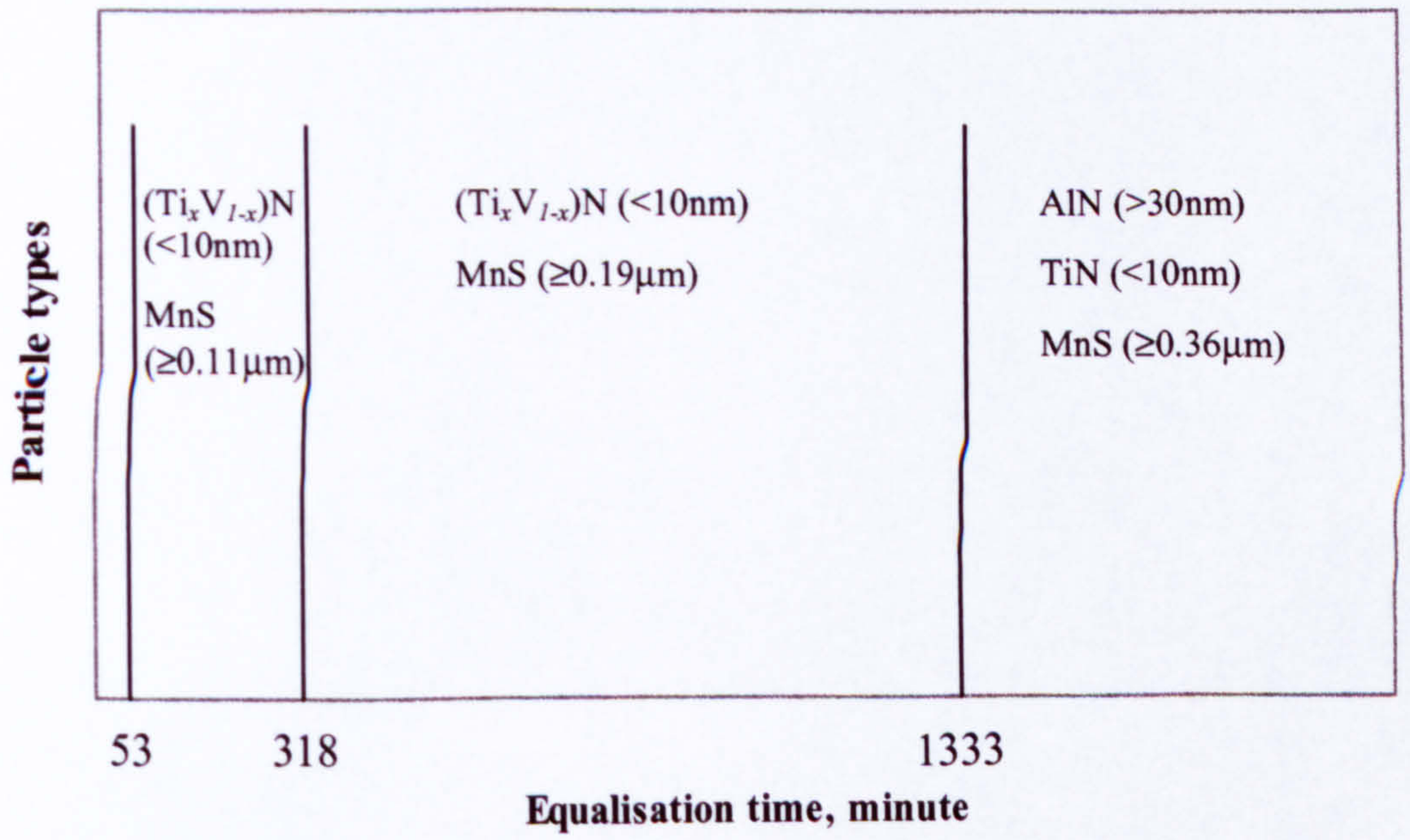

Fig. 5.27 The appearance of precipitates in austenite after the equalisation for three different times

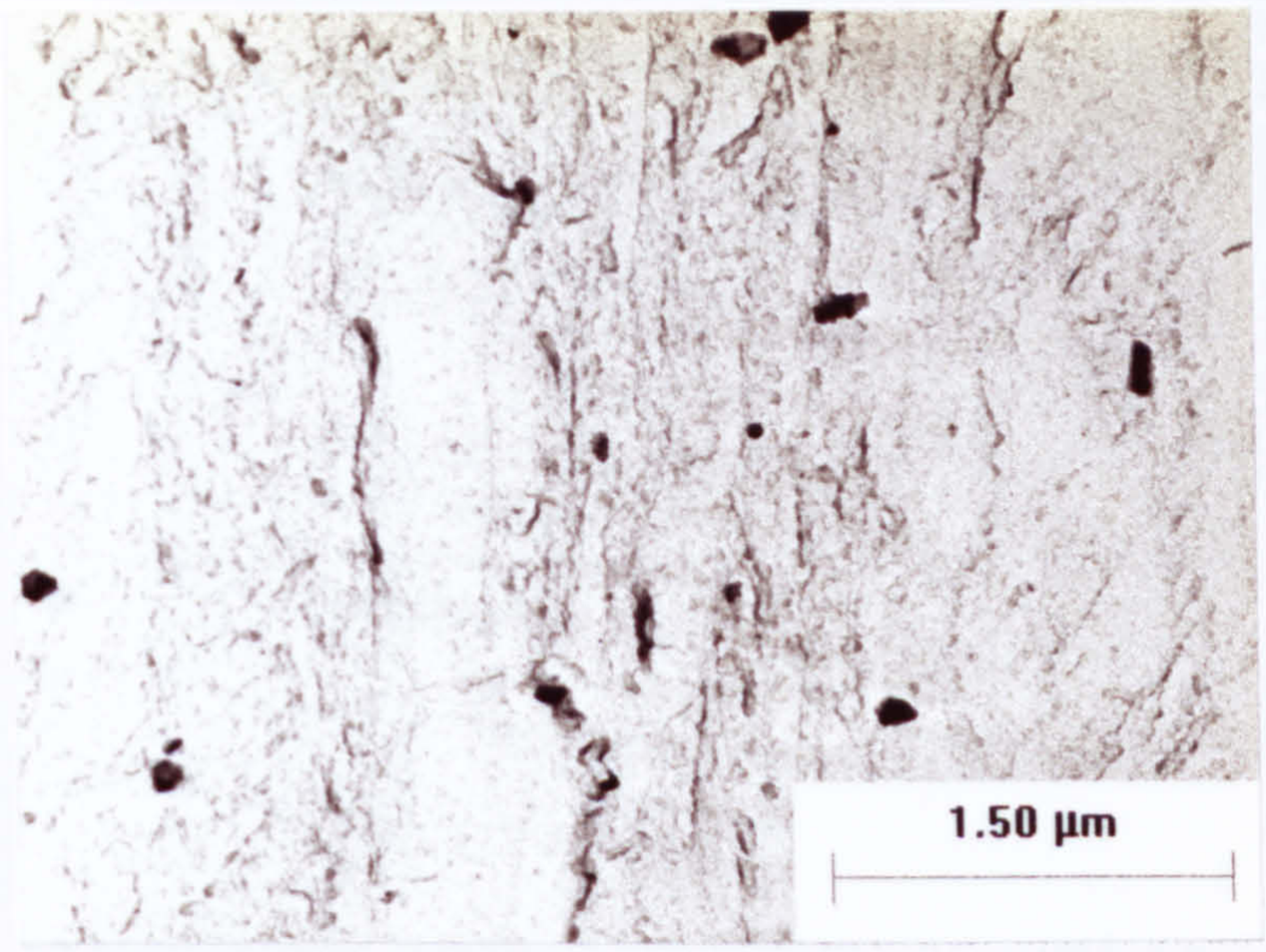

Fig. 5.28 AlN in austenite in Steel 2 reheated at 1150°C for 53 min

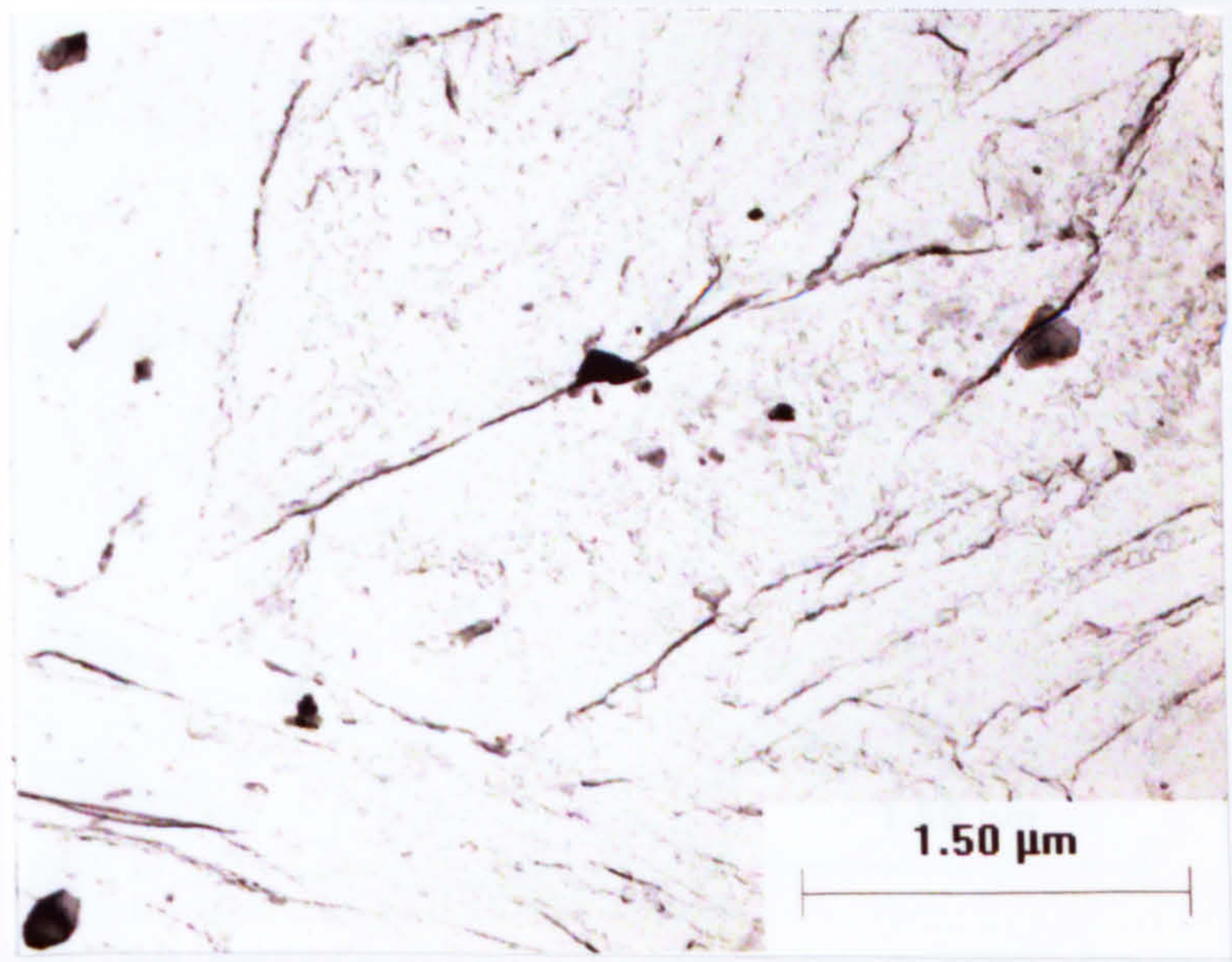

Fig. 5.29 AlN in austenite in Steel 2 reheated at 1150°C for 318 min

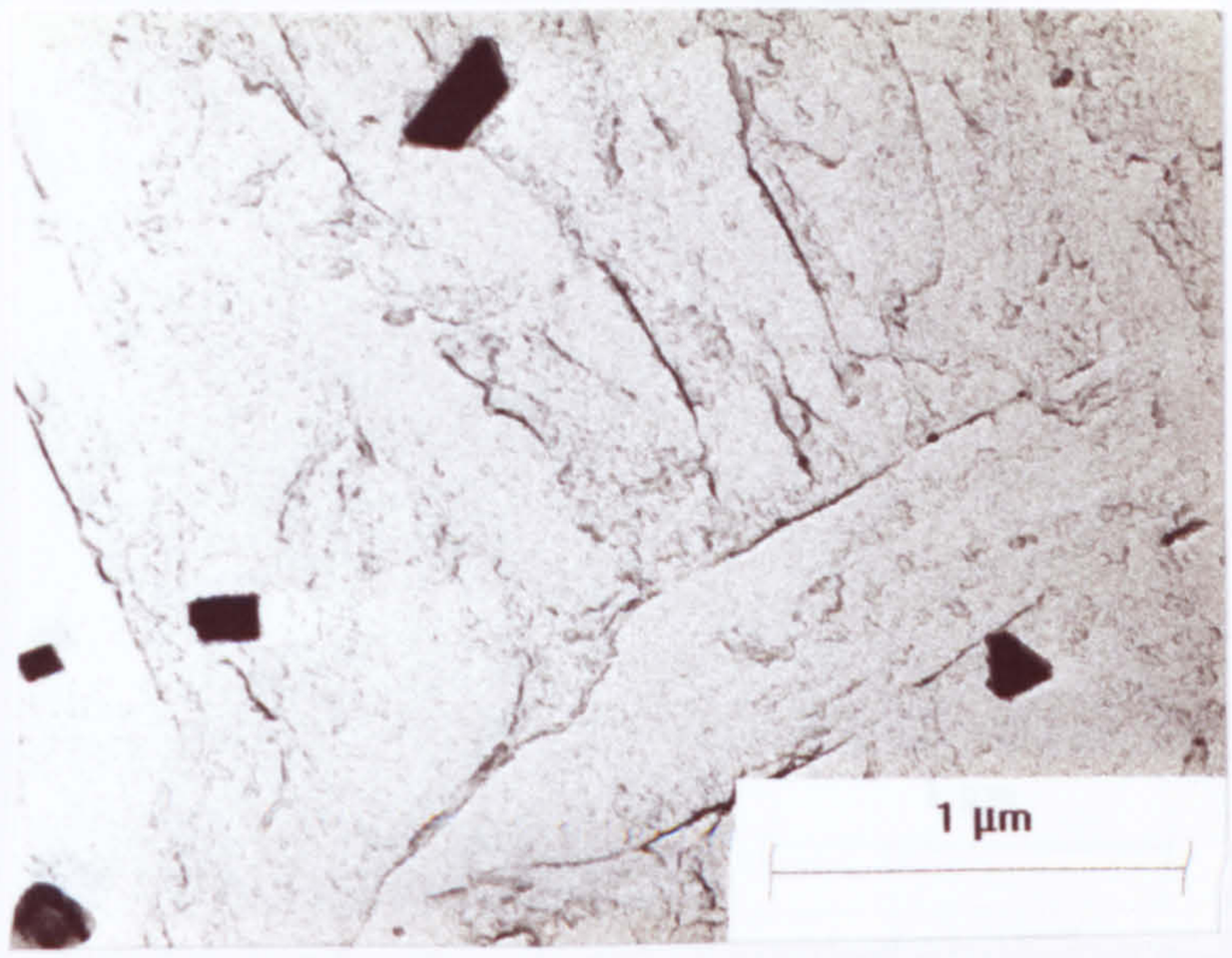

Fig. 5.30 AlN in austenite in Steel 2 reheated at 1150°C for 1333 min

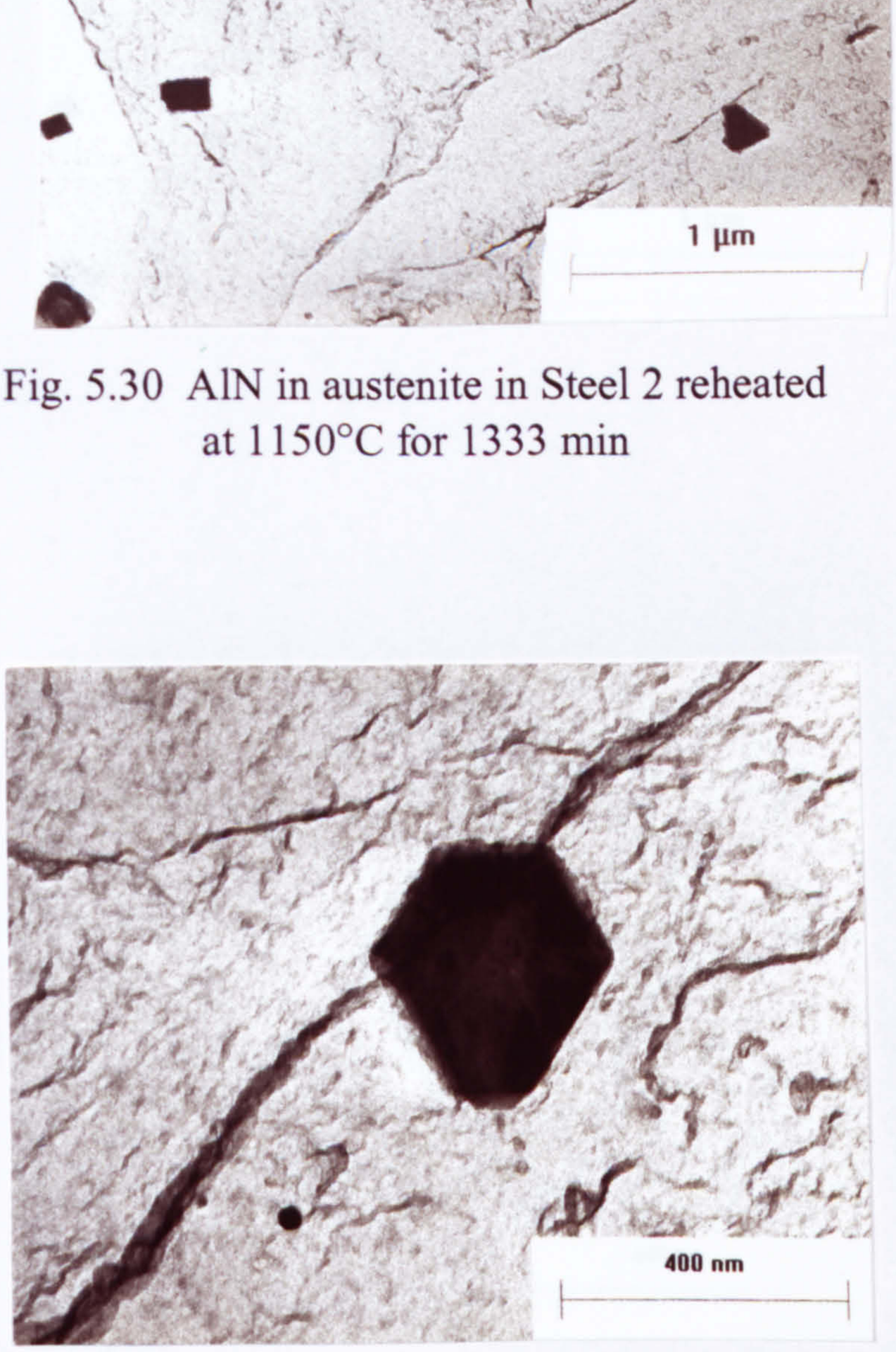

Fig. 5.31 AlN in austenite in Steel 3 reheated at 1150°C for 318 min

TABLES

Table 3.1 The composition of steels wt%

Steel	C	Si	Mn	P	S	Cr	Mo	Ni
1	0.073	0.40	1.83	0.014	0.002	0.08	0.50	0.08
2	0.067	0.39	1.52	0.016	0.004	0.08	0.02	0.09
3	0.067	0.39	1.52	0.016	0.004	0.08	0.02	0.09

Steel	Al	B	Cu	N	Nb	Ti	V
1	0.027	<0.005	0.08	0.021	<0.005	<0.005	0.16
2	0.03	<0.005	0.08	0.017	<0.005	<0.005	0.10
3	0.03	<0.005	0.08	0.017	<0.005	0.009	0.10

Table 5.1 Solubility expressions for VC, VN, AlN, TiN, and MnS in austenite

MX	Chemical Composition, wt%							Method	Temperature Range, °C	Heat time (h)	$Log_{10}K^{\gamma}$	REFERENCES
	C	Si	Mn	N	V	Al	Ti					
VC-1											-9500/T+6.72	Narita(1975)
VC-2											-8000/T+5.36	Aronsson(1973)
VC-3								A	900 ~1200		-10800/T+7.06	Robertson(1993)
VN-1	0.08	0.19			0.4			G			-8700/T+3.63	Narita(1975)
VN-2	0.16	0.31	0.92	0.007	0.027	0.066	0.009	A	900 ~1200		-7930/T+3.07	Robertson(1993)
VN-3	0.1	0.1	0.5	0.013	0.095			C	900 ~1100		-8330/T+3.46	Irvine(1967)
VN-4											-7733/T+2.99	Narita(1957)
VN-5								T			-7070/T+2.27	Frohberg(1960)
VN-6	0.2	0.2-2.33	0.55	0.006-0.011	0.003-0.26			C	900 ~1150	2	-6900/T+2.35	Erasmus(1964b)
VN-7	0.31	0.34	1.31	0.0082	0.18	0.022					-7840/T+3.03	Eckstein(1993)
VN-8	0.16		1.5		0.1			C	900 ~1100		-8330/T+3.40 +0.12[Mn%]	Irvine(1967)
AlN-1	0.08	0.41	1.46	0.0127		0-0.144		S	1050 ~1350	5 ~65	-7400/T+1.95	Eckstein(1993)
AlN-2	0.15	0.29	0.9	0.006	0.027	0.07	0.012		900 ~1200		-7410/T+1.69	Robertson(1993)
AlN-3	Fe-Al-N ternary alloys							B	800 ~1300	1	-7184/T+1.79	Narita(1975)
AlN-4	0.2	0.5	1.5	0.024		0.05		B	900 ~1350	1 ~3	-7750/T+1.80	Konig(1961)
AlN-5	0.05	0.01	0.35	0.005-0.0088		0.02-0.08		B	810 ~1260	15min ~3h	-6770/T+1.03	Leslie(1954)
AlN-6	0.1	0.24	0.8	0.004-0.014		0.023-0.15		B	950 ~1300	1~4min	-7500/T+1.48	Gladman(1976)

AlN-7	0.2	0.15	0.5	0.006		0-0.084		B	900 ~1200	2min	-6180/T+0.725	Erasmus(1964a)
AlN-8	0.17	0.2	0.4	0.007		0-0.216		B	900 ~1200	2min	-6015/T+0.309	Erasmus(1964a)
AlN-9	Pure Iron + Al-N								900 ~1250		-10020/T+3.577	Honer(1977)
AlN-10	0.4	0.6	0.8	0.025		0.005-0.03			900 ~1250		-9200/T+2.923	Honer(1977)
AlN-11	0.4	0.45	0.8	0.025		0.03-0.4			900 ~1250		-9295/T+3.079	Honer(1977)
AlN-12	0.06		0.24	0.006		0.035-0.137					-5675/T+0.18 +2.4[Al%]	Mayrhofer(1975)
TiN-1											-15020/T+3.82	Narita(1975)
TiN-2	0.16	0.3	0.89	0.006	0.063	0.027	0.016				-14840/T+4.36	Robertson(1993)
TiN-3											-8000/T+0.32	Matsuda(1978)
MnS-1		0.3	0.1						1000 ~1400		-10590/T+4.092	Wriedt(1976)
MnS-2	Pure Iron + 0.37%, 0.70%, 1.07%, 1.30% Mn								1200 ~1350		(-9020/T+ 2.929)/ f_S^{Mn}	Turkdogan(1955)
											$\log f_S^{Mn}$ =(-215/T+0.097)[Mn] in iron	

Note: Method A -- Average calculation; Method B -- Beeghly analysis; Method C -- Chemical method;
Method G -- Gaseous equilibrium; Method P -- Precipitation extraction; Method S -- Sieverts method.

Sieverts method: this method consists of holding the specimen in gaseous nitrogen, quenching (or cooling), and determining the nitrogen content by direct analysis (solution in acid followed by distillation of the ammonia).

Beeghly analysis: this involves separation of aluminium nitride from the steel by solution of the iron matrix in bromine and methyl acetate, followed by analysis of the residue for nitrogen.

Table 5.2 Calculated solubility products of V(C, N) in austenite considering and neglecting the effect of Al

Temperature ºC	Steel 1, w.t %							Temperature ºC	Steel 2, w.t %						
	Considering Al				Neglecting Al				Considering Al				Neglecting Al		
	C	N	V	Al	C	N	V		C	N	V	Al	C	N	V
700	0.0549	0.0005	0.0084	0.0004	0.0549	0.0005	0.0084	700	0.0590	0.0011	0.0058	0.0004	0.0588	0.0010	0.0058
750	0.0577	0.0006	0.0221	0.0010	0.0577	0.0006	0.0221	750	0.0607	0.0011	0.0145	0.0010	0.0608	0.0011	0.0143
800	0.0628	0.0008	0.0437	0.0020	0.0628	0.0008	0.0437	800	0.0630	0.0015	0.0269	0.0018	0.0631	0.0015	0.0271
850	0.0677	0.0013	0.0654	0.0029	0.0677	0.0013	0.0654	850	0.0650	0.0025	0.0385	0.0026	0.0651	0.0025	0.0385
900	0.0706	0.0024	0.0816	0.0038	0.0705	0.0023	0.0818	900	0.0661	0.0042	0.0492	0.0037	0.0661	0.0042	0.0494
950	0.0720	0.0040	0.0945	0.0045	0.0719	0.0041	0.0939	950	0.0666	0.0066	0.0605	0.0052	0.0666	0.0065	0.0605
1000	0.0725	0.0068	0.1060	0.0057	0.0725	0.0067	0.1059	1000	0.0669	0.0098	0.0734	0.0081	0.0669	0.0099	0.0734
1050	0.0728	0.0100	0.1200	0.0077	0.0728	0.0103	0.1202	1050	0.0670	0.0140	0.0890	0.0148	0.0670	0.0140	0.0889
1100	0.0730	0.0149	0.1377	0.0119	0.0730	0.0149	0.1375	1077					0.0670	0.0167	0.0988
1150	0.0730	0.0207	0.1593	0.0229	0.0730	0.0207	0.1590	1078	0.0670	0.0168	0.0989	0.0259			
1151	0.0730	0.0208	0.1593	0.0230	0.0730	0.0208	0.1591								

Table 5. 3 Calculated precipitation results of VC, VN, AlN, and MnS in austenite of Steel 1 without Ti by ChemSage

Temperature [°C]	VC/Carbonitride	VN/Carbonitride	Carbonitride	AlN	MnS
800	0.0003	0.0636	0.0639	0.0207	0.0054
825	0.0001	0.0641	0.0642	0.0200	0.0054
850	0.0001	0.0658	0.0658	0.0183	0.0054
875	0.0001	0.0680	0.0680	0.0163	0.0054
900	0.0000	0.0660	0.0660	0.0167	0.0054
925	0.0000	0.0637	0.0637	0.0171	0.0054
950	0.0000	0.0611	0.0611	0.0173	0.0054
975	0.0000	0.0582	0.0582	0.0175	0.0054
1000	0.0000	0.0548	0.0548	0.0176	0.0054
1025	0.0000	0.0508	0.0508	0.0175	0.0054
1050	0.0000	0.0463	0.0463	0.0173	0.0054
1075	0.0000	0.0412	0.0412	0.0171	0.0054
1100	0.0000	0.0355	0.0355	0.0167	0.0054
1125	0.0000	0.0291	0.0291	0.0161	0.0053
1150	0.0000	0.0220	0.0220	0.0155	0.0053
1175	0.0000	0.0142	0.0142	0.0147	0.0053
1200	0.0000	0.0057	0.0057	0.0138	0.0052
1225	0.0000	0.0000	0.0000	0.0121	0.0051
1250	0.0000	0.0000	0.0000	0.0089	0.0050
1275	0.0000	0.0000	0.0000	0.0056	0.0049
1300	0.0000	0.0000	0.0000	0.0022	0.0047

1325	0.0000	0.0000	0.0000	0.0000	0.0046
1350	0.0000	0.0000	0.0000	0.0000	0.0043
1375	0.0000	0.0000	0.0000	0.0000	0.0040
1400	0.0000	0.0000	0.0000	0.0000	0.0037
1425	0.0000	0.0000	0.0000	0.0000	0.0032
1440	0.0000	0.0000	0.0000	0.0000	0.0029
1441	0.0000	0.0000	0.0000	0.0000	0.0000

Table 5. 4 Calculated precipitation results of VC, VN, AlN, and MnS in austenite of Steel 1 with 0.005 wt.% Ti by ChemSage

Temperature [°C]	TiC/Carbonitride	TiN/Carbonitride	VC/Carbonitride	VN/Carbonitride	Carbonitride	AlN	MnS
800	0.0000	0.0065	0.0003	0.0660	0.0678	0.0181	0.0054
825	0.0000	0.0065	0.0002	0.0641	0.0682	0.0174	0.0054
850	0.0000	0.0065	0.0001	0.0635	0.0700	0.0157	0.0054
875	0.0000	0.0065	0.0001	0.0620	0.0725	0.0135	0.0054
900	0.0000	0.0065	0.0000	0.0616	0.0706	0.0140	0.0054
925	0.0000	0.0065	0.0000	0.0611	0.0685	0.0143	0.0054
950	0.0000	0.0065	0.0000	0.0597	0.0661	0.0146	0.0054
975	0.0000	0.0065	0.0000	0.0570	0.0635	0.0148	0.0054
1000	0.0000	0.0065	0.0000	0.0540	0.0605	0.0148	0.0054
1025	0.0000	0.0065	0.0000	0.0507	0.0571	0.0147	0.0054
1050	0.0000	0.0065	0.0000	0.0469	0.0533	0.0145	0.0054

1075	0.0000	0.0064	0.0000	0.0427	0.0491	0.0141	0.0054
1100	0.0000	0.0064	0.0000	0.0381	0.0445	0.0136	0.0054
1125	0.0000	0.0064	0.0000	0.0332	0.0396	0.0128	0.0053
1150	0.0000	0.0064	0.0000	0.0281	0.0345	0.0119	0.0053
1175	0.0000	0.0064	0.0000	0.0231	0.0295	0.0106	0.0053
1200	0.0000	0.0063	0.0000	0.0184	0.0247	0.0091	0.0052
1225	0.0000	0.0062	0.0000	0.0142	0.0204	0.0072	0.0051
1250	0.0000	0.0061	0.0000	0.0107	0.0169	0.0049	0.0050
1275	0.0000	0.0059	0.0000	0.0081	0.0140	0.0023	0.0049
1300	0.0000	0.0056	0.0000	0.0059	0.0115	0.0000	0.0047
1325	0.0000	0.0052	0.0000	0.0039	0.0091	0.0000	0.0046
1350	0.0000	0.0044	0.0000	0.0026	0.0070	0.0000	0.0043
1375	0.0000	0.0035	0.0000	0.0015	0.0050	0.0000	0.0040
1400	0.0000	0.0021	0.0000	0.0007	0.0029	0.0000	0.0037
1425	0.0000	0.0004	0.0000	0.0001	0.0005	0.0000	0.0032
1441	0.0000	0.0000	0.0000	0.0000	0.0000	0.0000	0.0000

Table 5. 5 Calculated precipitation results of VC, VN, AlN, and MnS in austenite of Steel 2 without Ti by ChemSage

Temperature [°C]	VC/Carbonitride	VN/Carbonitride	Carbonitride	AlN	MnS
800	0.0001	0.0265	0.0265	0.0323	0.0109
825	0.0000	0.0260	0.0260	0.0320	0.0109

850	0.0000	0.0257	0.0257	0.0312	0.0108
875	0.0000	0.0267	0.0267	0.0294	0.0109
900	0.0000	0.0249	0.0249	0.0292	0.0108
925	0.0000	0.0222	0.0222	0.0293	0.0108
950	0.0000	0.0191	0.0191	0.0293	0.0108
975	0.0000	0.0155	0.0155	0.0292	0.0108
1000	0.0000	0.0113	0.0113	0.0290	0.0108
1025	0.0000	0.0064	0.0064	0.0287	0.0108
1050	0.0000	0.0010	0.0010	0.0282	0.0108
1075	0.0000	0.0000	0.0000	0.0264	0.0108
1100	0.0000	0.0000	0.0000	0.0241	0.0108
1125	0.0000	0.0000	0.0000	0.0216	0.0107
1150	0.0000	0.0000	0.0000	0.0191	0.0107
1175	0.0000	0.0000	0.0000	0.0163	0.0106
1200	0.0000	0.0000	0.0000	0.0134	0.0106
1225	0.0000	0.0000	0.0000	0.0104	0.0105
1250	0.0000	0.0000	0.0000	0.0072	0.0104
1275	0.0000	0.0000	0.0000	0.0039	0.0102
1300	0.0000	0.0000	0.0000	0.0004	0.0100
1325	0.0000	0.0000	0.0000	0.0000	0.0098
1350	0.0000	0.0000	0.0000	0.0000	0.0095
1375	0.0000	0.0000	0.0000	0.0000	0.0091
1400	0.0000	0.0000	0.0000	0.0000	0.0087
1425	0.0000	0.0000	0.0000	0.0000	0.0082
1445	0.0000	0.0000	0.0000	0.0000	0.0000

Table 5. 6 Calculated precipitation results of VC, VN, AlN, and MnS in austenite of Steel 3 with 0.009 wt.% Ti by ChemSage

Temperature [C]	TiC/Carbonitride	TiN/Carbonitride	VC/Carbonitride	VN/Carbonitride	Carbonitride	AlN	MnS
800	0.0000	0.0116	0.0001	0.0247	0.0365	0.0259	0.0109
825	0.0000	0.0116	0.0001	0.0246	0.0363	0.0256	0.0109
850	0.0000	0.0116	0.0000	0.0249	0.0366	0.0247	0.0108
875	0.0000	0.0116	0.0000	0.0265	0.0381	0.0229	0.0109
900	0.0000	0.0116	0.0000	0.0255	0.0371	0.0227	0.0108
925	0.0000	0.0116	0.0000	0.0239	0.0355	0.0226	0.0108
950	0.0000	0.0116	0.0000	0.0221	0.0337	0.0224	0.0108
975	0.0000	0.0116	0.0000	0.0202	0.0318	0.0221	0.0108
1000	0.0000	0.0116	0.0000	0.0182	0.0298	0.0215	0.0108
1025	0.0000	0.0116	0.0000	0.0161	0.0277	0.0208	0.0108
1050	0.0000	0.0116	0.0000	0.0141	0.0256	0.0198	0.0108
1075	0.0000	0.0116	0.0000	0.0121	0.0237	0.0185	0.0108
1100	0.0000	0.0115	0.0000	0.0103	0.0219	0.0170	0.0108
1125	0.0000	0.0115	0.0000	0.0087	0.0202	0.0152	0.0107
1150	0.0000	0.0114	0.0000	0.0073	0.0188	0.0132	0.0107
1175	0.0000	0.0113	0.0000	0.0062	0.0175	0.0109	0.0106
1200	0.0000	0.0112	0.0000	0.0052	0.0164	0.0084	0.0106
1225	0.0000	0.0110	0.0000	0.0043	0.0154	0.0058	0.0105
1250	0.0000	0.0108	0.0000	0.0036	0.0144	0.0029	0.0104
1275	0.0000	0.0105	0.0000	0.0030	0.0135	0.0000	0.0102
1300	0.0000	0.0099	0.0000	0.0022	0.0122	0.0000	0.0100
1325	0.0000	0.0091	0.0000	0.0017	0.0108	0.0000	0.0098

1350	0.0000	0.0081	0.0000	0.0012	0.0093	0.0000	0.0095
1375	0.0000	0.0067	0.0000	0.0008	0.0075	0.0000	0.0091
1400	0.0000	0.0050	0.0000	0.0005	0.0055	0.0000	0.0087
1425	0.0000	0.0026	0.0000	0.0002	0.0028	0.0000	0.0073
1440	0.0000	0.0000	0.0000	0.0000	0.0000	0.0000	0.0012
1444	0.0000	0.0000	0.0000	0.0000	0.0000	0.0000	0.0000

Table 5.7 Diffusion data for microalloy and interstitial solutes in austenite and in ferrite (Kirk-Othmer Encyclopedia)

Element/Phase	C/α	C/γ	N/α	N/γ	Ti/α	Ti/γ	V/α
$D_0(m^2s^{-1})$	0.62×10^{-6}	0.10×10^{-4}	0.50×10^{-6}	0.91×10^{-4}	3.15×10^{-4}	0.15×10^{-4}	0.61×10^{-4}
$Q(kJ\ mol^{-1})$	80.4	135.7	77.0	168.6	248.0	251.2	267.1
Element/Phase	V/γ	Nb/α	Nb/γ	Al/α	Al/γ	Fe/α	Fe/γ
$D_0(m^2s^{-1})$	0.25×10^{-4}		5.30×10^{-2}	0.30×10^{-2}		1.67×10^{-4}	0.49×10^{-4}
$Q(kJ\ mol^{-1})$	264.2		344.6	234.5		256.7	284.1

Table 5.8 Density and lattice parameters of microalloy carbides, nitrides, and sulphide (at room temperature) (Leslie, 1981)

Compound/structure	NbC/fcc	NbN/fcc	VC/fcc	VN/fcc	TiC/fcc
Lattice parameter, nm	0.4462	0.4387	0.4154	0.4118	0.4313
Molecular per unit cell	4	4	4	4	4
Density, mg/mm^{-3}	7.84	8.41	5.83	6.18	4.89
Compound/structure	TiN/fcc	AlN/cph	α-MnS/fcc	β-Fe/fcc	α-Fe/bcc
Lattice parameter, nm	0.4233	c=0.4965, a=0.311	0.522	0.357	0.286
Molecular per unit cell	4	6	4	4	2
Density, mg/mm^{-3}	5.42	3.27	4.05	8.15	7.85

Table 5.9 The calculated and measured austenite grain size in Steel 1 by using Gladman equation

Equalisation time, min	MnS particle size, μm	Calculated austenite diameter, mm			Measured austenite diameter, mm
		$Z=\sqrt{2}$	Z=1.6	Z=2	
53	0.39	0.17	0.49	0.98	0.488
318	0.56	0.24	0.69	1.41	0.674
1333	0.75	0.32	0.94	1.89	0.710

Table 5.10 MnS particle mean diameter and volume fraction in each diameter section

MnS diameter section	MnS diameter, μm			MnS volume, mm^3			MnS volume percentage		
	53 min	318 min	1333 min	53 min	318 min	1333 min	53 min	318 min	1333 min
0 - 0.2	0.16	0.19	0	0.03	0.004	0	1.08%	0.04%	0%
0.2 - 0.4	0.3	0.28	0.36	0.27	0.20	0.10	9%	3%	1%
0.4 - 0.6	0.51	0.49	0.55	0.95	0.86	1.60	33%	10%	10%
0.6 - 0.8	0.7	0.67	0.75	1.30	2.07	2.91	45%	25%	18%
0.8 - 1.0	0.84	0.91	0.89	0.31	1.19	2.23	11%	14%	13%
>1.0	0	1.13	1.22	0	3.95	9.58	0%	48%	58%

Table 5.11 Austenite grain mean diameter and volume fraction in each diameter section

Austenite diameter section	Austenite diameter, mm			Austenite volume, mm^3			Austenite volume percentage		
	53 min	318 min	1333 min	53 min	318 min	1333 min	53 min	318 min	1333 min
0 - 0.3	0.20	0.27	0.26	0.15	0.12	0.09	1%	1%	0.4%
0.3 - 0.6	0.47	0.52	0.52	1.66	2.62	2.39	13%	12%	8%
0.6 - 0.9	0.80	0.80	0.78	3.32	3.53	4.66	26%	17%	15%
0.9 - 1.2	1.04	1.07	1.05	2.42	8.40	6.06	19%	40%	20%
1.2 - 1.5	0	1.50	1.40	0	1.77	4.35	0%	8%	14%
1.5 - 1.8	1.68	1.65	1.55	5.00	4.72	1.95	40%	22%	6%
>1.8	0	0	1.89	0	0	10.62	0%	0%	35%

Table 5.12 Comparison of measured and calculated austenite grain diameters

MnS mean size, μm	Measured austenite diameter, mm			Calculated austenite diameter, mm		
	53 min	318 min	1333 min	53 min	318 min	1333 min
0 - 0.2	0.20	0.27	0.26	0.19	5.79	-
0.2 - 0.4	0.47	0.52	0.52	0.53	2.1	3.5
0.4 - 0.6	0.80	0.80	0.78	0.49	1.0	1.0
0.6 - 0.8	1.04	1.07	1.05	0.36	1.3	1.0

Table 5.13 Calculated volume fraction value

By using Rios and Gladman equations

Reheating temperature, °C	1050			1150		
Reheating time, min	53	318	1333	53	318	1333
Austenite grain size, μm	35.4	37.1	46.5	251.7	268.5	286.5
AlN particle size, μm	0.18	0.26	0.42	0.71	0.87	0.98
f(Rios)	8.5×10^{-4}	1.2×10^{-3}	1.5×10^{-3}	4.7×10^{-4}	5.4×10^{-4}	5.7×10^{-4}
f(Gladman), $Z=\sqrt{2}\sim2$	$2.3\times10^{-4}\sim1.3\times10^{-3}$	$3.1\times10^{-4}\sim1.8\times10^{-3}$	$4.1\times10^{-4}\sim2.4\times10^{-3}$	$1.3\times10^{-4}\sim7.4\times10^{-4}$	$1.5\times10^{-4}\sim8.5\times10^{-4}$	$1.6\times10^{-4}\sim9.0\times10^{-4}$
f calculated from Eq. AlN-4	6.6×10^{-4}			3.8×10^{-4}		
f calculated from composition	1.1×10^{-3}					